UNIVERSITÉ DE LILLE

École Graduée Biologie - Santé de Lille

Doctoral specialisation

Research clinic, Innovation technology, Public health – MED

Scientific field

Biology, Medicine and Health

Design and development of a perifusion chamber for hormonal analysis and metabolic evaluation of islets of langerhans

Priyadarshini Gnanasekar, ME (Engineering)

A thesis submitted to the University of Lille
in fulfilment of the requirements for the degree of
Doctor of Life and Health Science

Jury Members :
Rachel DESAILLOUD, Professor – Examiner, President of the jury
Matthieu RAOUX, Professor – Reporter
Jérémie POURCHEZ, Professor – Reporter

Supervisors :
Patrice CODDEVILLE, Professor
Chiara SAPONARO, PhD, HDR
Valéry GMYR, PhD

December 16th, 2025

UNIVERSITÉ DE LILLE

École Graduée Biologie - Santé de Lille

Spécialisation doctorale

Recherche clinique, Innovation technologique, Santé publique – MED

Domaine scientifique

Biologie, Médicine et santé

Développement d'une chambre de périfusion pour l'analyse des sécrétions hormonales et l'évaluation du métabolisme des îlots de langerhans

Priyadarshini Gnanasekar, ME (Engineering)

Thèse soumise à l'université de Lille
en vue de l'obtention du diplôme de
Docteur en Science de la Vie et de la Santé

Membres du jury :
Rachel DESAILLOUD, Professeur – Examinateur, Président du jury
Matthieu RAOUX, Professeur – Rapporteur
Jérémie POURCHEZ, Professeur – Rapporteur

Superviseurs :
Patrice CODDEVILLE, Professeur
Chiara SAPONARO, PhD, HDR
Valéry GMYR, PhD

16 décembre 2025

Acknowledgements

I would like to express my sincere gratitude to the members of my thesis jury, Professor Matthieu RAOUX (Université de Bordeaux), Professor Jérémie POURCHEZ (Mines Saint-Etienne/Institut Mines-Telecom), and Professor Rachel DESAILLOUD (CHU Amiens-Picardie) for having accepted to examine this work. I'm truly honoured by your presence and by the time you have taken to read and discuss my thesis.

The PhD thesis work presented in this document is conducted at "Laboratoire U1190" at Pole recherche, Lille, France and at Fab Lab IMT Nord Europe, France, from September 2022 to February 2026, under the supervision of Research Engineer Dr Valéry GMYR and Dr Patrice Coddeville. The thesis theme with the title "Design and development of a perifusion chamber for hormonal analysis and metabolic evaluation of islets of Langerhans" was funded by the Biomedicine agency (ABM), EGID, Hauts de France and CPER TechSanté.

I would like to express my sincere gratitude to my supervisor, **Dr Valéry GMYR**, for everything he did for me in the past 3 years. First of all, I would like to thank him for allowing me to work in this project. I would also thank him for the trust he placed in me upon my work during these years, for his patience and for his availability. I still remember the phrase he said the first day, "family is first". Finally, I would like to thank him for his help and advice, his experience and the knowledge he generously shared, which have brought life and meaning to this work. Thank you **Dr Valéry GMYR.**

Likewise, I would like to express my sincere gratitude to co-supervisor **Dr Patrice CODDEVILLE** for his entire help in the fab lab during these years. I still remember the day he interviewed me and said the acceptance on the same day.

I would like to thank Professor **François Pattou**, Director of the INSERM UMR1190 and Professor **Julie Kerr-Conte** for accepting me in their lab for experiments. I am truly thankful for being welcomed as part of their team and for the generous support that enabled me to pursue this research.

I would like to express my deepest gratitude to Engineer **Mr Christophe CAPPLAERE**, a father figure, for his unwavering support throughout my PhD. His guidance, kindness, and human qualities have been truly inspiring, and his presence has been a source of strength and encouragement that I will always remember with gratitude.

I am deeply thankful to Engineer **Dr Vincent Martin** for his generous support in 3D Printing, his continuous support, and the engaging discussions that helped bring this thesis to completion.

I would like to thank **Mr Thomas Fagniez** - IMT Nord Europe, for his support in sensor selection; his valuable help contributed successful completion of my thesis work.

I would like to express my sincere thanks to **Dr Isabel González Mariscal** for her care, on-time motivation and her time for correcting the article.

I would like to thank **Dr Chiara Saponaro** for her tremendous support in slide correction during the PhD.

I would like to thank the team from UMR1190 laboratory — **Dr Caroline Bonner**, **Julien Thevenet, Nathalie Delalleau, Anaïs Coddeville, Gianni Pasquetti, Eva Gruson, Arnaud Hanssen, Bruno Lukowiak, Pauline Petit, and Audrey Quenon** — for their valuable support and collaboration.

I also extend my sincere thanks to the Human Resources and Administrative team — **Rofigua**

Hakem, Benjamin Legendre, and Alexandre Thevenot — for their assistance throughout my work.

This thesis would not have been possible without all the PhD students - **Jessica Abalos**, **Dr Omolara Tijani, Isaline Louvet, Valentin Lerique, Dr Rebecca Goutchtat**, **Dr Ana Acosta, Elise Wreven, and Tiffani Gencarelli.**

I am profoundly thankful to my family for their unconditional love, encouragement, and constant belief in me. My deepest gratitude goes to my father, **Mr Gnanasekar Ramalingam**, the pillar of my strength, my friend, and a truly wonderful father. His love, care, and guidance throughout my life have been my greatest support, always reminding me that I was never alone - Love you pa.

I also thank my beloved mother in heaven, whose blessings and love have guided me both in life and in reaching this achievement. Love you, Ma.

My sincere appreciation goes to my sisters, **Saravana Kumari** and **Sooriya Prabha**, and my brother, **Sathish Kumar**, for their constant encouragement and support throughout my journey.

Finally, I would like to express my heartfelt thanks to my husband, **Mr Manikannan**, for being my unwavering pillar of strength, a loving partner, and a devoted father. His patience, support, and love made this challenging journey possible. Love you, Bossu.

Finally, my deepest thanks to my dear son, **Mr Yojith Manikannan**, for his unconditional love, support, and understanding throughout this journey. I am deeply grateful for the sacrifices and adjustments he made for me. *Thank you, Da — and I'm sorry for the moments I wasn't there when you needed me most.*

Summary

Pancreatic Human islet of Langerhans (IL) transplantation is a promising clinical approach for the treatment of severe type 1 diabetes. However, the restoration of endogenous insulin secretion remains subject to many uncertainties (donor history, pancreas harvesting, cell islet processing, etc.), and the prediction of transplant success depends primarily on the quality of the insulin-secreting cells; hence the importance of being able to accurately evaluate a cell preparation before it is released to the transplant surgeon.

Among the various assessment techniques, the glucose-stimulated insulin secretion (GSIS) test remains the gold standard for evaluating beta cell function. However, the static or dynamic (perifusion) GSIS used have limitations in terms of information, as they focus exclusively on insulin stimulation. Increasing experimental throughput to facilitate parallel studies is a crucial aspect in refining perifusion systems for more efficient and comparative GSIS analysis.

Furthermore, due to the cellular heterogeneity of IL and inter-individual variability, it appears essential to combine other indicators for the evaluation of isolated IL.

This thesis establishes several advances: (1) to study the beta cell heterogeneity in human donors of islet Perifusions (2) by developing CAD (Computer Aided Design) modeled prototype, (3) by developing Stereolithography-based 3D-fabricated perifusion mono chambers, (4) assembling a 4-stream perifusion system with associated components to access parallel perifusion studies and (5) to adopt a measurement of oxygen consumption during the perifusion process.

The results of a single-center study of insulin secretion assessed by perifusion on a large number of IL preparations (n = 168) identified that donor physiological parameters, such as

Body Mass Index (BMI), Body Surface Area (BSA) and HbA1c, influenced insulin secretion, particularly at low glucose concentrations, independently of sex. This study confirmed the importance of fasting insulin secretion as an indicator of the functional quality of isolated IL.

In collaboration with IMT Nord Europe, we used CAD (SolidWorks) to model perifusion chambers and developed fluid flow analysis to ensure uniform perifusion that does not stress the IL during carbohydrate stimulation.

We therefore manufactured perifusion chambers (mono chambers) using 3D printing technology based on stereolithography (SLA). These chambers confirmed the uniformity of flow and stability during assembly.

Furthermore, an optical probe system was integrated post-chamber to monitor glucose-stimulated oxygen consumption rates (OCR). Our preliminary results confirmed measurable and reproducible metabolic responses in human islets within a single perifusion framework, and established a foundation for future studies.

This thesis has demonstrated the high intra- and inter-individual heterogeneity of insulin secretion by isolated human islets of Langerhans and have led to the development of a tool for evaluating the in vitro metabolic functionality of isolated IL used in clinical practice or in scientific studies. This tool should contribute to the development of standardised platforms for future research on IL hormone secretion and provide a better understanding of the physiology of insulin secretion.

(Graphical abstract page : 154)

Résumé (French)

La transplantation d'îlots pancréatiques humains de Langerhans (IL) est une approche clinique prometteuse pour le traitement du diabète de type 1 sévère. Cependant, la restauration de la sécrétion endogène d'insuline reste soumise à de nombreuses incertitudes (antécédents du donneur, prélèvement du pancréas, traitement des îlots cellulaires, etc.) et la prédiction du succès de la transplantation dépend principalement de la qualité des cellules sécrétrices d'insuline, d'où l'importance de pouvoir évaluer avec précision une préparation cellulaire avant qu'elle ne soit remise au chirurgien transplanteur. Parmi les différentes techniques d'évaluation, le test de sécrétion d'insuline stimulée par le glucose (GSIS) reste la référence pour évaluer la fonction des cellules bêta. Cependant, les tests GSIS statiques ou dynamiques (périfusion) utilisés présentent des limites en termes d'informations, car ils se concentrent exclusivement sur la sécrétion insulinique. De plus, du fait de l'hétérogénéité cellulaire des IL et de la variabilité interindividuelle, il semble essentiel de combiner d'autres indicateurs pour l'évaluation des IL isolées. Aussi perfectionner les analyses par périfusion semble crucial pour l'évaluation des cellules endocrines utilisées en clinique ou lors de protocoles expérimentaux.

Au cours de ce travail de thèse, nous avons pu : (1) étudier, à l'aide de la technique de périfusion, l'impact de l'hétérogénéité des IL humains sur la sécrétion d'insuline ; (2) développer et fabriquer, à l'aide de l'impression 3D, des chambres de réactionnelles adaptées à la physiologie fine de l'IL ; (3) développer un système de périfusion permettant plusieurs analyses en parallèle et (4) adapter une mesure de la consommation d'oxygène continue pendant le processus de périfusion.

Les résultats d'une étude monocentrique sur la sécrétion d'insuline évaluée par perfusion sur un grand nombre de préparations d'IL (n = 168) ont montré que les paramètres physiologiques

des donneurs, tels que l'Indice de Masse Corporelle (IMC), la Surface Corporelle (SC) et l'HbA1c, influençaient la sécrétion d'insuline, en particulier à de faibles concentrations de glucose, indépendamment du sexe. Cette étude a confirmé l'importance de la sécrétion d'insuline à jeun comme indicateur de la qualité fonctionnelle de l'IL isolée.

En collaboration avec l'IMT Nord Europe, nous avons utilisé la CAO (SolidWorks) pour modéliser des chambres de périfusion et développé une analyse des flux des fluides périfusés afin de garantir une périfusion uniforme qui ne stresse pas l'IL pendant la stimulation glucidique.

Nous avons fabriqué des chambres de périfusion individuelle (mono-chambre) à l'aide d'une technologie d'impression 3D basée sur la stéréolithographie (SLA). Ces chambres étaient chargées par le bas, et des tests itératifs ont confirmé l'uniformité du flux et la stabilité opérationnelle pendant la stimulation cellulaire. Un système de sonde optique a été intégré en aval de la chambre de perfusion afin de mesurer les taux de consommation d'oxygène (OCR) pendant la stimulation au glucose.

Cette thèse a démontré la grande hétérogénéité intra- et interindividuelle de la sécrétion d'insuline par les îlots de Langerhans humains isolés et a conduit au développement d'un outil permettant d'évaluer la fonctionnalité métabolique *in vitro* des IL isolés utilisés dans la pratique clinique ou dans les études scientifiques. Cet outil devrait contribuer au développement de plateformes standardisées pour les futures recherches sur la sécrétion d'hormones IL et permettre une meilleure compréhension de la physiologie de la sécrétion d'insuline.

(Page du résumé graphique : 154)

List of Abbreviations

BMI	Body Mass Index
BSA	Bovine serum albumin
BSA	Body surface area
CAD	Computer-aided Design
DMD	Digital Micromirror Device
DLP	Digital Light Processing
ETC	Electron Transport Chain
FC	Fraction collector
FDM	Fused Deposition modeling
FTC	Flow through cell
GSIS	Glucose-Stimulated Insulin Secretion
HbA1C	Hemoglobin A1C
IDF	International Diabetes Federation
IEQs	Islet Equivalents
IIC	Intra-Cellular Insulin Content
IL	Islets of Langerhans
IT	Islet Transplantation
KRB	Krebs Ringer Bicarbonate
LCD	Liquid Cristal Display
MSLA	Masked Stereolithography
OCR	Oxygen consumption rate
SI	Stimulation Index
SLA	Stereolithography
STL	Standard Triangle Language
T1D	Type 1 Diabetes
T2D	Type 2 Diabetes
TCA	Tricarboxylic Acid Cycle (Citric Acid Cycle)

Table of Contents

List of Figures

List of Tables

CHAPTER 1

Introduction

1 Chapter I: Introduction

1.1 Glucose homeostasis

Endocrine insufficiency plays a significant role in the development of diabetes, a group of metabolic disorders characterised by impaired glucose regulation. In most vertebrates, glucose serves as the primary energy source. After consuming food, glucose derived from complex carbohydrates enters the bloodstream and is transported to various tissues throughout the body. Once inside cells, glucose can be converted into energy, stored or used as a building block for other essential molecules (**Figure 1**). These metabolic conversions ensure that glucose is used efficiently to meet the cell's energy needs, support growth, repair, and maintenance.

Maintaining proper blood glucose levels is critical, as both low (Hypoglycemia, typically under 70 mg/dL) and high (Hyperglycemia, above 180 mg/dL after a meal, above 130 mg/dL during fasting) blood sugar levels create significant risks to the body, leading to severe health conditions (Amiel, 2021). Glucose homeostasis is regulated by a balance between glucose appearance (hepatic glucose production, intestinal absorption) and glucose disappearance (e.g., tissue uptake, storage) through the modulating effect of insulin, counterregulatory hormones (glucagon), and incretin hormones (Jiang and Zhang, 2003; Aronoff, Berkowitz et al., 2004). In healthy individuals, the endocrine pancreas maintains glucose homeostasis primarily through the coordinated secretion of insulin and glucagon.

1.2 Endocrine pancreas

The pancreas has three main regions: the head, the body, and the tail. On average, it measures around 15 centimetres in length and weighs approximately 70 to 150 grams. It is a soft, glandular organ with a somewhat elongated, flattened shape and a curved form, and the

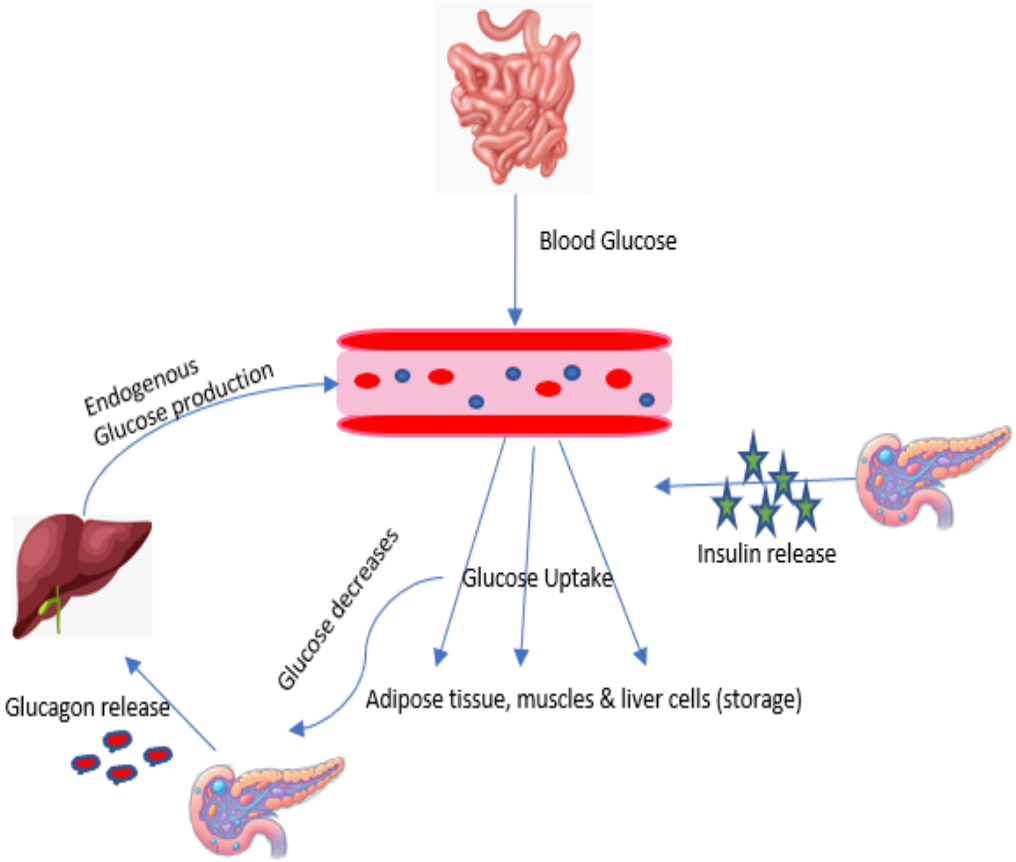

Figure 1: Glucose Homeostasis

The body tends to maintain a stable range, accomplished by a negative feedback loop that involves the release of two hormones. If the blood glucose increases beyond the normal range, for example, after a meal, it triggers the pancreas to release insulin that triggers body cells (adipocytes, myocytes), especially liver cells, to take up the glucose and convert it into glycogen for later use. If blood glucose decreases, it will also trigger the hormone glucagon, which will break down glycogen from the liver and release glucose into the blood, thereby bringing the levels back to normal (Fu, Gilbert et al., 2013; Podobnik, Korosak et al., 2020), figure adapted from (Richter, Albert et al., 2022).

organ exhibits a dual nature within its tissue glands. Firstly, the Endocrine function constitutes a mere 2% of the entire pancreas but carries a significant role (Longnecker, 2021). The small clusters in the endocrine called Islets of Langerhans (IL) encompass five distinct cell types: alpha cells (producing glucagon), beta cells (producing insulin), delta cells (producing somatostatin), PP cells (producing pancreatic polypeptide), and epsilon cells (producing ghrelin) (Cabrera, Berman et al., 2006). These cells consume over 25% of the organ's blood supply and collectively release hormones into the bloodstream, orchestrating the dynamic regulation of blood glucose levels. The IL are surrounded by the body's extracellular matrix and supported by a network of blood vessels, nerves, and other pancreatic cells. Secondly, a larger fraction of the pancreas is dedicated to its Exocrine gland aspect, characterised by duct and acinar cells that release enzymes and facilitate their conveyance to the duodenum (Zhou, Brown et al., 2008). Human islets exhibit a more heterogeneous and intermingled cellular composition compared to the organised structure seen in mouse islets (Brissova, Fowler et al., 2005).

1.3 Physiological regulation of insulin secretion:

1.3.1 Insulin biosynthesis and secretion

When food is consumed, the digestive system breaks it down into basic components, including carbohydrates, which are further digested into glucose. As blood glucose levels rise, beta cells from the pancreas detect these changes, and glucose enters through facilitated diffusion via glucose transporters. Inside the beta cells, glucose undergoes oxidative glycolysis, leading to the production of ATP, which plays a key role in the subsequent release of insulin (**Figure 2**) (Matschinsky and Ellerman, 1968; Fridlyand and Philipson, 2010; Navale AM, 2016). The

causes of diabetes may vary, but generally include insulin resistance, genetic influences, endocrine destruction or disorders & environmental factors.

1.3.2 Variability in insulin secretion

Research on insulin regulation consistently highlights that secretion and sensitivity are highly variable between individuals and across different stages of metabolic health (Hansen, Wium et al., 2020). Several studies emphasise that insulin secretion is not a fixed process but one that adapts to body composition, genetic background, and environmental influences (Ishida, Harada et al., 2025). Studies demonstrated that biphasic glucose-stimulated insulin secretion shows distinct changes over decades, and large inter-individual differences in insulin sensitivity are also observed, even among similar glucose levels (Peng, Wang et al., 2025). Besides glucose, other factors such as hormones and signals in the body can influence how insulin is produced (Henquin, 2021).

1.3.3 Biological and technical determinants of functional human islet quality

The functional beta cell mass at transplanted sites is influenced by various factors, including the preservation of islet yield after isolation, the condition of the donor pancreas, the effects of immunosuppressive therapy, the ability of islets to adapt to a new microenvironment, and the impact of hormones and neurotransmitters (Hiriart, Velasco et al., 2014; Rickels, Stock et al., 2018; Czarnecka, Dadheech et al., 2023; Langlois, Pinget et al., 2024). The integrity of the pancreatic islets is governed by complex biological processes involving the interplay of various cell types, variations in cellular composition, viability, ATP/ADP ratio, mitochondrial function and so on. Another layer of variability is heavily influenced by donor-specific factors, including age, BMI, cause of death, ischemia time and challenges to their standardization. Glucose remains the primary trigger for insulin release, entering beta cells through transporters. In

vitro models, such as perifusion and static incubation, stand as an important tool to study human islet secretion. Differences in perifusion methods, quantification, normalization which make the discrepancies in interpretation. Another layer of variability lies in donor-related factors such as islet purity, glycemic and weight-based parameters. Therefore, paying attention in in-vitro assays and reproducibility of data analysis is more important.

1.4 Diabetes trends, alternative therapy for Type 1 diabetes & evaluation procedures

1.4.1 Prevalences

In recent years, diabetes has become a significant global cause of death. In 2021 alone, approximately 6.7 million people lost their lives due to this condition. According to the international diabetes federation report, currently, there are around 589 million individuals (aged 20-79) living with diabetes, and this number is projected to rise to 643 million by 2030. This count is expected to rise to 853 million people in 2050 (IDF, 2024) . Diabetes is a chronic metabolic disorder characterised by elevated blood glucose levels (Hyperglycemia), often resulting from the progressive loss of pancreatic beta-cell function. Among the various types, Type 2 diabetes (T2D) is the most prevalent and arises from a combination of impaired insulin secretion and insulin resistance. During the progression of T2D, both fasting and postprandial glucose levels typically increase due to impaired insulin secretion and growing insulin resistance. Donor characteristics, such as genetic background, age, BMI (Body Mass Index), and metabolic health, can significantly influence the risk and severity of diabetes as they affect beta cell function and insulin sensitivity (how effectively the body responds to insulin). This dysfunction can lead to damage in multiple organs, including the kidneys, eyes, and heart. Management typically begins with lifestyle modifications and oral antidiabetic medications. Type 1 diabetes (T1D), on the other hand, is caused by an autoimmune destruction of beta

cells, leading to less or no insulin production. It requires immediate medical intervention. In 2024, an estimated 9.2 million people worldwide were living with Type 1 diabetes, including 1.8 million under the age of 20 (Atlas, 2024). Several challenges are involved in managing T1D due to the complexity of maintaining optimal glucose levels. The precise computation of insulin dosages and regular monitoring of glucose is taxing and invasive, but it is essential to avoid complications.

The requirement for ongoing observations and glucose modifications can affect day-to-day functioning and mental health (Ajjan, Battelino et al., 2024). Left untreated, the risk of hyper- and hypoglycaemia can result in serious health issues. It is important to bring alternative therapies for lifelong insulin dependence. (Shapiro AM, 2016; Dabas H, 2023).

1.4.2 Currently used therapy: Allogenic Islet Transplantation

There are numerous treatments available for managing T1D, such as continuous glucose monitors and insulin pumps. However, one of the most advanced and promising alternative approaches is Human Islet Transplantation (IT) (Shapiro, Lakey et al., 2000). This procedure involves transplanting insulin-producing islet cells from a donor pancreas into a person with T1D, aiming to achieve better glucose regulation. A significant milestone was recently achieved at Lille University Hospital, where the 10-year outcomes demonstrated sustained insulin independence (28% recipients) and improved metabolic control in patients (78% recipients) (Vantyghem MC, 2019). This success has been further validated by the French healthcare system, which has fully reimbursed for islet transplantation treatments since 2021, marking a significant step forward in the accessibility and recognition of this life-changing therapy. Despite significant advances in transplantation procedures, immunosuppression protocols, and safety concerns, the challenge of reliably assessing islet function before graft

remains a critical barrier to optimising clinical outcomes. After isolation, islets are chosen based on islet yield (should be more than 200,000 IEQs), viability (more than 80%) and sterility (to check the islets away from microbes). Most of the time, the in-vitro Glucose-Stimulated Insulin Secretion is performed after the transplant.

1.5 Glucose-Stimulated Insulin Secretion (GSIS)

Although several *in vitro* assays are available to evaluate pancreatic islet function, glucose-stimulated insulin secretion (GSIS) remains the most widely used and reliable method due to its direct assessment of beta cell responsiveness to glucose. Glucose-stimulated insulin Secretion closely mimics the physiological mechanism by which pancreatic beta cells secrete insulin in response to elevated blood glucose levels, thus serving as a functional indicator of beta cell health and viability. In this assay, isolated islets are sequentially exposed to low and high glucose concentrations, and the amount of insulin secreted is quantified. The difference between basal and stimulated insulin release reflects the cell's ability to sense glucose and mount an appropriate secretory response (Deepa Maheshvare, Raha et al., 2023; Lorza-Gil, Kaiser et al., 2023). The GSIS can be performed either statically or dynamically to evaluate the islet's beta cell function.

1.5.1 Static incubation

This widely used standard criterion for assessing islet function Measures glucose responsiveness by manually shifting islets from low to high glucose conditions. Although straightforward, the procedure is more time-consuming and requires careful attention to handling and filter activation. Insulin secretion is typically reported as the average response under low and high glucose stimulation (Molano, Pileggi et al., 2024).

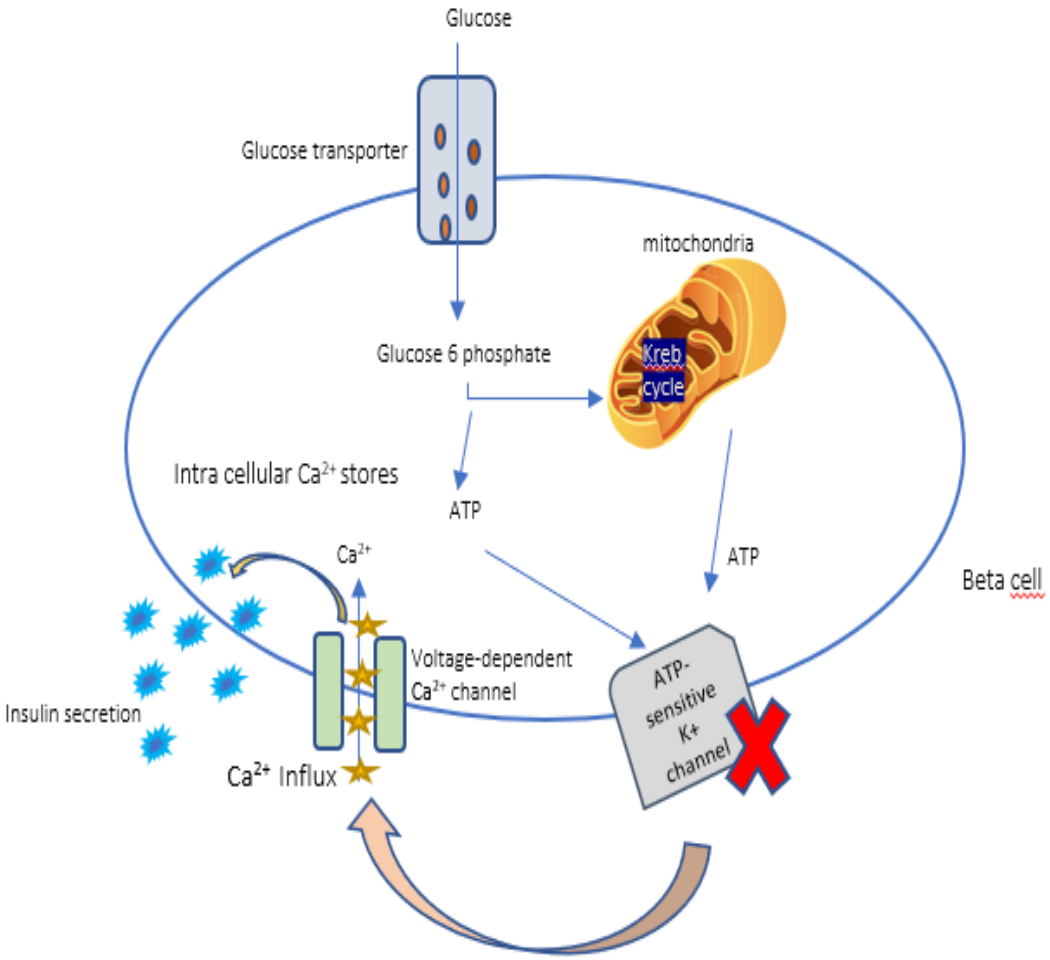

Figure 2: Beta Cell Metabolism

An increase in the ATP-ADP ratio causes ATP-sensitive potassium channels to close, leading to cell membrane depolarisation. This change prompts voltage-gated calcium channels to open, allowing calcium ions into the beta cell. The rise in intracellular calcium concentration triggers exocytosis, causing secretory vesicles to merge with the cell membrane and release insulin. This hormone is essential for maintaining stable blood sugar levels. In summary, this complex process ensures tight glucose regulation in the body (Gembal M, 1992; Rorsman P, 2018; Henquin JC, 2006), figure adapted from (Henquin, 2009; Petersen and Shulman, 2018).

1.5.2 Dynamic perifusion

Dynamic perifusion offers temporal resolution, allowing detailed insight into biphasic insulin secretion (Henquin, Dufrane et al., 2015; Alcazar and Buchwald, 2019; Hart and Powers, 2019; Misun, Yesildag et al., 2020). This release of kinetic provides crucial insights into beta cell function that static methods cannot capture.

Our laboratory has employed dynamic perifusion since 2017 to investigate insulin secretion and beta-cell function. In this technique, isolated pancreatic islets are maintained in a controlled environment to assess their functional response. The experiments require an assembled perifusion system with supporting components, operated according to a standardised protocol (**Figure 3**). A schematic representation of the setup is shown in **Figure 4**. The interpretation of insulin secretion data is complex and influenced by various factors, including donor characteristics, such as sex, age, Body Mass Index (BMI), Body surface Area (BSA), and islet preparation variables like size, purity and cold ischemia (Henquin, 2019). While perifusion techniques have become widely adopted for islet characterisation, the variability in protocols across different centers gives significant challenges for data comparison and standardisation (Nano, Kerr-Conte et al., 2020).

Quantification and normalisation strategies are essential in islet biology to ensure accurate interpretation of functional assays. Conventional normalisation methods typically rely on DNA or protein content (Squires, Harris et al., 2000; Keymeulen, Gillard et al., 2006; Hanley, Austin et al., 2010; Pisania, Papas et al., 2010; Chowdhury, Dyachok et al., 2013; Oh, Stull et al., 2014; Xie, Zhu et al., 2015; Qi, Bilbao et al., 2018), which may reflect not only endocrine but also exocrine cell contributions, thereby limiting their specificity. Moreover, these parameters may not fully capture the inherent variability between islet preparations. Therefore, it is important

to determine beta cell-specific parameters, in conjunction with purity-based normalisation, which can provide a more reliable and biologically relevant framework for analysing islet function.

Over the years, the GSIS technique has helped us to gather data across many donor samples, which we've used to build a large cohort study and allows us to perform quantitative and qualitative analysis of pancreatic islets. Considering the pronounced heterogeneity across donors and islet characteristics, how should these perifusion results be interpreted? Which parameters contribute most significantly to insulin secretory responses? As more labs turn to perifusion to assess islet function, especially in research and preclinical work, it's become increasingly important to understand what this data tells us and fits the bigger picture of islet quality assessment. It is also quite important to have a closer look at how perifusion itself changed and improved over time.

1.5.2.1 *Evolution: Perifusion techniques and their role in insulin secretion studies*

The first perfusions were performed on pancreatic tissues in 1969-70 by Burr in Wistar rats by stimulating with 3g/L of glucose, and the range of proinsulin secreted was 1-2%, detectable 30-40 minutes after stimulation (Burr, Balant et al., 1969). In 1972, Paul (Lacy, Walker et al., 1972) described a simple perifusion system for *in vitro* studies of insulin secretion from isolated rat islets. A biphasic pattern of insulin secretion by glucose is demonstrated, where the first phase of secretion is due to the release of beta granules already associated with the microtubular system, and the second phase is the result of stored and newly synthesised granules which are secondarily associated with the tubular system. The Geneva team (Kikuchi M, 1974) showed interest by comparing perifusion with a static method, several variables to compare samples from the same pancreas in parallel. The other pancreatic hormones are

studied, and Assan R et al. (Reach G, 1979) (Ashby JP, 1975) show that perifused pancreatic tissue releases glucagon in response to arginine, norepinephrine, and decreased glucose concentration in the medium. Insulin production from human pancreatic tissue in response to glucose stimulus *in vitro* by perifusion system was performed by Ferguson J et al (Ferguson J, 1977). The perifusion technique becomes essential to study the role of intracellular and extracellular calcium in the two phases of glucose-induced insulin release (Wollheim CB, 1978) showed the results on increased calcium uptake during the second phase rather than the first phase. The Orsetti team (Orsetti A, 1980) has shown that a double glycemic stimulation was a good physiological test and that viable isolated islets showed a significant increase in insulin during the second period at 16.5 mM glucose. Likewise, a model mathematical formula of insulin secretion was constructed by analysing insulin secretion induced by glucose using control theory (Nomura M, 1984). Perifusion also made it possible to test the physiology of pseudo-islets (Hopcroft DW, 1985). For this, pancreatic islets isolated from adult rats were dispersed and cultured in free suspension for 3 to 4 days, during which islet cells spontaneously reaggregate into spherical or pseudo-islands. The gross morphology of these tissues resembled that of undissociated islets, and insulin release dynamics assessed *in vitro* by perifusion showed a biphasic, dose-dependent response to glucose. In an automated method for isolating human pancreatic islets (Ricordi C, 1988), the team conducted purification of the islets by ficoll gradients remained morphologically and functionally intact for 7 days in culture at 24° C to allow their islet function before their transplantation. While evaluating cell preparations, Ricordi recommended using dithizone as a specific dye for immediate detection of beta cells to determine purity (Ricordi, Gray et al., 1990). Microfluidic devices have emerged as a tool for biomedical research (Hansen C, 2003), and they have been extended to observe mitochondrial potential changes in response to insulin (Cabrera O, 2008).

The multi-islets dynamic insulin secretion by microfluidics revolutionised in 2010 (Adewola, Wang et al., 2010). This study resulted in optical imaging by Lee and team (Lee D, 2012). Since its inception in 1969, perifusion has continuously evolved, reflecting advancements in technology and understanding of islet physiology. The currently used perifusion system in our laboratory (Using Professor Henquin's machine) has a set-up with two islet chambers assembled with supporting components such as a peristaltic pump, gas connection for carbogen, water bath and fraction collector **(Figure 5**). This perifusion setup provided a robust framework for dissecting islet behaviour, facilitating multiple layers of analysis that expanded our understanding of insulin dynamics.

1.5.3 Replicated perifusion system: Lab's need

To comprehend the perifusion system's action and also its need for the laboratory to perform more manipulations, the perifusion system was replicated using a 2-way chamber, appropriate tubing and readily available components, including a peristaltic pump, a heating immersion circulator, and a fraction collector (**Figure 6**). Altogether, as a functional element to run the perifusion system.

Perifusion System Overview:

1.5.3.1 *Peristaltic pump:*

The perifusion system primarily utilises a Master flex Ismatec peristaltic pump as its core component. This pump features a user-friendly touch interface that allows easy access and real-time monitoring. It ensures a consistent flow rate in a minimum volume, which is crucial for maintaining the islet suspension in a glucose medium, thereby facilitating continuous insulin measurement.

Preincubation G3	Low Glucose G3	High Glucose G15	Low Glucose -G3
60 mins	10 mins	40 mins	20 mins

Figure 3: Evaluation Protocol

The protocol involved a one-hour preincubation with fasting glucose at 3mM (G3) to allow islet stabilization, followed by sample collection at 10 minutes post-preincubation. Subsequently, the islets were continuously stimulated with high glucose for 40 minutes by 15mM to assess the biphasic insulin secretion profile, and then returned to basal glucose stimulation for an additional 20 minutes.

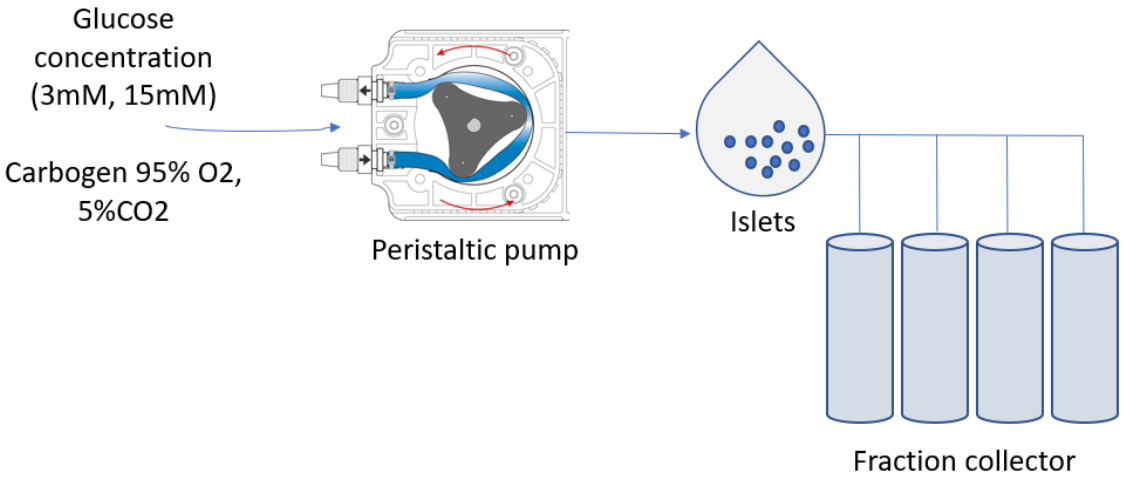

Figure 4: The schematic diagram

The Perifusions were performed with 300 IEQ per chamber with the flow rate of 1ml/min by using a peristaltic pump, and it was constant throughout the experiment with the continuous flow of carbogen and Bovine Serum Albumin (BSA) (1ml/100 ml) added with Krebs ringer bicarbonate (KRB) medium. In all experiments, the islets were maintained at 3mM glucose as basal before being stimulated with a high glucose concentrations 15mM; During the stimulation phase, sample were taken at every 2 minutes by fraction collector (FC), and the secreted insulin was measured, as well the intra cellular insulin content (IIC) after the recovery of the islets at the end of the procedure in order to calculate the % of insulin by taking the ratio of absolute and IIC and multiplied by 100.

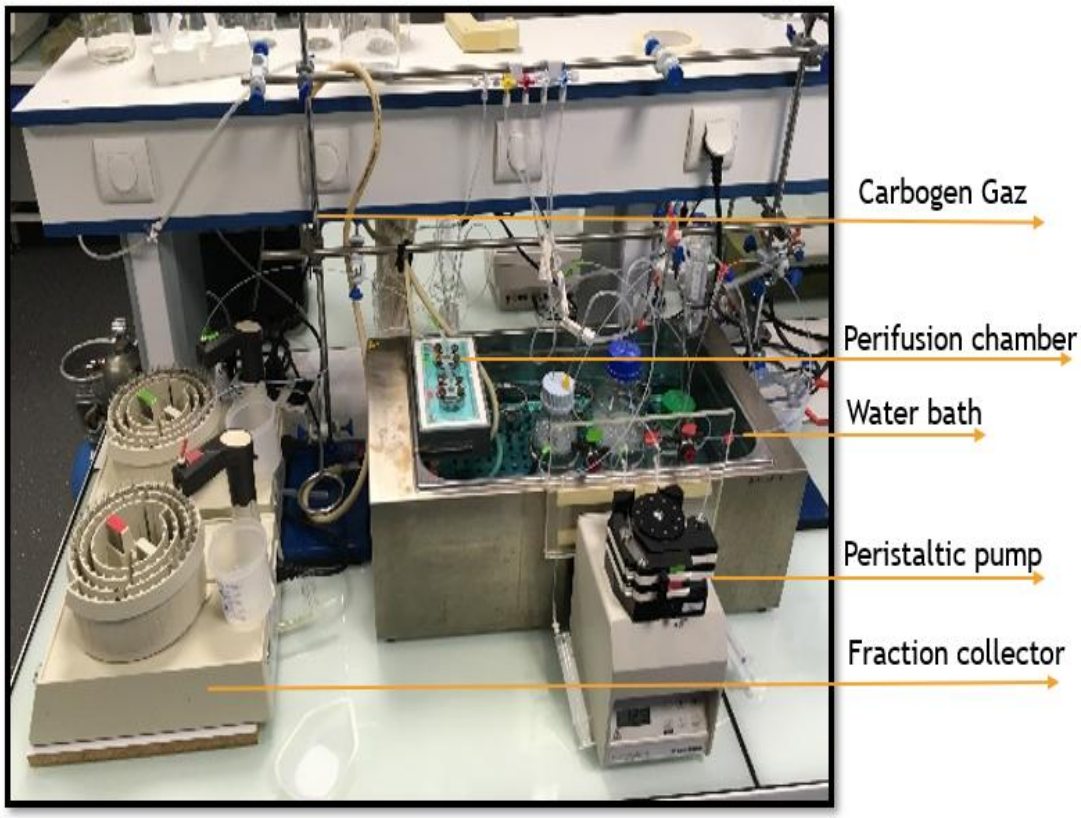

Figure 5: Dynamic perifusion set-up with all supporting components

Throughout the experiment, carbogen supply to the KRB (Krebs-Ringer Bicarbonate Buffer) medium, a Peristaltic pump to maintain a flow rate of 1 ml/min, the islet chambers facilitate the accommodation of 0.5ml of volume (300 IEQ approximately), a temperature regulator maintains 37° C, and a fraction collector – regular interval sample collection. A water bath, to maintain the samples at a regular temperature. This perifusion system is currently engaged with 2 chambers, accumulating 300IEqs per chamber, and two individual collector machines can be used to collect the samples by either number of drops or by minutes.

To achieve an optimal continuous flow rate of 1ml/min, a tube with an inner diameter of 1.5mm was used. This specific tube size was chosen to guarantee accurate delivery while minimising resistance and pressure drop. Selecting an appropriate tube diameter is vital to prevent those limitations. Furthermore, we adjusted the tube length to secure proper flow, lower energy loss, and further reduce pressure loss. This consideration for tube size and length is also crucial in minimising shear stress, preventing cell damage, and avoiding apoptosis in the beta cells.

1.5.3.2 *Current chamber information:*

The polished, smooth-surfaced dual chamber integrated in the same mini water bath, received from Arras Lab. It was well protected by using screws and sponges by avoid leakages. Each chamber was designed to hold 300 IEQs as the sample volume of 0.5mL.

1.5.3.3 *Fraction Collector (FC):*

Subsequent to the chamber is a piping connection, leading to a fraction collector, the Bio-Rad 2110. Each FC has one arm integrated with the sensor to count by either drops or minute-based flow. Each FC has a spiral holder to support 80 tubes, and each can bear up to 5 mL of sample. Its advanced automation and customizable settings permit effluent collection every 2 minutes during the perifusion process. FC takes a continuous fluid stream and automatically divides it into equal fractions by using a stepper the tube position. FC is composed of a collection arm/nozzle to guide the effluent into the current tube, a rack as a holder case controlled by motors, and Sensors for a drop counter.

1.5.3.4 *Temperature regulation:*

To ensure consistent results, the bath tank temperature remains steady at 37° Celsius throughout the perifusion. This consistency is made possible by the Julabo corio CD immersion circulator, which sustains the KRB medium at the required temperature.

1.5.3.5 *Tubing system*

These tubes mainly connect all the components and maintain the flow rate by calibrating through the pump, and it was maintained with the tube 1/16*30, which has an outer diameter of 1.6mm and a length of 30 inches (762mm).

1.5.3.6 *Assisted components:*

The water bath dimensions are 30 (width) *45 (length) *20 (height) cm to hold the sample containers and have the capacity to hold 25L of liquid, which will always be added with an antimicrobial additive (stabilising agent).

1.5.3.7 *Gas unit*

Carbogen (95%O2, CO2) connection was added to the system to gas the samples before experiment and during the experiment. Four separate gas tubes with regulators for whole set up used to control the flow.

1.5.4 Discrepancies in the classical set-up

This setup enables the capture of donor islet behavior based on donor characteristics, allowing for various analyses to be conducted. However, to refine and improve this process, it is necessary to develop a new perifusion chamber prototype. The classical setup consists of only two chambers, which is insufficient and not ideally suited for research applications.

A

B

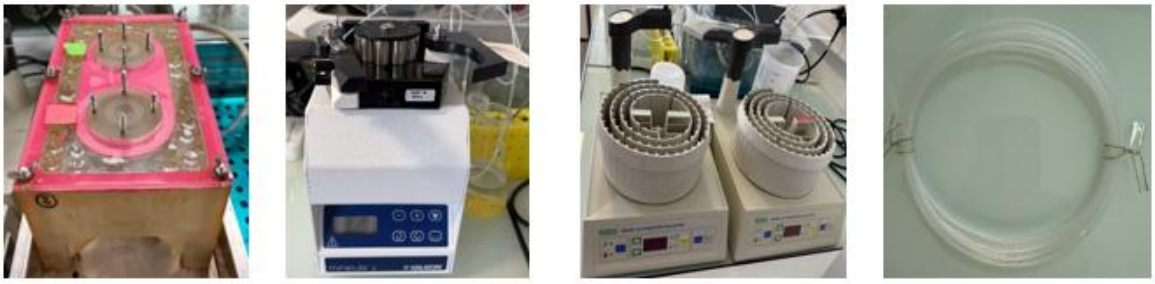

chamber

Peristaltic pump

Fraction Collector (FC)

Tubing

Figure 6: Replicated Perifusion system

A) illustrates the complete perifusion set-up assembly by connecting all individual components with tubing and the bath chamber, demonstrating the continuous flow path for the dynamic stimulation of beta cells. B) displays the individual parts of the replicated perifusion system, including the perifusion chamber, the peristaltic pump, the fraction collector, and silicone tubing (1.6 mm outer diameter) used for interconnection – engineering components for measuring biological information.

Representativeness of pancreatic islets: The current system is designed to accommodate 300 islet equivalents (IEQs) per chamber, enabling a total of 600 IEQs to be assessed simultaneously for beta-cell functionality through insulin secretion measurements. While this capacity may suffice for routine clinical evaluations, research applications often require additional experiments. These experiments are delayed due to the limited number of chambers, increasing the risk of islet loss, as a few hundred IEQs are typically lost each day in culture. This configuration also restricts comparative analyses between multiple treatments or replicates.

This limitation raises a key question: How can the existing two-chamber perifusion system be effectively expanded to improve experimental flexibility and efficiency?

One potential solution is the development of an advanced perifusion chamber prototype using microfluidic technology. However, microfluidic systems can restrict the number of islets that can be accommodated and may pose challenges in integrating new tools for monitoring islet behavior. Furthermore, due to the intrinsic heterogeneity of islets, using a single islet—or worse, a single cell—as a representative for the entire population is problematic. This laboratory previously attempted to assess glucose-stimulated insulin secretion in human islets using a Biorep-based perifusion system. Although the platform allowed dynamic monitoring of islet responses, several technical challenges limited its utility. The available quantity of human islets was relatively low (approximately 100 IEQs per run), which restricted the experimental reproducibility. Moreover, the structural configuration of the perifusion chamber imposed mechanical and shear stress on the islets, leading to instability of glucose stimulation assays. Therefore, the use of commercially available systems was discontinued, and the focus shifted toward establishing a customized experimental set-up capable of

accommodating the same islet equivalents by adding a number of chambers in parallel. After extensive consultations with industrial experts, the team concluded that an in-house solution would provide greater flexibility and experimental control than existing market options. Consequently, a decision was made to design and fabricate a bespoke chamber tailored to the specific requirements of human islet studies, utilising advanced 3D modeling and 3D printing technologies. This approach facilitates rapid prototyping and streamlines the platform tailored for islet physiology.

1.6 Engineering approach: Design & Fabrication of a novel chamber

1.6.1 Evolution and application of 3D modeling

The basic form of visual representation of 3D objects began with wireframes, constructed using curves, vertices, and edges, in the 1960s (Weiwei Fan a, Xinyi Liu a b 1 et al., 2025). Since then, 3D modeling has evolved dramatically, from simple geometric outlines to highly realistic, interactive, and physics-based simulations. Initially applied in engineering and architecture through computer-aided design (CAD) (Weisberg, 2023), its scope quickly expanded into diverse fields such as medicine, manufacturing, entertainment, and education (Fujita, 2020; Hunde and Woldeyohannes, 2022). Today, 3D modeling supports virtual prototyping, structural analysis, medical imaging, surgical planning, and the creation of customised biomedical devices, while also driving innovation in gaming, animation and virtual reality. Technological advancements over the past decades have been extensive, and the future of 3D modeling lies in its fusion with emerging technologies such as artificial intelligence and extended reality, making it an indispensable tool across scientific, industrial, and cultural domains (Huang, You-Min et al., 2005; Alghazzawi, 2016; Pokojski, Szustakiewicz et al., 2022; Shah, Khan et al., 2023).

1.6.2 Understanding 3D modeling and the use of SolidWorks

3D modeling is the process of creating a mathematical representation of a three-dimensional object (Chowdhury, Bhunia et al., 2023). Among many modeling approaches, parametric modeling is the primary approaches used in CAD. A 3D model represents the physical form of an object by defining its points, edges, faces and internal structure. Among various modeling techniques, solid modeling is one of the most widely used in product development (Requicha and Voelcker, 1983; Raghothama and Shapiro, 1998). It involves creating models by sketching 2D profiles and then using operations such as extrusion, feature addition, and feature removal to form 3D objects.

The integration of advanced design software has shortened development cycles, improved precision and enhanced collaboration across disciplines. One key enabler of this transformation is SolidWorks, a powerful computer–aided design (CAD) tool that has become essential for professionals and students alike across multiple areas. SolidWorks has become a game-changer across many industries by making it easier to bring ideas to life (Aboshweita, Masood et al., 2024). Whether it's designing complex mechanical parts in manufacturing, planning and visualising structures in construction, or creating precise models for medical devices like prosthetics and diagnostic tools, SolidWorks helps turn concepts into working models with accuracy (Bauer, Pobiel et al., 2023). With a multi-set of tools, it still stands as user-friendly, supports beginners. SolidWorks enables real-time simulations directly with the same platform used for modeling, eliminating the need to switch between separate software packages (Pant, Shukla et al., 2021; Rounak Mahakul, Dhirendra Nath Thatoi et al., 2021). Alongside the capabilities of advanced CAD tools like SolidWorks, technical guidance was sought through collaboration with Fab Lab, IMT Nord Europe, Douai. SolidWorks flow

simulation is a computational fluid dynamics (CFD) integrated within SolidWorks itself. It allows users to simulate real-world fluid flow and thermal behavior directly on their CAD models (Hunde, 2022), helping the model meet performance standards before physical prototypes are fabricated.

1.6.3 3D printing

Since the 1980s, 3D printing technology has undergone revolutionary development, finding applications in various fields and industries, ranging from small-scale to large-scale (Fujita, 2020). 3D printing, popularly known as additive manufacturing, building 3D objects layer by layer from the base upward by adding material (Ilbey Karakurt and Liwei Lin, 2020). 3D printing has advanced to the point where oral tablets can be fabricated directly from digital designs. This capability supports personalised therapy by tailoring dose and size and by integrating multiple drugs into a single polypill. As a result, 3D printing is emerging as a powerful tool that accelerates development and improves treatment precision (Kuldeep Rajpoot, Muktika Tekade et al., 2020). The development of 3D printing technology began with Stereolithography (SLA) by Charles Hull in 1986 (Bogue, 2013). Multiple embodiments of 3D printing are available; the commonly used additive manufacturing is FDM and SLA (Rami H. Awad and Sami A. Habash, 2018).

Types of 3D printing Technologies:

1.6.3.1 *Fused Deposition Modeling (FDM)*

Industrial use began with the emergence of Fused Deposition Modeling (FDM) in the 2000s, the Explosion of 3D printing in medical, automotive, aerospace, bioprinting development and multi-material printing in the 2010s (Berman, 2012) (Ngo, Kashani et al., 2018) (Sun Chunhua, 2020). FDM uses melted filaments to create objects layer by layer. This technique does not

require post-curing, but the removal of supports after fabrication can be challenging due to the hardened material. Though FDM is commonly employed for rapid prototyping, its suitability for biomedical applications remains uncertain, as the materials used may not always meet the necessary biocompatibility and performance requirements.

1.6.3.2 *DLP (Digital Light Processing)*

3D printing uses a digital projector as a source to cure the resin layer by layer, and it's widely used for high-detail models and functional prototypes. As a projector, it uses a digital micromirror device (DMD) that consists of thousands of tiny mirrors to project an entire image of one layer onto the resin surface using light from the UV projector. This light selectively solidifies the resin where the image I projected, forming the layer all at once. However, the print size is limited by the pixel resolution and field of view, and it is typically suitable for small to medium parts, not large-scale objects (Ge, Jiang et al., 2022; Yi, Yang et al., 2025).

1.6.3.3 *Masked Stereolithography (MSLA)*

MSLA has proven highly valuable in biomedical prototyping, offering higher throughput and the ability to produce intricate prints with fine detail, making it well-suited for creating complex biomedical models and small-scale devices (Ahmed, Sullivan et al., 2022; Stefan Junk, 2023). Despite these advantages, MSLA also presents notable drawbacks: the printed parts are often brittle, the built area is relatively small, and the LCD screens degrade quickly under prolonged UV exposure. Furthermore, the XY resolution is limited by the pixel size of the LCD, which may result in stair-stepping curves, while maintaining even light distribution is critical to avoid layer inconsistencies.

1.6.3.4 *Stereolithography (SLA)*

In contrast, SLA uses a precise laser spot that can trace smooth curves, achieving higher accuracy and better surface finish since it is one of the earliest and most established resin-based 3D printing technologies (Hideo, 1981). SLA supports a wide range of applications in biomedical research, product development and industrial design, where stable and durable models are prominent (Ngo, Kashani et al., 2018; Zhang, Zhu et al., 2021; Tasnim Tuli, Khatun et al., 2024). Due to the remarkable growth and advancements in 3D printing, we are keen to incorporate our innovations into this technology.

1.7 Collaboration with other labs

For innovation, we plan to collaborate with IMT Nord Europe, which is a leading French grande école d'ingénieurs that specialises in engineering, digital systems, energy & environment, and materials & processes. It's part of the institute Mines-Télécom (IMT) network, one of the largest groups of engineering and technology schools in France. We engaged with an experienced engineer from Fab Lab, which supports both student-based projects and community-oriented projects focused on 3D modeling and additive manufacturing.

To advance prototype development, we plan to collaborate with a Research Engineer from Centrale Lille, one of France's leading grandes écoles, renowned for its high-level scientific and technical education. The engineer brings extensive experience in various 3D printing technologies and has managed multiple research and industrial projects involving design optimization, additive manufacturing, and rapid prototyping.

This collaboration is expected to strengthen our technical capabilities, enhance design precision, and accelerate the transition from conceptual modeling to functional prototypes through the integration of advanced fabrication techniques.

1.8 Routine quality assessment in U1190

As part of a routine procedure for several years, systematically, 2% of the islet preparations after the isolation are used to perform quality checks, mainly focused on assessing purity, viability, islet yield post culture, and perifusion. Before grafting, a mandatory overnight cell culture is performed to detect potential contamination. Testing also allows performing other quality checks, QIVIPA (*in-vivo* model) (Caiazzo, Gmyr et al., 2008). The main parameter is that the consideration of islet yield should be greater than 200,000 islet equivalents, even when the donor is normoglycemic or prediabetic (Vantyghem, Kerr-Conte et al., 2009), with a viability of around 80%.

1.9 Cellular respiration as a key study for islet functionality

In recent years, numerous laboratories have focused on expanding the range of parameters used in evaluating islet functionality, aiming for a more comprehensive understanding of islet health and viability (Sweet, Gilbert et al., 2005). Among these parameters, cellular respiration has emerged as a critical indicator, providing direct insight into the metabolic activity and energy production capacity of the islets (Papas, Colton et al., 2007; Kelly, Smith et al., 2019). Respiration is essential for cellular survival, as it reflects the cell's ability to utilise oxygen to generate ATP, the primary energy currency required for maintaining normal physiological function (Goto, Holgersson et al., 2006). In the context of pancreatic beta cells, efficient respiration is not only vital for sustaining cellular integrity but also for supporting insulin secretion, which is tightly coupled to metabolic activity (Kitzmann, O'Gorman et al., 2014; Papas, Bellin et al., 2015). An increase in oxygen consumption (OCR) in response to glucose stimulation has emerged as a meaningful indicator of islet metabolic health; the dynamic metabolic shift offers a more functionally relevant measure of islet quality (Sweet, Gilbert et

al., 2008). In line with this, reports exploring the role of islet oxygen consumption rates in diabetes reversal are steadily increasing, reflecting growing interest in metabolic markers (Sweet, Khalil et al., 2002; Papas, Colton et al., 2007; Papas, Suszynski et al., 2009; Shang, Suzuki et al., 2025). Thus, investigating how beta cells respire under various conditions is central to understanding their functional competence.

1.10 Beta cell respiration mechanism:

In human pancreatic beta cells, glucose enters via facilitated diffusion through glucose transporters. Once inside the cell, glucose undergoes glycolysis in the cytosol, where it is broken down into pyruvate, generating small amounts of ATP and NADH. Glycolysis is, most common metabolic pathway that all cells use. Pyruvate is then transported into the mitochondria and converted into acetyl-CoA, which enters the tricarboxylic acid (TCA) cycle. Pyruvate is reduced to lactate where cells that lack mitochondria (anaerobic conditions).

The TCA cycle produces NADH, FADH2, CO2, and a small amount of ATP. In the inner mitochondrial membrane, NADH and FADH2 donate electrons to the electron transport chain (ETC). This drives the pumping of protons into the intermembrane space, creating a proton gradient. The return flow of protons through ATP synthase enables the production of a large amount of ATP. The resulting increase in the ATP-ADP ratio causes the closure of ATP-sensitive potassium (K^+-ATP) channels on the plasma membrane (Figure 7). This leads to membrane depolarisation, opening of voltage-dependent calcium channels, calcium influx and ultimately, insulin secretion. (Fernie, Carrari et al., 2004; Dashty, 2013). Dysfunction at any step of the cellular respiration pathway – from glycolysis to oxidative phosphorylation – can lead to metabolic impairments that may contribute to the development of pathological conditions,

including diabetes, cancer and various genetic disorders (Jucker, 2010; Ruggeri, Camp et al., 2014; Schmidt, Fisher-Wellman et al., 2021).

1.11 Techniques currently used to assess islet quality

To explore how these islets, breathe and produce energy, researchers have turned to a variety of experimental tools. Early approaches relied on traditional devices, such as Clark-type oxygen electrodes and classical respirometers, which measure the amount of oxygen cells consume (Li and Graham, 2012; Silva and Oliveira, 2018). In recent years, phosphorescence-based techniques using oxygen-sensitive dyes have enabled real-time monitoring and non-invasive tracking of oxygen levels within small chambers, providing insight into cellular respiration (Sweet and Gilbert, 2006; Rivera, Pozdin et al., 2019; Wang, Chen et al., 2021; Witthauer, Roussakis et al., 2023). At the cutting edge, platforms like Seahorse XY analyser have transformed the approach by integrating many assays to study mitochondrial activity. This system can measure multiple aspects of respiration simultaneously: basal respiration, ATP production, proton leak, and spare respiratory capacity by selected drugs (oligomycin, FCCP, Antimycin &Rotenone) to see how they respond under pressure (Papas, Colton et al., 2007; Wikstrom, Sereda et al., 2012; Plitzko and Loesgen, 2018; Rocha, Manucci et al., 2024). Many cell lines, such as INS-1 and MIN6, have been widely used to study metabolic function, particularly mitochondrial respiration, using the above-mentioned techniques. While all assess oxygen consumption, they differ significantly in protocols, sensitivity and biological context (Koshkin, et al., 2008; Li and Graham, 2012). However, it is challenging to find mitochondrial respiration data derived from a perifusion-based system with the same protocol in public datasets. Perifusion is more commonly used for studying islet physiology or insulin secretion by glucose stimulation rather than for direct measurement of mitochondrial

respiration. The context of glucose stimulation-based respiration through dynamic perifusion on specific beta cell lines is limited, scattered, and often not directly comparable to Seahorse data. For seahorse analysis, plates must undergo overnight preparation and calibration to ensure assay readiness. However, the system is not intended for direct measurement of insulin secretion in response to glucose. Given these growing limitations, can perifusion systems be evolved into platforms that not only assess dynamic hormone release but also capture key metabolic indicators such as oxygen consumption, thereby bridging the gap in functional islet assessment?

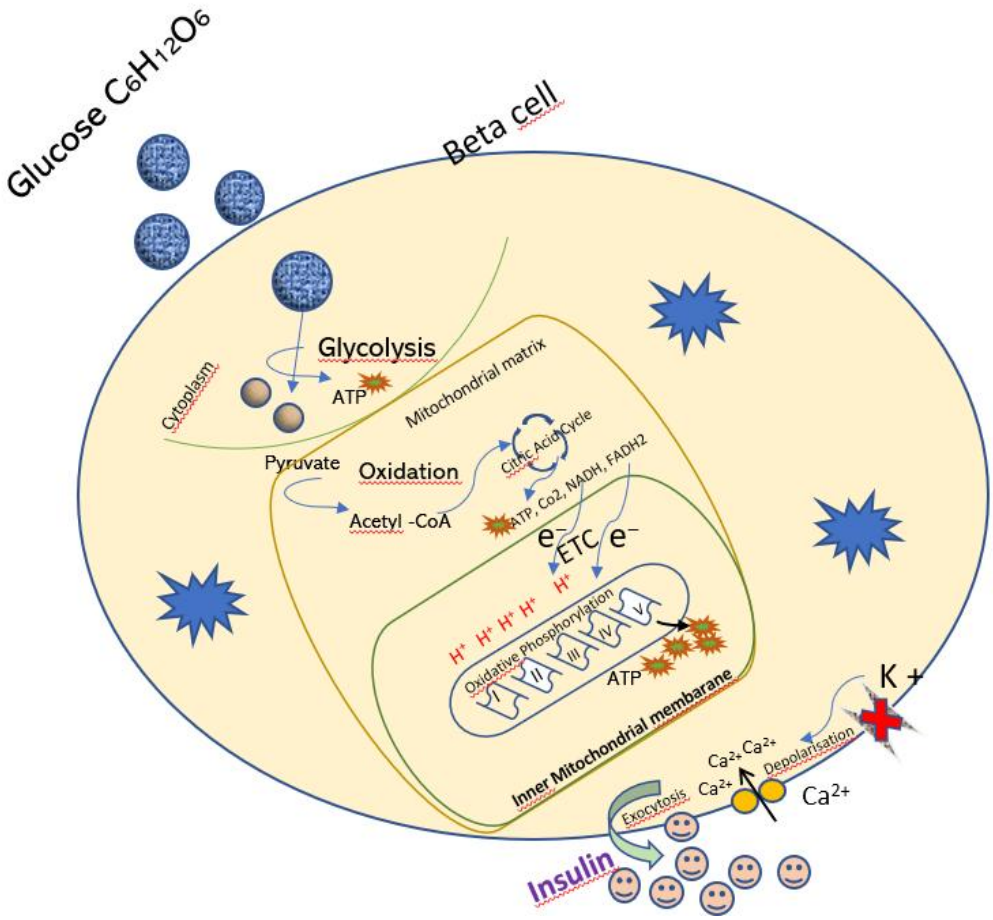

Figure 7: Mitochondrial ATP production through glycolysis, TCA cycle, ETC in pancreatic beta cells

Glut1&3 serves as a high-capacity glucose transporter in pancreatic β-cells, facilitating rapid glucose uptake. In the cytoplasm, glucose undergoes glycolysis, where one molecule is converted into two molecules of pyruvate. Pyruvate is then transported into the mitochondria and converted into acetyl-CoA, which enters the tricarboxylic acid (TCA) cycle. Within this cycle, substrates are oxidized and electrons are transferred to the coenzymes NAD^+ and FAD, reducing them to NADH and $FADH_2$. These reduced coenzymes subsequently donate electrons to the respiratory chain in the inner mitochondrial membrane, ultimately transferring them to molecular oxygen. The reoxidation of these coenzymes drives the proton gradient required for ATP synthesis through oxidative phosphorylation. Both the TCA cycle and oxidative phosphorylation occur in all cells that contain mitochondria, providing the primary source of cellular energy. Figure adapted from (Merrins, Corkey et al., 2022; Garcia, Gupta et al., 2023).

To address these limitations and also find the answers to the raised questions, this thesis aims to:

Chapter 3

Aim: To investigate how donor physiological variables – including age, HbA1c, body mass index (BMI), Body surface area (BSA), and sex -influence *in vitro* insulin secretion dynamics using perifusion assays in a large donor cohort. This study also aims to investigate the correlation of clinical data with *in-vitro* parameters to understand physiologically relevant assessment of beta cell function.

Chapters 4 & 5

Aim: The objective of this project is to design and develop a multi-perifusion chamber through computer-aided design (CAD) modeling and to fabricate a functional prototype using an appropriate 3D printing technology. The system will be assembled into a 4-stream perifusion setup capable of controlled, parallel flow operations. Additionally, the study includes the design and modeling of a fraction collector case – also created using CAD and additive manufacturing – to accommodate a 4-stream fraction collection system, thereby completing the integrated perifusion setup.

Chapter 6

Aim: To enhance the functional performance of the perifusion system by integrating a real-time sensing module capable of monitoring glucose-stimulated islet respiration. The system will be designed to enable precise, continuous measurement of key bioenergetic parameters such as oxygen consumption. By incorporating advanced sensor technology and optimized data acquisition, the developed set up aims to provide a robust, automated platform for

dynamic analysis of islet metabolism, improving reproducibility, and efficiency of perifusion-based studies.

To achieve these objectives, a retrospective analysis was conducted using a large cohort comprising 168 human donors to evaluate *in-vitro* insulin secretion under different experimental settings. This included a comparison between classical static incubation assays and dynamic perifusion-based assessments, allowing investigation of donor-specific heterogeneity in insulin secretion.

In parallel, a collaborative effort was established with IMT Nord Europe and TechSanté to design and fabricate a functional prototype.

Furthermore, to explore the bioenergetic behavior of human islets, two different oxygen sensing technologies were implemented without altering the standardized protocol to establish glucose-stimulated respiratory analysis.

CHAPTER 2

Materials and Methods

2 Chapter II: Materials and Methods

2.1 Biological part

2.1.1 Human islet donor information

Pancreata were procured from adult, brain-deceased donors through our clinical islet transplantation program (French “Agence de la BioMedecine”: PFS16-008). The study was conducted in accordance with French Regulations and approved by the Institutional Ethical Committee of the University of Lille and the Centre Hospitalier Universitaire (CHU) in Lille, France. Next of kin provided informed consent for scientific research following consultation with the French National Registry of Organ Refusal. The clinical characteristics of each donor are summarized in **Table 1**.

2.1.2 Primary islet culture

Human islets were isolated by the isolation team of the Translational Research for Diabetes laboratory UMR 1190 as described (Kerr-Conte J, 2010). Human pancreatic tissues were harvested from brain-dead donors in accordance with the traceability requirements (ClinicalTrials.gov, NCT01123187, NCT00446264, and NCT01148680). Islets were cultured in CMRL 1066 (Thermo Scientific, France) enriched with 0.625% human serum albumin along with penicillin (100IU/ml), streptomycin (100µg/ml), and insulin (0.18mg/l) (Kerr-Conte, Vandewalle et al., 2010) as supplements.

2.1.3 Evaluations of cell preparations

2.1.3.1 *Islet count*

Post cell culture, the quantification of islets was performed using Ricordi’s manual method with the aid of a microscope, which involved evaluating the size of the islets by dividing them

into classes since their sizes vary from 50µm to >500µm. One islet equivalent was approximately 150 micrometres in size, corresponding to a volume of 1.77nl (Ricordi, Tzakis et al., 1991).

2.1.3.2 *Viability*

The state of persistence is assessed using the staining method by Trypan Blue, which involves membrane penetration, which determines the ability to maintain metabolic activity and integrity of isolated pancreatic cells in islets. To provide a comprehensive assessment, the dithizone and trypan blue were used together to have a complete picture of viability (Avelar-Freitas, Almeida et al., 2014).

2.1.3.3 *Purity*

Achieving cell purity Is essential to ensure accurate and reliable results in experiments, which refers to the degree of the cell population of the desired cell type. The samples were taken in small Petri dishes with a few dithizone drops to assess the islet cell structures. This dye selectively stains insulin-producing beta cells within pancreatic islets. Dithizone binds to zinc ions, which are abundant in the insulin granules of beta cells, giving them a characteristic red colour. This helps to identify beta cells within the islets.

2.1.3.4 *Static incubation technique*

For static GSIS assessment, 40 IEQs were placed on cell culture inserts (3 µm pore size, PITP01250, Merck Millipore, Cork, Ireland). Each donor sample (from 2009-2017) underwent sextuplicate testing, utilizing 240 IEQ in parallel, islets were equilibrated for 50 minutes in KREBS buffer (124 mM NaCl, 4.8 mM KCl, 2.5 mM $CaCl_2$-H_2O, 1.2 mM $MgCl_2$-$6H_2O$, 25 mM NaHCO3, pH 7.3) containing 3mM glucose and 0.1% bovine serum albumin at 37°C. Glucose

stimulation was performed by transferring inserts to KREBS buffer containing 15mM glucose for 30 minutes. Following the collection of supernatants, islets were resuspended in acid-ethanol solution (1.5% HCl, 70% EtOH, 28.5% H_20), sonicated, diluted 1/400, and stored with supernatants at -20°C pending insulin measurement as described (Vandewalle, Douillard et al., 1999; Kerr-Conte, Vandewalle et al., 2010).

2.1.3.5 *Dynamic in vitro*

Dynamic perifusion studies utilized 300 IEQ per reaction chamber, with continuous flow maintained at 1 ml/min and fractions collected every 2 minutes, as described (Henquin, Dufrane et al., 2006). The protocol employed KREBS buffer supplemented with 1mg/ml Bovine Serum Albumin and consisted of three phases: 60-minute equilibration in 3mM glucose without sampling, followed by sequential collection at 3mM glucose (10 minutes, 0.54 g/L), 15mM glucose (40 minutes, 2.72 g/L), and return to 3mM glucose (20 minutes). Perifusion parameters, including flow rate (1 ml/min), temperature (37°C), and oxygenation (95% O_2 / 5% CO_2), were rigorously standardized across all experiments using automated, calibrated perifusion systems. Throughout the procedure, flow rate, pressure, temperature, and oxygen concentration remained constant. Each run included internal controls, and islet batches were randomly assigned across experimental days to minimize batch effects. Additionally, all experiments were conducted using identical buffer compositions and glucose ramping protocols, ensuring consistency in stimulus delivery and measurement conditions. Post-experiment, islets were processed in acid-ethanol, sonicated, serially diluted (1/2114, 1/3844, and 1/5761), and stored with outflow fractions at -20°C.

2.1.3.6 *Absolute and Insulin Content Measurement (IIC)*

Secreted and intracellular insulin was assessed using the automatic Unicell DXi 600 access immune assay System from Beckman Coulter (Beckman Coulter France, Villepinte, France). For the intracellular insulin determination, ethanol-acid-resuspended islets were ultrasonicated to release intracellular insulin into the solution. Secreted insulin was expressed as an absolute value (IU/ml/min) or as the percentage of secretion /time normalised to the intracellular insulin content. For perifusion experiments, the stimulation index (SI) was calculated from the mean of first-phase peak (S1) with or without second-phase plateau (S2) at 15 mM glucose, relative to baseline (B) secretion at 3 mM glucose. Static incubation SI was determined as the ratio of combined first and second phase secretion (S1 + S2) at 15 mM glucose to baseline (B) secretion at 3 mM glucose.

2.1.4 Cell culture – Ins-1 immortalized cell lines

Rat insulinoma cells clone 32 were cultured at 5% CO_2 at 37°c in RPMI 1640 11mM glucose (Gibco, cat No. 21875-034, UK) supplemented with 10% FBS (Eurobio, cat No CCVSVF06-oU, France), 100 U/ml P/S (Gibco, cat No 15140122, USA), 10 mM HEPES (Gibco, cat No 15630-080, USA), 1mM sodium pyruvate (Gibco, cat NO 11360-039, UK) and 50µM β-mercaptoethanol (Gibco, cat No 21985-023, USA).

2.1.5 Statistical analysis

Data analysis was performed using Prism 10.4.1 (GraphPad Software, La Jolla, USA), with results expressed as means ± SD or SEM. Statistical evaluation included Pearson correlation coefficients and linear regression analysis (beta coefficients and regression equations). Group comparisons were conducted using Kruskal-Wallis tests, with significance set at $p < 0.05$. Body

$$BSA\ (m^2) = \sqrt{\frac{Ht\ (cm) \times Wt\ (kg)}{3600}}$$

Surface Area (BSA) calculations employed Mosteller's formula (Mosteller, 1987), incorporating height (cm) and weight (kg).

2.1.6 Cluster analysis

Data stratification by cluster analysis performed by a biostatistician using R software with an unsupervised k-means algorithm; the number of clusters was chosen based on the silhouette method. The cluster stability was tested with Jaccard indices.

2.2 Engineering Part – 3D modeling

2.2.1 A CAD Tool 3D Model Design

Three-dimensional models were developed using SolidWorks CAD software (Dassault systems, version 2024). The software was employed to define geometrical constraints and perform preliminary fit and tolerance checks before fabrication.

2.2.2 Code conversion for 3D printing

The 3D parts were exported from SolidWorks in STL (Standard Triangle Language) (meshing) format and imported into the respective slicing software (Z-suite for FDM printing and Preform for SLA printing). The slicing software converted the STL models into machine-specific toolpaths, generating Z-code for FDM and G-code for SLA, which were subsequently used to guide the 3D printing process. For MSLA, the STL to G-code conversion method was used for 3D fabrication.

2.2.3 Flow simulation analysis

Flow analysis was carried out using the integrated SolidWorks flow simulation module. The computational domain was defined and discretised into an appropriate mesh, with boundary conditions specified for inlet and outlet parameters. The simulation was iterated until convergence, and flow behaviour was visualised through generated flow trajectories.

2.2.4 Pre-processing tool

Pre-processing of the finite element model was conducted in Hypermesh, and simulations were carried out in Optistruct with the assistance of an external collaborator to evaluate pressure, stress, and displacement responses.

2.2.5 3D modeling - 4-way fraction collector

For the 3D modeling of the fraction collector, we used SolidWorks, software that had already been used for modeling 4-chamber perifusion. The collector case sketches were modeled by using SolidWorks and handed over to IMT fab lab for further development. Further assembly for the arm, wooden base support, and provisions for the stepper motor were modeled from the same tool.

2.3 Engineering Part – 3D Printing

2.3.1 3D Printing technologies – 3D fabrication

2.3.1.1 *Fused Deposition Modeling (FDM) – for testing*

Fabrication was performed for initial testing using a Zortrax M200 3D printer (Fab Lab-IMT Douai) based on fused deposition modeling (FDM) technology. The thermoplastic filament Z-ABS was chosen, heated and extruded through a nozzle (diameter 0.4mm), depositing material layer by layer from bottom to top. Support structures were automatically generated

and printed as needed to maintain geometric stability during the build. The tolerance for dimensional accuracy is ± 0.2mm.

2.3.1.2 *MSLA (Masked Stereolithography) – for testing*

An Anycubic Mono X LCD-based 3d printer was used to fabricate the islet chamber with an integrated four-leg support alone without mini water bath.

2.3.1.3 *SLA (Stereolithography) – final fabrication*

The developed CAD model was sliced using Halot box slicing software for the CAD file edited, in Fusion 360°. The functional prototype was then fabricated using a Formlabs 3BL printer (Central Lille), which operates with a 3-litre resin tank capacity. A layer thickness of 50 microns was selected to achieve high-resolution detail. The tolerance used for dimensional accuracy ± 0.05mm.

2.3.1.4 *Post processing*

Supports were removed and washed in isopropyl alcohol (IPA) 90-99% to remove uncured resin with agitation for over 20-30 minutes. Parts were dried and exposed to UV light at a specific wavelength (405nm) at 65°C for 15 to 60 minutes for final strength quality.

2.3.2 3D materials

2.3.2.1 *FDM*

ABS (Acrylonitrile butadiene styrene) and HIPS (High Impact Polystyrene) thermoplastic filaments were used for testing a printing material for fabrication, which has a tensile strength between 26-45 megapascals. The hips have the property of being more flexible and brittle, and ABS is more rigid. The prints were performed using Zortrax M200, with a nozzle temperature of 290°C.

2.3.2.2 *SLA – Grey pro Resin*

Grey pro resin was employed as the printing material, undergoing layer-by-layer photopolymerization to construct the 3D object. This resin was selected for its toughness, tensile strength of 2.6 GPa, and heat resistance, with a thermal expansion range of 0-150°C, thermal conductivity 0.2 $w/m^{-1}/K^{-1}$, making it well-suited for durable applications.

2.4 Assembly part of the 4-stream Perifusion system

2.4.1 Islet chamber lid

The 4 holes were created on each islet chamber lid at equal distances using manual drilling with a 4.5 cm diameter. Small drilling with 1.98mm at the middle of the cap to insert inox and glued later. The rings with a thickness of 2.9mm were used to make it tight when it is closed.

2.4.2 Inox tube cutting

PRESI micro cutting machine was used for the inox tube to shape the inner dimension for both the islet chamber and lid, a butterfly nut was used for the 4 chambers to fix.

2.4.3 Mini water bath cover plate & drill

Aluminium material was cut to precise dimensions of 112 * 112 mm using the Trotec Speedy 400 laser cutting and engraving machine. Inlet and outlet holes were made on the aluminium plate for the water flow of 37°C with a dimension of 6mm.

2.4.4 Tubing

Male-female Luer locks were used for both inlet and outlet – combi stopper red has an inner diameter of 5 mm. The 1 ml/min flow rate was maintained with the silicone tube 1/16*30, which has an outer diameter of 1.6mm.

2.5 Bio sensor integration

2.5.1 PreSens technology – O_2 sensor, CO_2 sensor

A pre-calibrated, single-use disposable chemical optical oxygen sensor (Flow-through cell, FTC-Pst3, equipped with Luer lock connectors) was installed downstream of the chamber to measure the oxygen concentration in the sample. CO_2 sensor (0.3mL volume) is maintained in a saline solution to prevent drying, with a measurement range of 1-25% CO_2 and for O_2 – 45mg/L, the limit of detection for oxygen is 0.03%O_2. The response time achieved for both sensors is < 60s. Measurement Studio 2 software is employed for data analysis and processing.

2.5.2 Pyroscience technology

A Luer-Lock T connector with a removable oxygen probe is included, allowing a standard measurement range of 0 to 250% air saturation. Calibration is performed before the experiment using a two-point method: the lower point in an oxygen-free sample by using an oxygen-free capsule to take 0% oxygen point (Anoxic), and the upper point in either KRB medium or ambient air at experimental temperature. The sensor is positioned as close as possible to the chamber for optimal accuracy, with an inner diameter of 4.8 mm. After each experiment, the sensor is cleaned with ethanol, followed by distilled water. Real-time measurements are facilitated by a PC-controlled analyte meter via the Pyro Workbench software, and data analysis is carried out using the Pyro Data Inspector tool during or after the experiment. The curve resolution was obtained with an average number of values of 6 per minute.

CHAPTER 3

Importance of Glucose-Stimulated Insulin Secretion (GSIS): Uncovering islet dynamics by the perifusion technique

3 Results: Chapter III Importance of Glucose-Stimulated Insulin Secretion (GSIS): Uncovering islet dynamics by the perifusion technique

3.1 Introduction

Glucose-stimulated insulin secretion (GSIS) testing of isolated islets of Langerhans is crucial for assessing β-cell function, yet protocol variability complicates result interpretation. This study investigated insulin secretion heterogeneity across 576 donors and examined the influence of donor characteristics on secretory responses. We compared static incubation (*n* = 408) and dynamic perifusion (*n* = 168) techniques using standardized glucose stimulation protocols (3 mM versus 15 mM). While both methods showed comparable stimulation indices (r^2 = 0.652), dynamic perifusion uniquely captured temporal secretion patterns and revealed greater dynamic range in insulin responses. Notably, dynamic perifusion, with insulin content normalization, revealed a 22-fold variation in stimulation index across donors. BMI and HbA1c significantly influenced basal insulin secretion, particularly in donors with glucose intolerance and type 2 diabetes (T2D) (HbA1c ≥ 6.5%). Cluster analysis identified two distinct groups based on age, BMI/BSA, and HbA1c, which strongly predicted insulin secretion patterns, whereas donor sex had no measurable impact.

This large-scale study demonstrates the superiority of standardized perifusion over static incubation for resolving islet glucose responses. By capturing dynamic secretion profiles, perifusion reveals substantial donor heterogeneity, primarily driven by BMI and HbA1c through their effects on basal insulin secretion.

3.1.1 Dynamic characterization of insulin secretion

The perifusion system enabled real-time observation of insulin secretion kinetics from isolated human islets. When stimulated with glucose, islets (300 IEQ) demonstrated a characteristic biphasic response **(Figure 8A)**. At baseline (3 mM glucose), islets maintained stable basal secretion (B phase). Upon exposure to 15 mM glucose, insulin secretion exhibited two distinct phases: an initial rapid and intense peak (S1), followed by a sustained but lower plateau (S2). Return to 3mM glucose resulted in a gradual descent to baseline levels over 20 minutes. This secretion pattern remained consistent whether expressed in absolute terms (mIU/ml/min, Figure 8A) or as a percentage of total insulin content **(Figure 8B)**.

3.1.2 System reproducibility and method comparison

To validate system reliability, parallel perifusion chambers were tested using the same islet preparations and conditions. While absolute insulin measurements (μIU/ml/min) showed approximately 1.6-fold variation between chambers (**Figure 9A**), normalization to intracellular insulin content eliminated this sampling variation, yielding superimposable secretion profiles (**Figure 9B**). Comparative analysis of static versus dynamic glucose stimulation was performed using matched islet preparations from 10 donors. Perifusion demonstrated greater dynamic range in Stimulation Indices (SI) (SI: 1.8-13.4) compared to static incubation (SI: 0.9-2.6) while maintaining a significant positive correlation (r^2 = 0.652, p = 0.005) between methods (**Figure 10A**), same if both phases taken also gives the huge variation in stimulation index (r^2 = 0.683, p = 0.0034) (**Figure 10B**).

Large cohort study: stimulation indices & qualitative analysis

This enhanced sensitivity of perifusion was further confirmed across the first-time full dataset by non-islet selection, with significantly higher SI in the perifusion group (4.28 ± 3.25, n = 168)

compared to static incubation (1.88 ± 1.26, n = 408) (p < 0.0001, **Figure 11A**). Intracellular insulin content per IEQ showed comparable but statistically different values between static incubation (31.8 ± 21.9 ng) and perifusion (36.4 ± 22.8 ng) groups (P=0.024, **Figure 11B**), suggesting subtle variations in islet sampling or preparation methods between techniques.

3.1.3 Donor heterogeneity: substantial variations

Dynamic glucose stimulation of 168 islet preparations revealed substantial inter-individual variation in insulin secretion kinetics (**Figure 12A**). Mean secretion rates were 0.011% ± 0.009 at low glucose (B phase) and 0.038% ± 0.034 at high glucose (S1 phase), yielding an average stimulation index of 4.25 ± 3.22. While all preparations demonstrated glucose responsiveness (SI > 1), the magnitude varied dramatically. The highest responding preparation showed a SI of 5.70 (B = 0.0412%, S1 = 0.2351%), while the lowest had a SI of 1.28 (B = 0.0021%, S1 = 0.0027%), representing remarkable inter-individual variations: 19.5-fold in basal secretion, 87-fold in stimulated secretion, and 22-fold in stimulation indices. **Figure 12B** shows the minimum and maximum secretion levels noticed in this large cohort, expressed as percentages of content.

3.1.4 Donor characteristics impact on insulin secretion

Correlation analysis of donor variables

Multiple donor characteristics were found to significantly influence islet function, as summarized in **Table 2**. Basal insulin secretion correlated significantly with BMI, HbA1C, and BSA, whereas insulin secretion under high-glucose conditions was primarily associated with BMI. In contrast, the SI correlated with a broader range of factors, including age, HbA1C, ICU duration, and cold ischemia time. Given the strong correlation between BSA and BMI (r^2 = 0.62, p < 0.0001), the specific effects of BSA are detailed in Figure 13. Based on arbitrary and

using Mosteller's formula, BSA was calculated and compared with BMI and a positive correlation was noticed (**Figure 13A**), and the time course analysis showed groups with the BSA >2.1 have higher basal insulin secretion (**Figure 13B**). Basal and stimulated insulin secretion based on arbitrary notice and represented as mean ± SEM (**Figure 13C**).

3.1.5 Impact of glycemic status

Donors were stratified based on HbA1c levels, following the WHO criteria: normoglycemic (<5.7%), pre-diabetic (5.7-6.5%), and diabetic (≥6.5%). Diabetic donors showed significantly elevated basal insulin secretion compared to normoglycemic donors (1.8-fold increase, $p < 0.01$), while pre-diabetic donors displayed intermediate levels (**Figure 14**). Despite these differences in basal secretion, all groups retained robust glucose responsiveness, showing comparable secretion kinetics during both stimulation and return to baseline phases.

3.1.6 Effect of BMI on insulin secretion

Donors were grouped by BMI into normal weight (< 25 kg/m²), overweight (25–30 kg/m²), and obese (≥ 30 kg/m²). Clear differences in insulin secretion patterns emerged across groups (**Figure 15**). Both basal and glucose-stimulated insulin secretion increased progressively with BMI. Normal-weight donors showed significantly lower basal secretion compared to overweight ($p < 0.05$) and obese donors ($p < 0.01$). Under high-glucose conditions, obese donors demonstrated significantly higher insulin secretion compared to normal-weight donors ($p < 0.01$).

3.1.7 Impact of donor physiological variables on insulin responses: clustering analysis

3.1.7.1 *Identification of distinct donor clusters*

A multivariate factorial mapping was conducted, incorporating key physiological variables, including age, BMI, HbA1c, and BSA, to explore underlying donor phenotypes. Despite strong correlations between some variables, such as BMI and BSA, all variables were retained to maximize analytical depth. Data were standardized through centering and reduction to ensure comparability. Clustering via the silhouette method identified two optimal donor groups (**Figure 16A**), with no individuals excluded to ensure representation of clinically relevant extremes such as severe obesity and diabetes.

3.1.8 Cluster Characterization

Distinct metabolic profiles emerged between the two clusters. Cluster 1 (n = 102) comprised donors with normal metabolic variables: mean BMI of 25.1 kg/m^2, normal HbA1c (5.5%), and BSA of 1.9 m^2. In contrast, Cluster 2 (n = 56) reflected a metabolically impaired cohort characterized by obesity (mean BMI: 33.6 kg/m^2), elevated HbA1c (5.8%, pre-diabetic range), and higher BSA (2.3 m^2). Age distribution was comparable between clusters (52.7 vs 48.3 years). Cluster robustness was confirmed through bootstrap techniques, with high Jaccard indices for both Cluster 1 (0.98) and Cluster 2 (0.99), exceeding the accepted stability threshold of 0.75 (**Table 3**).

3.1.8.1 *Impact on insulin secretion dynamics*

Comparison of insulin secretion profiles revealed significant functional differences between clusters. Both basal (3 mM glucose) and glucose-stimulated (15 mM glucose) insulin secretion were significantly higher in Cluster 2 (**Figure 16B**; Wilcoxon test, p = 0.012 and p = 0.014,

respectively). These differences were further illustrated in the full dynamic secretion curves (**Figure 16C**), highlighting altered insulin kinetics in donors with metabolic dysfunction.

3.1.9 Gender analysis

Gender analysis revealed significant differences in the groups with normal BMI and BSA<1.9. These subgroups were further analyzed, while females showed a modest increase in (1.3-fold, p=0.023) glucose levels than males, there was no significant impact on insulin secretion variables during perifusion (low glucose: P=0.13; high glucose: P=0.18). This was further confirmed by Pearson's chi-squared analysis (*P*=0.08), indicating that metabolic variables, rather than gender, were the primary drivers of clustering (**Figure 17**). The sex-based cluster analysis shown in **Table 4.**

3.1.10 Islet function indices and graft performance

We evaluated the relationship between in-vitro islet function and the beta-2 score – a clinical index predicting graft success-measured 1 month after the final islet infusion (each recipient received 2-3 grafts). As reported by Bachul and colleagues (Bachul, Golebiewska et al., 2020), a BETa-2 score >17.4 during follow-up reflects islet function consistent with long-term insulin independence. In our cohort (n=12), lower perifusion basal secretion (<0.02%) tended to associate with higher BETA-2 scores, and an in-vitro stimulation index (SI) >2 likewise showed higher BETA-2 values. Although these patterns were evident, no statistically significant correlation was detected (**Figure 18**).

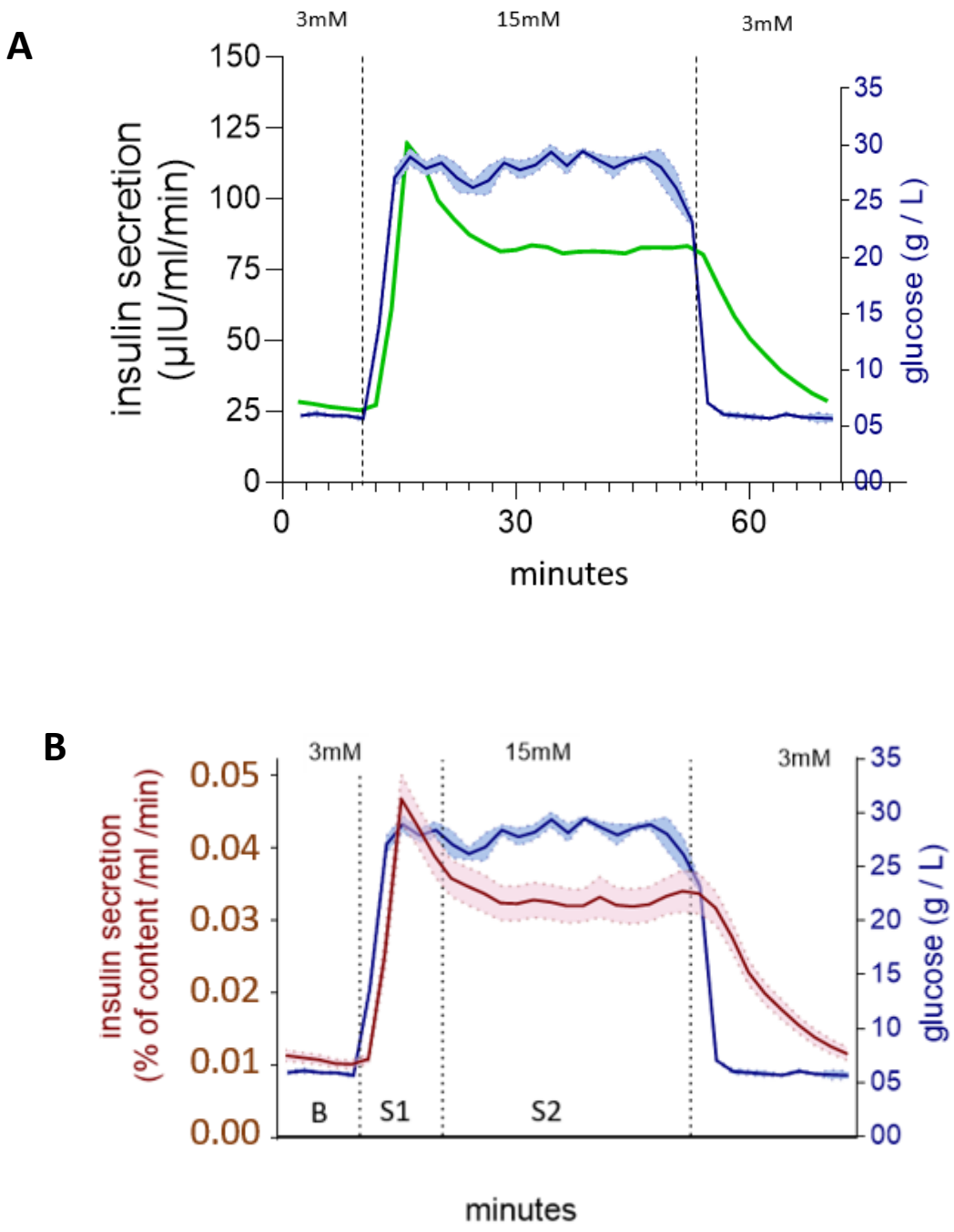

Figure 8: Dynamic glucose-stimulated insulin secretion profiles

Time-course analysis of insulin secretion from perifused islets (*n* = 168), expressed as A) absolute values (µIU/ml/min) and B) percentage of insulin content (%/ml/min). Phases of secretion are indicated: basal (B, 3 mM glucose), first-phase peak (S1), and second-phase plateau (S2) at 15 mM glucose. The blue line indicates glucose concentration. Data in (A-B) are presented as mean ± SEM.

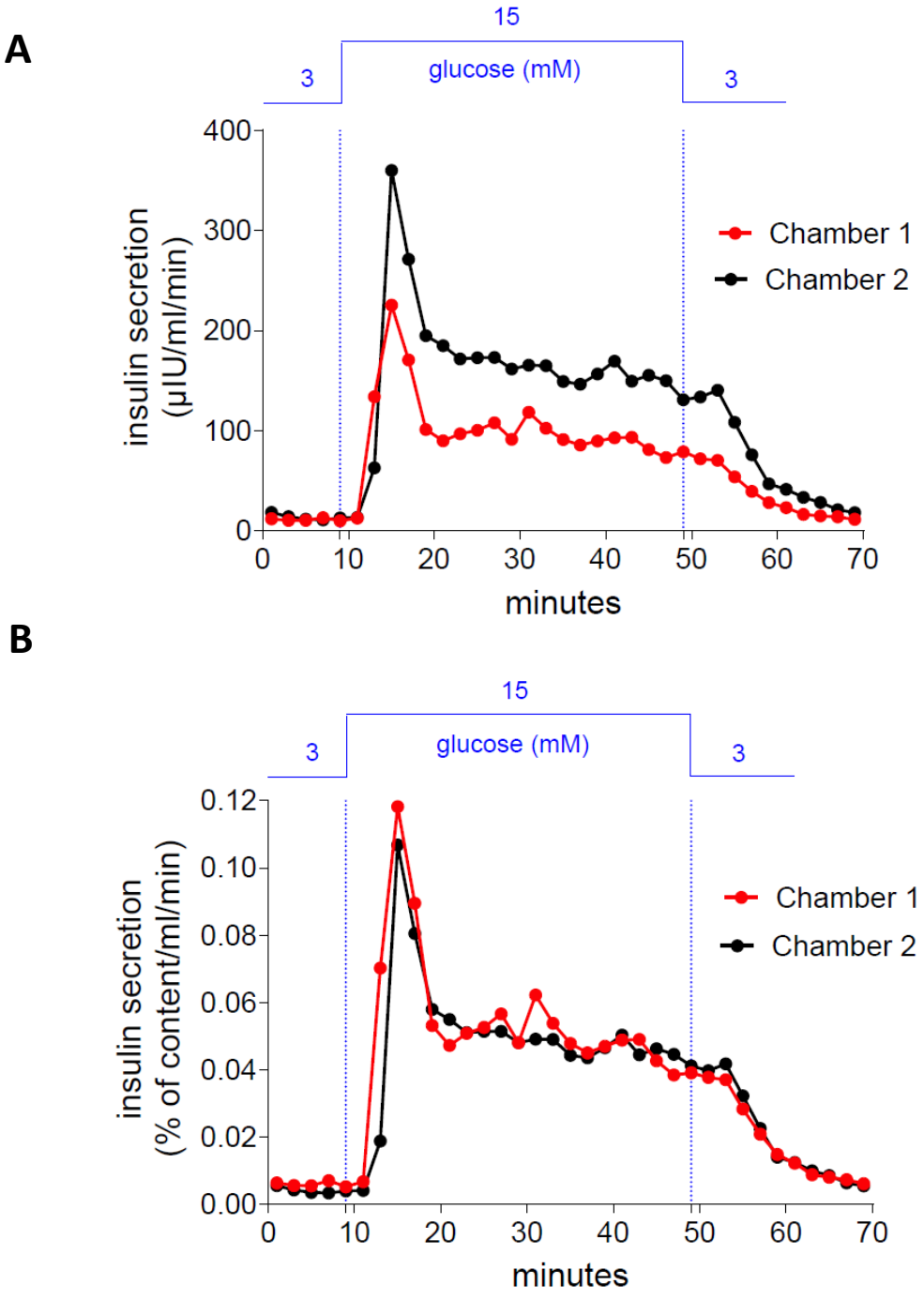

Figure 9: Method of comparison

Assessment of reproducibility using parallel perifusion chambers (300IEQ/chamber), showing insulin secretion expressed as A) absolute values and B) percentage of insulin content.

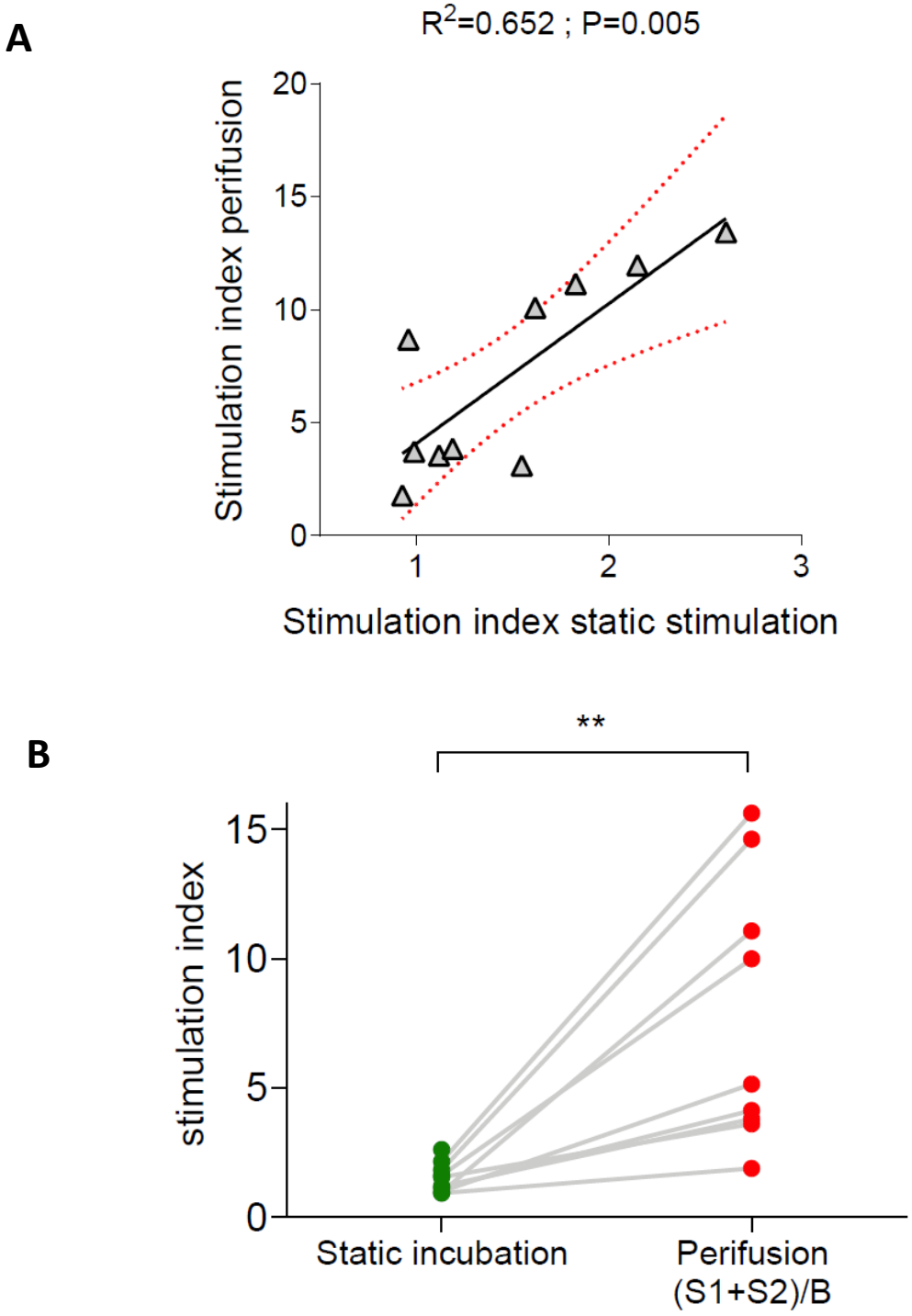

Figure 10: Correlation between static and dynamic

A) Stimulation indices (n = 10, r^2 = 0.652, p = 0.005); red dotted lines indicate 95% confidence intervals. Comparative analysis of static versus dynamic glucose stimulation was performed using matched islet preparations from 10 donors. Perifusion demonstrated a greater dynamic range in Stimulation Indices (SI) (SI: 1.8-13.4) compared to static incubation (SI: 0.9-2.6), while maintaining a significant positive correlation (r^2 = 0.652, p = 0.005) between the methods. B) huge heterogeneity if both phases are considered as the same as static (r^2 = 0.683, p = 0.0034).

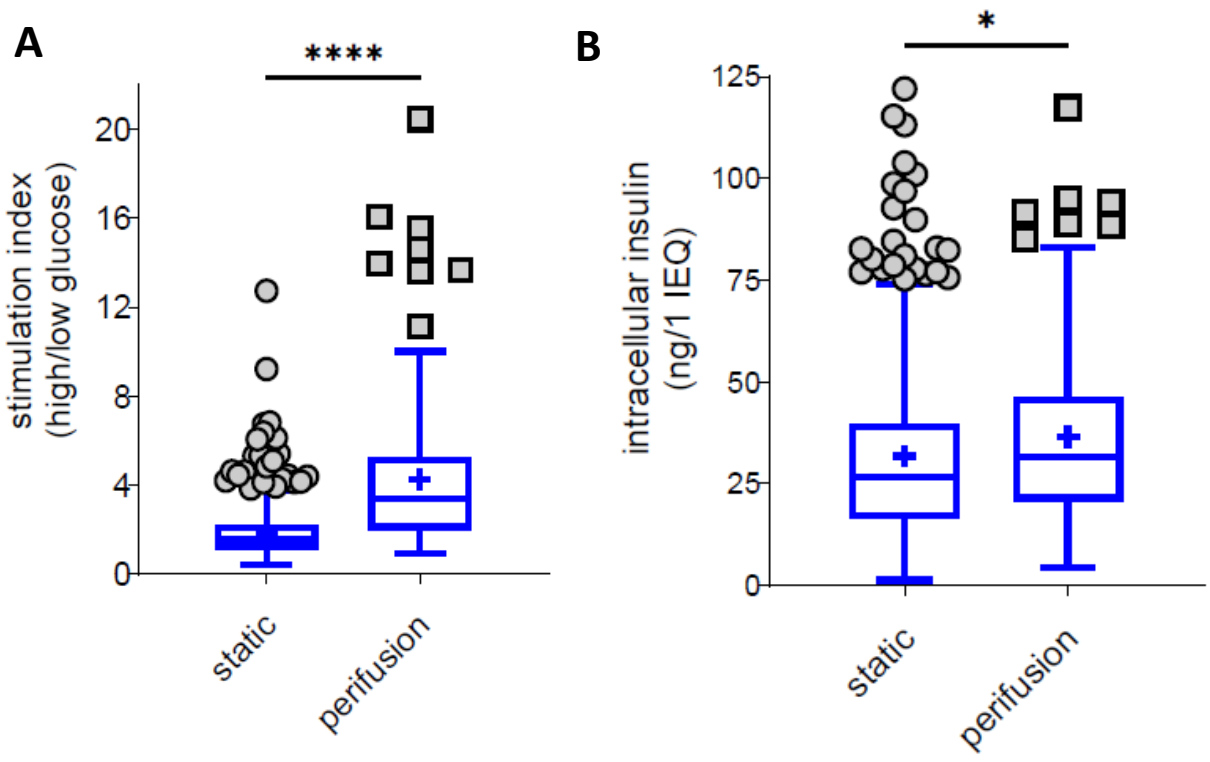

Figure 11: Large-scale study of comprehensive insulin secretion comparisons

A) Comparison of stimulation indices between static & dynamic, B) intracellular insulin content per islet equivalent (IEQ) between static incubation (*n* = 408) and perifusion (*n* = 168) techniques. Static IIC/IEQ is 31.8 ± 21.9 ng, dynamic IIC/IEQ is 36.4 ± 22.8 ng (revealed a closer mean in intracellular insulin content).

A

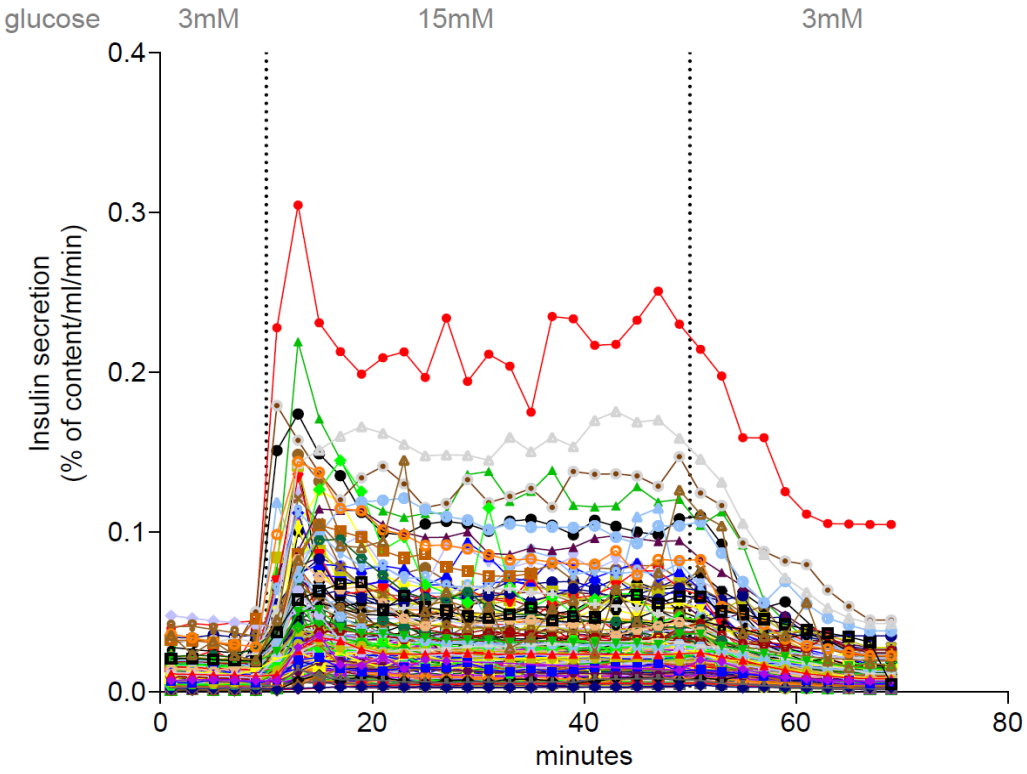

B

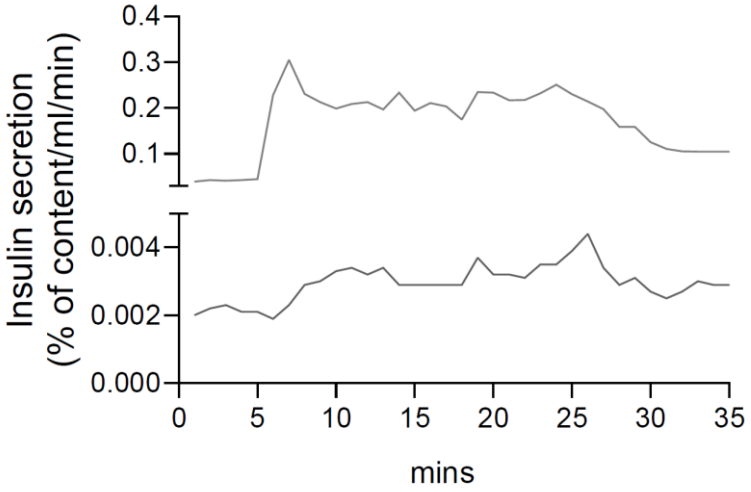

Figure 12: Heterogeneity of beta cells from 168 donors

A) Individual insulin secretion profiles from different categories (Normoglycemic, prediabetic & diabetic), n = 168 islet preparations during glucose stimulation (3 mM to 15 mM), expressed as percentage of insulin content. B) Representative maximum (red) and minimum (black) secretion profiles illustrate the range of response.

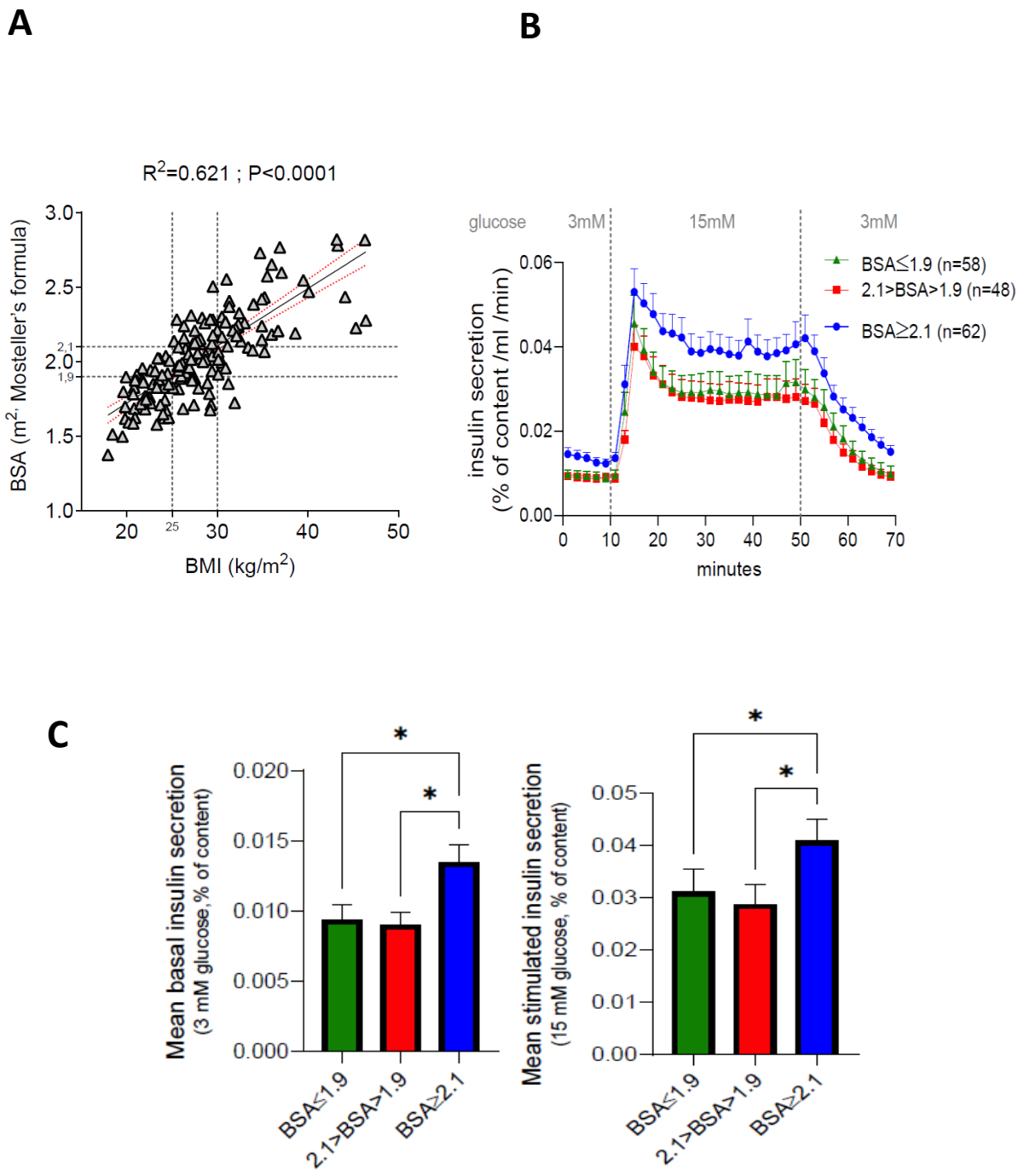

Figure 13: Analysis of Body Surface Area (BSA) influence on islet function

A) Correlation between BMI and BSA (calculated using Mosteller's formula) in the perifusion cohort (n = 168, r2 = 0.621, $p < 0.0001$). Dotted lines indicate BSA stratification thresholds. B) Time-course analysis of glucose-stimulated insulin secretion stratified by BSA: BSA ≤ 1.9 m2 (n = 58, green), 1.9 < BSA < 2.1 m2 (n = 48, red), and BSA ≥ 2.1 m2 (n = 62, blue). Data are presented as mean ± SEM. C) Comparison of mean insulin secretion at basal (3 mM glucose, left) and stimulated (15 mM glucose, right) conditions across BSA groups. Statistical significance was determined by an unpaired nonparametric t-test: *$p < 0.05$.

	Static incubation	Perifusion	Range (static+perif)	P value
N	**408**	**168**		
Sex (M/F) (n)	216 / 192	103 / 65		
Age (years)	48.9 ± 13.2	50.8 ± 13.0	13 - 86	0.111
Weight (kg)	78.2 ± 16.8	84.3 ± 19.9	42 - 150	*0.0002*
Height (cm)	170 ± 10	173 ± 10	140 - 203	*0.007*
BMI (kg/m^2)	26.8 ± 5.4	27.9 ± 5.6	16.6 - 46.9	*0.023*
BSA (m^2)	1.92 ± 0.23	2.03 ± 0.28	1.35 - 2.82	*<0.0001*
HbA1c (%)	5.7 ± 0.5	5.6 ± 0.6	4.2 - 9.3	0.175
ICU (days)	3.0 ± 2.7	2.9 ± 2.5	0.5 - 13	0.541

Table 1: Demographic and Clinical Characteristics of Islet Donors in Static and Dynamic Perifusion Studies

Comparison of donor characteristics between static incubation (n = 408) and perifusion (n = 168) groups. Data are presented as mean ± standard deviation or counts for categorical variables (sex). Range values represent the combined data from both groups. Statistical comparisons between groups were performed using unpaired nonparametric t-tests, with significant differences ($p < 0.05$) indicated in italics. BMI: Body Mass Index; BSA: Body Surface Area; HbA1c: Glycated Hemoglobin; ICU: Intensive Care Unit length of stay.

N=168	R^2	P value	significant
Age vs B	0.005	0.359	NS
—— vs S1	0.003	0.473	NS
vs S1/B	0.023	*0.047*	*
BMI vs B	0.034	*0.015*	*
vs S1	0.029	*0.026*	*
vs S1/B	0.001	0.628	NS
HbA1c vs B	0.042	*0.009*	**
vs S1	<0.001	0.827	NS
vs S1/B	0.040	*0.011*	*
BSA vs B	0.047	*0.005*	**
vs S1	0.018	0.079	NS
vs S1/B	0.002	0.526	NS
UCI vs B	0.001	0.640	NS
vs S1	0.001	0.200	NS
vs S1/B	0.035	*0.015*	*
Cold ischemia vs B	<0.001	0.866	NS
vs S1	0.011	0.179	NS
vs S1/B	0.034	*0.017*	*

Table 2: Correlation analysis of aonor characteristics with insulin secretion variables in dynamic perifusion studies

Linear regression analysis between donor physiological variables and insulin secretion kinetics (*n* = 168). Secretion variables were measured during basal stimulation (B, 3 mM glucose), the first-phase secretion peak (S1, 15 mM glucose), and calculated as the stimulation index (S1/B). R2 represents the coefficient of determination; p-values were determined using the Kruskal-Wallis multiple comparisons test. Statistical significance is indicated as: *$p < 0.05$, **$p < 0.01$, NS: not significant. BMI: Body Mass Index; BSA: Body Surface Area; HbA1c: Glycated Haemoglobin; ICU: Intensive Care Unit length of stay.

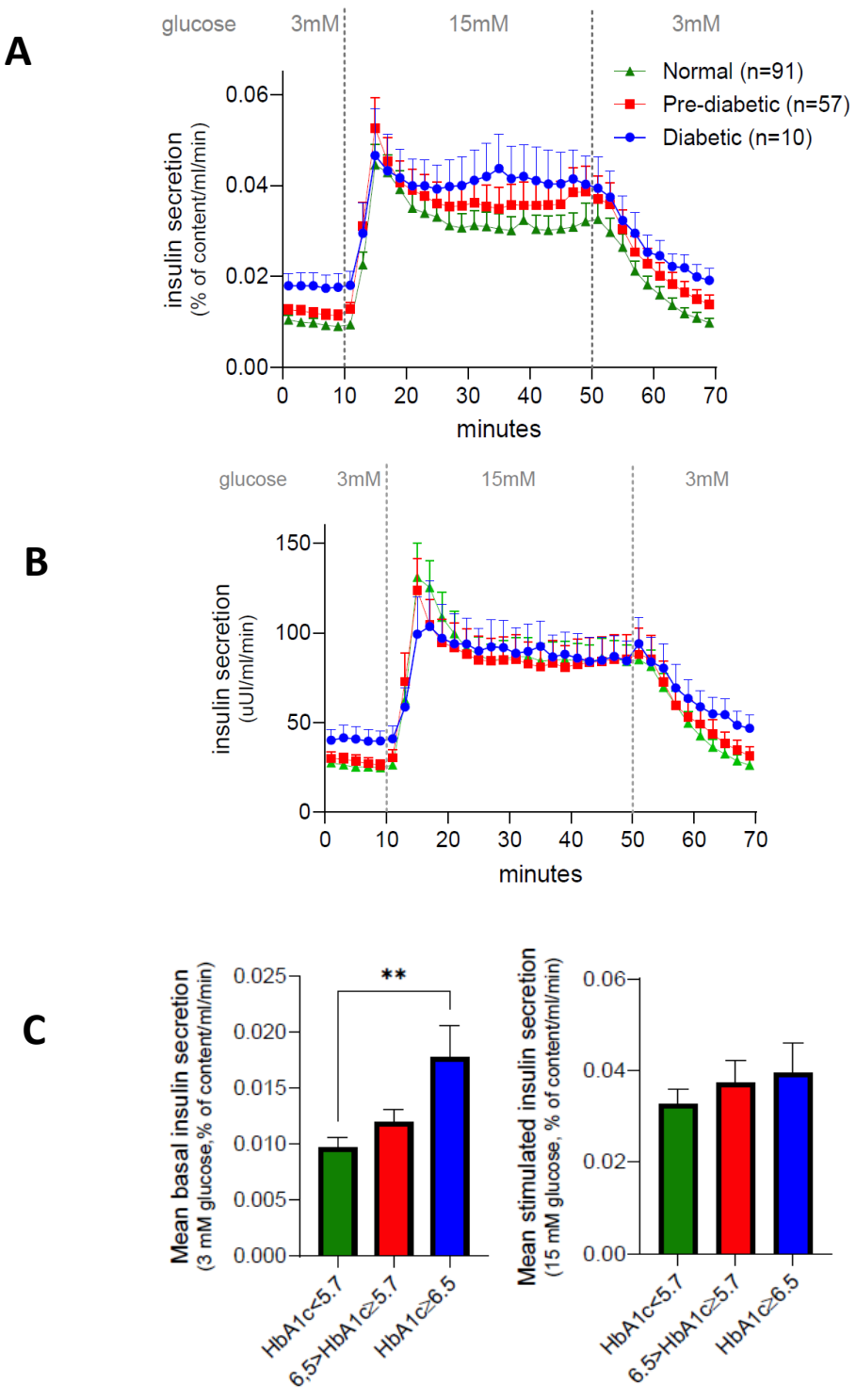

Figure 14: Insulin secretion heterogeneity and its stratification associated with donor HbA1c

A) Insulin secretion kinetics stratified by (normoglycemic: <5.7% n=91, pre-diabetic: 5.7-6.5% n=57, diabetic: ≥ 6.5% n=10); B) same kinetics in absolute value; C) Comparison of mean basal (3 mM glucose, left) and stimulated (15 mM glucose, right) insulin secretion across HbA1c groups. Data are presented as mean ± SEM, & Statistical significance was determined by an unpaired nonparametric t-test: *$p < 0.05$, **$p < 0.01$.

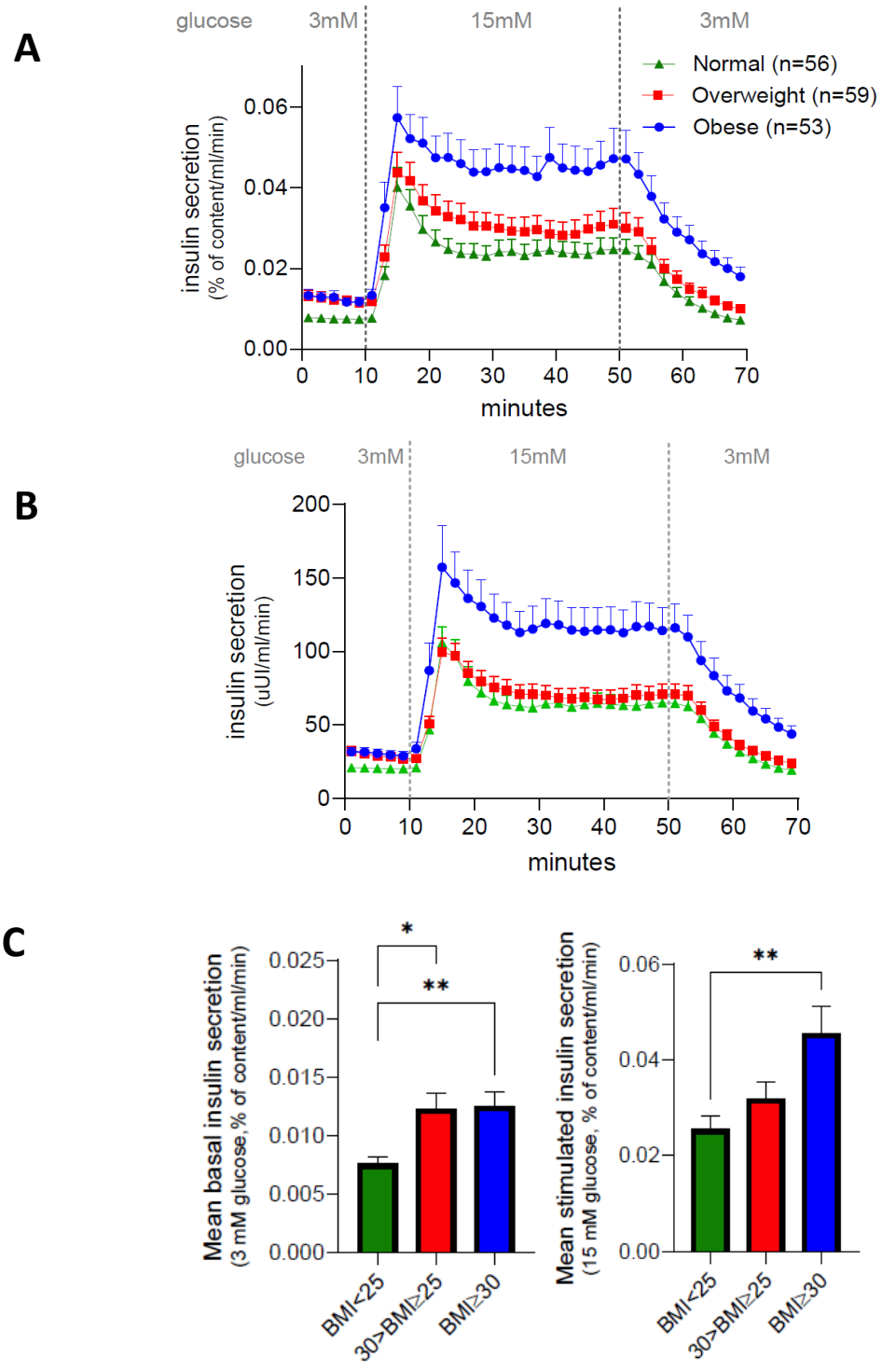

Figure 15: Insulin secretion heterogeneity and its stratification associated with donor BMI

A) BMI stratification (normal: < 25 kg/m^2 n=56, overweight: 25-30 kg/m^2 n=59, obese: ≥ 30 kg/m^2 n=53). B) same kinetics in absolute value. C) Comparison of mean basal (3 mM glucose, left) and stimulated (15 mM glucose, right) insulin secretion across BMI groups. Data are presented as mean ± SEM Statistical significance was determined by an unpaired nonparametric t-test: *$p < 0.05$, **$p < 0.01$.

A

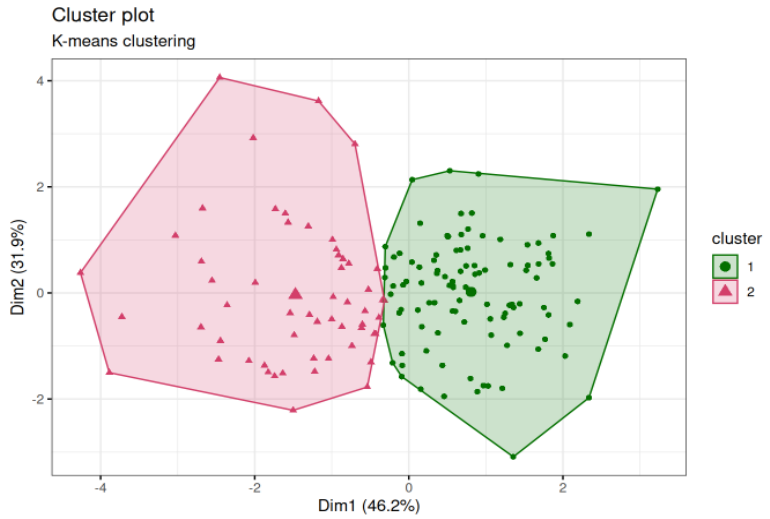
Cluster plot
K-means clustering
Dim2 (31.9%)
Dim1 (46.2%)
cluster
1
2

B

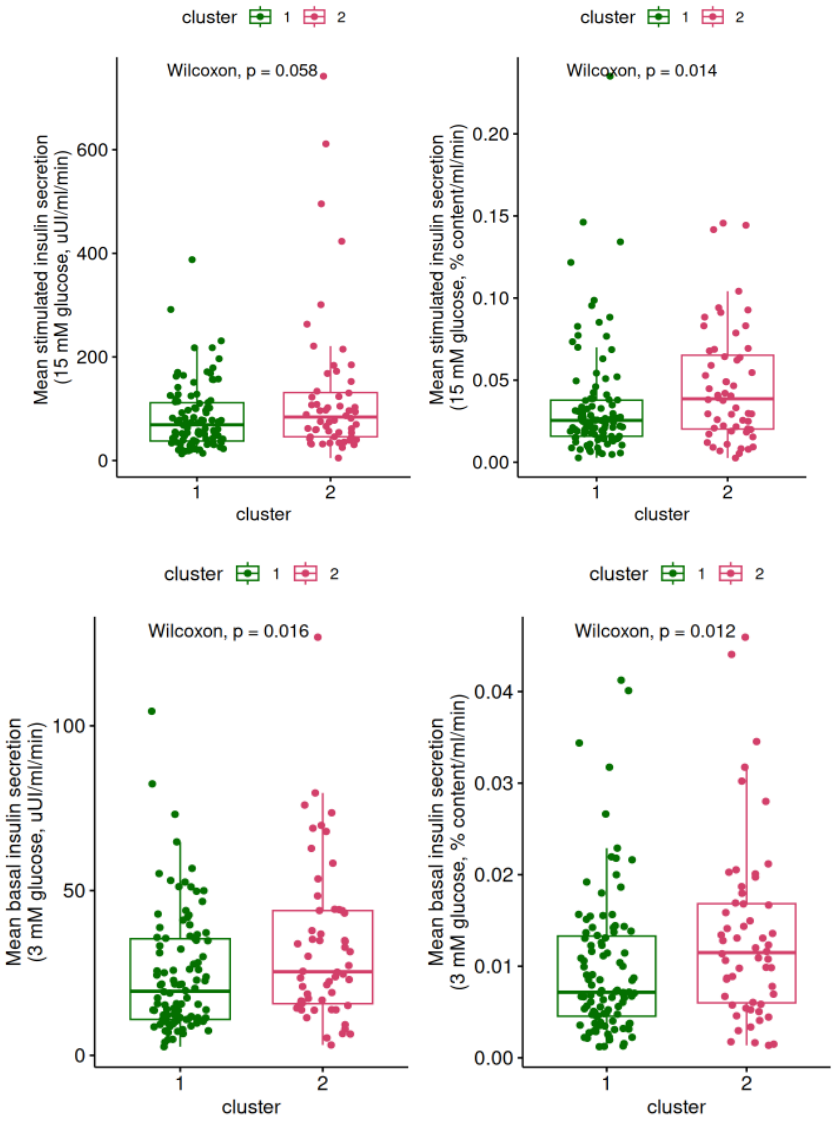
cluster 1 2
Wilcoxon, p = 0.058
Mean stimulated insulin secretion (15 mM glucose, uUI/ml/min)
cluster
Wilcoxon, p = 0.014
Mean stimulated insulin secretion (15 mM glucose, % content/ml/min)
Wilcoxon, p = 0.016
Mean basal insulin secretion (3 mM glucose, uUI/ml/min)
Wilcoxon, p = 0.012
Mean basal insulin secretion (3 mM glucose, % content/ml/min)

C

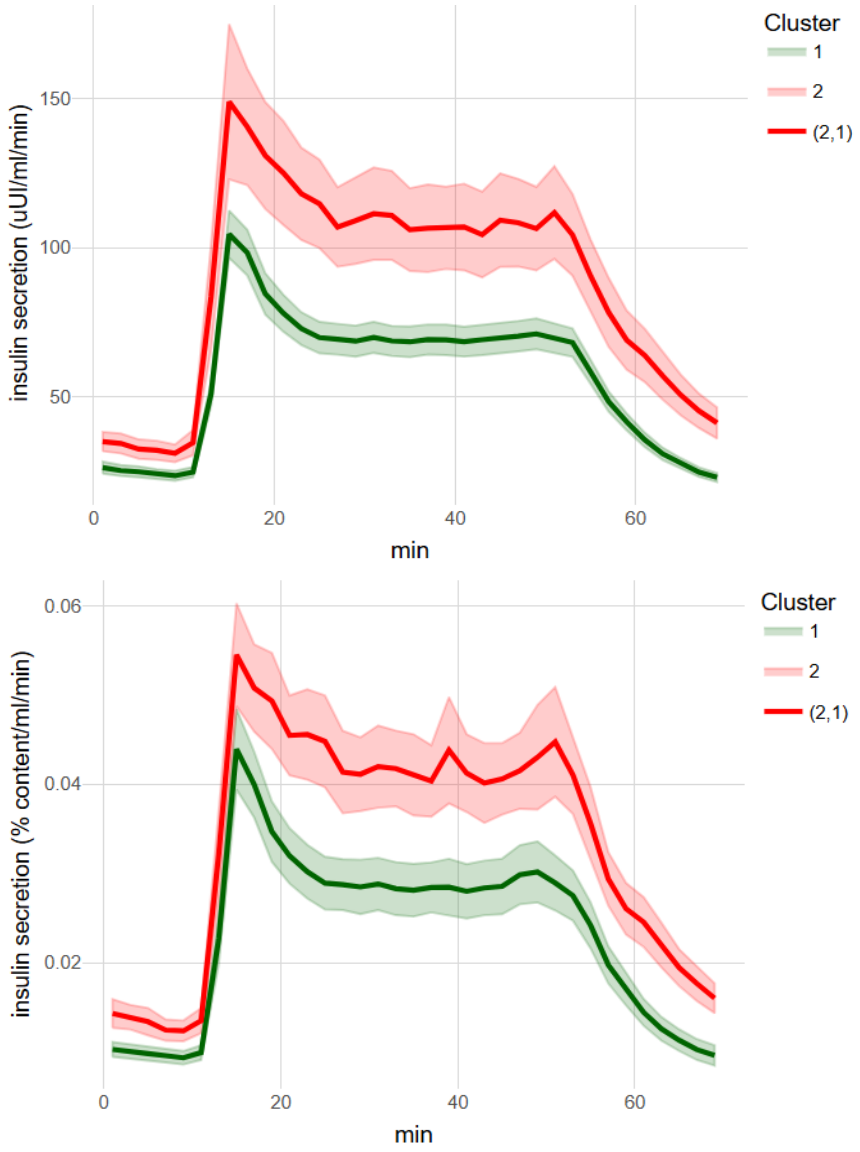

Figure 16: K-means clustering of donor characteristics in relation to insulin secretion.

16) K-means clustering was performed using donor age, BMI, HbA1c, and BSA about insulin secretion at low (3 mM) and high (15 mM) glucose. (A) Two distinct clusters emerged from the analysis. (B) Wilcoxon test comparing insulin secretion medians between clusters at low and high glucose levels. (C) Time-course profiles of insulin secretion (mean ± SEM) for the two clusters. Cluster-specific data with statistical comparisons of individual variables using an unpaired nonparametric t-test.

	Overall	1	2	p
n	158	102	56	
BMI (mean (SD))	28.15 (5.69)	25.13 (3.24)	33.65 (5.05)	<0.001
AGE (mean (SD))	51.13 (12.92)	52.69 (13.07)	48.29 (12.26)	0.040
HbA1c (mean (SD))	5.63 (0.57)	5.52 (0.41)	5.85 (0.73)	<0.001
BSA (mean (SD))	2.03 (0.27)	1.88 (0.17)	2.31 (0.19)	<0.001

Table 3: K-means clustering stratification based on donor characteristics

Cluster stratified groups based on donor characteristics: Age, BMI & HbA1c (n=158). R stratified groups, cluster 1 included normoglycemic and normal BMI groups, whereas Cluster 2 with obese and prediabetic & diabetic groups.

	All BMI	BMI<25	25≤BMI<30	BMI ≥30
Female (n)	65	23	19	23
male (n)	103	33	40	30
Female(mean±SD)	28.4 ± 6.8	21.8 ± 1.9	27.7 ± 1.2	35.5 ± 5.5
male (mean±SD)	27.7 ± 4.9	22.8 ± 1.6	27.3 ± 1.4	33.8 ± 3.5
P (t.test)	0.4857	0.0299	0.2901	0.1605
	All BSA	BSA<1.9	1.9≤BSA<2.1	BSA ≥2.1
Female (n)	65	35	17	13
male (n)	103	23	31	49
Female (mean±SD	1.9 ± 0.26	1.7 ± 0.11	1.99 ± 0.06	2.3 ± 0.18
male (mean±SD)	2.1 ± 0.25	1.8 ± 0.06	1.98 ± 0.05	2.3 ± 0.2
P (t.test)	<0.0001	<0.0001	0.5621	0.6188
	All HbA1c	HBA1c≤5.7	5.7≤HbA1c<6.5	HbA1c ≥6.5
Female (n)	62	36	25	1
male (n)	96	55	32	9
Female(mean±SD)	5.57 ± 0.58	5.28 ± 0.35	5.87 ± 0.18	8.80 ± 0.00
male (mean±SD)	5.67 ± 0.55	5.35 ± 0.24	5.87 ± 0.19	6.94 ± 0.65
P (t.test)	0.2781	0.2517	0.9377	0.0264

Table 4: Sex-stratified cluster analysis of a cohort study (n=168)

Comparison of donor characteristics in cluster-stratified groups based on sex (n = 168). Data are presented as mean ± standard deviation. Range values represent the combined data from both groups. Statistical comparisons between groups were performed using unpaired nonparametric t-tests, with significant differences ($p < 0.05$).

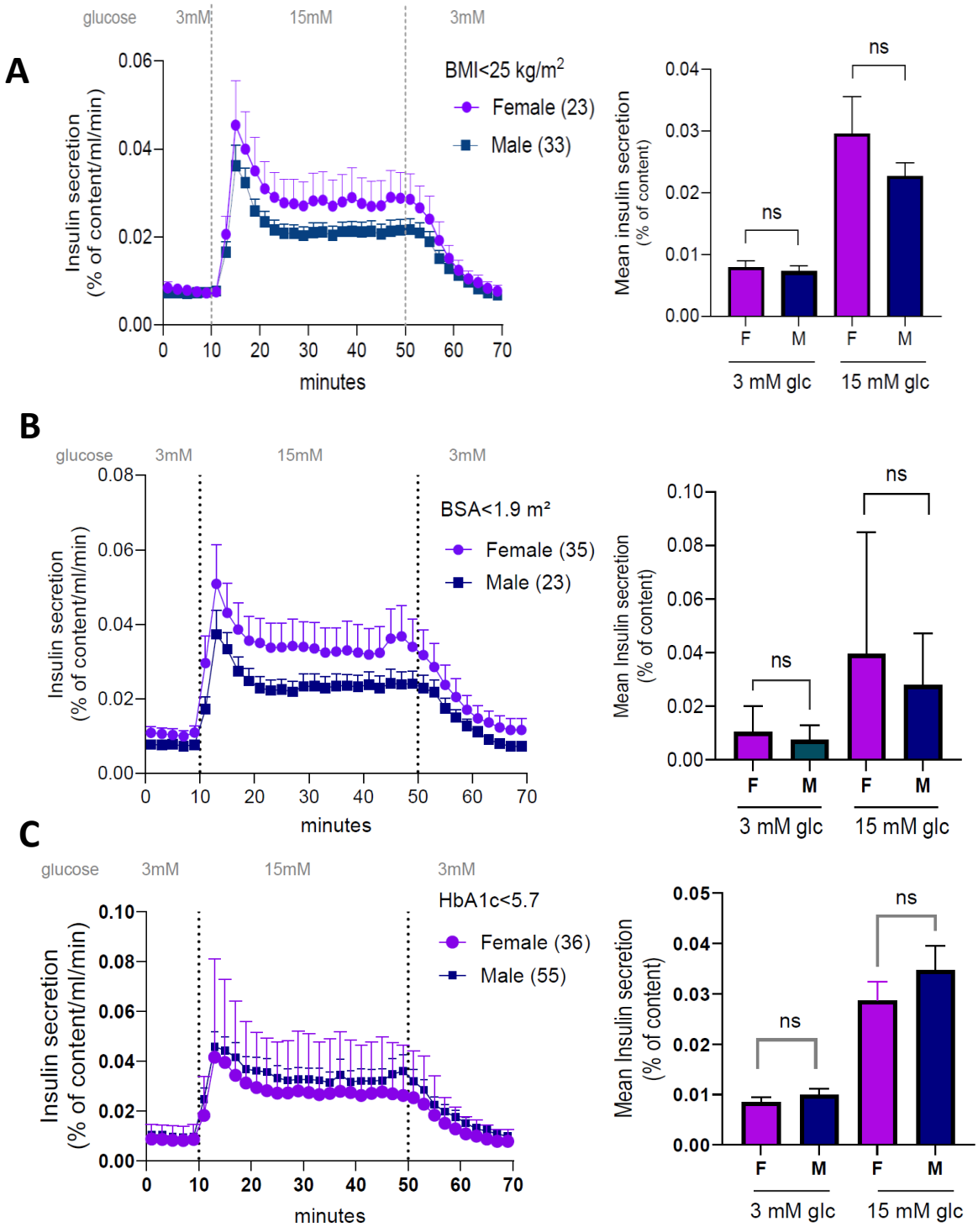

Figure 17: Sex stratified cluster analysis on cluster one based on the significance found

A) Comparison of mean insulin secretion between males and females under basal (3 mM glucose) and stimulated (15 mM glucose) conditions for the groups with Normal BMI; B) BSA less than 1.9, & C) group normoglycemic. Statistical analysis was assessed using an unpaired nonparametric t-test; ns: not significant.

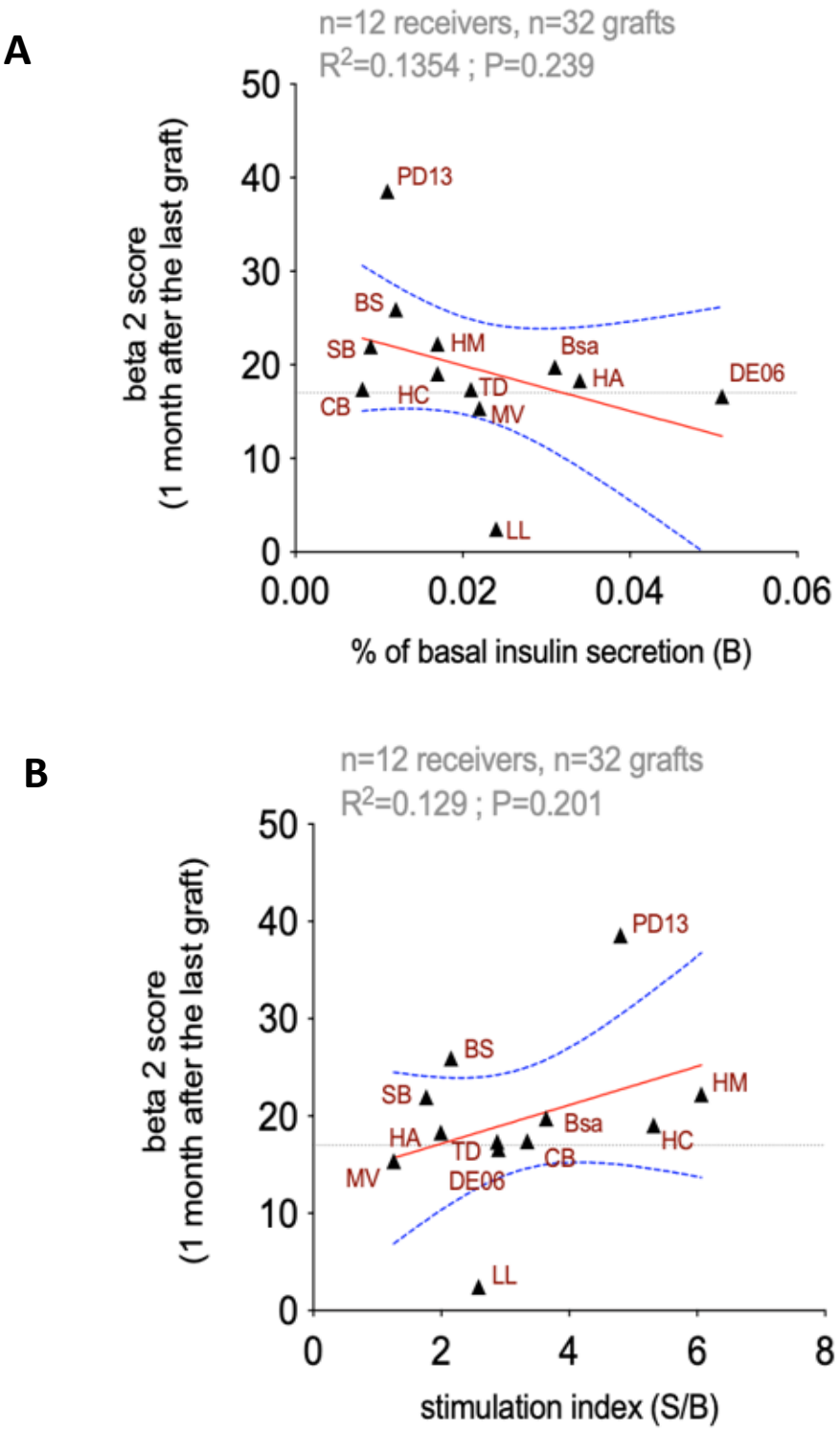

Figure 18: Directional and non-significant links between *in vitro* islet function and post-transplant Beta-2 score

A) Perifusion basal secretion (% content) vs BETA-2 score. B) Stimulation index vs Beta-2 score. Each point represents one recipient (n=12, 32 total grafts, 2-3 per recipient). BETA-2 was assessed 1 month after the final infusion. Trends observed.

3.2 Discussion

This large-scale, single-center study provides the first comprehensive comparison of insulin secretion between static (*n* = 408) and dynamic perifusion (*n* = 168) techniques using standardized experimental variables. While both methods showed comparable stimulation index measurements (r^2 = 0.652), dynamic perifusion offered superior resolution in assessing secretion kinetics relative to donor physiological variables. Standardization was crucial given the intrinsic heterogeneity of pancreatic islets in size, endocrine cell distribution, and molecular expression patterns (Dybala and Hara, 2019; Saponaro, Muhlemann et al., 2020). The observed variability in insulin secretion capacity, influenced by donor characteristics (Buemi, Mourad et al., 2024) and isolation center protocols (Kayton, Poffenberger et al., 2015; Henquin, 2018; Nano, Kerr-Conte et al., 2020), highlights the necessity for consistent assessment methods. Our approach of normalizing secretion to total islet insulin content effectively mitigated islet-specific heterogeneity (Henquin, Dufrane et al., 2006; Henquin, 2018). Notably, we observed higher intracellular insulin content (~34 ng/IEQ) compared to previous multi-center studies (13.3 ng/IEQ) (Henquin, 2019), emphasizing the impact of standardized protocols on measurement outcomes. The discrepancy likely reflects differences in islet isolation protocols, donor demographics (age, BMI, metabolic status), and measurement methodologies, including insulin quantification techniques and culture conditions. Variations in assay sensitivity and data normalisation may further contribute to inter-study variability.

Our perifusion studies revealed substantial heterogeneity in stimulation indices (ranging from 1 to 20), consistent with previous findings (Kayton, Poffenberger et al., 2015; Alcazar and Buchwald, 2019). The selected glucose concentrations (3 mM and 15 mM), while differing

from other studies using 4–16 mM or 5.6–16.7 mM (Alcazar and Buchwald, 2019) (Kayton, Poffenberger et al., 2015), were intentionally chosen. The use of 3 mM glucose, below physiological fasting levels, provided valuable insights into hypoglycemic responses, which may be predictive of islet graft function in T1D patients. Furthermore, the chosen 15 mM glucose as it reliably elicits robust, physiologically relevant insulin responses, enabling clear resolution of secretion kinetics without inducing non-specific stress.

Analysis of donor variables traditionally associated with islet isolation yields (O'Gorman, Kin et al., 2005) revealed novel insights into their influence on secretion kinetics. Our findings demonstrate that obesity and diabetes significantly affect both basal and stimulated insulin secretion, particularly under low glucose conditions. The enhanced insulin secretion observed under low glucose conditions in donors with obesity and prediabetes may reflect β-cell compensatory mechanisms in response to systemic insulin resistance. In these individuals, peripheral tissues exhibit reduced insulin sensitivity, prompting β-cells to increase basal insulin output to maintain euglycemia (normoglycemia). This chronic compensatory demand may lead to an upregulation of glucose-independent insulin secretion pathways, including enhanced basal exocytosis and altered ATP-sensitive potassium channel activity. Additionally, low-grade inflammation and lipotoxicity associated with obesity may modulate islet function by sensitizing β-cells to non-glucose stimuli, such as free fatty acids, further contributing to elevated basal secretion. These adaptations, while initially protective, may precede β-cell dysfunction and are consistent with early-stage hyperinsulinemia seen in prediabetic individuals.

The combination of advanced age (> 48 years), obesity (BMI > 33kg/m2), and pre-diabetes (HbA1c > 5.8%) was associated with higher insulin secretion kinetics. These results extend

previous observations about BMI's importance (Henquin, 2018) and challenge earlier conclusions regarding age effects. Our *in vitro* findings align with clinical observations of primary insulin hypersecretion (Trico, Natali et al., 2018) and underscore the role of basal insulin secretion in glycemic regulation (Investigators, Gerstein et al., 2012). The absence of gender-based differences in our study aligns with existing literature (Henquin, 2021), suggesting that while subtle hormone-mediated differences may exist, gender does not significantly impact insulin secretion capacity.

Regarding islet quality assessment, it's important to contextualize our findings alongside established donor scoring systems such as the North American Islet Donor Score (NAIDS) (Wang, Kin et al., 2016; Golebiewska, Bachul et al., 2019) and the Kansas City Islet Score (Ramachandran, Huang et al., 2015). These tools, developed to predict islet isolation outcomes based on donor characteristics like age, BMI, cold ischemia time, and HbA1c, have demonstrated utility in estimating islet yield and viability (Hering, Clarke et al., 2016). However, they do not directly assess functional potency. Our work aims to complement these predictive scoring systems by offering a high-resolution functional evaluation of islet insulin secretion via dynamic perifusion. By doing so, we provide additional insight into islet quality that may further inform graft selection and improve transplantation outcomes.

3.3 Conclusion

Dynamic perifusion reveals that inter-individual heterogeneity in isolated islet insulin secretion is primarily driven by donor BMI and HbA1c, especially under hypoglycemic conditions. These findings have important implications for donor selection and the optimization of islet transplantation protocols, reinforcing the value of standardized quality criteria in advancing cell therapy outcomes.

CHAPTER 4

CAD-based design and 3D modeling of a monochamber prototype simulation, and fabrication validation

4 Chapter IV: CAD – based design and 3D modeling of a monochamber prototype simulation, and fabrication validation

4.1 Introduction

3D modeling enables conceptual ideas to be turned into virtual representations that can be tested, optimized, and prepared for downstream processes such as additive manufacturing. Among the different software tools available, SolidWorks stands out as both an accessible and powerful solution for creating detailed models, ranging from simple to complex assemblies (Kurniawan, 2023). By considering geometry, functionality, and manufacturability, a parametric-based approach and integrated simulation features make it suitable for projects (Ciprian Dragne, Corina Radu (Frenț) et al., 2022). This tool is not merely seen as a tool for drawing, but an essential environment design where geometrical constraints, coupling strategies, and fluid interactions can be investigated before physical fabrication (Trojan, 2025).

The objective of this work is to design and model a functional chamber and its supporting components using Solidworks CAD software, with particular emphasis on defining the internal volume, liquid capacity, flow dynamics and coupling interfaces. Special attention is given to the islet chamber geometry, as it forms the foundation for subsequent analysis and reproducibility of perifusion conditions. The modeling process also focuses on achieving a smooth internal surface finish to support cell survival and facilitate uniform flow for biological applications. Several models were iteratively tested and fabricated using different 3D printing technologies to choose a suitable manufacturing approach and surface quality. The main focus is to develop 4 independent mono chambers to ensure that the performance of one chamber does not influence or interfere with the others. Each mono chamber is modeled with a mini

water bath, legs for support, an islet chamber with a volume of 0.5 ml, a Chamber lid and a dado joint for coupling interface.

4.2 Phases of developing a 3D model by CAD tool - SolidWorks

4.2.1 Base of the model, mini water bath and Lid

The water chamber base was designed on a sketch plane with dimensions of 112 X 112 mm and extruded to a height of 10 mm. An extrude cut of 1.96 mm diameter was made to insert the inox tube entry featuring 4 holes for samples to pass. The base serves as a foundational support for both the water chamber wall and the islet chamber. The side walls were extruded with a thickness of 6 mm and a height of 56.41 mm from the sketch plane, resulting in a final water chamber dimension of 100 x 100 mm.

Four legs, each measuring 15 x 15 mm, were created at the corners using the mirror tool, and small cuts of 9 x 6 mm were added to provide stability as stands, and the legs of the chamber were around 50 mm long. Fillets were applied to all edges to ensure smoothness and eliminate rigid corners, enhancing the structural integrity and usability of the model. The water chamber or mini water bath Lid sketches were made with the final dimension of 112 x 112 mm with a thickness of 3 mm to fit with the water chamber (**Figure 19A**).

4.2.2 Islet chamber 3D model

The sketches were created at the top plane, with a height of 52 mm and the islet volume is built with 8 mm. The design made sure to have a hole which passes through the islet chamber from the base with a diameter of 1.98 mm. From the axis, the revolution was made to have a configuration model of an islet chamber with support. For the 65 mm circular base, the cut was made to have the final dimension of 51.7 mm surface with 4 holes at equal spacing to fix

A

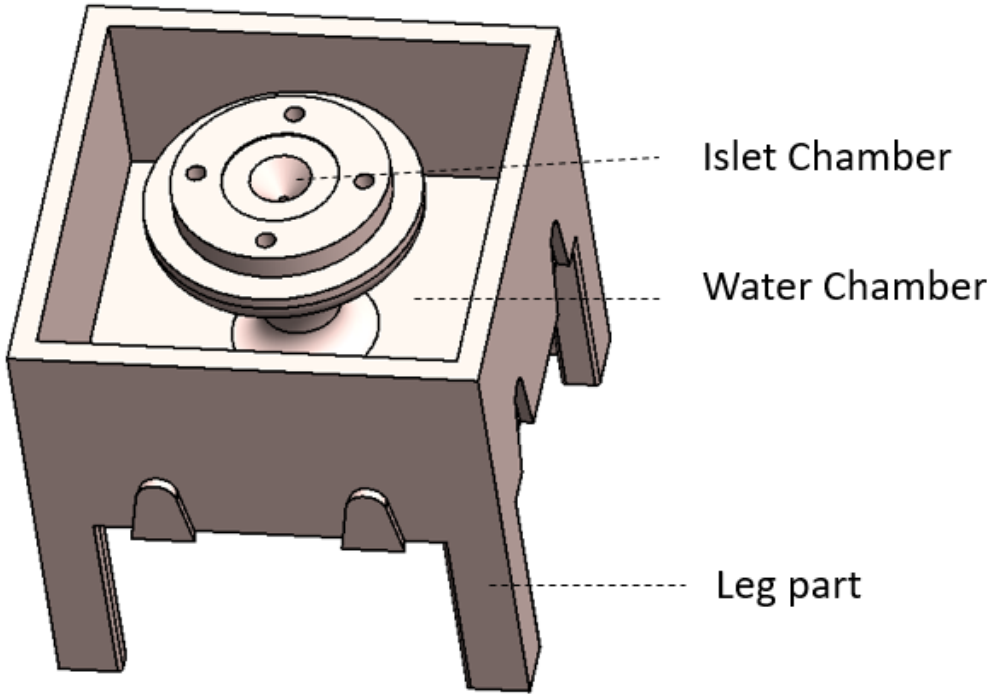

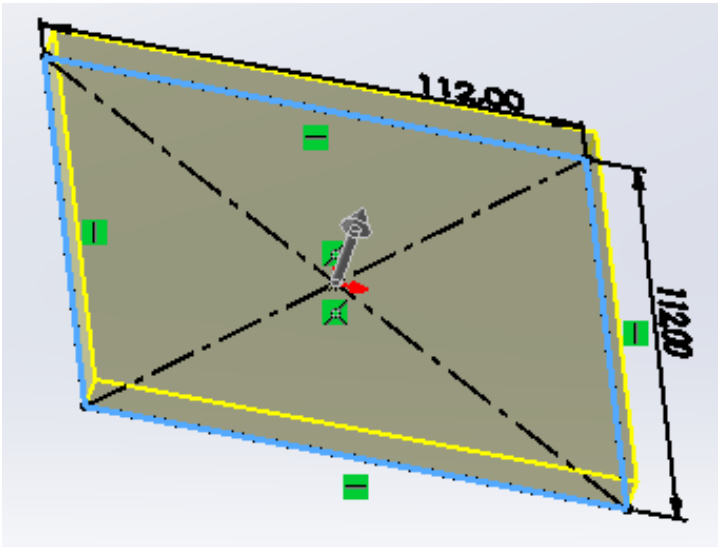

Figure 19: 3D sketches and models of the Mono chamber

A) Geometric model of water & islet chamber with its leg parts (Individual set-up 3D model without assembly) (Top figure), 3D sketch of water bath lid with the dimensions, extruded with 3 mm (Top plane view), bottom figure.

B

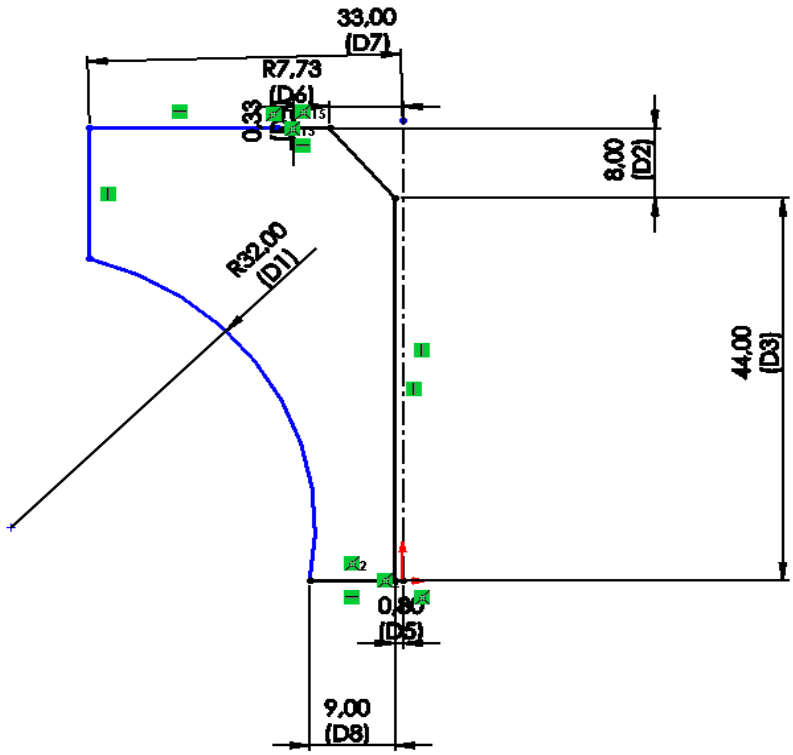

B) 3D sketch of the islet chamber revolution with its support dimensions. The sketch was developed at the front plane with a height of 52mm, 8mm for the islet chamber volume. The radius is 32 mm for the pillar support. The islet chamber with a pillar created with a 33mm radius for the revolution.

C

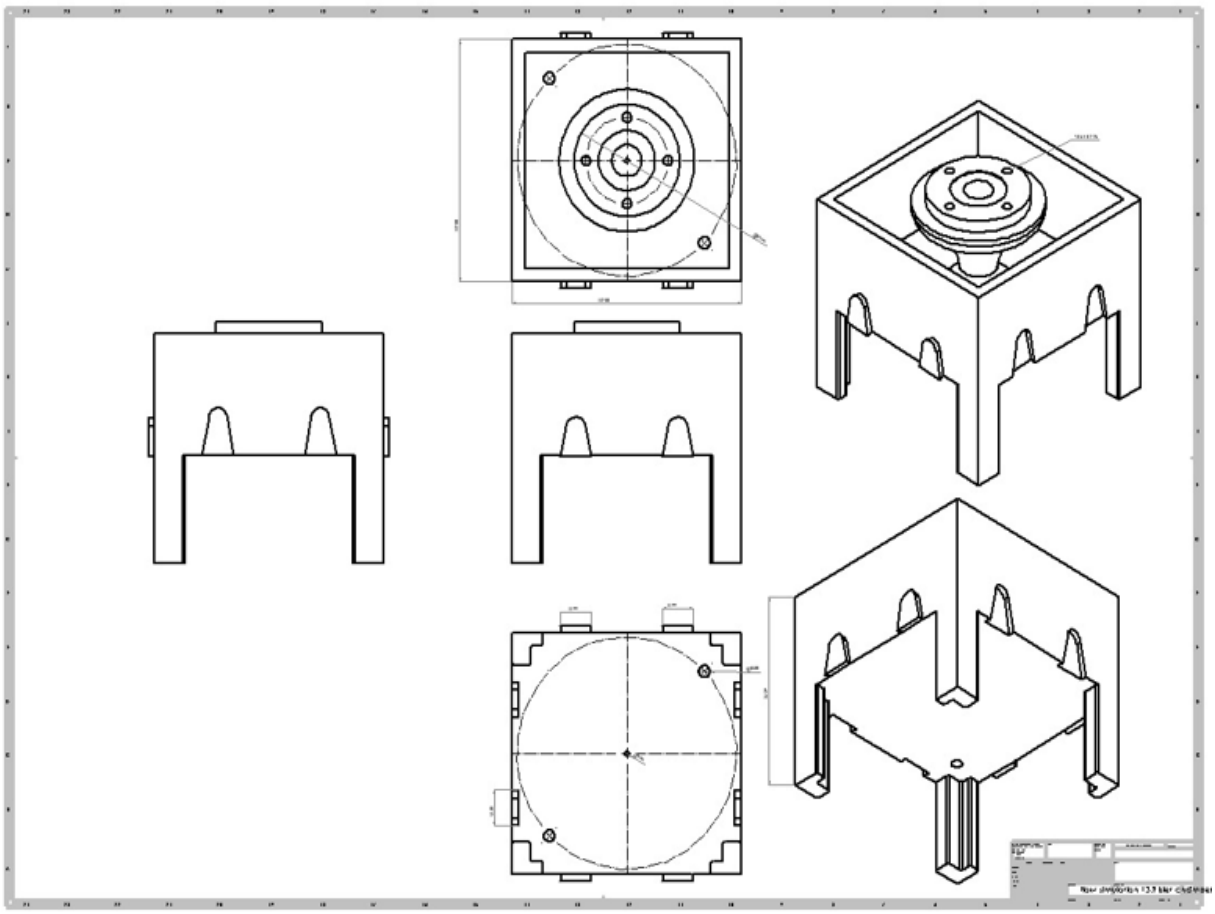

C) Generated 2D drawings with annotations of top, bottom and side views from the individual setup (Mono chamber).

the screws with a diameter of 4.5 mm, which facilitate screws fixation after fabrication. At the top of the surface, small cuts were made to fix the filter paper that is going to be used during the experiment with a porosity of 0.8µm in the islet chamber. The fillet was created at the base of the support with 8 mm (**Figure 19B**). The generated 2D drawings with annotations are shown in **Figure 19C**.

4.2.3 Islet chamber lid sketch

The height of the lid was modelled for 25 mm concerning the axis, with the hand of 7 mm from the middle to the top at a distance of 15 mm, and these sketches were made before the revolved cut. A small deep cut of 6 mm was created for the ring provision at the bottom of the lid at a distance of 12 mm from the base of the Lid (**Figure 20A**). The small plus symbol cut at the bottom of the lid created a rectangular form with a dimension of 12.6 x 6.3 mm at the middle of the bottom lid (**Figure 20B**), and on the top screw provisions were given. The entire 2D sketch with annotations is shown in **Figure 20C & D**.

4.2.4 Dado's joint

These joints were made to fix the other chamber set-up in parallel or adjacent to make a complete set-up of the assembly. These joints were made and tested with different clearances to have a fit coupling.

4.2.4.1 *Extrude cut (Female part)*

These joints were made by choosing a distance of 25 mm from the origin front plane. The base of the joint was sketched with a dimension of 16.6 mm, and the two parallel lines from the base narrowed with the same angle of 80°. The draft dimensions were made with a radius of

4.35 mm at the top of the joint. The mirror tool was used to replicate the same dimension on the opposite face, and the thickness used for the inside cut is 3.2 mm (**Figure 21**).

4.2.4.2 *Extrude boss (male part)*

This joint needs to be bigger than the extruded cut joint. The Broader base with a length of 14.9 mm and the two connecting perpendicular lines were narrowed down by drafting the part with a radius of 4.45 mm to fix a tight fit when both parts connect. The middle of the joint was distanced 25mm from the mid-plane, and it was replicated by the mirror option in the opposite plane. The thickness was around 3mm for the boss joint (**Figure 22**).

4.2.5 Individual set-up & assembly of 3D parts

The final assembly of individual parts, including the water chamber lid, islet chamber lid, inox tube, and dado joints, is shown in **Figure 23**. The mating has been done in assembly between the lid and the islet chamber to bring the whole setup, shown in **Figure 24**.

4.2.6 Testing dado joints clearances

The initial dimensions for the draft phase of the dado joint clearances were tested, but due to post-processing effects, the joints did not achieve a perfect fit. To address this, we plan to test various clearance settings on the extrude cut (female part) phase using the Halot Box 3D printing slicing software, which supports Fusion 360° (**Figure 25**). Support structures were manually selected to avoid any negative impact on the extruder boss and cutting areas, ensuring precise results during the printing process. The final 0.1 mm clearance allowed the joints to fit properly with the extruder boss. With this adjustment, a 0.1 mm increase was applied to both sides of the base, and a 0.1 mm clearance was maintained for the draft from its original value. These versatile joints on the exterior of the water bath enabled multiple

connections to be made simultaneously. **Figure 26** shows the printed form of checking final clearance for the dado joint fix (0.1mm).

4.2.7 Pre-analysis of prototype

Testing a prototype before it is introduced to real-world applications is essential to reduce the risk of costly errors, save materials, and ensure easier maintenance and repairability. The flow analysis was divided into two key phases. The first phase focused on assessing the durability of the 3D model surfaces, ensuring that they could withstand the applied water load over time. The second phase was centered around evaluating the specific area within the chamber where the islets would reside. This region was subjected to detailed scrutiny, as it is crucial to maintain the prescribed flow rate conditions that are conducive to the islet's survival throughout the experiment.

4.2.8 Water chamber flow analysis – static test

The pre-processing analysis of the finite element model was conducted using Hypermesh and tested through OptiStruct by applying Hydrostatic pressure (outside source). In this simulation, pressure was applied at intervals of every 10 cm in height, assuming a constant water density throughout. The goal was to generate contour plots that highlight areas of maximum structural variation. This approach allowed us to evaluate the model's response to pressure, focusing on structural integrity.

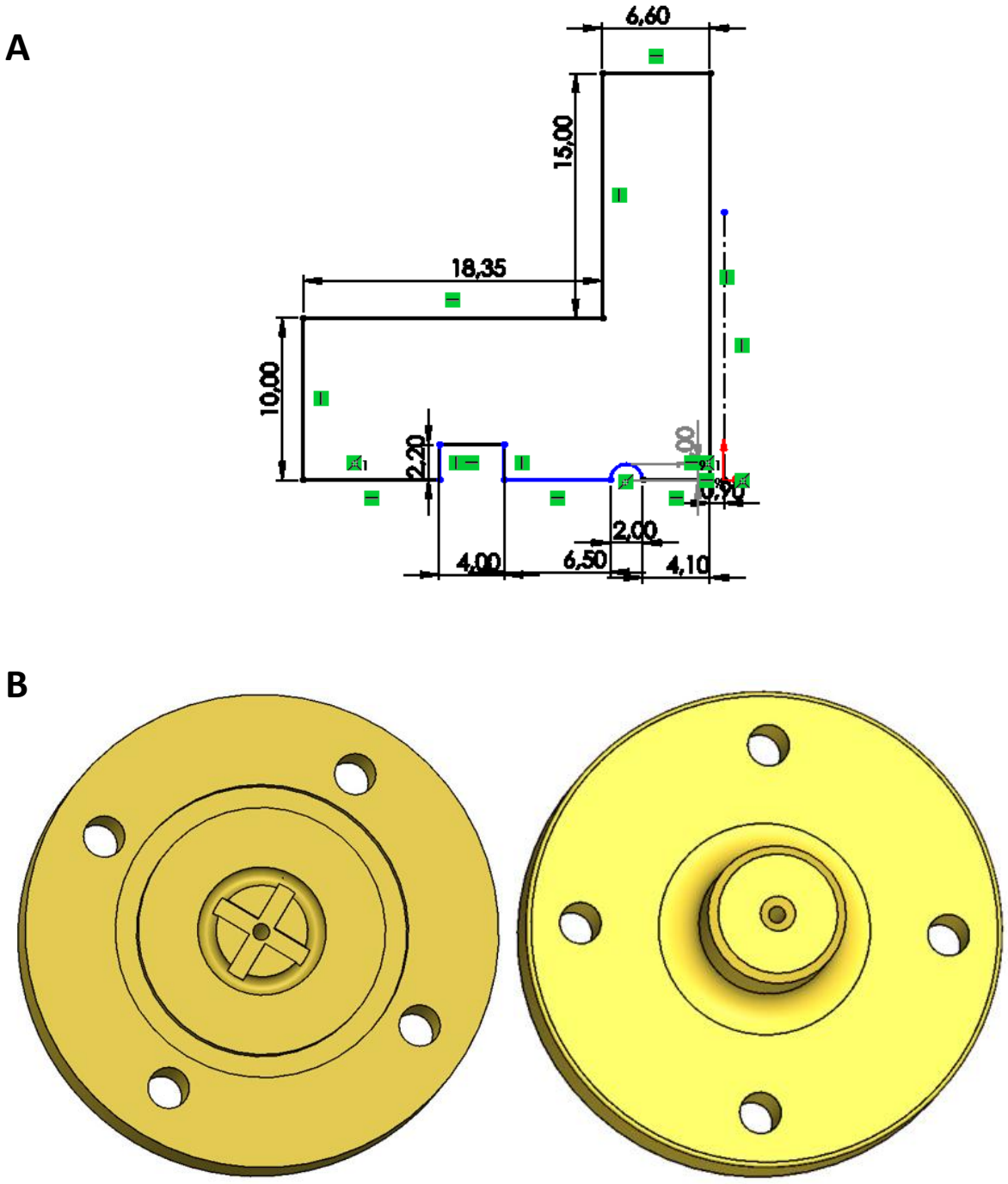

Figure 20: 3D sketch of the islet chamber lid for a 0.5 mL volume and its top and bottom views

A) Geometrical 3D sketch of the islet chamber lid with a 2mm ring cut, B) bottom view of the islet chamber cap 3D model, with a small plus sign to support a nitrocellulose filter (0.8µm) (left). Top view of 3D model with 4 screw holes (4.5mm) (right), islet chamber lid 3D model front and back side sketch view.

C

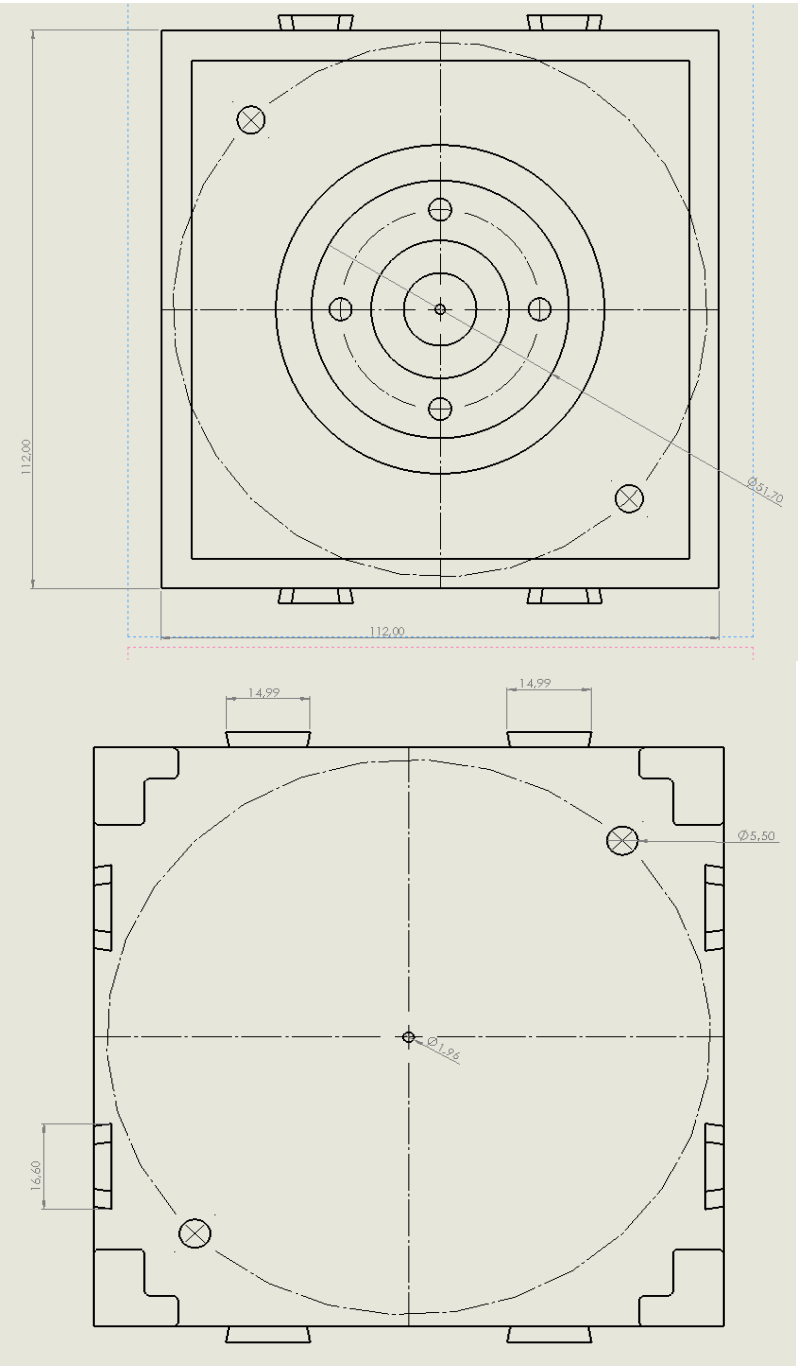

C) 2D drawings of the islet chamber include a top view that illustrates the annotation of the tube inox (middle hole) (top figure), a bottom view that illustrates the male and female parts annotations with inlet and outlet (5.5mm) dimensions (bottom figure).

D

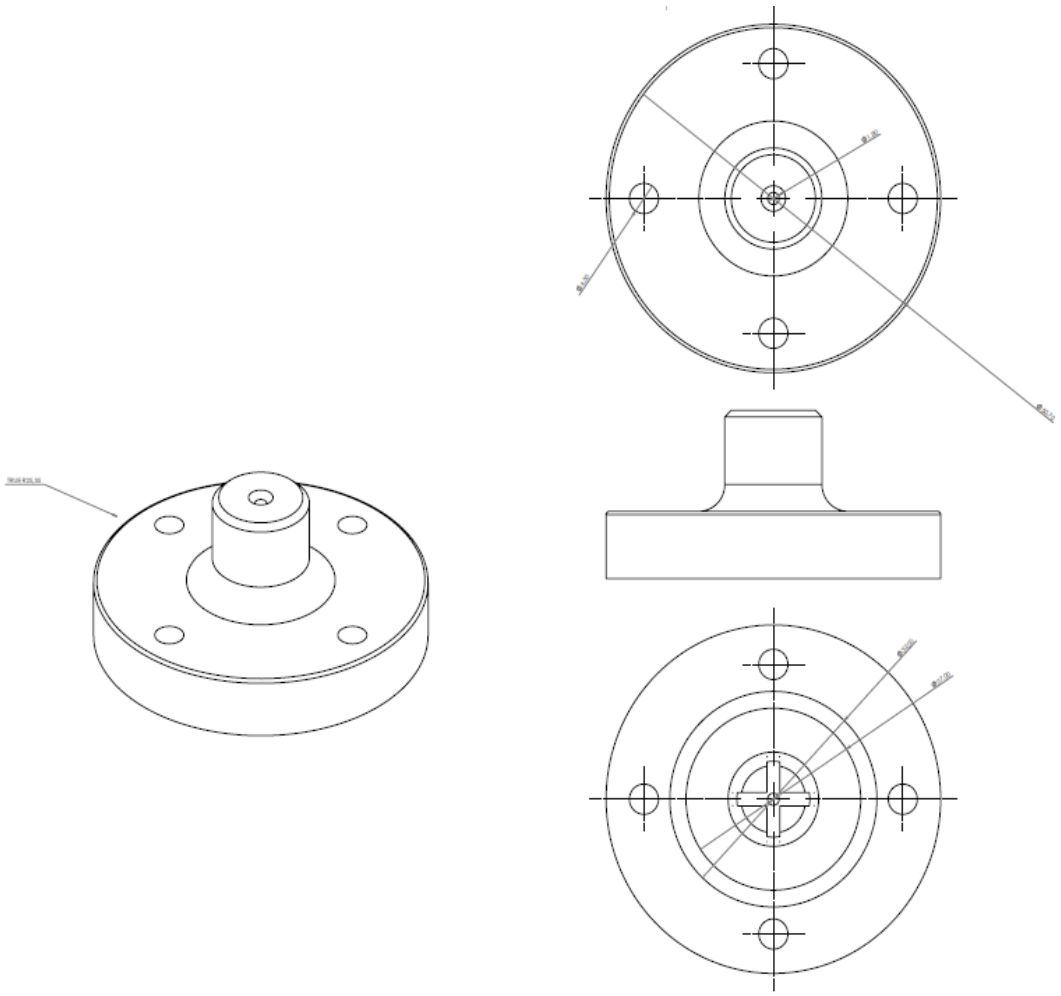

D) 2D drawings of side, top and bottom views of the islet chamber lid with annotations generated from the SolidWorks Drawing tool. The middle of the cap is extruded with a 1.96mm dimension for the inox insert. The four holes with a dimension of 4.5mm are created for screw fixation.

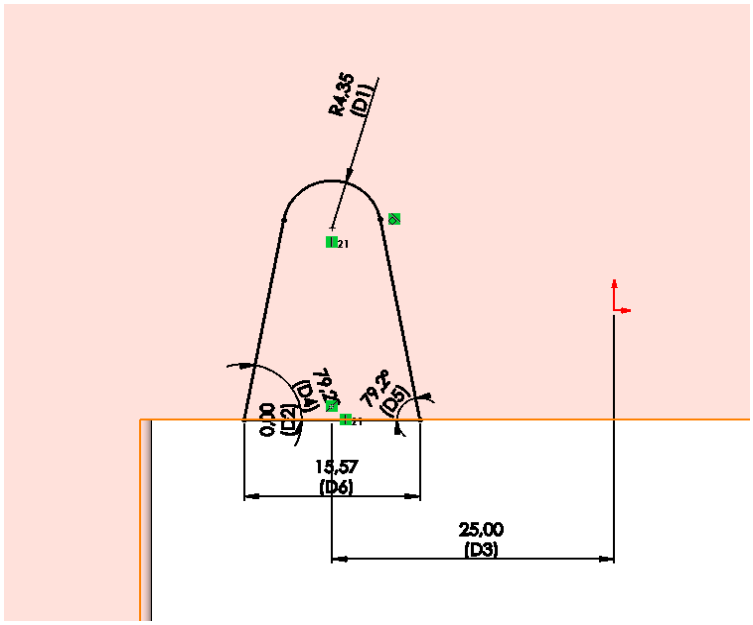

Figure 21: Dado's joint female 3D sketch with geometrical dimensions

Female part, Dado's joint extrudes a cut 3D sketch with dimensions, with a draft radius of 4.35mm. The elevation from both sides, angle of 79.2°, was chosen.

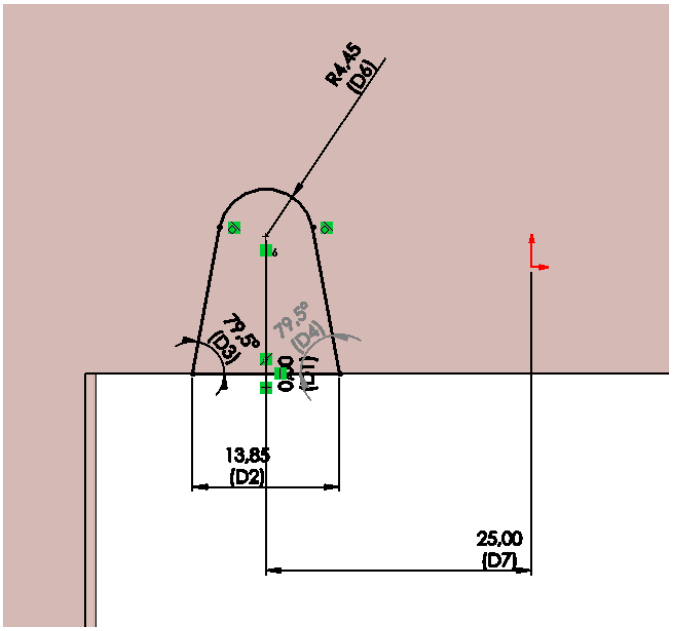

Figure 22: Dado's joint male 3D sketch with geometrical dimensions

Male part, Dado's joint Boss 3D sketch with dimensions, with draft radius of 4.45mm. The base of this sketch is dimensioned with 13.85mm, and the radius of the draft and midpoint of the base were positioned vertically to avoid misalignment. The elevation angle between the two faces is adjusted as per the female part dado fix.

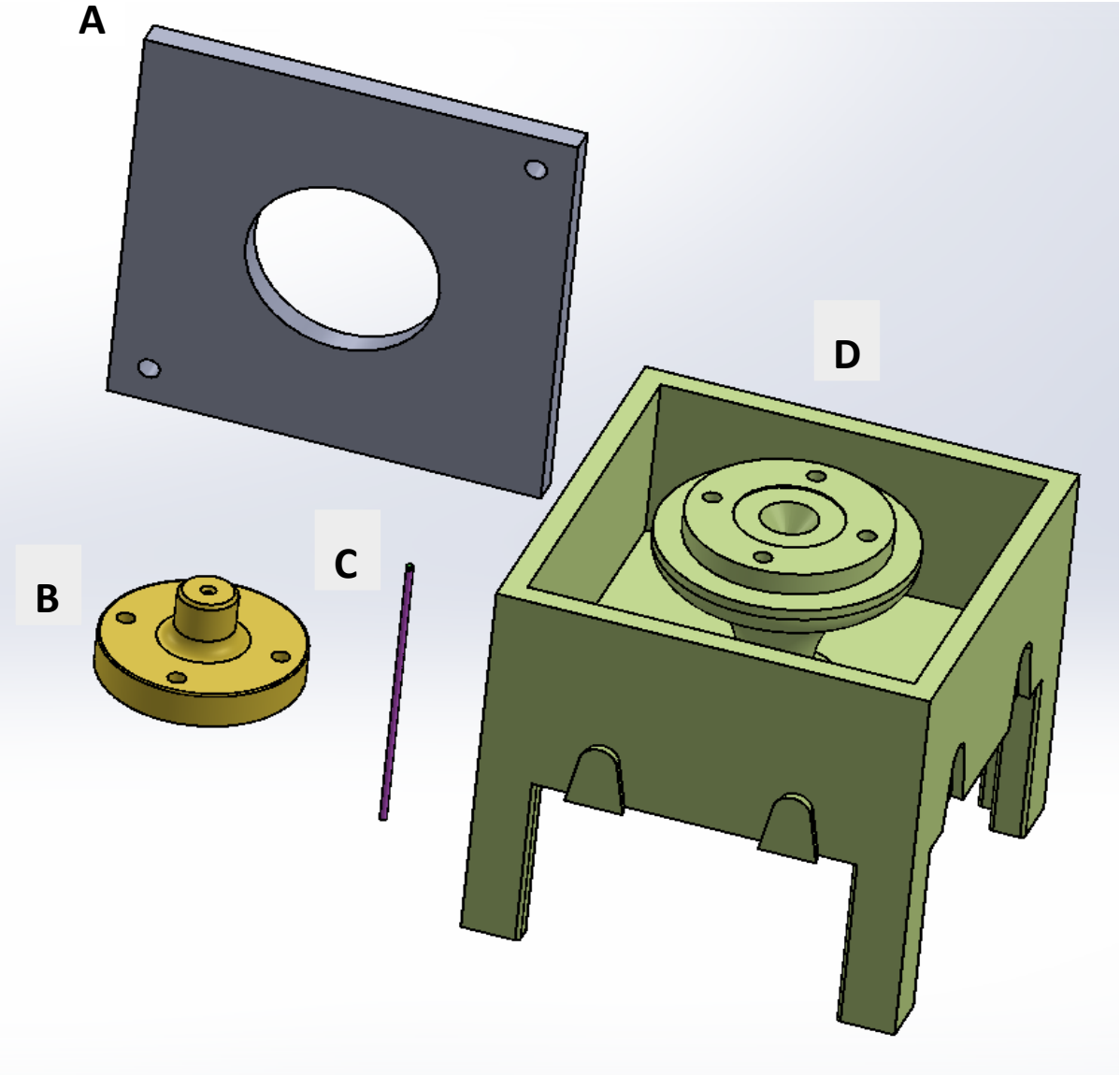

Figure 23: All parts of the individual set up (mono chamber)

A) 3D view of water bath lid with the dimensions of 112*112mm with the hole of 6mm on 2 corners, B) Top view of the Islet chamber, C) 3D model of the tube (to represent inox) with 4 tiny holes at the top end, D) 3D view of water bath with islet chamber. (one set up to accommodate 300IEQs)

A

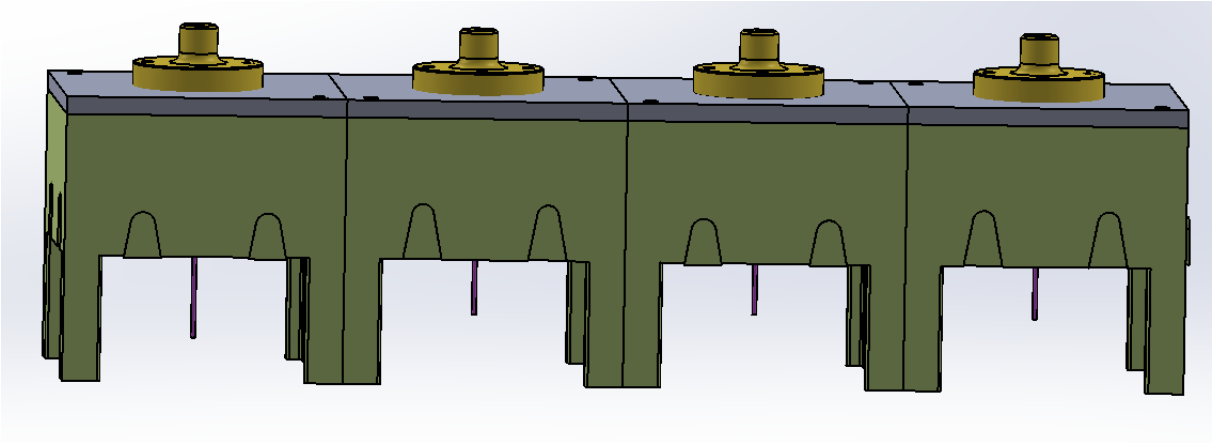

B

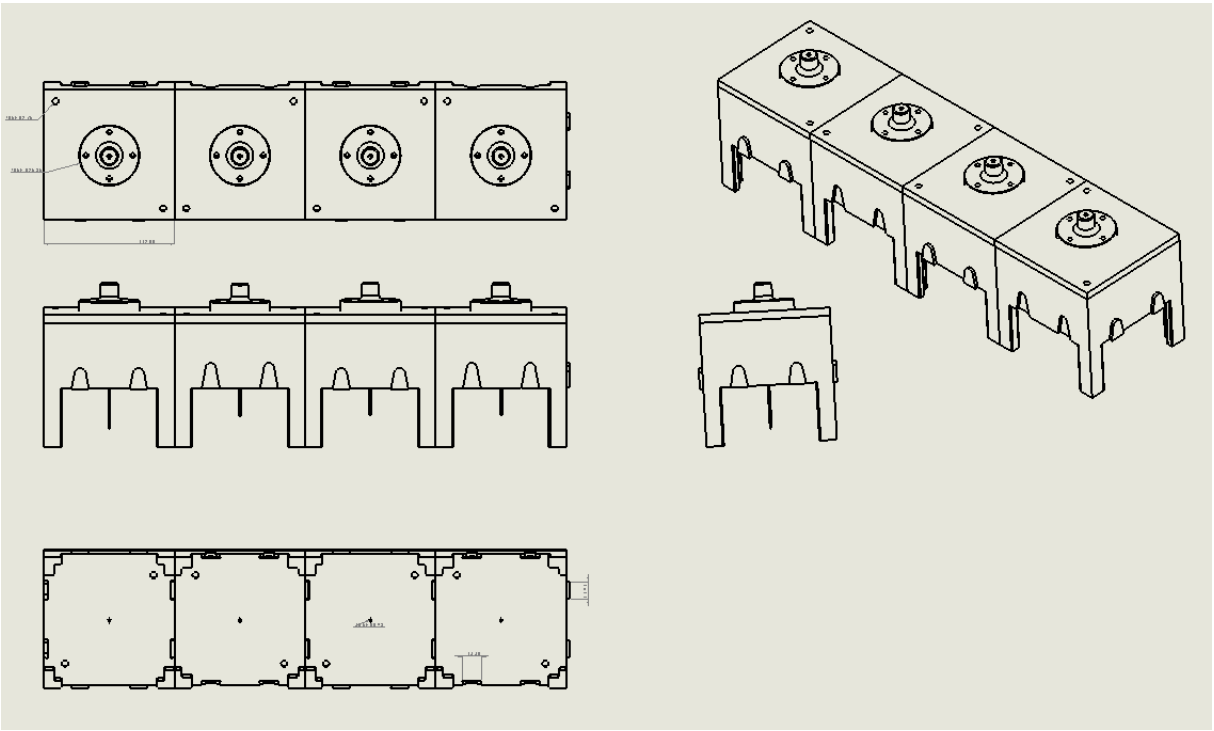

Figure 24: Assembly 3D view in parallel connection and its 2D drawings

A) Parallel assembly of all four-chamber set up, and Figure B) 2D drawings after the mating in assembly of their top, side and bottom views.

A

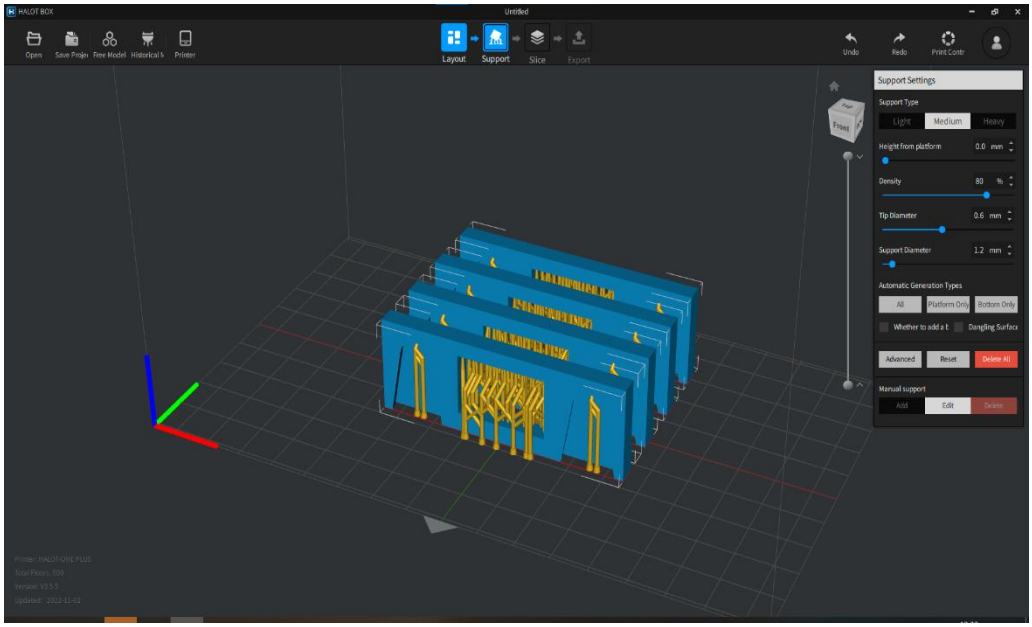

B

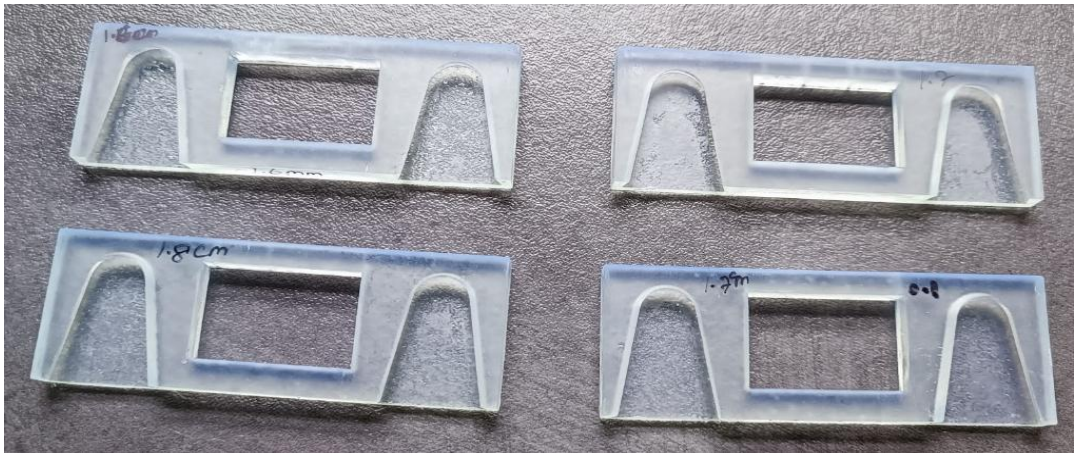

Figure 25: 3D printed different clearances by MSLA for perfect draft fitting

A) Manual support placement for clearance checking (Female part), performed all in the same window; the analysis is performed by Halot box slicing software (supported version of Fusion 360°). B) clearances checked in MSLA for Dado's joint.

A

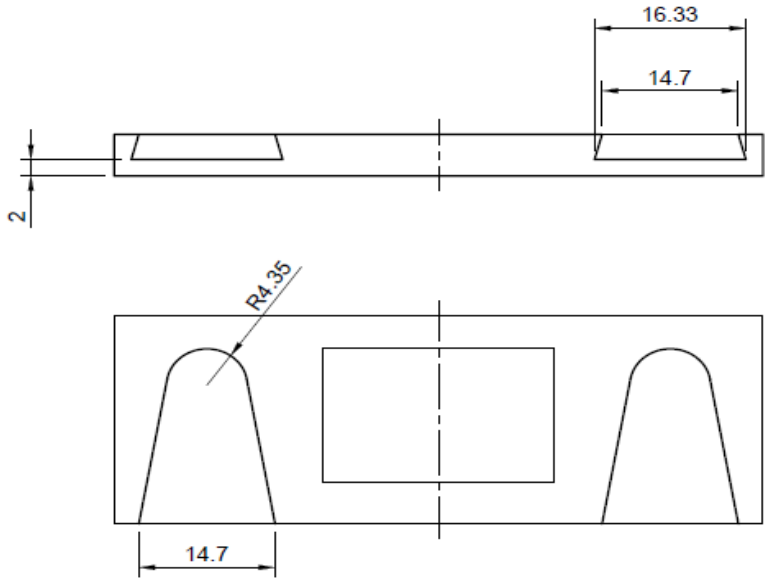

Actuel Clearance – Extrude cut

B

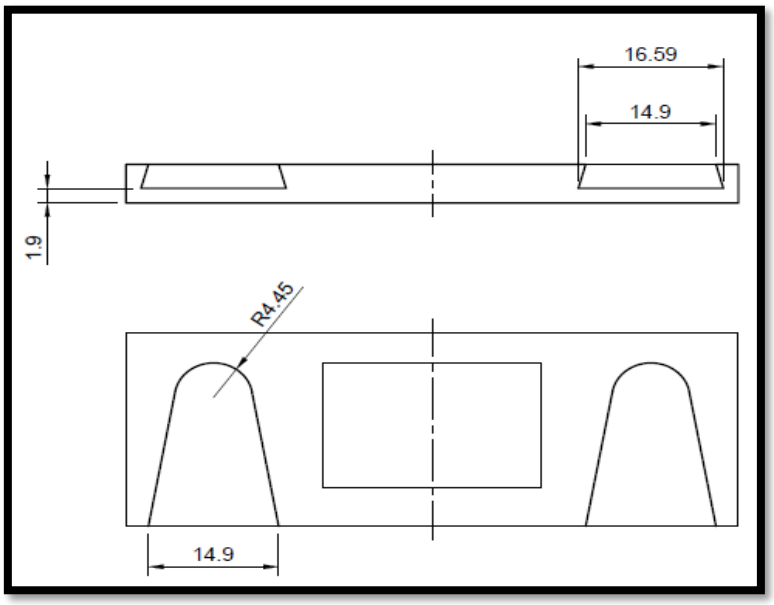

0.1 mm Clearance – Extrude cut

C

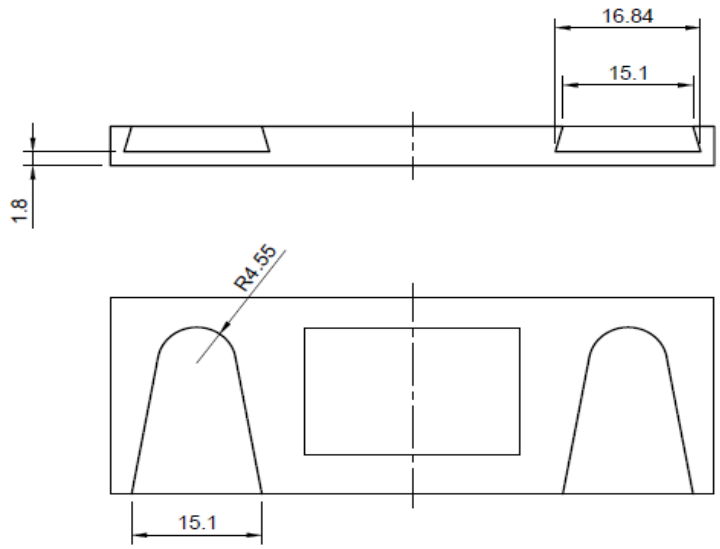

0.2 mm Clearance – Extrude cut

D

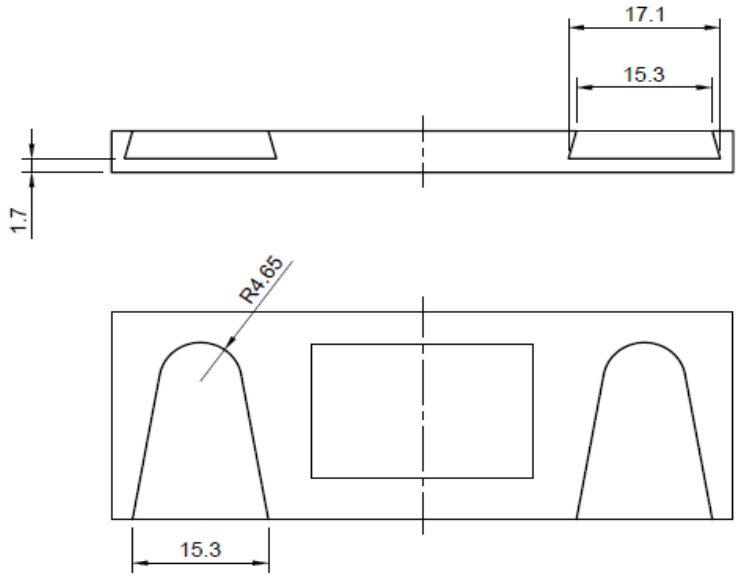

0.3 mm Clearance – Extrude cut

Figure 26: Geometrical view of testing clearances with various dimensions for MSLA

A) Female part actual draft dimensions with the base of 14.7, with a draft radius of 4.45mm (with a tight fit), B, C, D) draft modifications with 0.1mm, 0.2mm & 0.3mm with corresponding radius adjustments. The final fit was achieved with 0.1mm clearances.

A

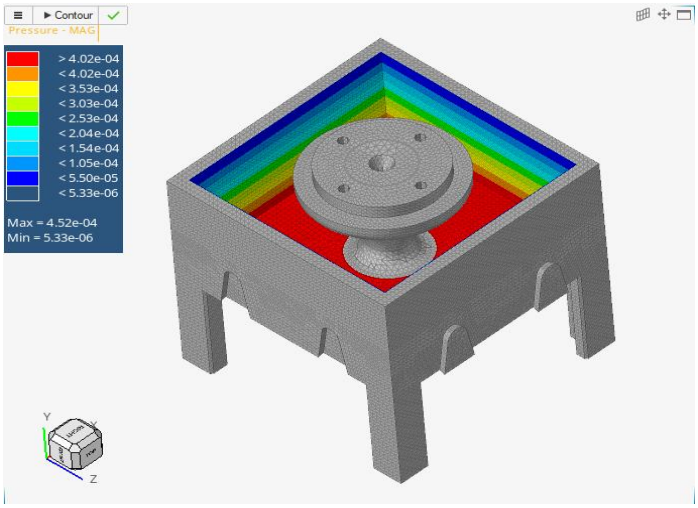

B

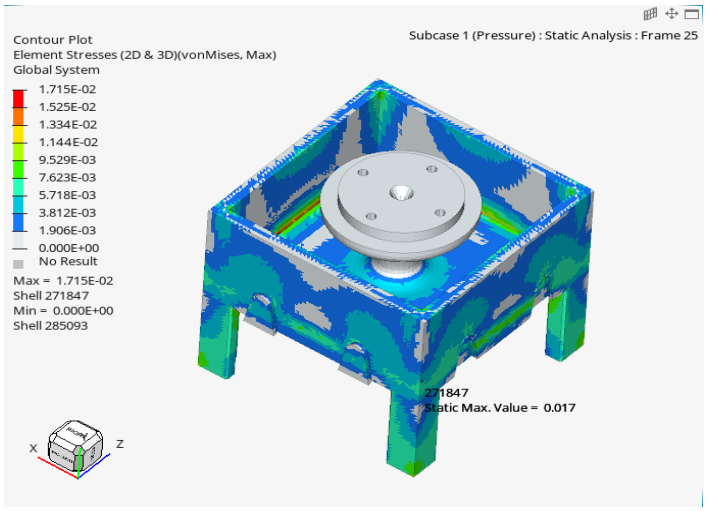

C

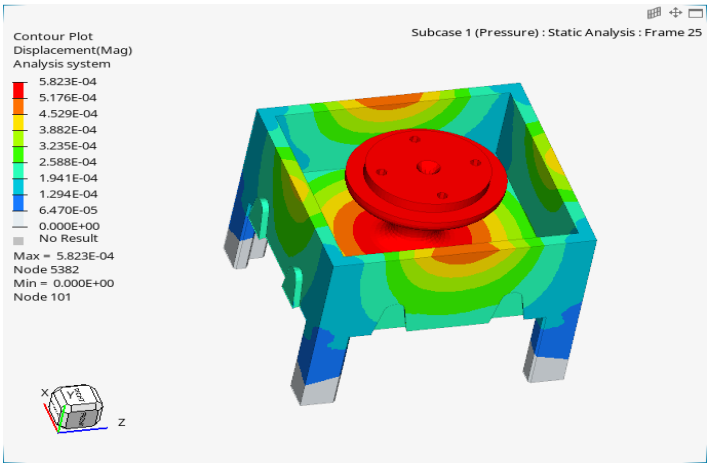

Figure 27: Hypermesh modeling, a contour plot of pressure, stress & displacement analysis

A) simulated pre-processing result by applying pressure at every 10 cm, negligible effect (4.52x10^-7 kPa), B) negligible stress (1.715x10^-5 kPa), C) and negligible displacement (5.823x10^-7 kPa) due to the water load.

The results revealed minimal variations in pressure, stress, and displacement, as demonstrated in **figure 27**. The variations during stimulation as pressure reached a maximum of 4.52x10^-7 kPa. When this pressure was used as input, to calculate stress (1.715x10^-5 kPa) and displacement (5.823x10^-7 kPa), which is a small pressure compared to the atmospheric value (**Figure 27A, B & C**).

The input was applied using the hydrostatic equation, where the pressure was calculated as:

Pressure=ρ (0.99 g/cm^3) × gravity (9.81 m/s2) × height

4.3 Flow simulation in SolidWorks

4.3.1 Islet chamber flow analysis

Flow simulation in SolidWorks follows a systematic process for solver analysis. First, the geometry is divided into small cells to create a computational mesh, enabling fluid behavior to be analysed at discrete points. Next, boundary conditions such as pressure, velocity, and temperature are applied to the model's inlets, outlets, and surfaces. The solver then uses numerical methods to solve fundamental fluid dynamics equations across the mesh.

Through an iterative process, the solver refines the solution until convergence is achieved, ensuring accuracy (**Figure 28**). Once the calculations are complete, the results are visualized using plots that display velocity, pressure, and temperature distributions.

In real time, the islet chamber operates with a flow rate of 1 ml/min. A crucial parameter for the simulation is the density of the medium. Given that the KRB medium is primarily composed of water with dissolved salts, its density is similar to water's.

Therefore, the flow rate can be calculated in terms of kg/s as follows:

1 milliliter (ml) = 1 x 10^-6 cubic meters (m^3)

So, 1ml/min = 1 x 10^-6 m^3/min

To convert minutes to seconds

1 minute = 60 seconds

Therefore, 1 ml/min = (1 x 10^-6 m^3/min) ÷ 60 = 1.67 x 10^-8 m^3/s

Apply the density of KRB medium (1000 kg/m^3)

Mass (Q x ρ) Kg/s = 1.67 x 10^-8 m^3/s x 1000 kg/m^3

For the KRB medium, 1 ml/min is equivalent to 1.67 x 10^-5 kg/s.

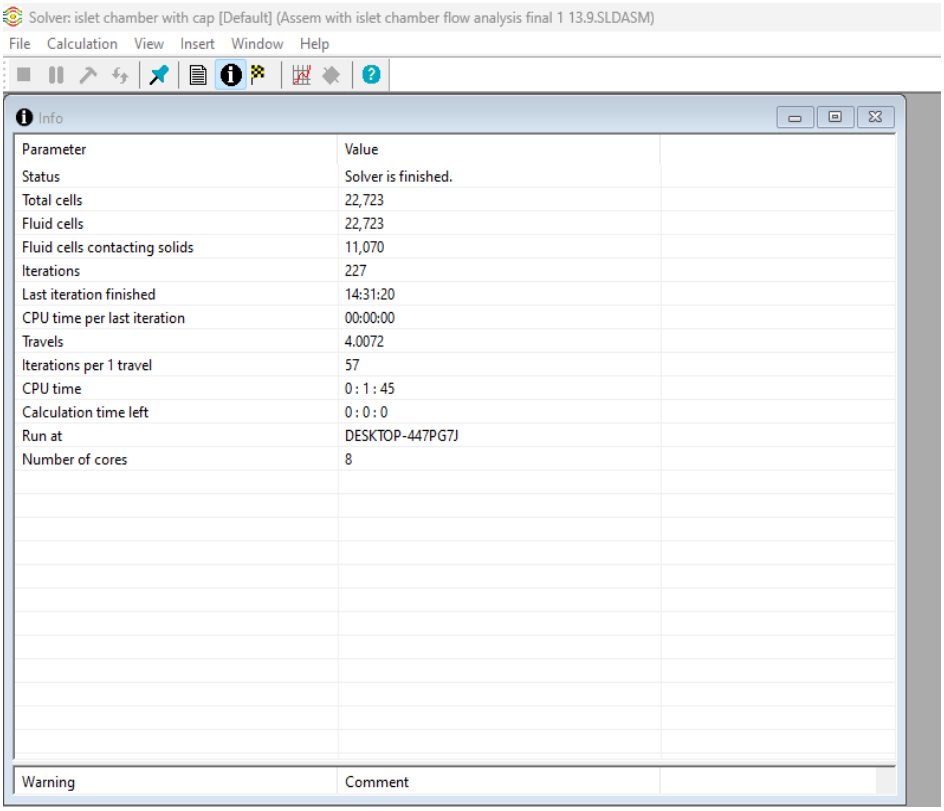

Figure 28: Solver performance metrics

227 iterations have been taken by the solver to reach a converged solution (stop changing significantly between steps).

A

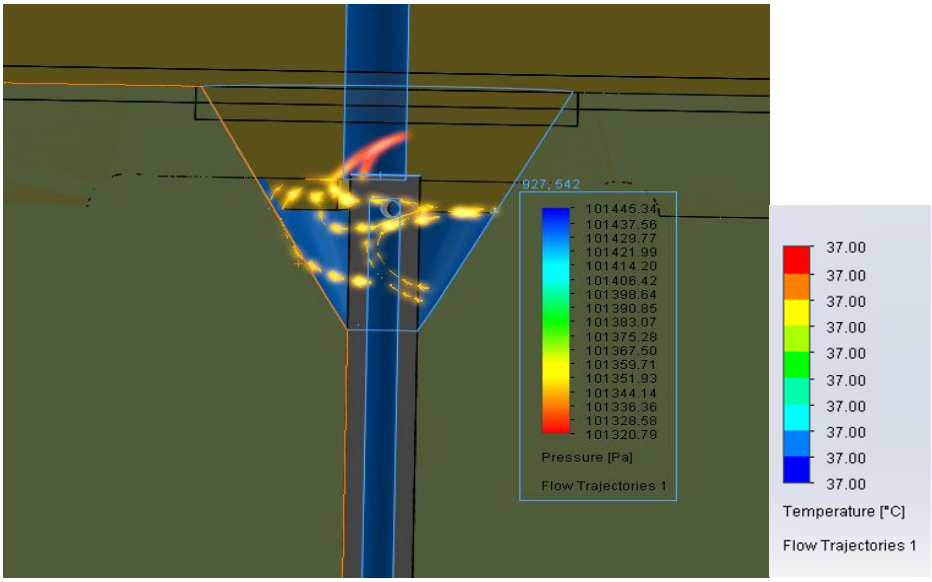

B

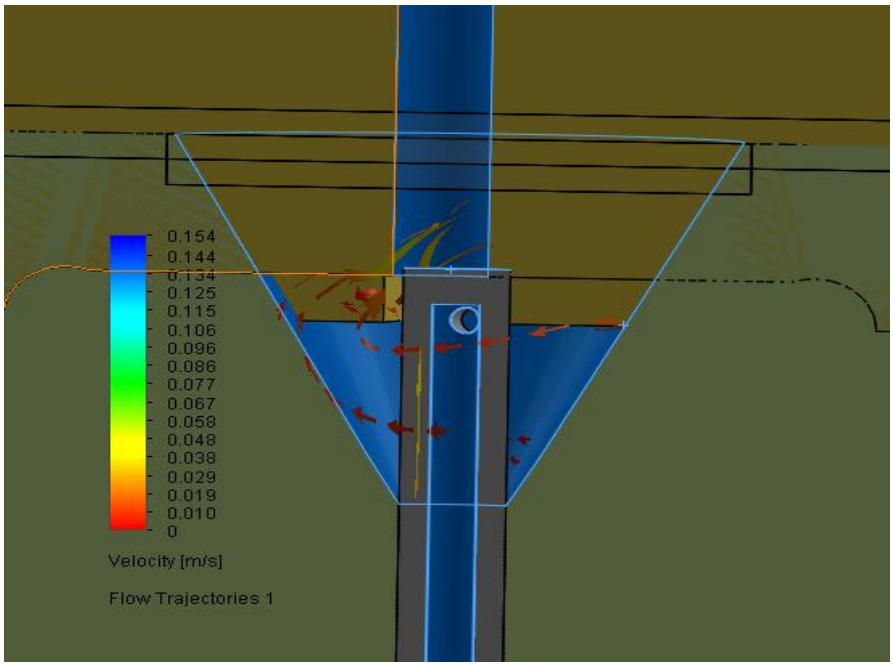

Figure 29: A) pressure plot flow analysis in the islet chamber, B) velocity plot flow analysis in the islet chamber

The simulation has been performed in the islet chamber with a 1mL/min flow rate (1.6667×10−5kg/s) and observed negligible pressure (101.3Kpa) (A) and velocity (0.01 m/s), no change in temperature inside islet chamber (B) by SolidWorks flow simulation. The flux observed due to the flow from the pierced tube to the islet chamber.

this simulation, the pressure within the system ranged from a minimum of 101320 pascals to a maximum of 101445 pascals. These slight variations in pressure indicate a well-controlled environment with minimal fluctuations and consistent with atmospheric pressure, ensuring stability within the islet chamber (**Figure 29A**). The relatively narrow pressure range demonstrates that the design can effectively manage the internal forces, providing consistent conditions necessary for maintaining the functionality of the islets.

With this flow rate of 1.67 x 10-5 kg/s, the velocity has slight variations from 0.01 m/s to 0.15 m/s observed in the islet chamber as shown in **Figure 29B**. The controlled variation in flow velocity prevents potential turbulence or stress on the islets, which could improve the cell function. This steady and manageable flow pattern highlights the effectiveness of the chamber design in maintaining optimal conditions for the experiment, ensuring both consistency and protection for the biological system.

4.3.2 Water chamber flow analysis through the inlet by integrated SolidWorks simulation

The flow simulation of the bottom-fed mini water bath demonstrated stable hydraulic behavior under the applied conditions. With an inlet flow rate of 125ml/min and a mass flow input of 0.00208kg/s, the chamber reached full capacity (500 ml) within four minutes, consistent with experimental expectations. The solver achieve convergence after 40 iterations, during which the pressure and temperature variation within the chamber were negligible. This uniformity indicates a steady and laminar filling behavior, suggesting that the bottom-fed configuration promotes even fluid distribution without significant thermal or pressure gradients (**Figure 30**).

A

Infos

Paramètre	Valeur
Etat	Calcul t
Nombre total de cellules	5,013
Cellules fluides	5,013
Cellules fluides en contact avec le solide	2,771
Itérations	40
Dernière itération terminée	12:27:17
Temps de calcul pour la dernière itération	00:00:03
Transferts	
Itérations par transfert	40
Temps de calcul	0 : 0 : 9
Temps de calcul restant	0 : 0 : 0
Exécuter sur	PC-411
Nombre de coeurs	16

Avertissement	Comme
Pas d'avertissement	

Log

Evénement	Itération	Temps
Génération du maillage démarrée	0	11:50:54 , Oct 09
Génération du maillage terminée avec succès	0	11:50:56 , Oct 09
Préparation des données pour le calcul	0	11:50:57 , Oct 09
Calcul démarré	0	11:50:59 , Oct 09
Le calcul a convergé puisque les critères suivants...	40	11:51:08 , Oct 09
Les objectifs ont convergé	40	
Calcul terminé	40	11:51:11 , Oct 09
Préparation des données pour le calcul	0	12:27:17 , Oct 09
Calcul terminé	40	12:27:17 , Oct 09

B

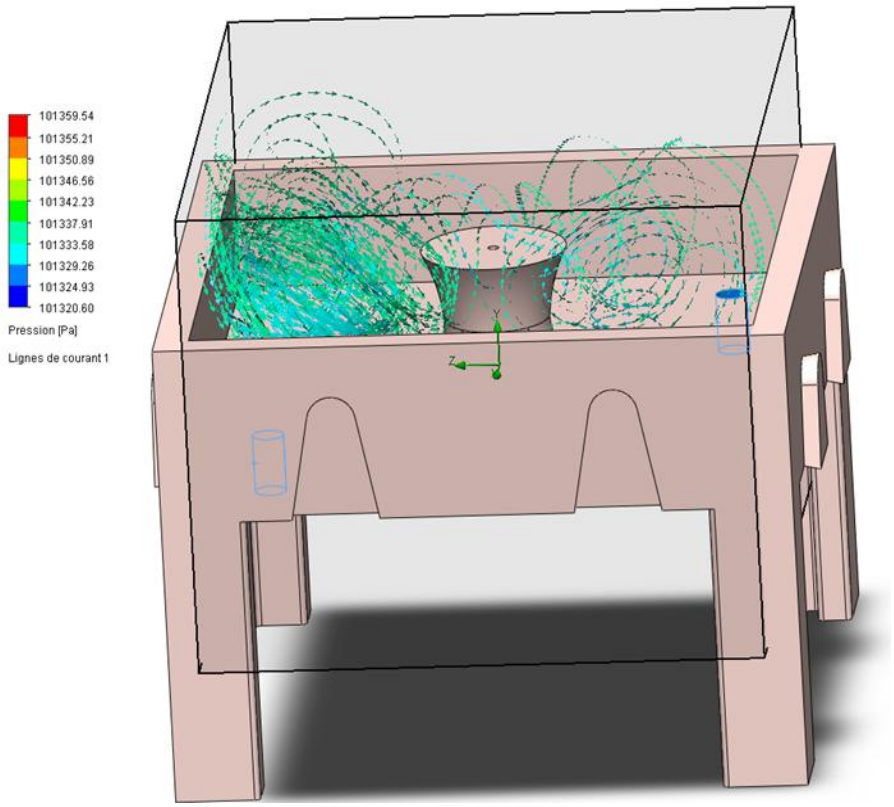

C

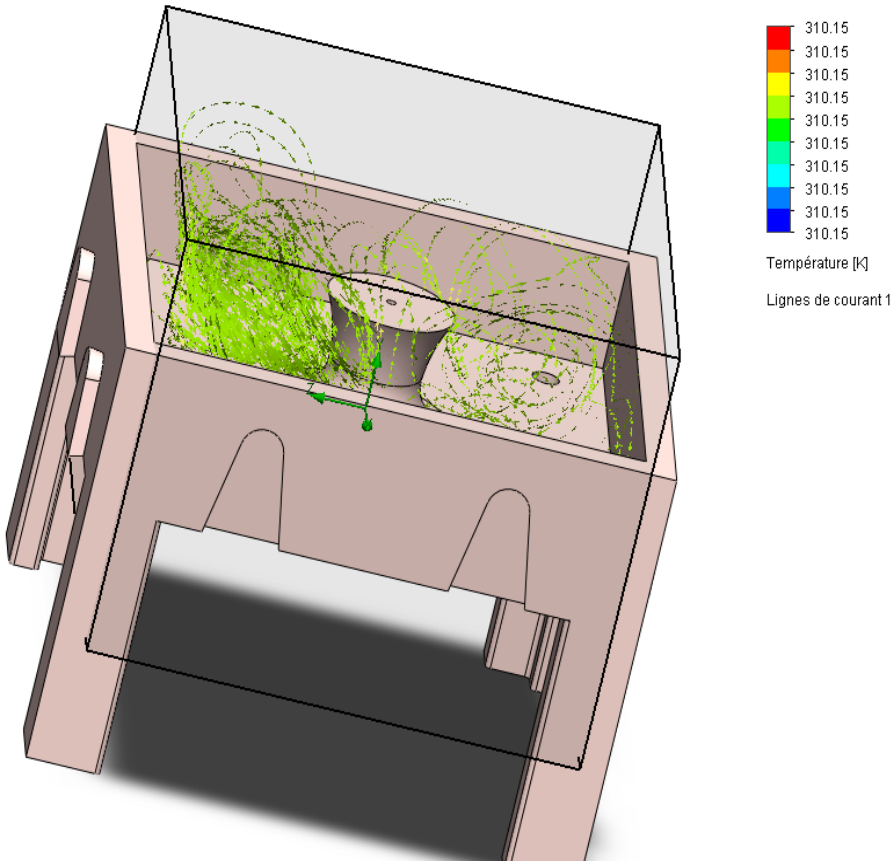

Figure 30: Flow simulation setup and results for bottom-fed mini water bath

The inlet of the mini water bath received water at a flow rate of 125ml/min supplied by the pump. Each Monochamber was filled with 500 ml of water over a duration of 4 minutes. The inlet area was defined as 100*100 mm, and with the density of water (1000 kg/m^3), the corresponding mass flow rate was calculated as 0.00208 kg/s and applied as the input boundary condition. The computational mesh was generated, and the solver was iterated until 40 convergence steps (Figure A), resulting in negligible pressure (Figure B) and temperature variations (Figure C) throughout the mini water bath, indicating stable flow conditions during bottom feeding.

4.4 Fabricated part 3D printing

4.4.1 Trial fabrication

4.4.1.1 *Test components by FDM*

The 3D prototype was initially tested using Fused Deposition Modeling due to its low cost, minimal post-processing requirements, and high geometrical accuracy. This technology was applied to trial a developed model ranging from a single chamber to four-well perifusion chambers using a swept pipe configuration, 4 wells in the same water bath, and a dovetail coupling trial (**Figure 31**). A classical water chamber was also modeled as a swept pipe and tested for successful fluid flow; however, it was excluded from further development due to temperature-related issues. Additionally, male and female parts of the dado joints were tested and successfully validated for geometrical accuracy. None of the trialled 3D sketches were shown here. After the joint fabrication for both male and female parts, the amount of material used after removing the raft and support was 41 g and 34g, respectively. Although this technology can achieve the required geometry, the resulting prototype exhibits surface roughness and porosity that may trap cells, making it unsuitable for perifusion experiments.

4.4.1.2 *MSLA-based tested component – mono islet chamber with support alone*

During the trial phase, different models and printing technologies were tested. For instance, a complete individual set-up was attempted using MSLA-based technology; however, alignment issues were observed. In another case, a mono-chamber unit with four single supports was fabricated using MSLA with tough resin, though this approach also presented certain limitations (**Figure 32**).

4.4.2 Final version of 3D printed monochamber prototype: SLA

After evaluating different approaches, the limitations associated with thermoplastic properties and the misalignments caused by the LCD-based curing process led to both methods being discarded. Consequently, the final prototype was fabricated using SLA Grey Pro resin through stereolithography (**Figure 33**). This technique relies on laser-based curing, in which each layer is solidified sequentially, and the process was carried out on a Formlabs 3BL printer (maximal printable volume is 335*200*300mm), capable of producing layer thickness between 25 and 200 microns. Since increasing the layer thickness can negatively impact the dimensional accuracy of the model (Salmi, 2016), a layer thickness of 50 microns was selected to ensure both efficiency and precision in fabrication. Upon completion of printing, the following post-processing steps were performed.

4.4.2.1 *Post processing*

Once fabrication was complete, the printed part was carefully detached from the build platform, and the supports were removed manually and partially by tool with caution, as shown in **Figure 34**. The part was then immersed in isopropyl alcohol (90-99%) for several minutes to eliminate any residual uncured resin. Following this, compressed air was applied to ensure the surface was fully cleaned and dried. Finally, the component was placed in a Formlabs UV curing oven, where it was exposed to multidirectional light at a controlled temperature of 60°C for 40 minutes, allowing the resin to fully polymerize and stabilize its mechanical properties. No surface finishing was performed to enhance the look.

A

B

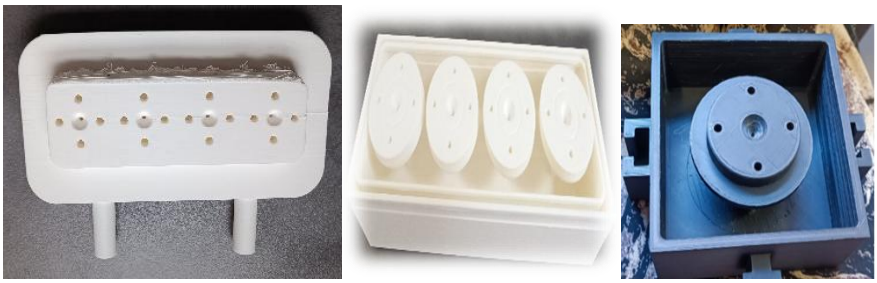

C

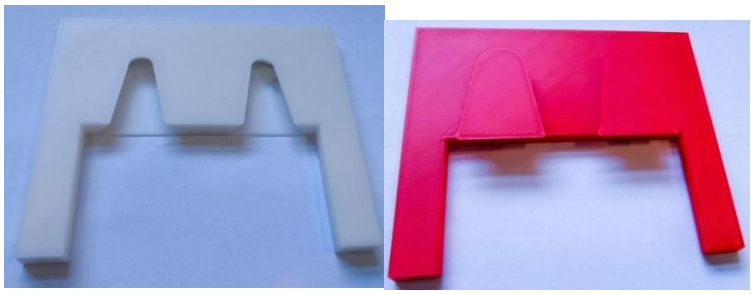

Figure 31: FDM 3D printed trial parts

A) FDM-based Zortrax 3D printer (200*200*180mm), B) several models of fabricated prototypes tested by FDM with individual well (mono) and four combined, C) male and female parts fabrication by ABS material for dado joint clearances. After the fabrication process, the male joint weighed 54g, but its weight was reduced to 41g once the support material was removed. Similarly, the Female joint initially weighed 48g with the raft, but it decreased to 34g after the raft (extra support) was removed.

A

B

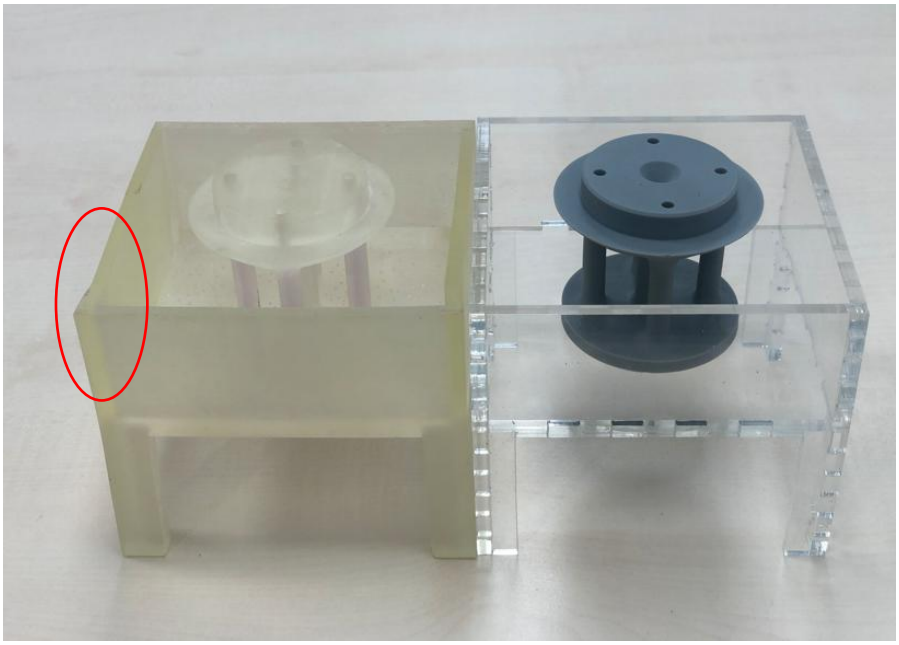

Figure 32: Trailed MSLA parts

A) 3D printer any cubic mono MSLA-LCD based, volume part (192*120*245 mm) B) 3D printed parts MSLA parts, noticed misalignment in the corner of the water bath, made with tough resin– shown in red (left), glass cut water bath with the same dimensions and the legs were assembled by zigzag cutting (big pores – not suitable). The separately 3D-fabricated middle part is shown in blue; made with Form Futura Grey - not water-tight.

4.4.2.2 *SLA printed parts*

A

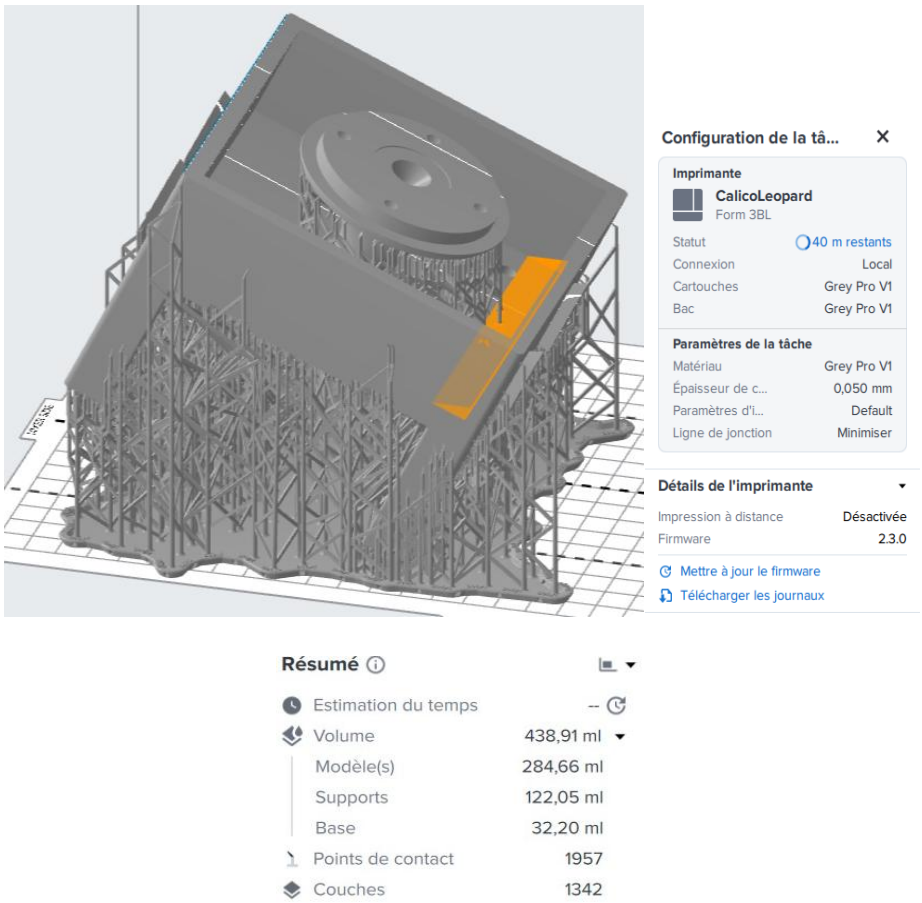

B

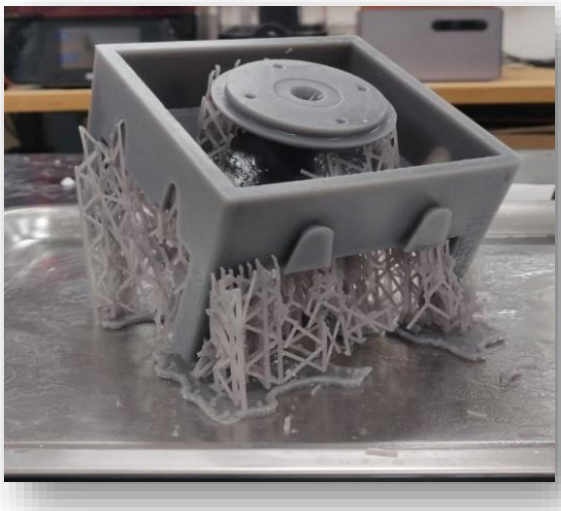

C

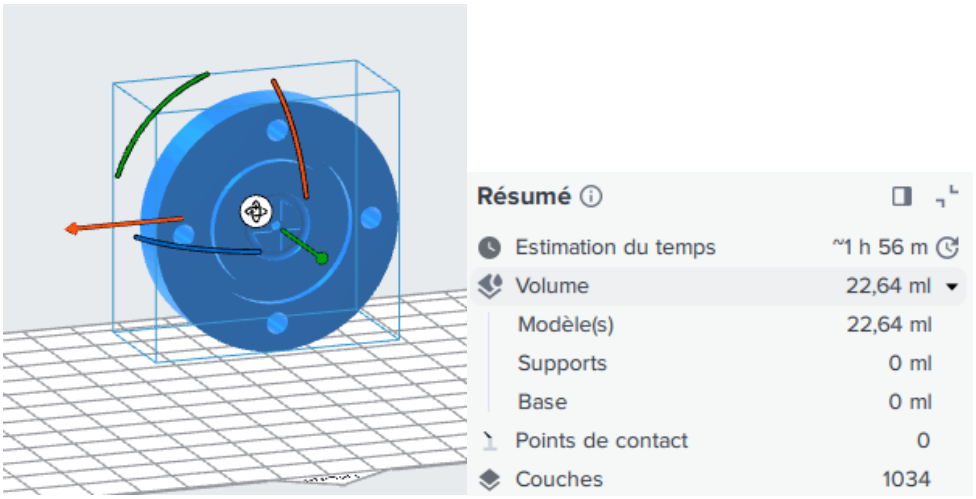

Figure 33: Removed the monochamber from the build platform and fabricated the lid

A) 3D fabricated mono chamber- modeled by Solidworks, transferred to Simulation software (mesh) - Slicing tool (Halot box) developed by using Autodesk Fusion 360° CAD Tool. B) fabricated parts, half-removed supports. A printer used volume to fabricate a mono-chamber 284.66 ml. 1957 supports were created, and the number of layers used was 1342. C) Top view of the fabricated 3D mono chamber (islet chamber) lid. The simulated STL file (bottom left) for and generated quantity of material and supports used for the fabrication is shown in the figure (right bottom).

A

B

C

Figure 34: Post-processing steps after fabrication

A) post-processing set-up, showing a cleaning tank containing isopropyl alcohol (IPA) used for rinsing the printed material. B) an air machine to dry the material for removing residual solvent. C) UV curing unit used to complete polymerization of the printed Monochamber, typically operated for 20-40 minutes to achieve full material hardening.

4.5 Discussion

In the process of developing a 4-stream perifusion chamber, after several iterations smooth surface was achieved through an SLA-based fabrication technique without missing any alignment. This was achieved by engaging continuous design optimization, simulation analysis, and consultation with domain experts, which guided the evolution of our prototypes toward a feasible final solution.

The design journey began with three-dimensional modeling using SolidWorks, where successive prototypes were developed to conceptualize the perifusion system. This stage proved relatively straightforward, as the software's integration of simulation tools allowed us to visualize and test our designs before moving into fabrication. Integrated simulation analyses within SolidWorks facilitated an early assessment of feasibility, enabling us to predict material behavior and to identify areas of potential weakness in the prototypes.

To validate structural robustness, the analysis under hydrostatic pressure was performed to test parameters. Simulations were conducted to assess stress and displacement across pressure conditions due to water load on the water bath. The result demonstrated that the impact of hydrostatic pressure on the mono-chamber water bath was negligible. Complementary computational fluid dynamics (CFD) simulations were carried out in SolidWorks to analyse flow dynamics in the islet chamber and its water bath. By defining appropriate boundary conditions for the inlets and outlets, and by applying static pressures, we were able to replicate realistic flow conditions. Meshing and iterative process imposed minimal additional velocity, temperature and turbulence on both the islet chamber geometry and mini water bath. The structurally cone-shaped islet chamber facilitated laminar flow with

a central stream at the flow rate of 1ml/min. These results strengthened our confidence that the design was mechanically viable and could be translated into fabrication.

While the design phase was completed, the choice of fabrication technology emerged as a critical decision point. Selecting an inappropriate technique would not only compromise prototype functionality but also risk both time and resources. Thus, we systematically evaluated multiple additive manufacturing approaches. Initially, FDM (Fused Deposition Modeling) was considered due to its accessibility and widespread use in rapid prototyping. However, FDM is based on thermoplastic materials, which solidify upon cooling. The resulting surfaces were consistently rough, and the fabricated parts lacked the fine resolutions required for cell survival. Furthermore, the mechanical finish was unsuitable for the precise alignment demanded in a perifusion setup. So, FDM was excluded from further consideration.

We next explored MSLA (Masked Stereolithography) printing, which uses LCD-based photopolymer curing. Although MSLA offered advantages in speed and resolution, practical limitations soon became apparent. The available build volume restricted the scale of the device, making it difficult for large integrated structures. When testing a mono chamber set-up, adhesion using glue for stability within a water environment proved unsustainable, as it weakened under liquid exposure. These challenges made MSLA unsuitable for the long-term stability and robustness that our perifusion system required.

Learning from these limitations, we turned our attention to SLA (Stereolithography) printing, specifically using Grey Pro Resin. The printer offered superior precision and large volume compared to MSLA. Moreover, SLA produced a smooth surface finish, eliminating many of the issues encountered with FDM. Grey pro resin itself has favourable mechanical and thermal properties; tensile strength of approximately 61MPa, and an elongation break of 13% post-

curing. Importantly, a heat resistance of 77.5-78°C, excellent for functional prototype, fit testing, and low creep deformation compared to standard resins, which makes it highly suitable for the conditions expected in our perifusion protocol. These properties reassured us that the material could withstand the operational environment without deformation, brittleness, or failure.

An additional consideration was the practicality of printing the entire setup as a single unit rather than fabricating smaller components and assembling them afterward. This approach eliminated the need for adhesives. By leveraging the build capacity of the Formlabs Form 3BL printer – with a maximum printable volume of 335 × 200 × 300 mm – we were able to fabricate complete structures within a single print cycle by simplifying the post-processing workflow.

By considering this, the evolution of the chamber development underscores the importance of choosing fabrication technologies aligned with functional requirements. The final decision to adopt SLA with grey Pro Resin was not simply a matter of material compatibility, but rather a culmination of iterative learning and problem-solving.

4.6 Conclusion

In summary, through successive rounds of design, expert feedback and fabrication trials, we successfully developed and fabricated four individual components of the mono chamber. The discussion of these trials emphasizes that, though multiple technological pathways exist, the responsibility lies in critically matching the technology to the specific needs of the application. Once a fabrication path is chosen, reverting to earlier options becomes impractical. Therefore, the lessons learned in this development process not only shaped the present prototype but also provided a framework for future iterations of perifusion system assembly in islet research.

CHAPTER 5

Four Independent Monochamber (islet chamber with supports) Assembly and validation

5 Chapter V: Four independent monochamber assembly and validation

In preparing for the assembly of the perifusion system, several key design and operational requirements were carefully evaluated to ensure both functionality and reliability.

5.1 Considerations for assembly

5.1.1 Space requirement:

Operating a perifusion set-up with multiple chambers presents significant practical challenges in terms of coordination and workflow. Even with two chambers, switching between collection points, monitoring flow, and ensuring synchronised sampling requires constant attention and manual handling. When the number of chambers increases to four, this workload effectively doubles, demanding precise timing and efficient organization to prevent errors or sample overlap.

Therefore, a major focus during system assembly was to determine the optimal placement and accessibility of each component – including the chambers, tubing layout, fraction collector, and sampling ports to streamline operation.

The arrangements of the chamber were planned in parallel so that each would receive equal flow from the peristaltic pump, avoiding discrepancies in tube length that could affect experimental results. I also took great consideration for the entire tube length, which needed to match the pump and flow lines, while being resistant to repeated use and compatible with the fluids involved. Particular attention was also given to the sealing of the chamber lids, since leakage or poor closure could compromise both sample collection and sterility.

5.1.2 The cover of the mono-chamber water bath

The choice of cover plate for a mini water bath also focused on ensuring a secure closure. The initial decision of selecting the glass-based cover with the application of glue didn't fix well, and when there was testing of liquid sample leakage noticed we then moved to choosing an aluminium-based cover plate set up to fix with a 3D printed mono chamber prototype. Initially, a glass-based cover was selected and attached to the 3D printed Monochamber prototype using adhesive. However, this approach did not provide a reliable seal, and leakage was observed during liquid testing. Consequently, the design was revised to incorporate an aluminium-based cover plate, which offered a leak-proof fit and high surface energy with the 3D printed chamber (**Figure 35**). The parallel fixation by dado joint is established with iterative clearances (**Figure 36**).

5.1.3 Tubing placement

The choice of connectors and tubing was also critical. As a standard routine, a 1/16*30-dimensional tube was used for connection to maintain the flow rate from the pump. All the tubes are placed at the same distances from the pump to have an equal flow.

5.1.4 Temperature regulation

Temperature stability represented another important consideration, as the system relies on a water bath to maintain controlled conditions. The regulation mechanism was also anticipated, and a proper water bath outlet was also fixed on the assembly area.

5.1.5 4-stream peristaltic pump

The peristaltic pump allows the fluid path for each stream. I have used identical tubing to reach maximal accuracy of delivering a sample to the chamber by enforcing the calibration for

the chamber volume of 0.5 ml in 20 seconds. The real calculation of the flow rate will take place once the assembly of the fraction collector is installed.

5.1.6 Flow direction-driven pressure balancing in mono-chambers

To ensure uniform temperature distribution across each individual mono-chamber (112*112mm), inlet and outlet provisions were incorporated to facilitate pressure release and flow regulation. When the fluid entered from the top of the chamber, leakage was observed along the sidewalls. This is likely due to the pressure gradient generated by the vertical inflow, which creates localized turbulence and uneven pressure distribution against the chamber walls, exceeding the sealing tolerance at certain points.

In contrast, when the inlet and outlet were positioned at the bottom of the chamber with flow introduced through the bottom port and released through another-lo leakage occurred. This configuration promotes a more stable and laminar flow, minimizing vertical pressure buildup and preventing fluid from accumulating near the upper seals. The bottom-to-bottom flow path also allows better hydrostatic balance and pressure equalization within the chamber, maintaining structural integrity and ensuring more uniform temperature transfer (**Figure 37**).

5.1.7 The whole assembly set up (without FC)

The perifusion system was successfully assembled and calibrated to establish stable flow dynamics prior to biological experimentations. The configuration incorporated a regulated gas line and assisted components to ensure uniform perifusion. Preliminary calibration verified steady flow rates and pressure balance, indicating that the system is mechanically stable and ready for subsequent islet perifusion studies. Although no biological samples were tested at this stage, the calibration confirmed the reliability of the assembled setup for future experimental applications (**Figure 38**).

A

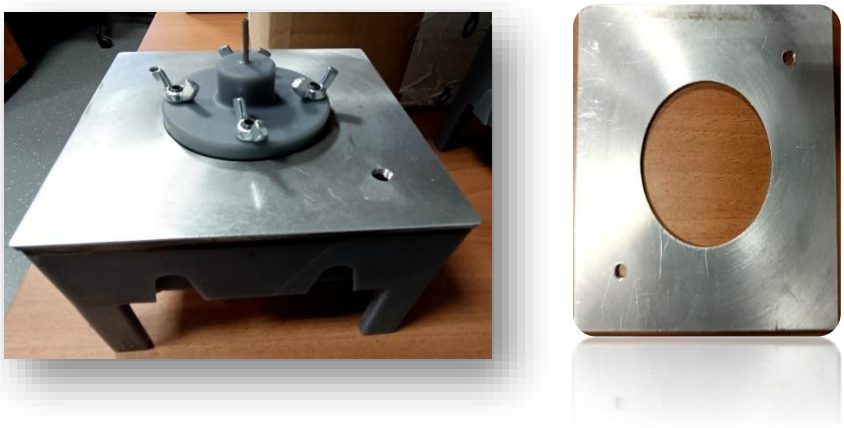

B

Figure 35: Plexiglas replaced by aluminium cover plate

A) The chosen Aluminium-based sheet to cover the mono chamber water bath with a thickness of 3mm, with the dimensions of 112*112mm, with the inlet and outlet holes with a diameter of 4.5mm. SLA printed parts tested with 3D printed lids, which were locked with butterfly nuts, B) glass-based water chamber lid, the glue doesn't have much effect on the resin edges.

A

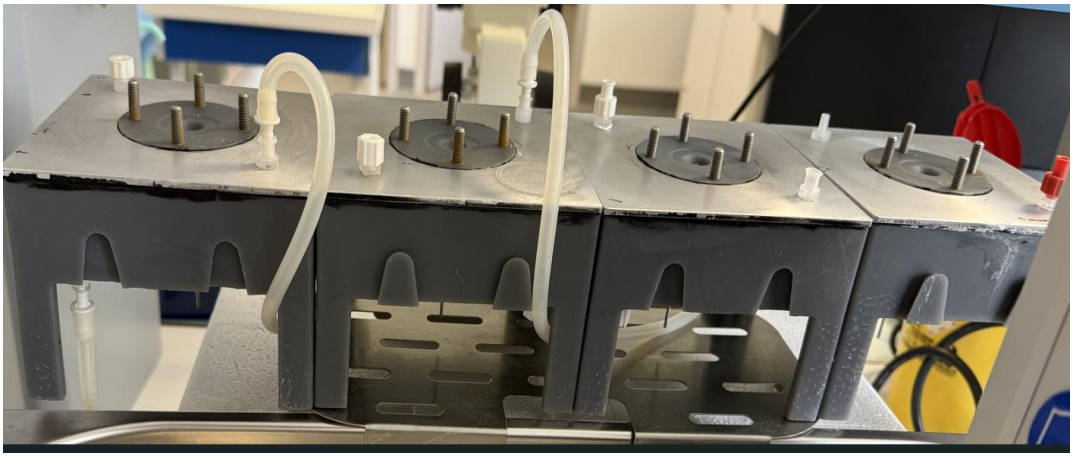

B

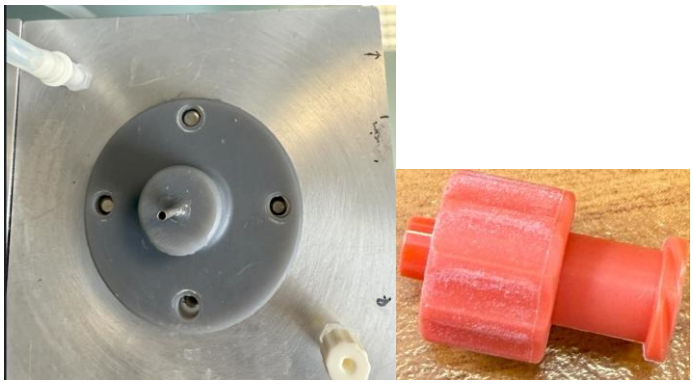

Figure 36: 3D-fabricated 4-stream perifusion mono chamber

parallel connection of a mono chamber by using dado joints (A), and each assembled with 4 inox screws to facilitate the lid, aluminium cover plate with the dimension of 112*112mm fixed tightly to avoid leakage, each Monochamber designed with 2 inlets and outlets, the unused were properly closed with a combi stopper red has an inner diameter of 5 mm (B), between the hole of aluminium plate and stopper there was a connector used. The liquid flow is 125 ml/min, achieved through a separate peristaltic pump (Masterflex). Each Mono chamber has a volume capacity of approximately 490ml, so it takes around 4 minutes to fill the water chamber.

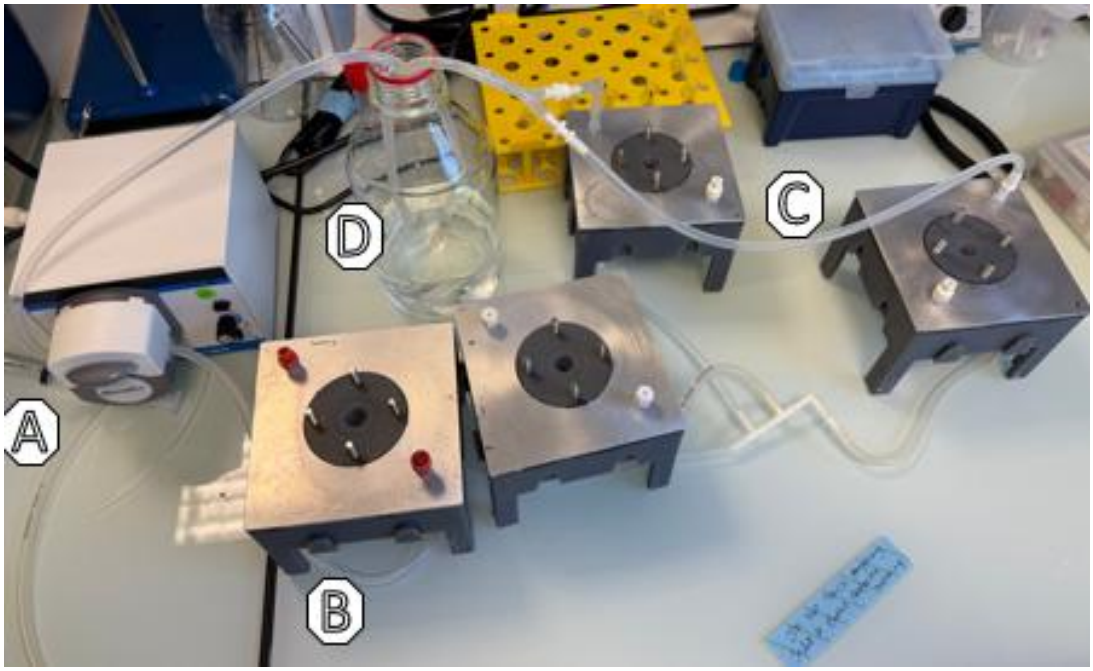

Figure 37: Bottom-fed set-up for flow distribution

Flow is initiated by a peristaltic pump (A) and introduced through a tube connected to the bottom inlet of the first chamber. The flow exited from the bottom outlet (B) and continued sequentially through the subsequent chambers using the same bottom-fed configuration. The system was designed such that water exited through 2 outlets located at the top (C), which then merged and returned to the same container serving as the reservoir (D) for continuous circulation. All chambers were filled simultaneously, ensuring uniform water distribution and stable circulation throughout the system.

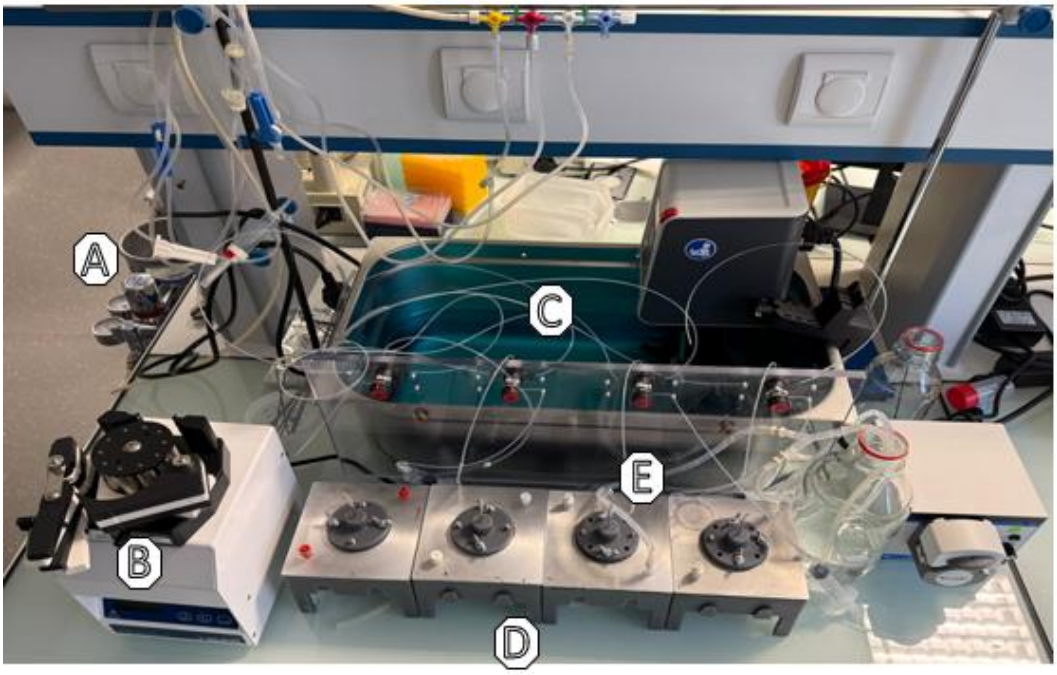

Figure 38: Assembled 4-stream perifusion system

The perifusion system was fully assembled to enable continuous and controlled medium circulation through all components. The set-up included a regulated gas supply (A) to maintain a desired environment for cell survival, a 4-way peristaltic pump system (B) to ensure uniform flow distribution, and a large water bath (C) providing stable thermal control for all chambers. Four mono chambers (D), each equipped with individual caps, were connected in parallel using dado joints to achieve simultaneous perifusion and consistent flow dynamics across all units. The inlet and outlines (E) were carefully configured to establish a closed-loop water circulation between the bath of mono chambers. However, the final assembly set-up will be completed with the real-time fraction collection.

5.2 Four - stream fraction collectors

5.2.1 Challenges

As the individual Bio-Rad fraction collector model previously used for perifusion assays was discontinued, a custom four-stream fraction collector was developed to accommodate simultaneous sample collection from four independent chambers. The system was designed to be modular, efficient, and compatible with the perifusion set-up, ensuring synchronised collection across all channels.

5.2.2 Collector unit

Each collector unit was equipped with a rotating sample holder capable of accommodating 35 collection tubes for a single rotation, with a dimension of 192mm with a height of 70 mm. For tube placement, the dimension of the sketch is shown in Figure B. The collector case model was fabricated by using FDM-based technology **(Figure 39)**. The total weight of the collector case is about 400g. After placing all the tubes of 5mL, the total weight becomes 650-700g based on the weight of the tube. However, the regular protocol of collecting samples is every 2 minutes (1ml/min).

5.2.3 Assembled 4-way FC set up – half done

The system was mounted on a custom-fabricated wooden base that provides stability during operation. 4 individual Stepper motors were integrated to control the rotation of each collector disc, providing precise movement and timing for all four collection channels. The entire assembly was made in IMT Nord Europe Douai-Fab lab **(Figure 40).**

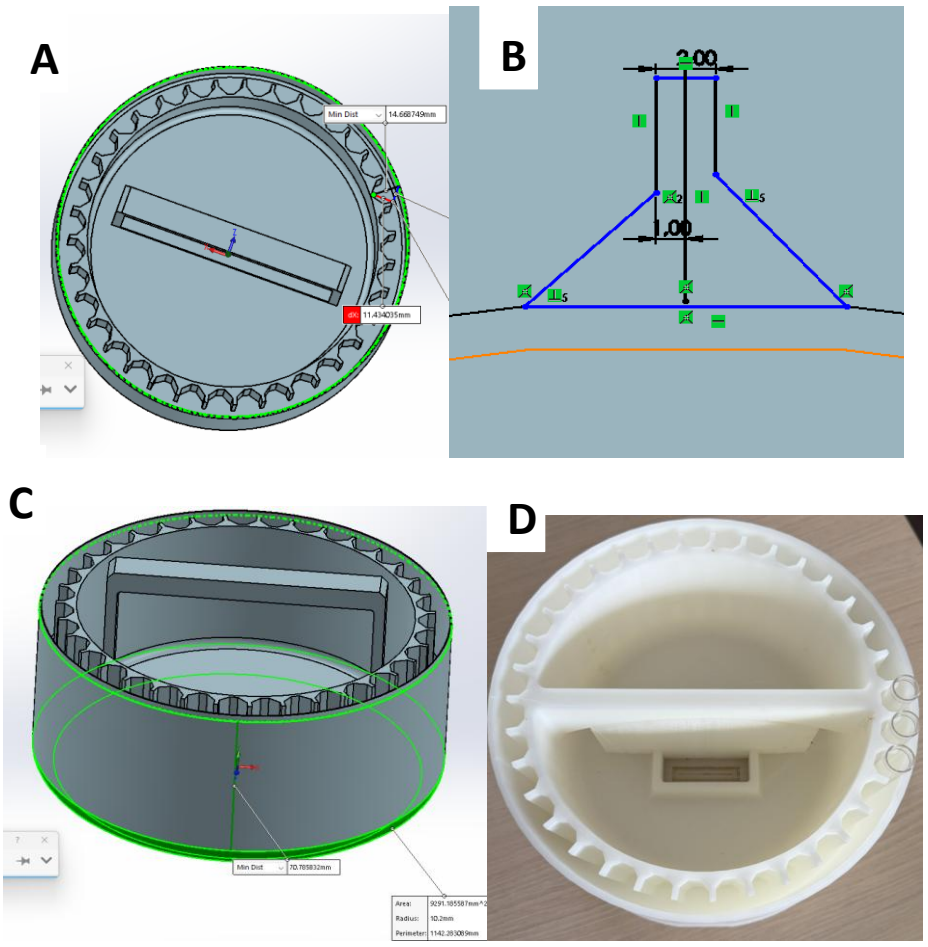

Figure 39: 3D modeled and fabricated single-unit collector case

A) Top view of a 3D model of one collector case with the dimensions of 192 mm, extruded with a height of 70 mm, B) sketch design for tube (~1.7mm) placement is elevated, C) side view of the collector case with a handle. D) FDM fabricated the collector case (~400 g) and tested it with tube placements. (FDM: Fused Deposition Modeling)

A

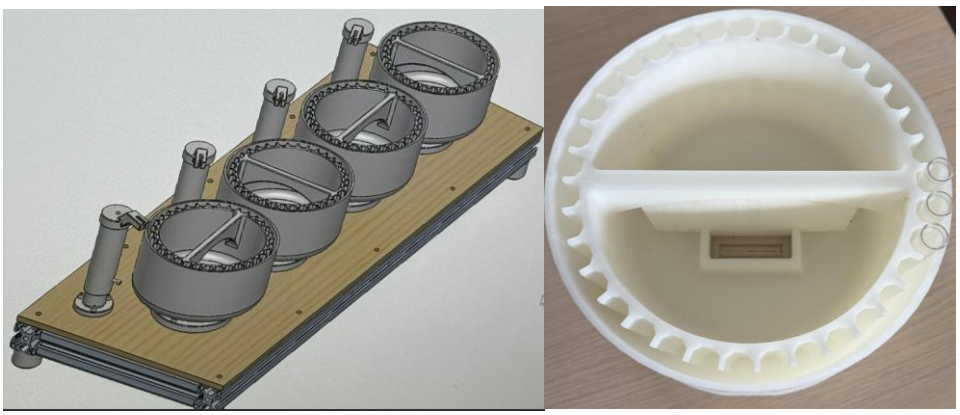

B

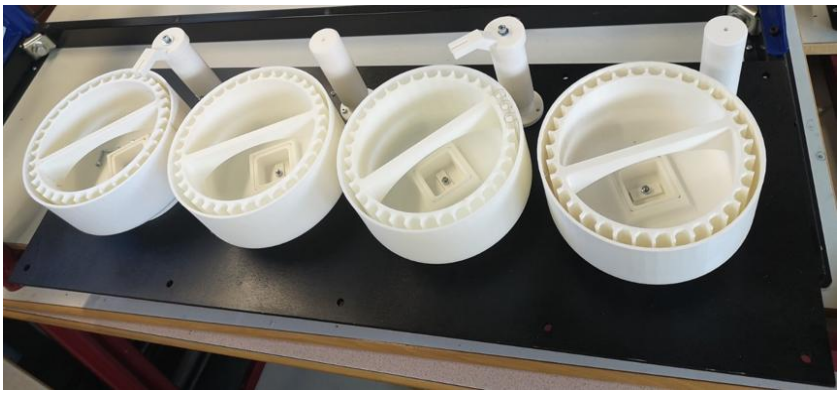

C

Figure 40: Assembly set-up of FC without display unit

A) Entire 4-stream fraction collector 3D modeling set-up, including collector case (screwed with stepper motor), arm provisions, wood base and stepper motor provisions. On the right, the printed single collector case was shown, and it was tested to see if the tube could fit into the provisions. B) 3D printed set-up of partially assembled on a wooden base. C) 4 independent stepper motors (NEMA 17) were fixed for each collector case.

5.2.4 Electronic control unit and coding support

The development of the interface kit and associated coding is currently managed by the Fab Lab team. As these tasks involve technical customization, the completion of the assembly setup has been postponed until the integration is finalized.

5.3 Discussion

Proper spacing, tubing organization, and gas provisions are essential for establishing a stable and reproducible perifusion environment. The water chamber lid is made up of aluminium because its higher surface energy compared to engineered plastics provides better adhesion for gluing (Zdziennicka, Krawczyk et al., 2017). These parameters directly influence flow uniformity, oxygenation, and temperature maintenance, all of which are crucial for preserving islet viability during extended experimental runs. Hence, the physical layout of the setup — including the placement of chambers, tubing length, and accessibility of connectors — must be carefully planned before initiating a new perifusion configuration.

The overall success of the perifusion system assembly depends strongly on the effective integration of its associated components. This collector serves as a critical element for enabling simultaneous and synchronised sampling from multiple chambers, thereby improving experimental throughput and data comparability. Precise control of the peristaltic pump remains the most vital factor. The pump governs the perifusion rate and ensures that each islet chamber receives an equal and uninterrupted flow of media. Inconsistent flow or pressure fluctuations could alter oxygen and nutrient delivery, thereby affecting the metabolic and secretory responses of the islets. Consequently, optimising pump calibration, tubing diameter, and connection tightness becomes essential for maintaining experimental reliability.

The direction and position of the fluid entry critically affect the internal pressure distribution. A top-fed system tends to create uneven vertical pressure gradients and local turbulence, which stresses the side seals. Bottom-fed designs support laminar, pressure-balanced flow, leading to structural stability and leak prevention. By considering all aspects, the system components were assembled properly, and it will be completed as a full setup once integrated with multiple FCs. The geometry of the 3D-modeled collector case, designed to accommodate 35 collector tubes based on their specific dimensions, was successfully fabricated four times. All assemblies, including the arms and the collector case, were precisely aligned and mounted on a properly dimensioned wooden base. This complete setup will undergo final evaluation following the integration of the control coding developed by the Douai team.

5.4 Conclusion

The successful flow analysis confirms the perifusion system's ability to maintain controlled conditions and support functional performance during dynamic assays. However, the proper installation and integration of the fraction collector, completion of coding and interface development, and the availability of human islets will together ensure the full operational readiness of the perifusion system for validation.

CHAPTER 6

Sensor-based Measurements of Islet Respiratory Dynamics - Preliminary data

6 Chapter VI: Sensor based measurements of islet respiratory dynamics – preliminary data

6.1 Introduction

In pancreatic islets, energy metabolism is primarily governed by nutrient availability and cellular respiration, which are tightly linked to insulin secretion. The coupling between glucose metabolism and ATP production serves as a key signal for insulin release. In 2006, Ian R Sweet demonstrated that glucose-driven respiration in perifusion assays can serve as a predictor of islet quality and highlighted its islet-specific nature (Henquin, Dufrane et al., 2006; Sweet and Gilbert, 2006). This work also compared handpicked islets with non-islet tissue, underscoring the specificity of the metabolic response. The tools for assessing mitochondrial activity have progressed from Clark electrodes (dissolved oxygen during glucose challenges), to optical perifusion (islet-specific OCR), to stirred microchambers (OCR scaled to viable mass), and finally to partitioning of profiling by Seahorse (Papas, Pisania et al., 2007; Sweet, Gilbert et al., 2008; Silva and Oliveira, 2018; Shirato, Hsueh et al., 2024). This study also pointed out that OCR increased linearly with the number of viable cells in the perifusion chamber.

Following their work, I performed the sensor integration in the perifusion set-up by using a PreSens rented sensor to measure partial oxygen concentration within islet samples (n=3). Although oxygen concentration (PO_2-mg/L) could be monitored, respiration rate could not be derived since it requires temporal changes in oxygen levels; benchmark CO_2 release (%CO_2) was also observed, despite its importance as a key byproduct of energy metabolism. The subsequent transition to the Pyro Science tool, which enabled real-time measurement of both oxygen concentration and respiration rate (ΔOCR µmol/L/min). The accompanying pyro developer software was used to process data and perform multiple analytical specific

intervals, converting oxygen units across more than four different scales, and applying smoothing algorithms. Initially, the pyro tool was tested using INS-1 cell clusters to assess respiration rates at varying cluster sizes. The observed results supported the groundwork to test the sensor in human islets (13 donors), and measure their oxygen consumption in real time, parallel to insulin secretion.

6.2 Oxygen Concentration-based PreSens technology measurements

The perifusion system has lower operational complexity due to the sensor connection. The tested sensor was commercially rented from PreSens Technology (limit of detection ~0.03%O_2; ~0.015-0.020 mg/L), which is a T-type miniaturised chemical optical oxygen sensor integrated into flow-through cells that allows non-invasive online monitoring of oxygen measurement by integrating post chamber placement. 300 IEQ of human islets per chamber were perifused with non-stimulatory glucose (basal; 3mM) for 10 mins, then stimulated with 15 mM glucose for 20 mins, then cells are challenged with inhibitor oligomycin (5µM-20mins) and an uncoupling agent carbonyl cyanide-4-(trifluoromethoxy) phenylhydrazone FCCP (1µM-20mins) to see the metabolic activity changes in islet behaviour, and the used concentrations inspired from previous studies (Pradhan, Lee et al., 2022). We noticed during high stimulation (G15), increased CO_2 range for a few minutes and decreased O_2 concentrations, consistent with increased mitochondrial oxidation under stimulatory conditions (Umeda, Ishizaka et al., 2021). The drug-evoked shifts during ATP synthase inhibition (oligomycin) were observed next 20 mins. In contrast, during the uncoupling effect (FCCP), both PO_2 (mg/L), PCO_2(%) had reduced concentrations. These preliminary experiments were performed in non-diabetic donors (n=3), and the metabolic function and efficiency of their mitochondria were monitored under stimulated perifusion **(Figure 41)**. Donor characteristics are represented in **Table 5**.

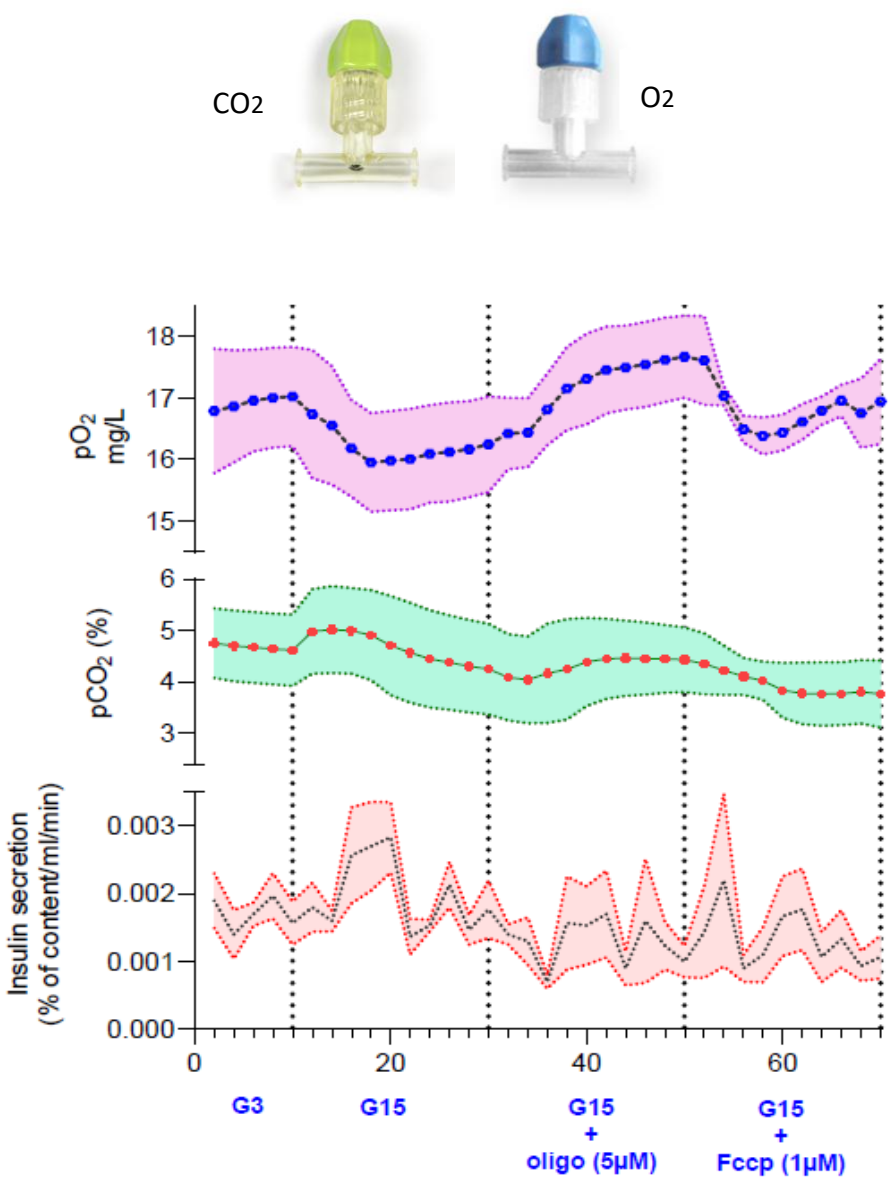

Figure 41: Oxygen concentration and CO_2 measurement from non-diabetic donors

Partial pressure of dissolved oxygen over time, PO_2 (mg/l) (pink in colour): basal concentrations reduced over 20 mins due to consumption and increased again due to complex V inhibition (oligo), then decreased due to the uncoupling effect of FCCP. CO_2 (%) (green) concentrations at 2-minute intervals; basal concentration increased slightly during G15 and went down during the second phase (second 10 minutes). The insulin secretion profile due to metabolic flux is shown in red. Data represented as mean ± SEM from N = 3 non-diabetic donors. Respiration measurements by integrating PreSens Technology (response time<60s). (G3 = 3 mM glucose; G15=15 mM glucose; Oligo = oligomycin (5 µM), FCCP=6 µM), (Limit of Detection ~0.03%O_2).

6.3 Pyroscience tool measurement for respiration

Under this technology, only the O_2 sensor (firesting probe) was implemented in the perifusion experiments by placing it close to the chamber, to assay the respiration behavior of human islets. It starts to detect the oxygen concentration from ~0.01mg/L (as per the manual). The manufacturer describes the sensor uses a REDFLASH optical dye, which was designed to minimise drift.

6.3.1 Preliminary assessment of cellular respiration using cell lines before human islet analysis by using Pyro Tool

The Pyroscience oxygen sensors were connected to the parallel chambers to measure the change in oxygen drop over time; both were connected to the post chamber. The full setup of sensor attachment with the perifusion system is shown in **Figure 42**. The functional capacity of pancreatic beta cells remains a primary focus in diabetes research, given their critical role in glucose-stimulated insulin secretion. While multiple cell types contribute to overall islet physiology, beta cells occupy a unique role as the primary mediators of insulin release. Insulin secretion is tightly coupled to glucose metabolism and the efficiency of mitochondrial respiration (Place, Domann et al., 2017), linking cellular bioenergetics to endocrine function. Recent studies have emphasized the importance of directly quantifying respiration in beta cells to better understand the metabolic mechanism of insulin secretion (Kener, Munk et al., 2018; Hertig, Maddah et al., 2021). The experiments were performed by using INS-1 832/13 cells, which were cultured, seeded, and organised into clusters to evaluate their bioenergetic responses. Mitochondrial respiration was assessed under varying glucose concentrations to capture the dynamic interplay between cellular metabolism and insulin secretion. Practically,

A

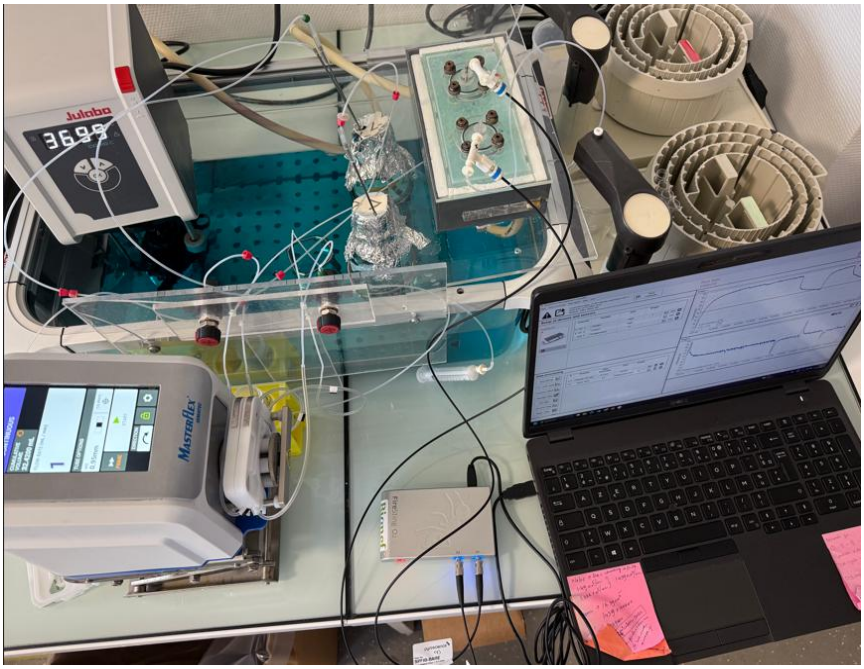

B

Figure 42: The pyro sensor tool setup with the perifusion system

A) Both O_2 sensors (Sterile Oxflow - firestring) were connected at the post chamber connectivity. The flow cell is a glass tube with a sensor spot attached to its inner wall. The fiber optic cable from firesting connected to the optical port of the flow cell and reads the lights emitted from the spot. The dye inside the spot changes its intensity based on the local oxygen concentration in the flowing medium. B) Flow through cell with the attached sensor spot (left figure), Multi-channel analyte meter (firesting) (right figure).

A

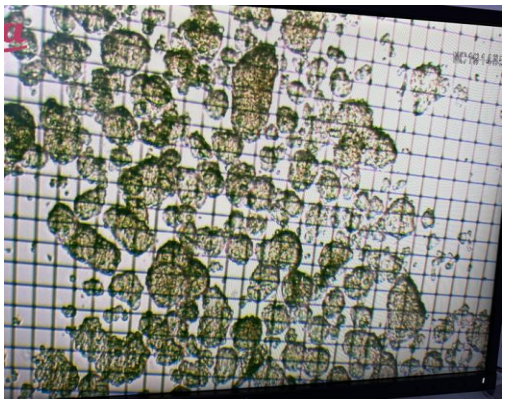

B

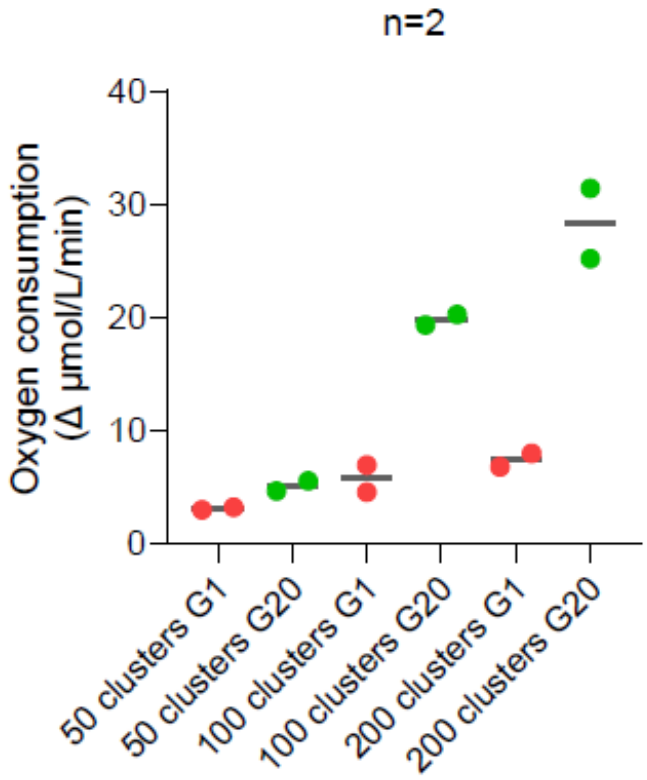

Figure 43: Glucose-dependent respiration in INS-1 clusters of increasing density

A) An image of dispersed clusters from a cell line is shown. B) Ins 1 clusters from 50 to 200 stimulated with low glucose 1 mM (G1), shown in red, and high glucose 20 mM (G20), shown in green. Value showed 10 minutes of stimulation in each condition. The graph represented a change in oxygen concentration over time as consumption, with the unit of delta µmol/L/min. pyro tool-generated data plotted in Prism and represented as mean ± SD (n=2). (O_2 – FTC (flow through cell), LOD: 0.02%) (LOD: Limit of Detection), (Response time<30s).

as the number of cells within a chamber increases, the rate of oxygen consumption also rises proportionally. To examine the effect of cell density, 50, 100, and 200 clusters were seeded per chamber and analysed for glucose-stimulated respiration. I observed a progressive increase in oxygen consumption (ΔOCR µmol/L/min) with higher cluster densities, following 20 mM glucose exposure over 40 minutes **(Figure 43)**. These results show that both low and stimulated respiratory capacity correlate with cluster density, highlighting the metabolic resilience of beta cell populations and offering a framework to evaluate this phenomenon in human islets. The observed increased OCR in G20 in a cluster number-dependent manner also allowed for a greater difference from basal G1, indicating that a minimum number of islet-like clusters is required for the proper analysis of cell metabolism.

6.3.2 Pyro tool assessment with human donors

Following the cell lines' observations, the sensor was tested in the human islets. The corresponding superimposed profiles of insulin secretion and oxygen consumption (OCR) are shown in the figure, obtained from experiments using islets isolated from 13 donors. Insulin secretion is expressed as concentration (uUI/ml/min) to minimise potential misinterpretation in cases where the tested compound may influence the insulin content (IIC) of the islets. The unit of oxygen consumption shown here is delta µmol/L/min. The superimposed curve demonstrated that the integration of the sensor did not interfere with or alter the dynamic insulin secretion profile (**Figure 44**). The donor characteristics are shown in **Table 6.**

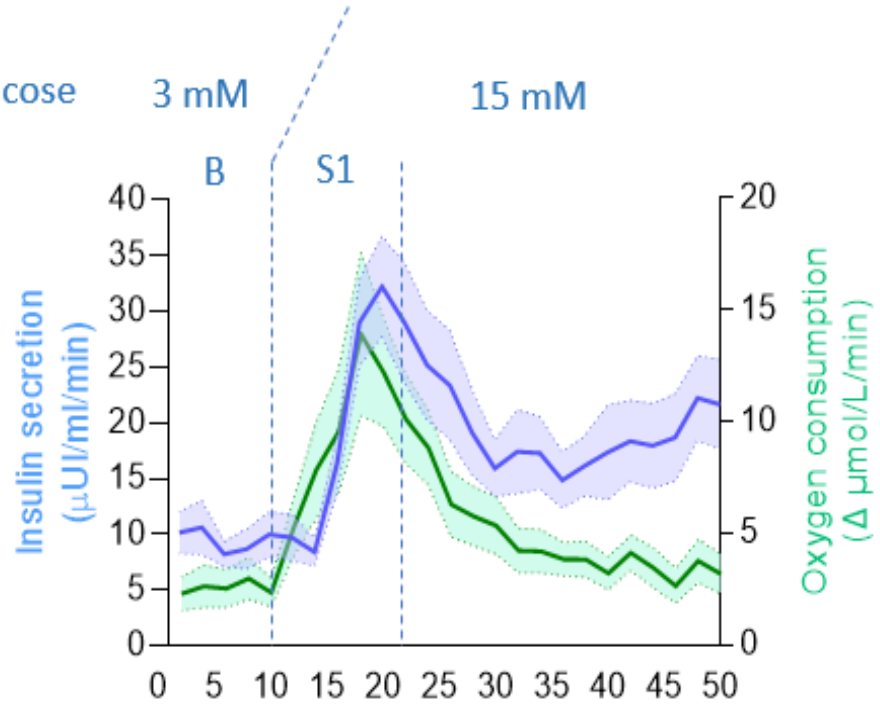

Figure 44: The superimposing of insulin secretion and OCR (consumption) curve

Superimposed profiles of insulin secretion (uUI/ml/min) and oxygen consumption rates (OCR - delta µmol/L/min) in response to glucose stimulation (n=13). Isolated islets were first perifused for 10 minutes with basal glucose (3mM), followed by 40 minutes with stimulatory glucose (15 mM). Samples were collected every 2 minutes. The increased consumption and insulin release during the second phase than the basal B (SI>1). The overlaid traces illustrate that the increase in oxygen consumption occurs prior to insulin secretion, indicating enhanced mitochondrial activity and ATP production that drive the subsequent exocytotic release of insulin.

A

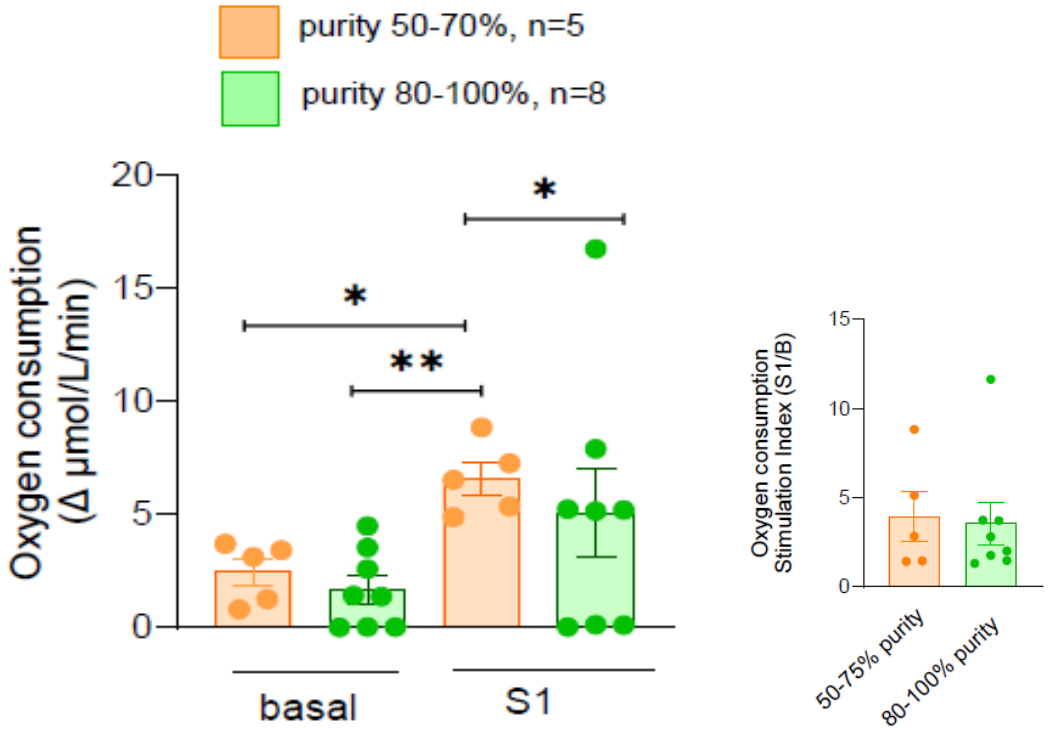
purity 50-70%, n=5
purity 80-100%, n=8
Oxygen consumption (Δ µmol/L/min)
20
15
10
5
0
*
*
**
basal
S1
Oxygen consumption Stimulation Index (S1/B)
15
10
5
0
50-75% purity
80-100% purity

B

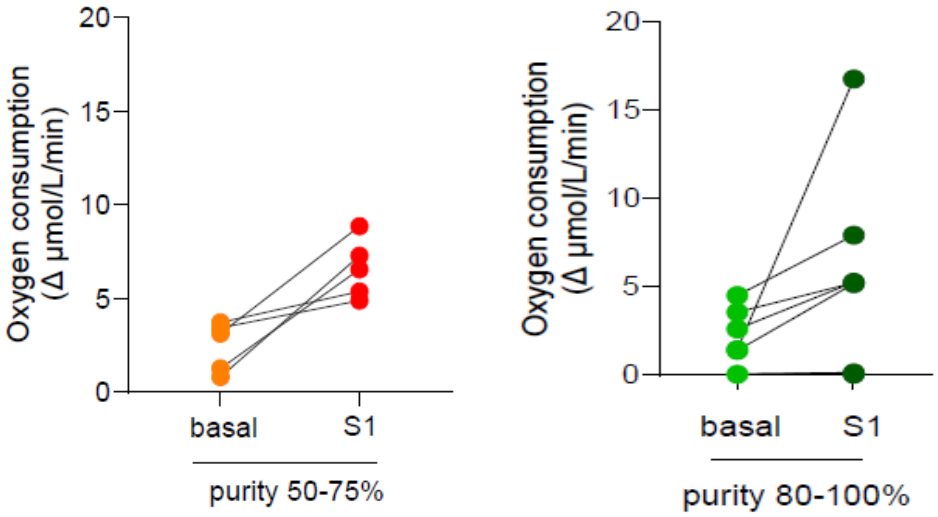
Oxygen consumption (Δ µmol/L/min)
20
15
10
5
0
basal
S1
purity 50-75%
Oxygen consumption (Δ µmol/L/min)
20
15
10
5
0
basal
S1
purity 80-100%

C

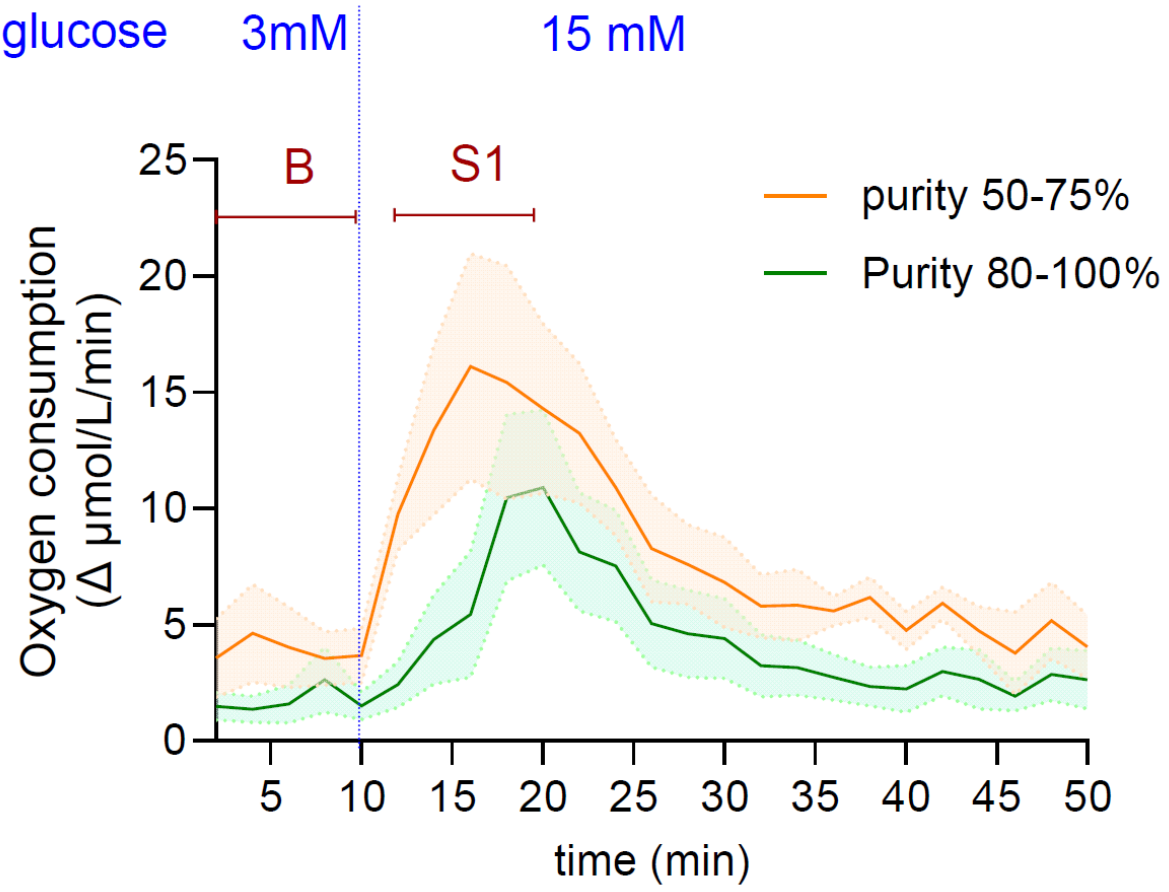

Figure 45: Analysis of oxygen consumption association with low (50-75%, n=5) and high purity (80-100%, n=8)

A) Low purity S1 has an independent effect with low purity basal (p=0.018), high purity basal (p=0.0043) & high purity S1 (p=0.00349). B) The mean donor in each group, orange: basal, red: stimulated, is shown in symbols & lines. C). The oxygen consumption rate (Δ µmol/L/min) curve for both purity comparisons observed, low purity has increased in mean both at basal and S1. Data are represented as mean ± SEM.

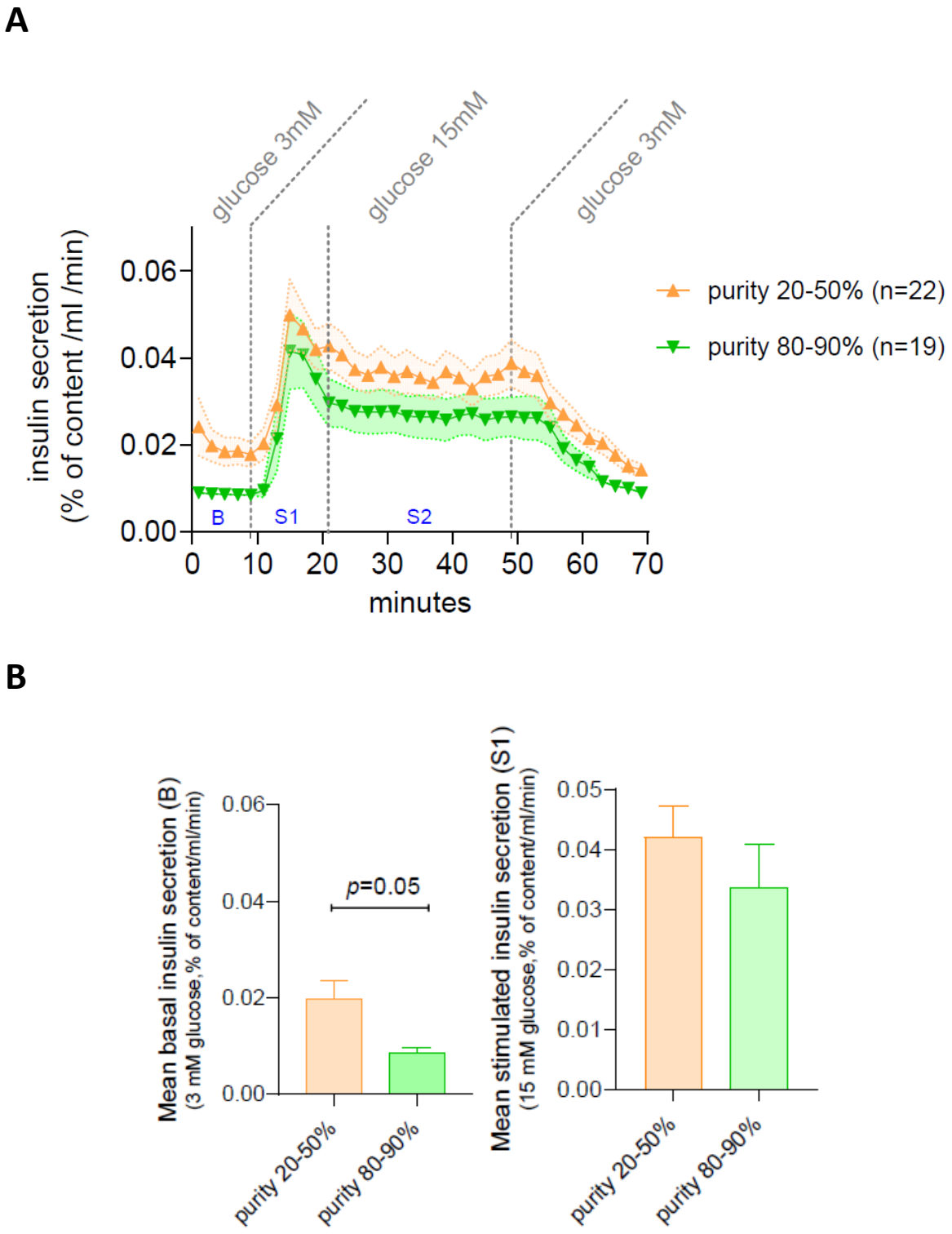

Figure 46: Purity-based insulin secretion – lab data

A) Insulin secretion of low (20-50%) (in orange) and high-purity groups (80-90%) (in green), including 41 donors. B) Low purity (n=22) has more insulin secretion both in basal and stimulated glucose stimulation than groups (19). Samples were collected every 2 minutes. Data are represented as Mean ± SEM.

A

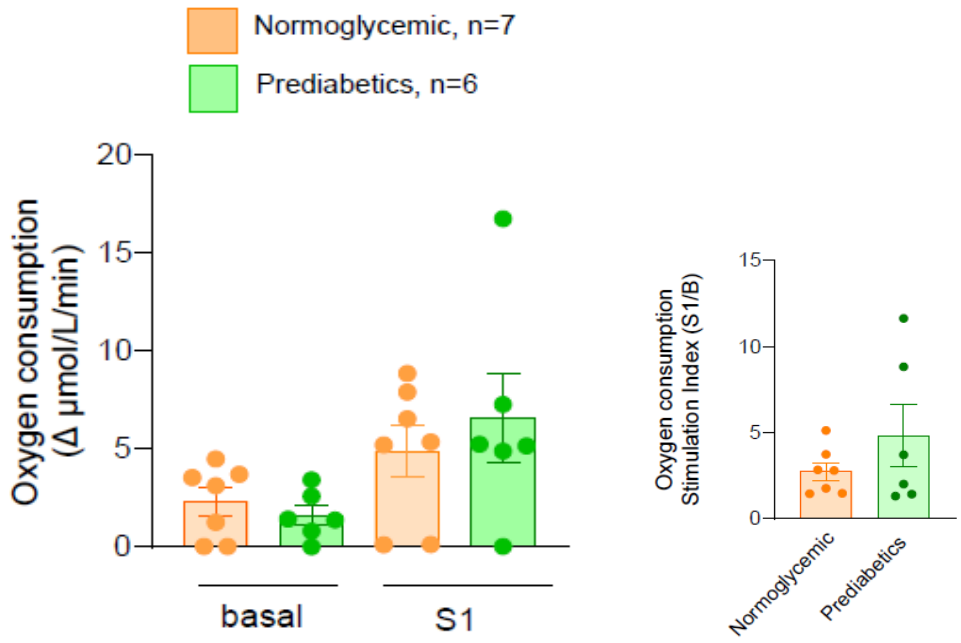
Normoglycemic, n=7
Prediabetics, n=6
Oxygen consumption (Δ µmol/L/min)
20
15
10
5
0
basal
S1
Oxygen consumption Stimulation Index (S1/B)
15
10
5
0
Normoglycemic
Prediabetics

B

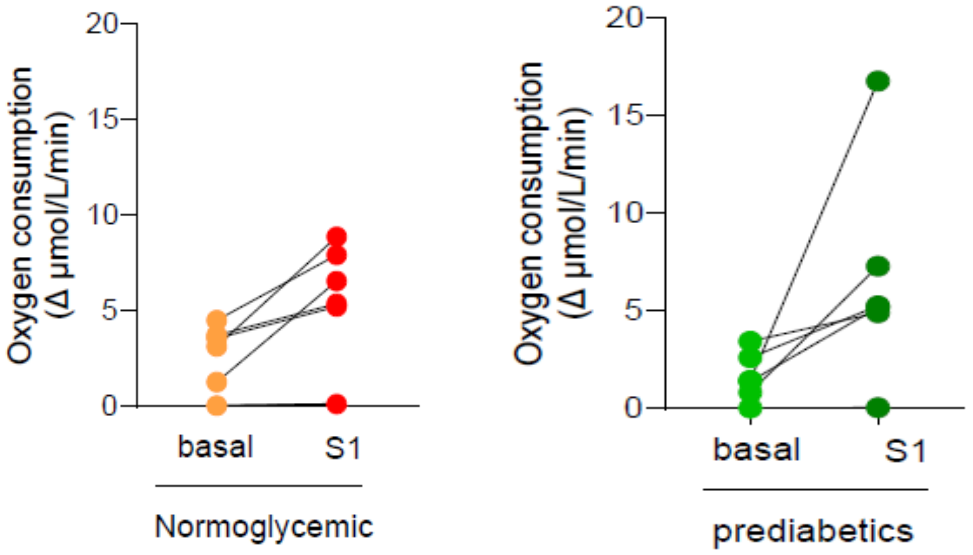
Oxygen consumption (Δ µmol/L/min)
20
15
10
5
0
basal
S1
Normoglycemic
Oxygen consumption (Δ µmol/L/min)
20
15
10
5
0
basal
S1
prediabetics

C

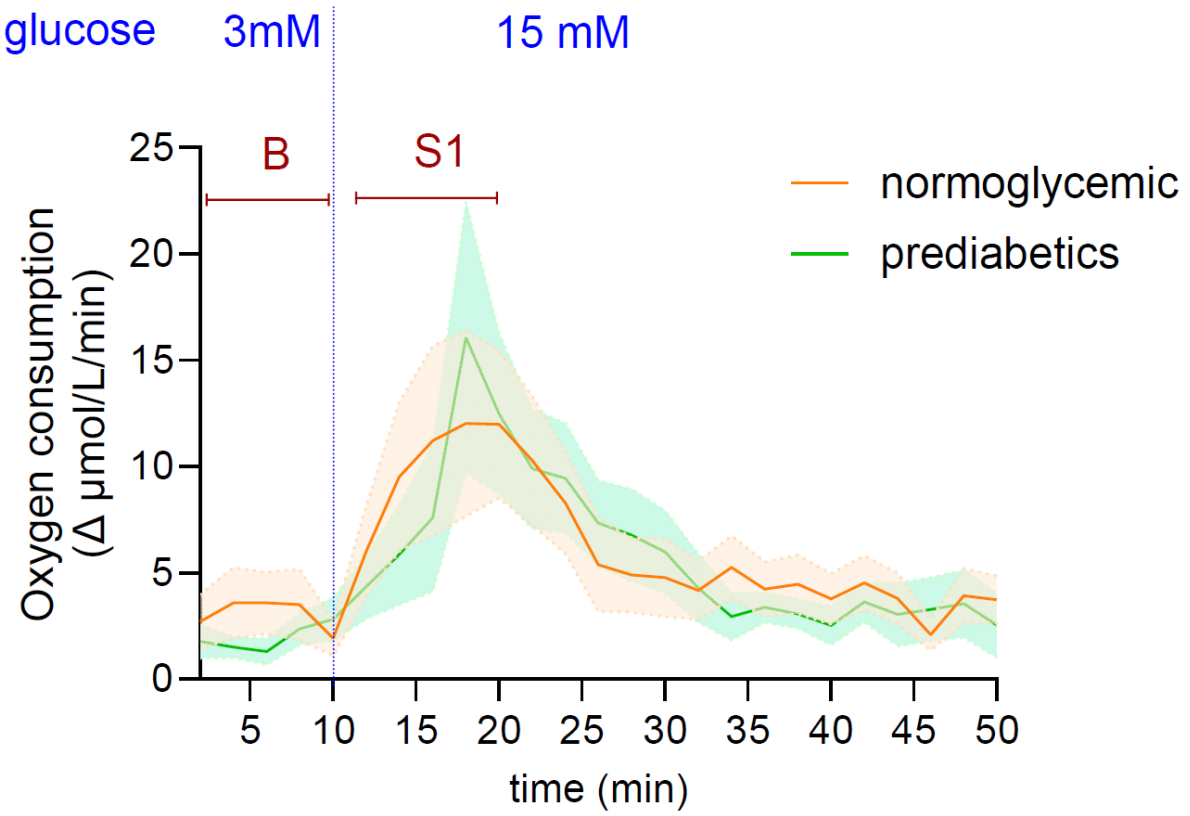

Figure 47: Analysis of oxygen consumption (OCR) association with normoglycemic (HbA1c<5.7, n=7) and prediabetic (6.5>HbA1c≥5.7, n=6)

A) individual consumption at basal (3mM-10mins) & stimulated (15mM-10 mins) expressed as Δ µmol/L/min per 300IEQs. B) means of individual points (donors) at each condition in symbols & lines, the dispersion of donors same in both basal and S1, C) the Oxygen consumption curve for both glycemic comparisons. Non-difference effect between glycemic conditions. Data are represented as mean ± SEM.

A

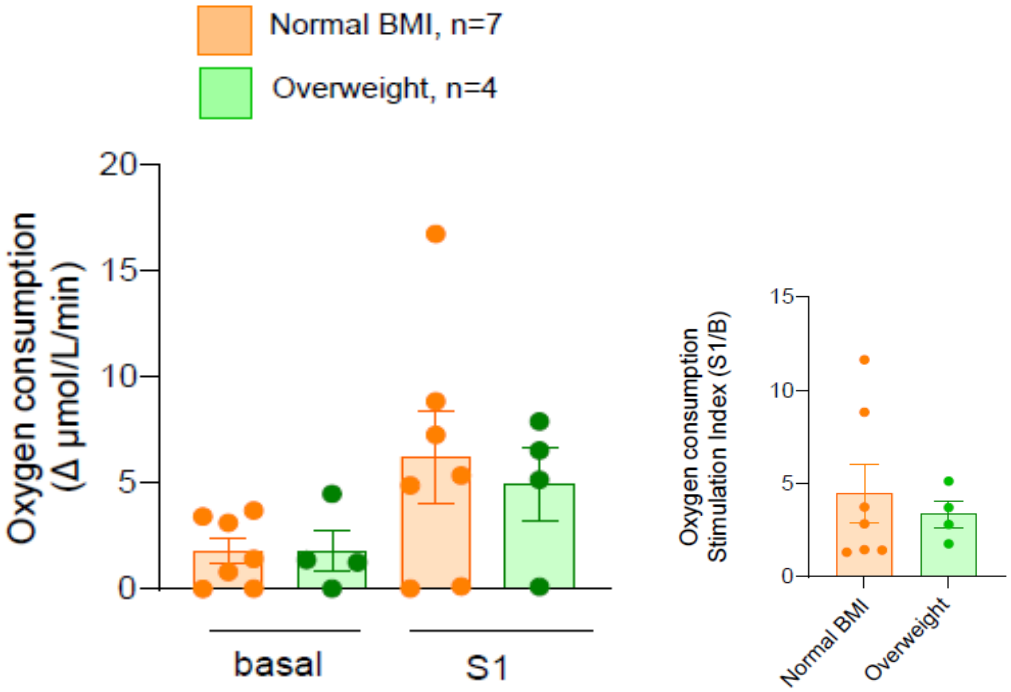
Normal BMI, n=7
Overweight, n=4
Oxygen consumption (Δ µmol/L/min)
20
15
10
5
0
basal
S1
Oxygen consumption Stimulation Index (S1/B)
15
10
5
0
Normal BMI
Overweight

B

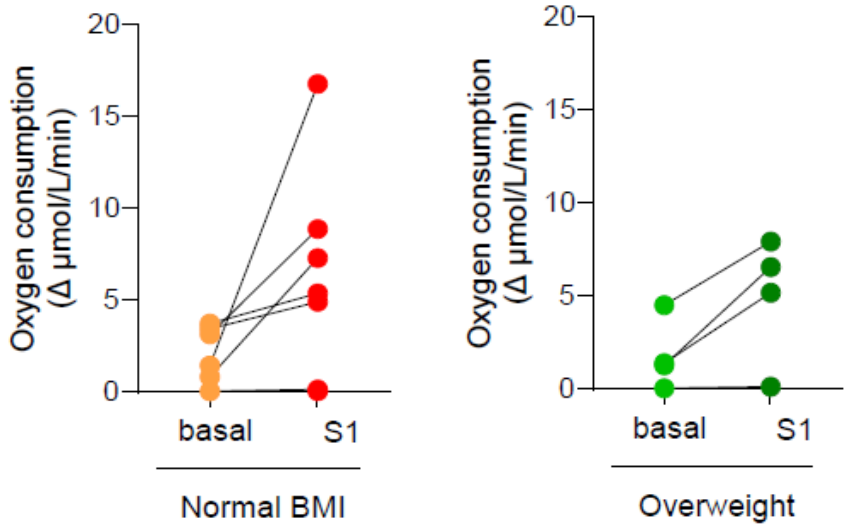
Oxygen consumption (Δ µmol/L/min)
20
15
10
5
0
basal
S1
Normal BMI
Oxygen consumption (Δ µmol/L/min)
20
15
10
5
0
basal
S1
Overweight

C

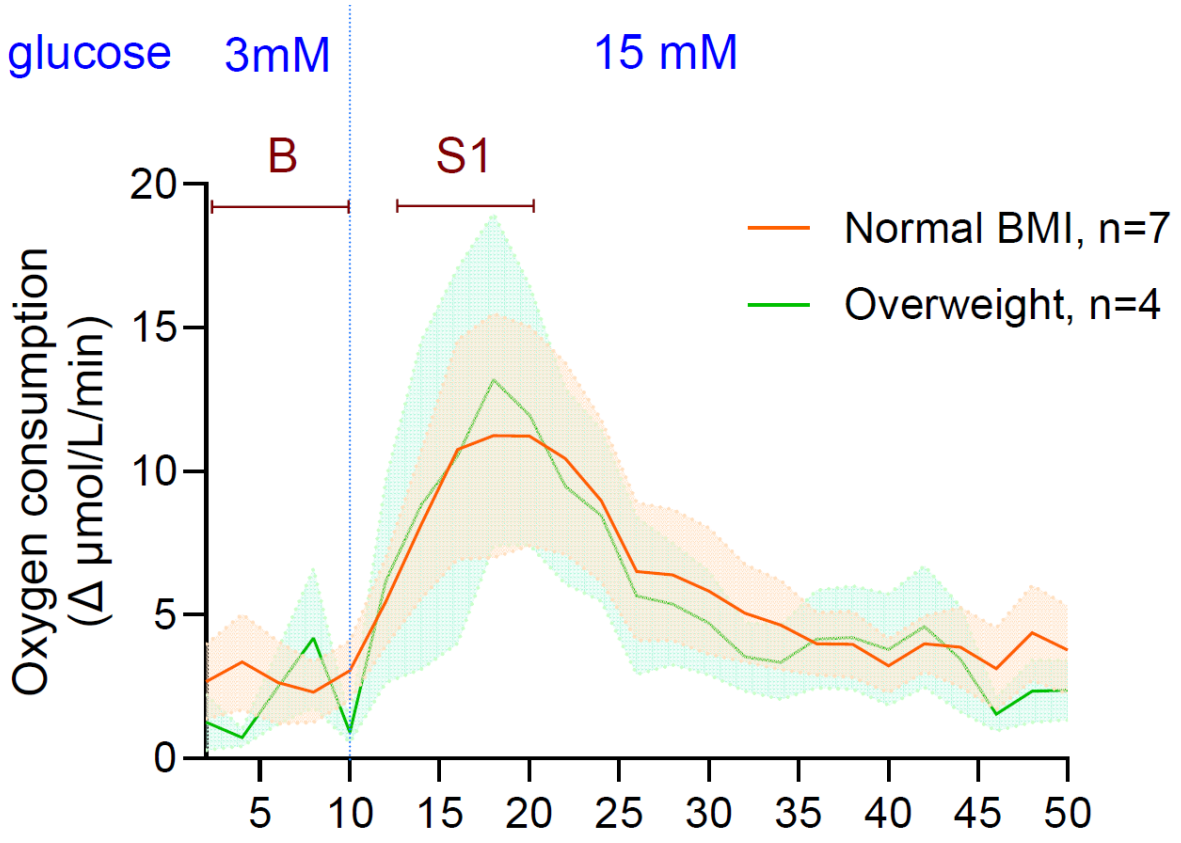

Figure 48: Analysis of oxygen consumption association with normal BMI (<25, n=7) and overweight (30>BMI≥25, n=4)

A) individual consumption at basal (3mM-10mins) & stimulated (15mM-10 mins) expressed as Δ µmol/L/min per 300IEQs. B) means of individual points (donors) at each condition in symbols & lines. C). Oxygen consumption curve shown as ± SEM. Data are represented as mean ± SEM.

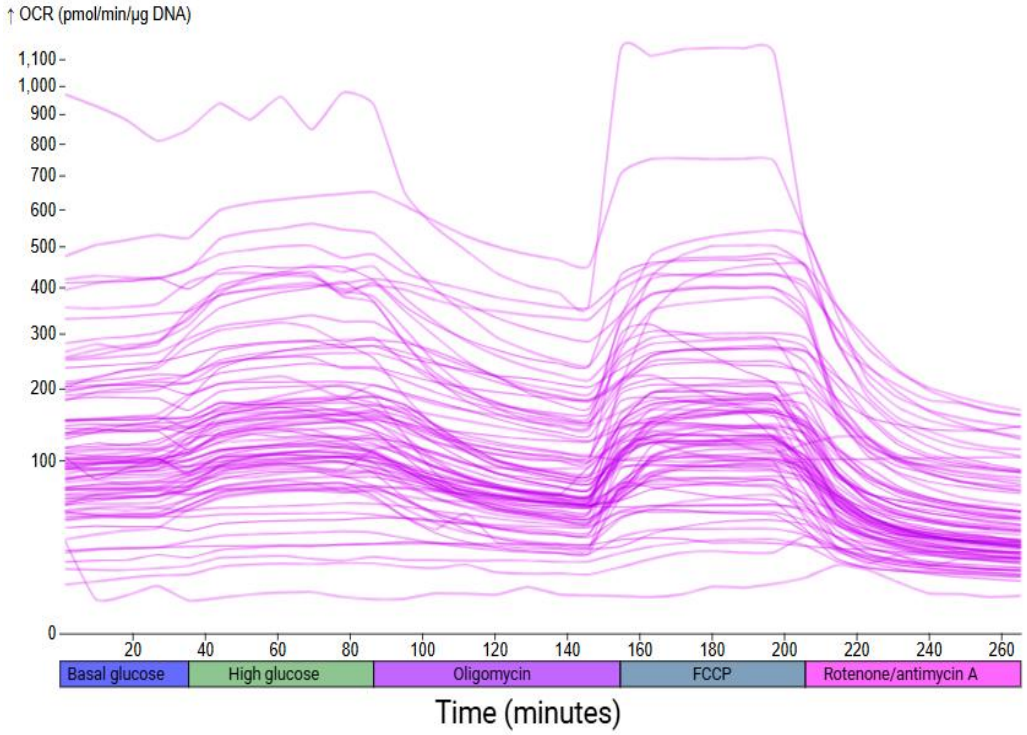

Figure 49: Mitochondrial function from Seahorse analysis

Mitochondrial respiration profile of human islets (>125 donors) under basal (2.8 mM) and stimulated glucose conditions (20 mM). Oxygen consumption rate (OCR) was measured in human islets exposed sequentially to basal glucose (2.8mM) and high glucose (20mM) to assess glucose-stimulated mitochondrial function. Oligomycin (5µM) inhibited ATP synthase (complex V) and determined the proportion of ATP-linked respiration. FCCP (6µM) induced mitochondrial uncoupling and revealed the maximal respiratory capacity. Finally, rotenone and antimycin A (5µM each) were added to inhibit complex I and complex III, respectively, defining the non-mitochondrial respiration component. (data source: www.humanislets.com/#/donor).

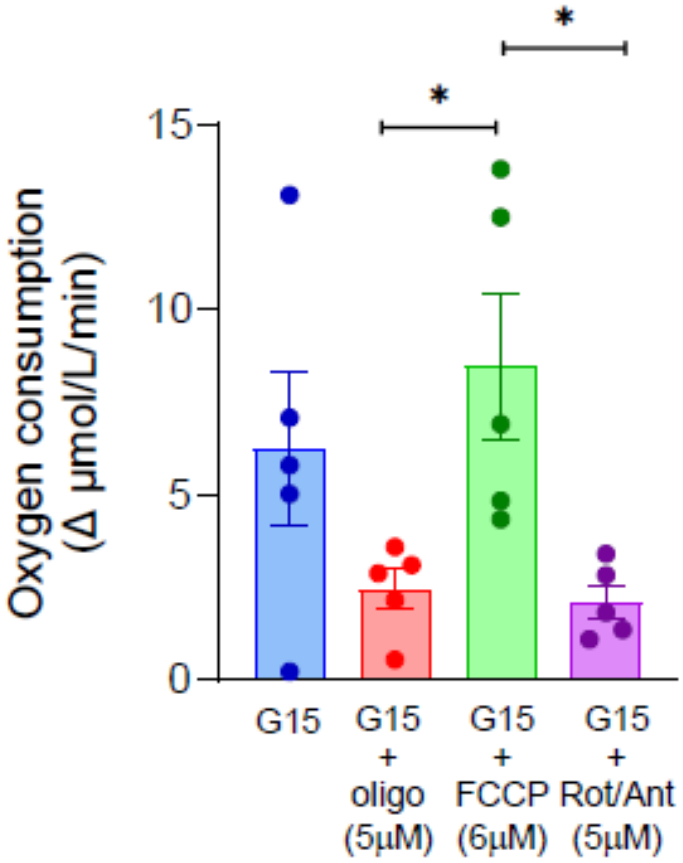

Figure 50: Inhibitors and modulator effects analysed in human islet donors by the integrated pyro tool (n=5)

In blue: islets stimulated by high glucose (30 minutes) as control, red: complex 5 inhibited by oligomycin (5µM-30 minutes), green: the uncoupling effect by Fccp (6 µM), purple: Antimycin and Rotenone to shut down complex I & III. All drug effects are carried in high glucose concentration. The statistical difference was noticed between oligo and maximum coupling (p=0.0183), rot/Ant effect (*p*=0.0133). The statistical significance was shown in Asterix, and a non-parametric t-test for comparisons, data represented by Mean ± SEM. Statistical significance was defined as $p<0.05$ (*), $p<0.01$ (**).

6.3.2.1 *Purity-dependent differences in islet respiratory function*

This preliminary study included 13 donors for perifusion-based respiratory measurements, and their characteristics are shown in **Table 7**. Glucose concentrations of 3mM (0.54 g/L) for basal conditions and 15mM (2.72 g/L) for high stimulation were applied, following the standard protocol of our laboratory. Donor samples were stratified by islet purity: the low-purity group (ranging from 50-75%; n=5) and the high-purity group (80-100%; n=8). The low-purity group exhibited higher respiratory consumption under both basal and stimulated conditions compared with the high-purity group, potentially reflecting the influence of exocrine contamination. Nonetheless, preparations in both groups demonstrated a stimulation index (SI) greater than 1 (**Figure 45A & B**). The mean SI was 3.93 ± 1.40 for low purity preparations and 3.55 ± 1.20 (mean ± SEM) for high purity preparations. The findings of this graph imply S1 response is purity independent (between low purity Basal – S1; p=0.018, high purity basal to low purity S1; p=0.0043, and finally both purity groups of S1; p=0.0349). The OCR curve shows a clear picture of increased consumption at stimulation in **Figure 45C**. Although experiments were conducted in a relatively small cohort in this study, the basal and stimulated conditions were consistent with our previous lab observations (**Figure 46**) in insulin secretions.

6.3.2.2 *Glycemic-based analysis in islet respiratory function*

A second analysis, samples were stratified by glycemic condition, revealed distinct consumption patterns. Under basal conditions, normoglycemic donors (HbA1c<5.7%, n=7) have a higher mean than prediabetic donors (HbA1c 5.7-6.5%, n=6). In contrast, upon stimulation, prediabetic donors exhibited higher consumption in mean compared to normoglycemic donors (**Figure 47A**). Consequently, the stimulation index was greater in the

prediabetic group (4.818 ± 1.784) relative to the normoglycemic group (2.736 ± 0.5099) (**Figure 47B**), representing a 1.52-fold increase. Notably, all donors demonstrated a stimulation index above 1, indicating robust consumption responsiveness across all groups (**Figure 47C**). The comparison between basal consumption in prediabetic donors and stimulated consumption in normoglycemic donors showed a trend toward significance (p = 0.0535) (**Table 8**).

6.3.2.3 *The effect of BMI on islet oxygen consumption*

Donors were stratified based on normal BMI (<25Kg/m², n=7) and overweight (25-30 kg/m², n=4) (**Table 9**). Both groups showed a closer mean at basal (Normal BMI; 1.808 ± 0.6080, overweight; 1.807 ± 0.9503), with no significant changes between groups (**Figure 48A)**. Oxygen consumption had a stimulation index greater than 1 for both groups (**Figure 48B**), even though less oxygen consumption was noticed in a few donors at both basal and S1. The corresponding curve is shown in **Figure 48C**, and the unit is oxygen consumption Δμmol/L/min.

6.3.2.4 *Deciphering mitochondrial function*

To assess mitochondrial function, islets from 5 independent human donors were analysed following a protocol adapted from the Seahorse XF Cell Mito stress test. All islets were initially incubated for one hour with 3mM to establish basal respiration. Subsequently, islets were exposed to G15 (40 min), oligomycin (5μM, 30min) to assess ATP-linked respiration, FCCP (6μM, 30min) to evaluate maximal respiratory capacity, and Rotenone/Antimycin A (5μM, 30min) to inhibit complex I and III, thereby determining non-mitochondrial oxygen consumption. Fccp treatment produced the highest consumption rate among all conditions, consistent with a maximal respiration response. Statistical analysis confirmed a significant difference between FCCP and both oligomycin (p=0.0183) and rotenone/Antimycin

(*p*=0.0133). The observed OCR profile mirrored the pattern found in a classical Seahorse mitochondrial stress assay (**Figure 49**), with increased response in glucose, suppression with oligomycin, rise in FCCP, and an inhibition after rotenone/antimycin addition (**Figure 50**). These results suggest that our new system could be potentially used to calculate maximal respiration, spare capacity, ATP production and non-mitochondrial respiration in human islets.

6.4 Discussion

In this preliminary study, a preSens fluorescence-based oxygen sensor was used to monitor human islet respiration in real time by measuring the partial pressure of dissolved oxygen, demonstrating islet metabolic activity during the different glucose-stimulated insulin secretion phases. The reduced oxygen concentration at G15, with a parallel effect of slightly increased concentration of CO_2 (first 10 mins), is consistent with glucose oxidation (Keppler; Vasa Radonic). Because the preSens tool was not available for long-term use, preliminary tests with a Pyroscience optical sensor were carried out and observed increased oxygen consumption by an increasing number of clusters, highlighting the proportional response, which is consistent with previous results (Sakata-Kato and Wirth, 2016). This preliminary perifusion-based study (n=13) demonstrates that human islet preparations exhibit clear oxygen consumption responses by using the pyro sensor tool under both basal and stimulated (S1) conditions, reflecting active mitochondrial respiration. The stimulation index (SI>1) across all donors confirms preserved metabolic function or functionally active. However, the magnitude of oxygen consumption differed by islet purity: low purity preparations showed higher basal and stimulated respiration than high purity ones and consistent with previous studies (Sweet, Gilbert et al., 2008). The statistically significant difference between low purity S1 -low purity basal showed a real effect, and the same was observed in high purity basal and

low purity S1 (p= 0.0043), between S1 at low and high purity (p=0.0349). Upon stimulation, the sensor tool captured prediabetic nuances from basal resting tone to observed consumption. Even though no significant differences were noticed when comparing groups based on their HbA1c or BMI, the consistent stimulation index showed preserved mitochondrial responsiveness among all donors despite differences among classifications. Responses to various inhibitors of the respiratory chain and uncoupling agents serve as functional readouts of islet mitochondrial performance (Dott, Mistry et al., 2014).

6.5 Conclusion

Insulin secretion is tightly linked to oxidative metabolism, and the cells' oxygen consumption reflects the metabolic demand required for secretion. The perifusion system supported the sensor integration on the outlet chamber connectivity with non-invasive and showed potential applications of real-time monitoring flow-based optical measurements in human islets, proving practical, consistent & revealing the temporal resolution of islet physiology studies in a small cohort (n=13). This approach has the advantage of adaptability, flexibility and demonstrates the potential for continuous, parallel measurement of metabolic parameters under flow conditions.

Table 5 : Donor characteristics, used by preSens sensor

No	Donor	Age (years)	BMI (Kg/m^2)	HbA1c (%)	Islet Purity (%)	Islet Viability (%)
1	H1255	62	25.9	5.4	85	86.9
2	H1256	65	32.1	5.1	85	88
3	H1257	58	24.5	5.1	80	90.3

Number of donors (n=3) used to test the preSens technology to measure the oxygen and CO_2 concentrations. (All donors are non-diabetic donors).

Table 6: Characteristics of the donor for islet respiration measurement by using the pyro tool

No	Donor	Age (years)	BMI (Kg/m^2)	HbA1c (%)	Islet Purity (%)	Islet Viability (%)
1	H1308	57	26.3	5.3	85	93.6
2	H1313	64	29.6	5.7	80	93.7
3	H1318	41	24.7	5.5	90	91.5
4	H1322	67	30.5	5.9	90	91
5	H1329	33	19	6	65	91.5
6	H1333	37	23.6	5.3	75	92.7
7	H1341	54	34.1	5.6	80	93
8	H1345	61	22	6	80	94.5
9	H1352	52	25.1	5.3	94.5	70
10	H1358	57	26.8	5.6	60	91
11	H1359	56	22.2	5.9	80	92.8
12	H1361	44	21.9	5.3	60	95.3
13	H1371	27	23.1	5.7	50	91.3

Table 7: Purity-based analysis in islet respiration (purity 50-75%, n=5 & purity 80-100%, n=7)

		p	
basal 50-75%	Basal 80-100%	0.3978	NS
basal 50-75%	S1- 50-75%	**0.018**	*
basal 50-75%	S1- 80-100%	0.627	NS
basal 80-100%	S1- 50-75%	**0.0043**	**
basal 80-100%	S1- 80-100%	0.101	NS
S1 80-100%	S1- 50-75%	**0.0349**	*

Purity-based comparisons: Consumed data under each group compared with non-parametric t-tests. Statistical significance is indicated as: *p<0.05, **p<0.01, Ns: not significant. B – Basal, S1-first peak (10-12 mins).

Table 8: Glycemic-based analysis in islet respiration (Normoglycemic n=7, prediabetic n=6)

		p	
B normoglycemic	B prediabetic	0.446	NS
B normoglycemic	S1 normoglycemic	0.1445	NS
B normoglycemic	S1 prediabetic	0.0814	NS
B prediabetic	S1 normoglycemic	0.0535	NS
B prediabetic	S1 prediabetic	0.0586	NS
S1 prediabetic	Si normoglycemic	0.5192	NS

Comparisons between normoglycemic and prediabetic groups were performed using non-parametric t tests. Statistical difference of *p* values is shown here: NS-Not significant. B – Basal, S1-first peak (10-12 mins).

Table 9: Weight-based analysis in islet respiration (Normal BMI, n=7, Overweight, n=4)

		p	
B Normal BMI	B (overweight, n=4)	0.9992	NS
B Normal BMI	S1 Normal BMI	0.0746	NS
B Normal BMI	S1 (overweight, n=4)	0.0633	NS
B (overweight, n=4)	S1 Normal BMI	0.1786	NS
B (overweight, n=4)	S1 (overweight, n=4)	0.1586	NS
S1 Normal BMI	S1 (overweight, n=4)	0.7024	NS

Comparisons between normal BMI and overweight donors were performed using non-parametric t tests. Statistical difference of *p* values is shown here: NS-Not significant. B – Basal, S1-first peak (10-12 mins).

CHAPTER 7

General Discussion

7 Chapter VII General Discussion

7.1 Impact of donor characteristics on insulin secretion

7.1.1 Discussion:

Diabetes is the leading cause of death, and its prevalence is growing worldwide (Diabetes, 2024). Among various types, T1D has a major impact; the alternative solution currently used is allogenic islet transplantation (Vantyghem MC, 2019). Determining the quality of the islets is crucial due to donor variability and heterogeneity of the islet size and their performance (Henquin, Dufrane et al., 2015). The variability in insulin secretion greatly influenced by donor characteristics and isolation center protocols, requires consistent assessments (Buemi, Mourad et al., 2024). This study investigated insulin secretion variability across a large cohort of human islets using both static and dynamic GSIS, and also investigated the impact of donor physiological variables on insulin secretion phases during glucose stimulation via perifusion.

7.1.2 Key findings:

The large cohort single-center study revealed variation in insulin secretion kinetics while comparing both static (n=408) and dynamic experiments (n=168). This dynamic study revealed the importance of fasting insulin secretion as an indicator of the functional quality of the isolated Islets. The key findings suggest that despite similar SI overall (r^2=0.625), perifusion resolved a greater dynamic response by capturing both nuances in stimulation, which has donor influence. The stimulation index varied from 1-20 and was consistent (Alcazar and Buchwald, 2019). Normalizing with intra-cellular insulin content mitigated the exocrine involvement and varied higher (~34ng/IEQ) in this cohort than in multi-center studies (~13.3ng/IEQ) (Henquin, 2019), elucidating protocol differences. In this study, the obese and prediabetic group secreted more insulin, particularly under basal and stimulated conditions.

Sex based analysis was not shown as an important parameter in perifusion-based analysis and was consistent with previous studies (Henquin, 2021).

7.1.3 Relation to existing literature:

Integrating 3mM as basal, which is below the physiological range, facilitates hypoglycemic responsiveness, whereas 15mM showed physiological range, implies robust glucose stimulation *in vitro* studies. The observed result in elevated basal insulin secretion in both obese and prediabetic groups might be the influence of a compensatory mechanism, which results in higher secretion in insulin resistance. The combined effects of age, BMI & HbA1c donor characteristics highlighted the amplified kinetics in the determination of in-vitro dynamics.

Our results aligned with broad SI heterogeneity and BMI-based insulin secretion (Kayton, Poffenberger et al., 2015; Trico, Natali et al., 2018). The absence of sex differences matches prior findings. Higher intracellular insulin content compared to multi center studies extended highlighting how protocol harmonization can shift the results. The work complements NAIDS (Wang, Kin et al., 2016)/ Kansas city scores (Ramachandran, Huang et al., 2015) by supplying functional potency rather than yield and viability alone.

7.1.4 Methodological reflection:

Improved internal consistency by performing standard stimuli protocol (3mM, 15mM) that reveals basal, peak, second phase and recovery phase under resolved static endpoints. Reproducibility has been achieved by considering purity, normalization factor, stimulation time and assay conditions.

7.1.5 Strengths, limitations and future directions:

This study benefited from a large cohort study by using standardized procedures, direct comparisons, and mitigating heterogeneity by normalizing the beta cell-specific parameter (IIC). Variations in assay sensitivity and data normalization may further contribute to inter-study variability. Incorporating more variables, including consumption-based parameters to broadens the analysis framework to add more meaningful insights for donor selection. Scaling the integrated effects of insulin secretion and OCR may provide a predictive framework for post-transplantation outcomes.

7.1.6 Concluding statement:

Dynamic, content-normalized perifusion provides a standardized, donor-aware readout of human islet function that complements yield-focused scores and better captures the biology that matters for interpretation and graft selection.

7.2 Prototype 3D model, fabrication, assembly & validation

7.2.1 Discussion:

Perifusion is a valuable technique used to study how cells or tissues respond to various stimuli, such as hormones, by continuously supplying fresh media and collecting the outflow. It plays an important role in evaluating islet function. Since 2017, this technique has been routinely used in our laboratory. In this study, the goal was to improve the perifusion system to handle a larger number of cells. To achieve this, a new perifusion chamber was designed, simulated, and fabricated. The system consists of four individual mono-chambers (each 112*112mm in dimension), assembled to form a four-chamber perifusion unit. This design focused on creating smooth internal surfaces for better flow, accurate alignment for proper sealing, and

strong mechanical stability. The selected SLA based 3D printing allowed quick production of complex parts with smoother surfaces directly from computer-aided designs, and proper post-processing made this tool reliable for assembly (Soni, Kumar et al., 2018).

7.2.2 Key findings:

The iterative CAD development in SolidWorks enabled a solid design of the perifusion chamber development by considering base, side walls, islet chamber, lid, and insert interfaces, along with Islet chamber fluid dynamics simulations. Each element optimized for functionality and manufacturability before assembly. Dedicated provisions were made for filtering paper and proper ring sizes on the cap (lid) early in the model reduced complications and helped the coupling interfaces. The used tolerance of ± 0.05mm and the technique SLA, and its proper post-processing, improved the fabrication process. Added fillets and chamfers, specified smooth internal surfaces, and prevented sharp edges. Proper drilling at the cap avoided the closure leakage issues and promoted the linear flow. Proper gluing of the inox insert enabled no leakage in the setup.

The high surface energy from the aluminium plate with a size of 112*112mm overcame the leakage issue during the water flow in the mini water bath of each mono chamber. The MSLA-assisted clearances of 0.1mm facilitated the proper interface couplings. Performed Simulations to determine the pressure and leakage effects reflected with no further complications in the water bath.

7.2.3 Integration:

The engineering workflow -CAD-Simulation -fabrication – tightened feedback loops between concepts and performance. Solid works simulations showed that, with realistic boundary conditions, the chamber geometry sustains stable, low-turbulence flow compatible with islet

health. SLA printing reproduced these geometries with a smooth surface, improving hydrodynamics and sealing without resorting to adhesives. Printing the chamber as a single unit minimized stack-ups and alignment errors, directly serving the biological objective of consistent perifusion across four independent streams.

7.2.4 Existing literature:

SLA based Additive manufacturing is widely used for surface finish, and dimensional control remains an important aspect (Lu, Wang et al., 2023). This work prioritized the production of a prototype with surface quality required by reducing assembly complexity and adhesive interfaces.

7.2.5 Methodological reflection:

Designs were performed through repetitive iterations, refined with clearances for interface coupling and alignment. Integrated simulation in Solidworks analysed under hydrostatic loading confirmed negligible displacement, solver iterations to reach convergence, low velocity, and temperature perturbations under expected operating conditions. FDM (Fused Deposition Modeling) was deprioritized due to rough surfaces and poor fine-feature fidelity. MSLA (Masked Stereolithography) was limited by build volume and aqueous adhesion issues; SLA Grey Pro Resin (Stereolithography) provided the balance of precision, surface finish, and thermal properties.

7.2.6 Strengths and limitations

Objective simulation criteria before fabrication: material properties (~61 Mpa tensile strength (Maximum force that it can withstand before it breaks), ~13° elongation, ~78°C heat

reflection), compatible with perifusion experiments. Tolerance claims depend on printer calibration and post-processing; long-term soak/ thermal testing remains to be completed.

7.2.7 Implications and applications:

The final chamber design provides a mechanically stable, hydraulically consistent platform for four independent perifusion streams, simplifying setup and improving experimental throughput. Smooth internal surfaces and accurate alignment reduce shear hotspots, enhancing data quality for islet studies.

7.2.8 Future directions:

To validate the chamber across cells, tissues, and organoids with time-resolved drug perturbations, thereby establishing tight control of the perifusion microenvironment, and mechanical stability under long-term culture.

7.2.9 Concluding statement:

SLA with grey pro resin, guided by targeted structural and CFD simulations, enabled a smooth, precisely aligned, adhesive-dependent assembly robust, fabrication-ready perifusion platform. All these nuances served as a solid background for assembling the perifusion system, thereby standing as a strong tool for future perifusion experiments, benefiting research and pharmacological studies by maximising utilization of the islet resource in a limited time.

7.3 Assembly & validation

Flow setup and validation: spacing for component layout was optimized for access and safety, tubing length matched and secured, pump was calibrated for 1ml/min under operating conditions. Gas delivery was tuned for cell stable oxygenation/CO_2 balance, and inlet/outlet lines were leak tested to confirm the steady state flow. Initial leaking disappeared with the

bottom-fed design by achieving laminar flow. This experiment highlights how simple geometric and directional changes in flow design can dramatically improve system reliability. It supports a general principle: horizontal or balanced inflow-outflow configurations often outperform vertical top-fed ones in sealed microfluidic or thermal chambers. These findings can be generalized to other systems like lab-on-a-chip devices and biomedical applications.

Outstanding Integration: The only missing component is the integrated 4-stream fraction collector, which remains in the coding phase with Fab Lab -IMT Nord Europe; synchronization of motion control.

Next steps: Once the collector is synchronized, the system will undergo end-to-end verification before proceeding to islet validation. In the interim, a temporary collection can support short pilot trials, but full kinetic studies will require a finalized 4-way Fraction collector.

7.4 Glucose-stimulated respiration analysis by optical tools

7.4.1 Key findings & methodological reflection

Many research studies have promoted the prediction of islet quality by measuring mitochondrial activity (Dott, Mistry et al., 2014; Kelly, Smith et al., 2019). By aiming this, the feasibility established by optical, perifusion-based respiration measurements in human islets as a preliminary study (PreSens, n=3, Pyroscience, n=13) and observed respiratory readouts by two sensor platforms. Basal to S1, OCR rise in both tools, implying the functional ability observations in human islets.

Measuring the respiration from the same islet preparations, which were simultaneously stimulated by glucose, is the main key finding in this study; all the donors showed increased consumption varying in magnitude (S1>1) when stimulated by glucose (15mM-40mins). The

segregation among donors based on purity, glycemic and weight-based analysis was established in a perifusion framework.

7.4.2 Integration & existing literature:

Drug challenges further dissected the pathway: oligomycin (5µM, n=5) suppressed ATP-linked respiration, FCCP (6µM, n=5) unmasked maximal electron-transport capacity, and rotenone/antimycin (5µM, n=5) collapsed mitochondrial respiration. These results explain the sensitive readouts of coupling efficiency and respiratory reserve (Papas, Bellin et al., 2015) (Abe, Sakairi et al., 2010; Plitzko and Loesgen, 2018). By combining both practices were established biological patterns and true metabolic responses.

7.4.3 Strengths & limitations

Real-time measurement of oxygen consumption (Δ µmol/L/min per 300IEQs) of the same islet preparations, which are stimulated for insulin analysis, and this study established consistent stimulatory responses across donors (S1>1), drug responses mimic the same secretion profile of the internationally used technique, Seahorse analyser. A small cohort study from both sensors limits the power of donor stratified statistics. A limited study reported on OCR in a single perifusion framework, highlighting the need for broader validation across multiple experimental settings.

7.4.4 Future aspects:

Scaling up this work, by repeated readouts and simultaneous implementation of both O_2 and CO_2, may bring insights into consumption dynamics. Link the OCR kinetics with Glucose Stimulated Insulin Secretion with large cohorts and implement in clinical practices. From our data, the perifusion technique demonstrated stable performance and reliable readouts for

measuring oxygen consumption, confirming its suitability in glucose-stimulated islet studies. To further enhance its analytical capability, future development could focus on integrating in situ sensors within the chamber. By employing non-tearing, high-strength filter paper or similar support materials, these sensors could be positioned inside the chamber without disturbing the perifusion flow. This modification would allow earlier and more precise detection of metabolic fluxes as they occur, thereby improving temporal resolution and data accuracy.

Moreover, while our current results highlight consistent responses, glucagon-stimulated consumption data – particularly from small donor samples – were not evident in this setup. Implementing these improvements would expand the chamber's utility for dual-hormone studies and provide a more comprehensive understanding of islet physiology across variable donor sizes.

7.4.5 Conclusion:

The classical perifusion chamber and system cooperated well for the tool integration during dynamic stimulation, enabling high resolution in bioenergetic human islet profile by measuring real-time oxygen consumption, thereby supporting clinical decision making and guiding the pharmacological strategies.

7.5 Combined conclusions:

The present study highlights significant inter-individual heterogeneity in isolated insulin secretion and identifies donor metabolic characteristics as the primary determinants of this variation. Among the analysed parameters, body mass index (BMI) and glycated haemoglobin (HbA1c) emerged as the most influential factors affecting insulin secretory capacity. The increased basal secretion reflects compensatory beta cell activity associated with insulin resistance and impaired beta cell function.

These findings emphasize that donor metabolic background plays a crucial role in pancreatic islet function, even under standardized experimental conditions. Consequently, BMI and HbA1c should be considered key covariates in the interpretation of insulin secretion data from isolated islet studies and in donor selection for both research and clinical applications. Understanding these relationships contributes to a more accurate assessment of beta cell physiology and may pave the way for optimization for personalized approaches to diabetes prevention and treatment.

A 3D-modeled and fabricated prototype of the perifusion chamber (mono chamber) was developed as per lab need with precise geometrical specifications to ensure efficient nutrient delivery and uniform environmental conditions across all chambers.

The application of computational fluid dynamics (CFD) enabled a detailed assessment of parameter analysis within the islet chamber and water bath setups. The prototype was assembled successfully with all associated mechanical and electronic components, except for the fraction collector, due to assembly and synchronised programming, which temporarily hinders full system integration. However, upon completion, the assembly will be finalised and

synchronised across four perifusion chambers, allowing parallel, high-throughput testing of multiple islet preparations or experimental conditions.

To complement secretion data, oxygen consumption rate (OCR) analysis was successfully performed under perifusion conditions by integrating 2 distinct sensors-one for oxygen tension measurement and another for flow control or metabolic activity monitoring. Preliminary experiments using cell lines served as a platform to engage in the validation of system functionality in human islets. This dual-sensor integration provided reliable real-time data on the coupling between glucose metabolism and insulin secretion, establishing the technical feasibility and accuracy of perifusion-based respiration analysis.

The perifusion platform effectively maintained islet integrity under continuous flow conditions, providing a physiologically relevant environment. Collectively, the integration of biological and technical advancements establishes a solid framework for precise, real-time evaluation of metabolic and secretory interactions, paving the way towards improved *in vitro* islet research, metabolic research, and the development of personalized strategies for diabetes investigation and therapeutic optimization.

7.6 Graphical Abstract

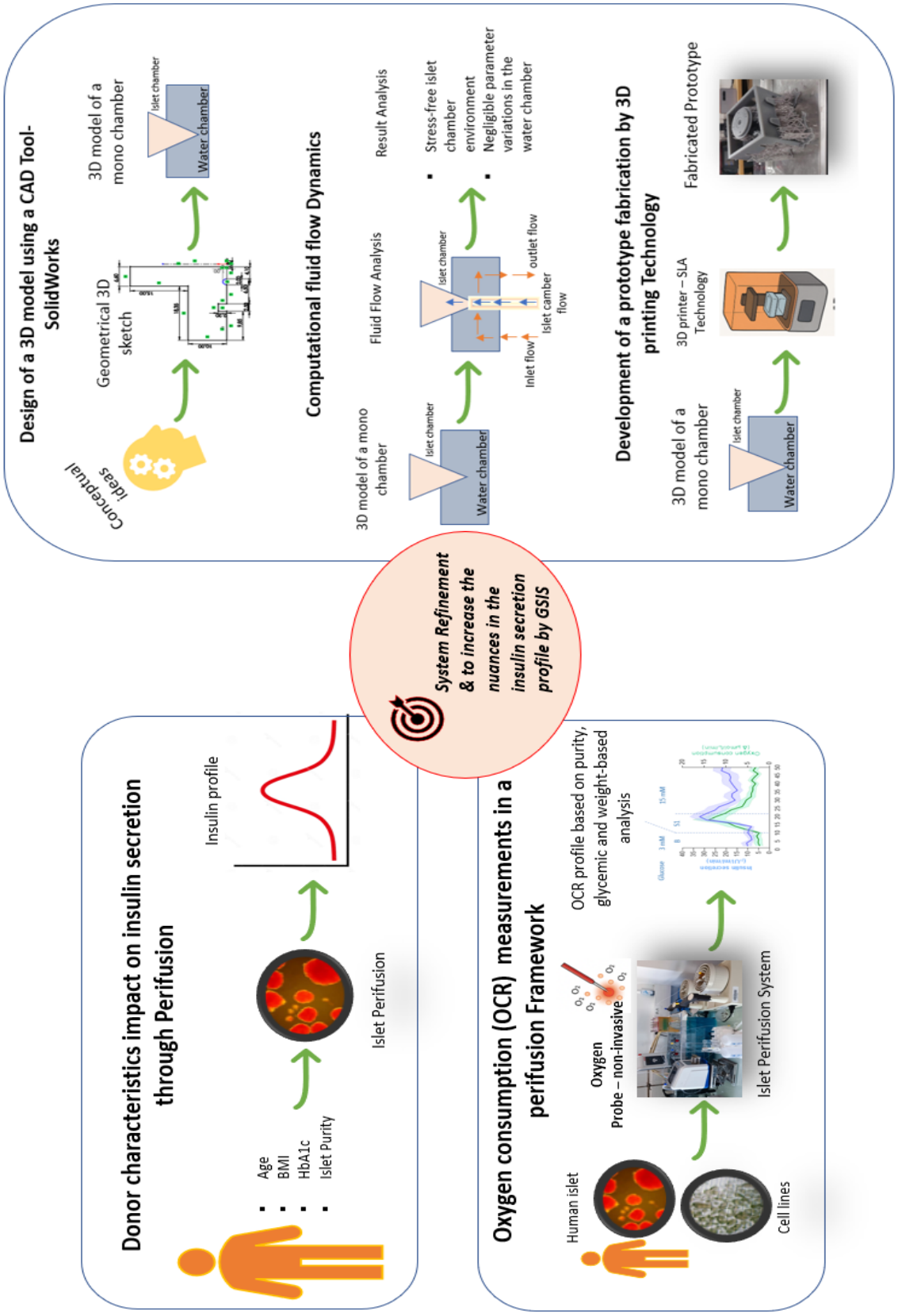

8 Scientific Contributions and Dissemination

8.1 Oral presentations

1. Think Tank - 7th Egid Symposium – Title “Standardized dynamic glucose Testing Reveals Donor-Dependent Heterogeneity in Human Islet Function, Lille, 30th June 2025. (15 mins)

2. Moodle platform – Ecole Doctoral – “A Novel 3D printing perifusion chamber for insulin secretion measurement & fibre optic biosensing for islet analysis”- 2 September 2024. (5 mins)

3. Summer school graduate programme – Title “Enhancing Islet Analysis: Advancing fibre optic biosensing and novel 3D printing perifusion chambers for insulin secretion measurement” – Onco Lille – July 1-3, 2024. (15 mins)

4. National Conference - ESSR -Lille (2022)—participated in the First conference with research titled “Dynamic assessment of human islet secretion: the amount of insulin released after glucose stimulation” – June 29-30, 2023. (15 mins)

8.2 Poster Presentations

1. 13th EPITA symposium - Improved metabolic analysis of islets of Langerhans: detection of O2 consumption during phases of dynamic insulin secretion - Innsbruck-Igls, Austria – 26-28 January, 2025

2. The graduate Programme - CALL for PhD Poster Presentation within the Frame of Transition Week – “Assessing Human islets through Fiber optic biosensing: Unravelling bioenergetic Dynamics” Lille – 18th March 2024.

3. Summer school graduate programme – Title “Enhancing Islet Analysis: Advancing fibre optic biosensing and novel 3D printing perifusion chambers for insulin secretion measurement” – Onco Lille – July 1-3, 2024.

4. 6th Egid Summer School at Bruges - “Enhancing Islet Analysis: Advancing fibre optic biosensing and novel 3D printing perifusion chambers for insulin secretion measurement” – 26-27 September, 2024.

5. Journée du CPER Tecsanté -Technologique au service de la SANTÉ de précision aiguë et chronique – at l'Université de Compiègne – 10th July, 2024.

8.3 Publication

Priyadarshini G, Chiara S, Markus M, Chimene AA, Anais C, Julien T, Nathalie D Pauline P, Arnaud H, Gianni P, Valentin L, Mikael C, Violeta R, Isabel GM, Vantyghem MC, Bonner C, Pattou F, Kerr-Conte J, Gmyr V. Standardized Dynamic Glucose Testing Reveals Donor-Dependent Heterogeneity in Human Islet Function. *Cell Transplantation*, 2025 (volume 34: 1-11) – **Annexe 1**

8.4 Professional Development and Contributions during PhD

Mentoring and Supervision of Students

- Mentored cell line cultures

  Yasine – high school Student

- Assisted projects in solid SolidWorks CAD tool for an Engineering student and showed the FabLab - Douai

  Michaël Leblanc – an Engineering student

Training and certifications

Solid Works – CAD Tool and Simulations - 2023

Ethical and Research Integrity - 2025

9 Bibliography

Abe, Y., T. Sakairi, H. Kajiyama, S. Shrivastav, C. Beeson and J. B. Kopp (2010). "Bioenergetic characterization of mouse podocytes." Am J Physiol Cell Physiol **299** (2): C464-476.

Aboshweita, I. M., M. A. Masood, A. A. M. Idris and W. Abotbina (2024). "Evaluation of the Freeform Feature of Solid works Parametric." International Journal of Latest Engineering and Management Research (IJLEMR) **09** (05): 35-44.

Adewola, A. F., Y. Wang, T. Harvat, D. T. Eddington, D. Lee and J. Oberholzer (2010). "A multi-parametric islet perifusion system within a microfluidic perifusion device." J Vis Exp(35).

Ahmed, I., K. Sullivan and A. Priye (2022). "Multi-Resin Masked Stereolithography (MSLA) 3D Printing for Rapid and Inexpensive Prototyping of Microfluidic Chips with Integrated Functional Components." Biosensors (Basel) **12** (8).

Ajjan, R. A., T. Battelino, X. Cos, S. Del Prato, J. C. Philips, L. Meyer, J. Seufert and S. Seidu (2024). "Continuous glucose monitoring for the routine care of type 2 diabetes mellitus." Nat Rev Endocrinol **20** (7): 426-440.

Alcazar, O. and P. Buchwald (2019). "Concentration-Dependency and Time Profile of Insulin Secretion: Dynamic Perifusion Studies With Human and Murine Islets." Front Endocrinol (Lausanne) **10**: 680.

Alghazzawi, T. F. (2016). "Advancements in CAD/CAM technology: Options for practical implementation." J Prosthodont Res **60** (2): 72-84.

Amiel, S. A. (2021). "The consequences of hypoglycaemia." Diabetologia **64** (5): 963-970.

Aronoff, S. L., K. Berkowitz, B. Shreiner and L. Want (2004). "Glucose Metabolism and Regulation: Beyond Insulin and Glucagon." Diabetes Spectrum **17** (3): 183-190.

Ashby JP, S. R. (1975). "Insulin and glucagon secretion from isolated islets of Langerhans. The effects of calcium ionophores." Biochem J **150** (1): 89-96.

Atlas, D. (2024). from https://diabetesatlas.org/data-by-indicator/type-1-diabetes-estimates/people-with-type-1-diabetes-all-age-groups/.

Avelar-Freitas, B. A., V. G. Almeida, M. C. Pinto, F. A. Mourao, A. R. Massensini, O. A. Martins-Filho, E. Rocha-Vieira and G. E. Brito-Melo (2014). "Trypan blue exclusion assay by flow cytometry." Braz J Med Biol Res **47** (4): 307-315.

Bachul, P. J., J. E. Golebiewska, L. Basto, K. Golab, R. Anteby, L. J. Wang, M. Tibudan, C. Thomas, W. Fendler, A. Lucander, D. J. Grybowski, A. Debska-Slizien, J. Fung and P. Witkowski (2020). "BETA-2 score is an early predictor of graft decline and loss of insulin independence after pancreatic islet allotransplantation." Am J Transplant **20** (3): 844-851.

Bauer, D. L., B. Pobiel, K. Hilber, A. K. Verma, J. Wang, J. Vitek, M. Johnson and L. Johnson (2023). "3D printed guide tube system for acute Neuropixels probe recordings in non-human primates." J Neural Eng **20** (3).

Berman, B. (2012). "3-D printing: The new industrial revolution." Business Horizons **55** (2): 155-162.

Bogue, R. (2013). "3D printing: the dawn of a new era in manufacturing?" Assembly Automation **33** (4): 307-311.

Brissova, M., M. J. Fowler, W. E. Nicholson, A. Chu, B. Hirshberg, D. M. Harlan and A. C. Powers (2005). "Assessment of human pancreatic islet architecture and composition by laser scanning confocal microscopy." J Histochem Cytochem **53** (9): 1087-1097.

Buemi, A., N. I. Mourad, J. Ambroise, D. Hoton, A. Devresse, T. Darius, N. Kanaan, P. Gianello and M. Mourad (2024). "Donor- and isolation-related predictive factors of in vitro secretory function of cultured human islets." Front Endocrinol (Lausanne) **15**: 1345351.

Burr, I. M., L. Balant, W. Stauffacher, A. E. Renold and G. Grodsky (1969). "Dynamic aspects of proinsulin release from perifused rat pancreas." Lancet **2** (7626): 882-883.

Cabrera, O., D. M. Berman, N. S. Kenyon, C. Ricordi, P. O. Berggren and A. Caicedo (2006). "The unique cytoarchitecture of human pancreatic islets has implications for islet cell function." Proc Natl Acad Sci U S A **103** (7): 2334-2339.

Cabrera O, J.-S. M., Berman DM, Fachado A, Echeverri F, Poo R, Khan A, Kenyon NS, Ricordi C, Berggren PO, Caicedo A. (2008). "Automated, high-throughput assays for evaluation of human pancreatic islet function." Cell Transplant **16** (10): 1039-1048.

Caiazzo, R., V. Gmyr, B. Kremer, T. Hubert, B. Soudan, B. Lukowiak, B. Vandewalle, M. C. Vantyghem, F. Pattou and J. Kerr-Conte (2008). "Quantitative in vivo islet potency assay in normoglycemic nude mice correlates with primary graft function after clinical transplantation." Transplantation **86** (2): 360-363.

Chowdhury, A., O. Dyachok, A. Tengholm, S. Sandler and P. Bergsten (2013). "Functional differences between aggregated and dispersed insulin-producing cells." Diabetologia **56** (7): 1557-1568.

Chowdhury, P. N., A. K. Bhunia, A. Sain, S. Koley, T. Xiang and Y.-Z. Song (2023). "Democratising 2D Sketch to 3D Shape Retrieval Through Pivoting." 2023 IEEE/CVF International Conference on Computer Vision (ICCV): 23218-23229.

Ciprian Dragne, Corina Radu (Frenț) and M. Iliescu (2022). "Mechanical Engineering of Robotic Systems by SolidWorks." International journal of modern manufacturing technologies (IJMMT) **14** (2): 61-68.

Czarnecka, Z., N. Dadheech, H. Razavy, R. Pawlick and A. M. J. Shapiro (2023). "The Current Status of Allogenic Islet Cell Transplantation." Cells **12** (20).

Dabas H, S. J., Madhu SV.. (2023). "Insulin Adherence in Adolescents with Type 1 Diabetes Mellitus." Indian J Endocrinol Metab. **27** (5): 394-397.

Dashty, M. (2013). "A quick look at biochemistry: carbohydrate metabolism." Clin Biochem **46** (15): 1339-1352.

Deepa Maheshvare, M., S. Raha, M. Konig and D. Pal (2023). "A pathway model of glucose-stimulated insulin secretion in the pancreatic beta-cell." Front Endocrinol (Lausanne) **14**: 1185656.

Diabetes, A. (2024). from https://idf.org/about-diabetes/what-is-diabetes/.

Dott, W., P. Mistry, J. Wright, K. Cain and K. E. Herbert (2014). "Modulation of mitochondrial bioenergetics in a skeletal muscle cell line model of mitochondrial toxicity." Redox Biol **2**: 224-233.

Dybala, M. P. and M. Hara (2019). "Heterogeneity of the Human Pancreatic Islet." Diabetes **68** (6): 1230-1239.

Ferguson J, A. R., Taylor RM, Johnston ID (1977). "Isolation of viable human pancreatic islets." World J Surg. **1** (1): 69-75.

Fernie, A. R., F. Carrari and L. J. Sweetlove (2004). "Respiratory metabolism: glycolysis, the TCA cycle and mitochondrial electron transport." Curr Opin Plant Biol **7** (3): 254-261.

Fridlyand, L. E. and L. H. Philipson (2010). "Glucose sensing in the pancreatic beta cell: a computational systems analysis." Theor Biol Med Model **7**: 15.

Fu, Z., E. R. Gilbert and D. Liu (2013). "Regulation of insulin synthesis and secretion and pancreatic Beta-cell dysfunction in diabetes." Curr Diabetes Rev **9** (1): 25-53.

Fujita (2020). "AI-based computer-aided diagnosis (AI-CAD): the latest review to read first. Radiol Phys Technol." Radiol Phys Technol. **13** (1): 6-19.

Garcia, G. C., K. Gupta, T. M. Bartol, T. J. Sejnowski and P. Rangamani (2023). "Mitochondrial morphology governs ATP production rate." J Gen Physiol **155** (9).

Ge, Q., B. Jiang and H. Li (2022). "Shaping soft materials via digital light processing-based 3D printing: A review." Forces in Mechanics **6**: 100074.

Gembal M, G. P., Henquin JC. . J Clin (1992). "Evidence that glucose can control insulin release independently from its action on ATP-sensitive K+ channels in mouse B cells." J Clin Invest. **89** (4): 1288-1295.

Golebiewska, J. E., P. J. Bachul, L. J. Wang, S. Matosz, L. Basto, M. R. Kijek, N. Fillman, K. Golab, M. Tibudan, A. Debska-Slizien, J. M. Millis, J. Fung and P. Witkowski (2019). "Validation of a New North American Islet Donor Score for Donor Pancreas Selection and Successful Islet Isolation in a Medium-Volume Islet Transplant Center." Cell Transplant **28** (2): 185-194.

Goto, M., J. Holgersson, M. Kumagai-Braesch and O. Korsgren (2006). "The ADP/ATP ratio: A novel predictive assay for quality assessment of isolated pancreatic islets." Am J Transplant **6** (10): 2483-2487.

Hanley, S. C., E. Austin, B. Assouline-Thomas, J. Kapeluto, J. Blaichman, M. Moosavi, M. Petropavlovskaia and L. Rosenberg (2010). "beta-Cell mass dynamics and islet cell plasticity in human type 2 diabetes." Endocrinology **151** (4): 1462-1472.

Hansen, A. M. B., C. Wium, S. Lee, A. C. Tierney, D. McCarthy, H. M. Roche, C. A. Drevon, K. I. Birkeland and H. L. Gulseth (2020). "Substantial inter-individual variations in insulin secretion and sensitivity across the glucometabolic spectrum." Scand J Clin Lab Invest **80** (4): 282-290.

Hansen C, Q. S. (2003). "Microfluidics in structural biology: smaller, faster em leader better." Curr Opin Struct Biol. **13** (5): 538-544.

Hart, N. J. and A. C. Powers (2019). "Use of human islets to understand islet biology and diabetes: progress, challenges and suggestions." Diabetologia **62** (2): 212-222.

Henquin, J. C. (2009). "Regulation of insulin secretion: a matter of phase control and amplitude modulation." Diabetologia **52** (5): 739-751.

Henquin, J. C. (2018). "Influence of organ donor attributes and preparation characteristics on the dynamics of insulin secretion in isolated human islets." Physiol Rep **6** (5): 13646.

Henquin, J. C. (2019). "The challenge of correctly reporting hormones content and secretion in isolated human islets." Mol Metab **30**: 230-239.

Henquin, J. C. (2021). "Glucose-induced insulin secretion in isolated human islets: Does it truly reflect beta-cell function in vivo?" Mol Metab **48**: 101212.

Henquin, J. C. (2021). "Non-glucose modulators of insulin secretion in healthy humans: (dis)similarities between islet and in vivo studies." Metabolism **122**: 154821.

Henquin, J. C., D. Dufrane, J. Kerr-Conte and M. Nenquin (2015). "Dynamics of glucose-induced insulin secretion in normal human islets." Am J Physiol Endocrinol Metab **309** (7): E640-650.

Henquin, J. C., D. Dufrane and M. Nenquin (2006). "Nutrient control of insulin secretion in isolated normal human islets." Diabetes **55** (12): 3470-3477.

Hering, B. J., W. R. Clarke, N. D. Bridges, T. L. Eggerman, R. Alejandro, M. D. Bellin, K. Chaloner, C. W. Czarniecki, J. S. Goldstein, L. G. Hunsicker, D. B. Kaufman, O. Korsgren, C. P. Larsen, X. Luo, J. F. Markmann, A. Naji, J. Oberholzer, A. M. Posselt, M. R. Rickels, C. Ricordi, M. A. Robien, P. A. Senior, A. M. Shapiro, P. G. Stock, N. A. Turgeon and C. Clinical Islet Transplantation (2016). "Phase 3 Trial of Transplantation of Human Islets in Type 1 Diabetes Complicated by Severe Hypoglycemia." Diabetes Care **39** (7): 1230-1240.

Hertig, D., S. Maddah, R. Memedovski, S. Kurth, A. Moreno, M. Pennestri, A. Felser, J. M. Nuoffer and P. Vermathen (2021). "Live monitoring of cellular metabolism and mitochondrial respiration in 3D cell culture system using NMR spectroscopy." Analyst **146** (13): 4326-4339.

Hideo, K. (1981). "Automatic method for fabricating a three-dimensional plastic model with photo-hardening polymer. ." Review of Scientific Instruments: , 52(11):1770-1773.

Hiriart, M., M. Velasco, C. Larque and C. M. Diaz-Garcia (2014). "Metabolic syndrome and ionic channels in pancreatic beta cells." Vitam Horm **95**: 87-114.

Hopcroft DW, M. D., Scott RS. (1985). "Insulin secretion from perifused rat pancreatic pseudoislets." In Vitro Cell Dev Biol. **21** (8): 421-427.

Huang, H. H., You-Min, Lan and Hsiang-Yao (2005). "CAD/CAE/CAM integration for increasing the accuracy of mask rapid prototyping system." Computers in Industry **56** (5): 442-456.

Hunde, B. R. (2022). "Future prospects of computer-aided design (CAD) – A review from the perspective of artificial intelligence (AI), extended reality, and 3D printing." Results in Engineering **14**.

IDF. (2024). from https://idf.org/about-diabetes/diabetes-facts-figures/.

Ilbey Karakurt and Liwei Lin (2020). "3D printing technologies: techniques, materials, and post-processing." Current Opinion in Chemical Engineering **28**: 134-143.

Investigators, O. T., H. C. Gerstein, J. Bosch, G. R. Dagenais, R. Diaz, H. Jung, A. P. Maggioni, J. Pogue, J. Probstfield, A. Ramachandran, M. C. Riddle, L. E. Ryden and S. Yusuf (2012). "Basal insulin and cardiovascular and other outcomes in dysglycemia." N Engl J Med **367** (4): 319-328.

Ishida, N., S. Harada, R. Toki, A. Hirata, M. Matsumoto, N. Miyagawa, M. Iida, S. Edagawa, A. Miyake, K. Kuwabara, T. Shibuki, S. Kato, K. Arakawa, K. Kinoshita, M. Sakurai-Yageta, G. Tamiya, K. Nagashima, H. Muraoka, Y. Sato and T. Takebayashi (2025). "Causal relationship between body mass index and insulin resistance: Linear and nonlinear Mendelian randomization study in a Japanese population." J Diabetes Investig **16** (7): 1305-1314.

Jiang, G. and B. B. Zhang (2003). "Glucagon and regulation of glucose metabolism." Am J Physiol Endocrinol Metab **284** (4): E671-678.

Jucker, M. (2010). "The benefits and limitations of animal models for translational research in neurodegenerative diseases." Nat Med **16** (11): 1210-1214.

Kayton, N. S., G. Poffenberger, J. Henske, C. Dai, C. Thompson, R. Aramandla, A. Shostak, W. Nicholson, M. Brissova, W. S. Bush and A. C. Powers (2015). "Human islet preparations distributed for research exhibit a variety of insulin-secretory profiles." Am J Physiol Endocrinol Metab **308** (7): E592-602.

Kelly, A. C., K. E. Smith, W. G. Purvis, C. G. Min, C. S. Weber, A. M. Cooksey, C. Hasilo, S. Paraskevas, T. M. Suszynski, B. P. Weegman, M. J. Anderson, L. E. Camacho, R. C. Harland, T. Loudovaris, J. Jandova, D. S. Molano, N. D. Price, I. G. Georgiev, W. E. Scott, 3rd, D. M. D. Manas, J. A. M. Shaw, D. O'Gorman, T. Kin, F. M. McCarthy, G. L. Szot, A. M. Posselt, P. G. Stock, T. Karatzas, A. M. J. Shapiro, R. M. Lynch, S. W. Limesand and K. K. Papas (2019). "Oxygen Perfusion (Persufflation) of Human Pancreata Enhances Insulin Secretion and Attenuates Islet Proinflammatory Signaling." Transplantation **103** (1): 160-167.

Kener, K. B., D. J. Munk, C. R. Hancock and J. S. Tessem (2018). "High-resolution Respirometry to Measure Mitochondrial Function of Intact Beta Cells in the Presence of Natural Compounds." J Vis Exp(131).

Keppler, G. D. a. J. "Simultaneous pH, CO2 and O2 Measurements in Algae Photobioreactor." from https://www.presens.de/knowledge/publications/application-note/simultaneous-ph-co2-and-o2-measurements-in-algae-photobioreactor-1061?utm_source=chatgpt.com.

Kerr-Conte, J., B. Vandewalle, E. Moerman, B. Lukowiak, V. Gmyr, L. Arnalsteen, R. Caiazzo, A. Sterkers, T. Hubert, M. C. Vantyghem and F. Pattou (2010). "Upgrading pretransplant human islet culture technology requires human serum combined with media renewal." Transplantation **89** (9): 1154-1160.

Keymeulen, B., P. Gillard, C. Mathieu, B. Movahedi, G. Maleux, G. Delvaux, D. Ysebaert, B. Roep, E. Vandemeulebroucke, M. Marichal, P. In 't Veld, M. Bogdani, C. Hendrieckx, F. Gorus, Z. Ling, J. van Rood and D. Pipeleers (2006). "Correlation between beta cell mass and glycemic control in type 1 diabetic recipients of islet cell graft." Proc Natl Acad Sci U S A **103** (46): 17444-17449.

Kikuchi M, R. A., Blackard WG, Renold AE. (1974). "Perifusion of pancreas fragments. A system for the study of dynamic aspects of insulin secretion." Diabetes. **23** (6): 550-559.

Kitzmann, J. P., D. O'Gorman, T. Kin, A. C. Gruessner, P. Senior, S. Imes, R. W. Gruessner, A. M. Shapiro and K. K. Papas (2014). "Islet oxygen consumption rate dose predicts insulin independence for first clinical islet allotransplants." Transplant Proc **46** (6): 1985-1988.

Koshkin, V., , F. F. Dai, , C. A. Robson-Doucette, , C. B. Chan, and M. B. Wheeler (2008). "Limited Mitochondrial Permeabilization Is an Early Manifestation of Palmitate-induced Lipotoxicity in Pancreatic β-Cells." Journal of Biology Chemistry **283** (12): 7936-7948.

Kuldeep Rajpoot, Muktika Tekade, Mukesh Chandra Sharma, Nagaraja Sreeharsha, Basel Arafat and Rakesh K. Tekade (2020). "3D printing as an emerging tool in pharmaceutical product development." The Future of Pharmaceutical Product Development and Research: 27-71.

Kurniawan, R. N. A., Romahadi, D., Fitri, M., & Karim, M. R. (2023). "Implementation of the finite element method in SolidWorks to optimize the front cast wheel design for motorcycles." International Journal of Innovation in Mechanical Engineering and Advanced Materials **4**: 66-73.

Lacy, P. E., M. M. Walker and C. J. Fink (1972). "Perifusion of isolated rat islets in vitro. Participation of the microtubular system in the biphasic release of insulin." Diabetes **21** (10): 987-998.

Langlois, A., M. Pinget, L. Kessler and K. Bouzakri (2024). "Islet Transplantation: Current Limitations and Challenges for Successful Outcomes." Cells **13** (21).

Lee D, W. Y., Mendoza-Elias JE, Adewola AF, Harvat TA, Kinzer K, Gutierrez D, Qi M, Eddington DT, Oberholzer J. (2012). "Dual microfluidic perifusion networks for concurrent islet perifusion and optical imaging." Biomed Microdevices **14** (1): 7-16.

Li, Z. and B. H. Graham (2012). "Measurement of mitochondrial oxygen consumption using a Clark electrode." Methods Mol Biol **837**: 63-72.

Longnecker, D. S. (2021). "Anatomy and Physiology of the Pancreas." https://api.semanticscholar.org/corpusID:10104610.

Lorza-Gil, E., G. Kaiser, C. Carlein, M. D. A. Hoffmann, G. M. Konig, S. Haug, L. Prates Roma, E. Rexen Ulven, T. Ulven, E. Kostenis, A. L. Birkenfeld, H. U. Haring, S. Ullrich and F. Gerst (2023). "Glucose-stimulated insulin secretion depends on FFA1 and Gq in neonatal mouse islets." Diabetologia **66** (8): 1501-1515.

Lu, Y., L. Wang, A. M. O. Dal Piva and I. N. J.P.M. Tribst, C.J. Kleverlaan, A.J. Feilzer, (2023). "Influence of surface finishing and printing layer orientation on surface roughness

and flexural strength of stereolithography-manufactured dental zirconia." Journal of the Mechanical Behavior of Biomedical Materials **143**: 1-18.

Matschinsky, F. M. and J. E. Ellerman (1968). "Metabolism of glucose in the islets of Langerhans." J Biol Chem **243** (10): 2730-2736.

Merrins, M. J., B. E. Corkey, R. G. Kibbey and M. Prentki (2022). "Metabolic cycles and signals for insulin secretion." Cell Metab **34** (7): 947-968.

Misun, P. M., B. Yesildag, F. Forschler, A. Neelakandhan, N. Rousset, A. Biernath, A. Hierlemann and O. Frey (2020). "In Vitro Platform for Studying Human Insulin Release Dynamics of Single Pancreatic Islet Microtissues at High Resolution." Adv Biosyst **4** (3): e1900291.

Molano, R. D., A. Pileggi, H. M. Tse, C. L. Stabler and C. A. Fraker (2024). "A static glucose-stimulated insulin secretion (sGSIS) assay that is significantly predictive of time to diabetes reversal in the human islet bioassay." BMJ Open Diabetes Res Care **12** (2).

Mosteller, R. D. (1987). "Simplified calculation of body-surface area." N Engl J Med **317** (17): 1098.

Nano, R., J. A. Kerr-Conte, H. Scholz, M. Engelse, M. Karlsson, F. Saudek, D. Bosco, B. Antonioli, F. Bertuzzi, P. R. V. Johnson, B. Ludwing, Z. Ling, D. L. De Paep, B. Keymeulen, F. Pattou, T. Berney, O. Korsgren, E. de Koning and L. Piemonti (2020). "Heterogeneity of Human Pancreatic Islet Isolation Around Europe: Results of a Survey Study." Transplantation **104** (1): 190-196.

Navale AM, P. A. (2016). "Glucose transporters: physiological and pathological roles." Biophys Rev **8** (1): 5-9.

Ngo, T. D., A. Kashani, G. Imbalzano, K. T. Q. Nguyen and D. Hui (2018). "Additive manufacturing (3D printing): A review of materials, methods, applications and challenges." Composites Part B: Engineering **143**.

Nomura M, S. M., Kawamori R, Yamasaki Y, Iwama N, Abe H (1984). "A mathematical insulin-secretion model and its validation in isolated rat pancreatic islets perifusion." Comput Biomed Res **17** (6): 570-579.

O'Gorman, D., T. Kin, D. McGhee-Wilson, A. M. Shapiro and J. R. Lakey (2005). "Multi-lot analysis of custom collagenase enzyme blend in human islet isolations." Transplant Proc **37** (8): 3417-3419.

Oh, E., N. D. Stull, R. G. Mirmira and D. C. Thurmond (2014). "Syntaxin 4 up-regulation increases efficiency of insulin release in pancreatic islets from humans with and without type 2 diabetes mellitus." J Clin Endocrinol Metab **99** (5): E866-870.

Orsetti A, B. N. (1980). "Insulin receptors in dog lymphocytes." C R Seances Soc Biol Fi **173** (6): 1113-1119.

Pant, H., D. Shukla, S. Rathor and S. Senthur Prabu (2021). "Heat transfer analysis on different pin fin types using Solid Works." IOP Conference Series: Earth and Environmental Science **850**.

Papas, K. K., M. D. Bellin, D. E. Sutherland, T. M. Suszynski, J. P. Kitzmann, E. S. Avgoustiniatos, A. C. Gruessner, K. R. Mueller, G. J. Beilman, A. N. Balamurugan, G. Loganathan, C. K. Colton, M. Koulmanda, G. C. Weir, J. J. Wilhelm, D. Qian, J. C. Niland and B. J. Hering (2015). "Islet Oxygen Consumption Rate (OCR) Dose Predicts Insulin Independence in Clinical Islet Autotransplantation." PLoS One **10** (8): e0134428.

Papas, K. K., C. K. Colton, R. A. Nelson, P. R. Rozak, E. S. Avgoustiniatos, W. E. Scott, 3rd, G. M. Wildey, A. Pisania, G. C. Weir and B. J. Hering (2007). "Human islet oxygen consumption rate and DNA measurements predict diabetes reversal in nude mice." Am J Transplant **7** (3): 707-713.

Papas, K. K., A. Pisania, H. Wu, G. C. Weir and C. K. Colton (2007). "A stirred microchamber for oxygen consumption rate measurements with pancreatic islets." Biotechnol Bioeng **98** (5): 1071-1082.

Papas, K. K., T. M. Suszynski and C. K. Colton (2009). "Islet assessment for transplantation." Curr Opin Organ Transplant **14** (6): 674-682.

Peng, X., K. Wang and L. Chen (2025). "Biphasic glucose-stimulated insulin secretion over decades: a journey from measurements and modeling to mechanistic insights." Life Metab **4** (1): loae038.

Petersen, M. C. and G. I. Shulman (2018). "Mechanisms of Insulin Action and Insulin Resistance." Physiol Rev **98** (4): 2133-2223.

Pisania, A., K. K. Papas, D. E. Powers, M. J. Rappel, A. Omer, S. Bonner-Weir, G. C. Weir and C. K. Colton (2010). "Enumeration of islets by nuclei counting and light microscopic analysis." Lab Invest **90** (11): 1676-1686.

Place, T. L., F. E. Domann and A. J. Case (2017). "Limitations of oxygen delivery to cells in culture: An underappreciated problem in basic and translational research." Free Radic Biol Med **113**: 311-322.

Plitzko, B. and S. Loesgen (2018). "Measurement of Oxygen Consumption Rate (OCR) and Extracellular Acidification Rate (ECAR) in Culture Cells for Assessment of the Energy Metabolism." Bio Protoc **8** (10): e2850.

Podobnik, B., D. Korosak, M. Skelin Klemen, A. Stozer, J. Dolensek, M. Slak Rupnik, P. C. Ivanov, P. Holme and M. Jusup (2020). "beta Cells Operate Collectively to Help Maintain Glucose Homeostasis." Biophys J **118** (10): 2588-2595.

Pokojski, J., K. Szustakiewicz, Ł. Woźnicki, K. Oleksiński and J. Pruszyński (2022). "Industrial application of knowledge-based engineering in commercial CAD / CAE systems." Journal of Industrial Information Integration **25**.

Pradhan, G., J. H. Lee, C.-S. Wu, H. Wang, L. Lin, T. Donti, B. H. Graham, A. S. Rajan, A. Balasubramanyam, S. L. Samson, S. Guo and Y. Sun (2022). "Mechanistic Investigation of GHS-R Mediated Glucose-Stimulated Insulin Secretion in Pancreatic Islets." Biomolecules **12** (3): 407.

Qi, M., S. Bilbao, E. Forouhar, F. Kandeel and I. H. Al-Abdullah (2018). "Encompassing ATP, DNA, insulin, and protein content for quantification and assessment of human pancreatic islets." Cell Tissue Bank **19** (1): 77-85.

Raghothama, S. and V. Shapiro (1998). "Boundary representation deformation in parametric solid modeling." ACM Trans. Graph. **17** (4): 259–286.

Ramachandran, K., H. H. Huang and L. Stehno-Bittel (2015). "A Simple Method to Replace Islet Equivalents for Volume Quantification of Human Islets." Cell Transplant **24** (7): 1183-1194.

Rami H. Awad and C. J. H. Sami A. Habash (2018). "3D Printing Methods." 3D Printing Applications in Cardiovascular Medicine: 11-12.

Reach G, A. R. (1979). "Glucagon and diabetes mellitus." Diabete Metab **5** (1): 63-70.

Requicha, A. A. G. and H. B. Voelcker (1983). "Solid modeling: current status and research directions." IEEE Computer Graphics and Applications **3**: 25-37.

Richter, L. R., B. I. Albert, L. Zhang, A. Ostropolets, J. L. Zitsman, I. Fennoy, D. J. Albers and G. Hripcsak (2022). "Data assimilation on mechanistic models of glucose metabolism predicts glycemic states in adolescents following bariatric surgery." Front Physiol **13**: 923704.

Rickels, M. R., P. G. Stock, E. J. P. de Koning, L. Piemonti, J. Pratschke, R. Alejandro, M. D. Bellin, T. Berney, P. Choudhary, P. R. Johnson, R. Kandaswamy, T. W. H. Kay, B. Keymeulen, Y. C. Kudva, E. Latres, R. M. Langer, R. Lehmann, B. Ludwig, J. F. Markmann, M. Marinac, J. S. Odorico, F. Pattou, P. A. Senior, J. A. M. Shaw, M. C. Vantyghem and S. White (2018). "Defining Outcomes for beta-cell Replacement Therapy in the Treatment of Diabetes: A Consensus Report on the Igls Criteria From the IPITA/EPITA Opinion Leaders Workshop." Transplantation **102** (9): 1479-1486.

Ricordi, C., D. W. Gray, B. J. Hering, D. B. Kaufman, G. L. Warnock, N. M. Kneteman, S. P. Lake, N. J. London, C. Socci, R. Alejandro and et al. (1990). "Islet isolation assessment in man and large animals." Acta Diabetol Lat **27** (3): 185-195.

Ricordi C, L. P., Finke EH, Olack BJ, Scharp DW (1988). "Automated method for isolation of human pancreatic islets." Diabetes **37** (4): 413-420.

Ricordi, C., A. Tzakis, R. Alejandro, Y. J. Zeng, A. J. Demetris, P. Carroll, D. H. Mintz and T. E. Starzl (1991). "Detection of pancreatic islet tissue following islet allotransplantation in man." Transplantation **52** (6): 1079-1080.

Rivera, K. R., V. A. Pozdin, A. T. Young, P. D. Erb, N. A. Wisniewski, S. T. Magness and M. Daniele (2019). "Integrated phosphorescence-based photonic biosensor (iPOB) for monitoring oxygen levels in 3D cell culture systems." Biosens Bioelectron **123**: 131-140.

Rocha, D. S., A. C. Manucci, A. Bruni-Cardoso, A. J. Kowaltowski and E. A. Vilas-Boas (2024). "A practical and robust method to evaluate metabolic fluxes in primary pancreatic islets." Mol Metab **83**: 101922.

Rorsman P, A. F. (2018). "Pancreatic β-Cell Electrical Activity and Insulin Secretion: Of Mice and Men." Physiol Rev **98** (1): 117-214.

Rounak Mahakul, Dhirendra Nath Thatoi, Sasanka Choudhury and Pragyan Patnaik (2021). "Design and numerical analysis of spur gear using SolidWorks simulation technique." Materials Today: Proceedings **41**: 340-346.

Ruggeri, B. A., F. Camp and S. Miknyoczki (2014). "Animal models of disease: pre-clinical animal models of cancer and their applications and utility in drug discovery." Biochem Pharmacol **87** (1): 150-161.

Sakata-Kato, T. and D. F. Wirth (2016). "A Novel Methodology for Bioenergetic Analysis of Plasmodium falciparum Reveals a Glucose-Regulated Metabolic Shift and Enables Mode of Action Analyses of Mitochondrial Inhibitors." ACS Infect Dis **2** (12): 903-916.

Salmi, M. (2016). "Possibilities of Preoperative Medical Models Made by 3D Printing or Additive Manufacturing." J Med Eng **2016**: 6191526.

Saponaro, C., M. Muhlemann, A. Acosta-Montalvo, A. Piron, V. Gmyr, N. Delalleau, E. Moerman, J. Thevenet, G. Pasquetti, A. Coddeville, M. Cnop, J. Kerr-Conte, B. Staels, F. Pattou and C. Bonner (2020). "Interindividual Heterogeneity of SGLT2 Expression and Function in Human Pancreatic Islets." Diabetes **69** (5): 902-914.

Schmidt, C. A., K. H. Fisher-Wellman and P. D. Neufer (2021). "From OCR and ECAR to energy: Perspectives on the design and interpretation of bioenergetics studies." J Biol Chem **297** (4): 101140.

Shah, I., A. Khan, M. Ali, S. Shahab, S. Aziz, M. A. A. Noon and J. A. K. Tipu (2023). "Numerical and Experimental Analysis of Horizontal-Axis Wind Turbine Blade Fatigue Life." Materials (Basel) **16** (13).

Shang, K. M., T. Suzuki, H. Kato, T. Toyoda, Y. C. Tai and H. Komatsu (2025). "Oxygen dynamics and delivery strategies to enhance beta cell replacement therapy." Am J Physiol Cell Physiol **328** (5): C1667-C1684.

Shapiro AM, P. M., Ricordi C (2016). "Clinical pancreatic islet transplantation." Nat Rev Endocrinol **13** (5): 268-277.

Shapiro, A. M. J., J. R. T. Lakey, E. A. Ryan, G. S. Korbutt, E. Toth, G. L. Warnock, N. M. Kneteman and R. V. Rajotte (2000). "Islet Transplantation in Seven Patients with Type 1 Diabetes Mellitus Using a Glucocorticoid-Free Immunosuppressive Regimen." New England Journal of Medicine **343** (4): 230-238.

Shirato, Y., A. J. Hsueh, N. A. Ab Mutalib, Y. Deng, R. Suematsu, A. Kato, B. M. Kearney, M. Kinoshita and H. Suzuki (2024). "Bipolar Clark-Type Oxygen Electrode Arrays for Imaging and Multiplexed Measurements of the Respiratory Activity of Cells." ACS Omega **9** (9): 10825-10833.

Silva, A. M. and P. J. Oliveira (2018). "Evaluation of Respiration with Clark-Type Electrode in Isolated Mitochondria and Permeabilized Animal Cells." Methods Mol Biol **1782**: 7-29.

Soni, A., S. Kumar and B. (Singh (2018). "Prediction of tensile strength of 3D printed part using response surface methodology." JOURNAL OF THE BRAZILIAN SOCIETY OF MECHANICAL SCIENCES AND ENGINEERING **40** (12): 566.

Squires, P. E., T. E. Harris, S. J. Persaud, S. B. Curtis, A. M. Buchan and P. M. Jones (2000). "The extracellular calcium-sensing receptor on human beta-cells negatively modulates insulin secretion." Diabetes **49** (3): 409-417.

Stefan Junk, F. B. (2023). "Design guidelines for Additive Manufacturing using Masked Stereolithography mSLA." Procedia CIRP **119**: 1122-1127.

Sun Chunhua, S. G. (2020). "Application and Development of 3D Printing in Medical Field"." Modern Mechanical Engineering **10** (3): 25-33.

Sweet, I. R. and M. Gilbert (2006). "Contribution of calcium influx in mediating glucose-stimulated oxygen consumption in pancreatic islets." Diabetes **55** (12): 3509-3519.

Sweet, I. R., M. Gilbert, R. Jensen, O. Sabek, D. W. Fraga, A. O. Gaber and J. Reems (2005). "Glucose stimulation of cytochrome C reduction and oxygen consumption as assessment of human islet quality." Transplantation **80** (8): 1003-1011.

Sweet, I. R., M. Gilbert, S. Scott, I. Todorov, R. Jensen, I. Nair, I. Al-Abdullah, J. Rawson, F. Kandeel and K. Ferreri (2008). "Glucose-stimulated increment in oxygen consumption rate as a standardized test of human islet quality." Am J Transplant **8** (1): 183-192.

Sweet, I. R., G. Khalil, A. R. Wallen, M. Steedman, K. A. Schenkman, J. A. Reems, S. E. Kahn and J. B. Callis (2002). "Continuous measurement of oxygen consumption by pancreatic islets." Diabetes Technol Ther **4** (5): 661-672.

Tasnim Tuli, N., S. Khatun and A. B. Rashid (2024). "Unlocking the future of precision manufacturing: A comprehensive exploration of 3D printing with fiber-reinforced composites in aerospace, automotive, medical, and consumer industries." Heliyon **10** (5): e27328.

Trico, D., A. Natali, S. Arslanian, A. Mari and E. Ferrannini (2018). "Identification, pathophysiology, and clinical implications of primary insulin hypersecretion in nondiabetic adults and adolescents." JCI Insight **3** (24).

Trojan, J. e. a. (2025). "Component Design for Streamlining the Manufacturing Process" — the project included 3D scanning and creation of a model using SolidWorks software, and then fabrication via 3D printing." processes **13** (5): 1282.

Umeda, A., M. Ishizaka, A. Ikeda, K. Miyagawa, A. Mochida, H. Takeda, K. Takeda, I. Fukushi, Y. Okada and D. Gozal (2021). "Recent Insights into the Measurement of Carbon Dioxide Concentrations for Clinical Practice in Respiratory Medicine." Sensors (Basel) **21** (16).

Vandewalle, B., C. Douillard, J. Kerr Conte, V. Gmyr, R. Riachi, M. D'Herbomez, F. Pattou and J. Lefebvre (1999). "Human pancreatic islet quality control: easy assessment of metabolic functions." Exp Clin Endocrinol Diabetes **107** (3): 214-219.

Vantyghem MC, C. M., Gmyr V, Jannin A, Espiard S, Le Mapihan K, Raverdy V, Delalleau N, Machuron F, Hubert T, Frimat M, Van Belle E, Hazzan M, Pigny P, Noel C, Caiazzo R, Kerr-Conte J, Pattou F (2019). "Ten-Year Outcome of Islet Alone or Islet After Kidney Transplantation in Type 1 Diabetes: A Prospective Parallel-Arm Cohort Study." Diabetes Care **42** (11): 2042-2049.

Vantyghem, M. C., J. Kerr-Conte, L. Arnalsteen, G. Sergent, F. Defrance, V. Gmyr, N. Declerck, V. Raverdy, B. Vandewalle, P. Pigny, C. Noel and F. Pattou (2009). "Primary graft function, metabolic control, and graft survival after islet transplantation." Diabetes Care **32** (8): 1473-1478.

Vasa Radonic, I. P., Mila Djisalov, Teodora Knezic, Ivana Gadjanski. "O2, pH and CO2 Monitoring in Microfluidic Mammalian Cell Culture." from https://www.presens.de/knowledge/publications/application-note/o2-ph-and-co2-monitoring-in-microfluidic-mammalian-cell-culture-1772.

Wang, F., L. Chen, J. Zhu, X. Hu and Y. Yang (2021). "A Phosphorescence Quenching-Based Intelligent Dissolved Oxygen Sensor on an Optofluidic Platform." Micromachines (Basel) **12** (3).

Wang, L. J., T. Kin, D. O'Gorman, A. M. J. Shapiro, B. Naziruddin, M. Takita, M. F. Levy, A. M. Posselt, G. L. Szot, O. Savari, B. Barbaro, J. McGarrigle, C. C. Yeh, J. Oberholzer, J. Lei, T. Chen, M. Lian, J. F. Markmann, A. Alvarez, E. Linetsky, C. Ricordi, A. N. Balamurugan, G. Loganathan, J. J. Wilhelm, B. J. Hering, R. Bottino, M. Trucco, C. Liu, Z. Min, Y. Li, A. Naji, L. A. Fernandez, M. Ziemelis, J. S. Danobeitia, J. M. Millis and P. Witkowski (2016). "A Multicenter Study: North American Islet Donor Score in Donor Pancreas

Selection for Human Islet Isolation for Transplantation." Cell Transplant **25** (8): 1515-1523.

Weisberg, D. (2023). "History of CAD." from https://www.shapr3d.com/history-of-cad/introduction.

Weiwei Fan a, Xinyi Liu a b 1, Yongjun Zhang a b c 1, Dong Wei a, Haoyu Guo c and D. Y. a (2025). "3D wireframe model reconstruction of buildings from multi-view images using neural implicit fields." Automation in construction, **174**.

Wikstrom, J. D., S. B. Sereda, L. Stiles, A. Elorza, E. M. Allister, A. Neilson, D. A. Ferrick, M. B. Wheeler and O. S. Shirihai (2012). "A novel high-throughput assay for islet respiration reveals uncoupling of rodent and human islets." PLoS One **7** (5): e33023.

Witthauer, L., E. Roussakis, J. P. Cascales, A. Goss, X. Li, A. Cralley, D. Yoeli, H. B. Moore, Z. Wang, Y. Wang, B. Li, C. A. Huang, E. E. Moore and C. L. Evans (2023). "Development and in-vivo validation of a portable phosphorescence lifetime-based fiber-optic oxygen sensor." Sci Rep **13** (1): 14782.

Wollheim CB, K. M., Renold AE, Sharp GW (1978). "The roles of intracellular and extracellular Ca++ in glucose-stimulated biphasic insulin release by rat islets." J Clin Invest **62** (2): 451-458.

Xie, L., D. Zhu, S. Dolai, T. Liang, T. Qin, Y. Kang, H. Xie, Y. C. Huang and H. Y. Gaisano (2015). "Syntaxin-4 mediates exocytosis of pre-docked and newcomer insulin granules underlying biphasic glucose-stimulated insulin secretion in human pancreatic beta cells." Diabetologia **58** (6): 1250-1259.

Yi, J., s. Yang, L. Yue and l. M. Lei (2025). "Digital light processing 3D printing of flexible devices: actuators, sensors and energy devices." Microsystems & Nanoengineering **11** (1): 51.

Zdziennicka, A., J. Krawczyk, K. Szymczyk and B. Jańczuk (2017). "Components and parameters of liquids and some polymers surface tension at different temperature." Colloids and Surfaces A: Physicochemical and Engineering Aspects **529**: 864-875.

Zhang, F., L. Zhu, Z. Li, S. Wang, J. Shi, W. Tang, N. Li and J. Yang (2021). "The recent development of vat photopolymerization: A review." Additive Manufacturing **48**.

Zhou, Q., J. Brown, A. Kanarek, J. Rajagopal and D. A. Melton (2008). "In vivo reprogramming of adult pancreatic exocrine cells to beta-cells." Nature **455** (7213): 627-632.

10 Annexe 1:

Original Article

Cell Transplantation
Volume 34: 1–11

DOI: 10.1177/09636897251350654
journals.sagepub.com/home/cll
Sage

Standardized dynamic glucose testing reveals donor-dependent heterogeneity in human islet function

Priyadarshini Gnanasekar[1*], Chiara Saponaro[1*], Markus Mühlemann[1], Chimene Amayene Amassogo[1], Anais Coddeville[1], Julien Thevenet[1], Nathalie Delalleau[1], Pauline Petit[1], Arnaud Hanssen[1], Gianni Pasquetti[1], Valentin Lericque[1], Mikael Chetboun[1], Violeta Raverdy[1], Isabel Gonzales-Mariscal[1], Marie-Christine Vantyghem[1], Caroline Bonner[1], François Pattou[1], Julie Kerr-Conte[1], and Valery Gmyr[1]

Abstract

Glucose-stimulated insulin secretion (GSIS) testing of isolated islets of Langerhans is crucial for assessing β-cell function, yet protocol variability complicates result interpretation. This study investigated insulin secretion heterogeneity across 576 donors and examined the influence of donor characteristics on secretory responses. We compared static incubation (n = 408) and dynamic perifusion (n = 168) techniques using standardized glucose stimulation protocols (3 vs 15 mM). While both methods showed comparable stimulation indices (r^2 = 0.652), dynamic perifusion uniquely captured temporal secretion patterns and revealed greater dynamic range in insulin responses. Notably, dynamic perifusion, with insulin content normalization, revealed a 22-fold variation in stimulation index across donors. Body mass index (BMI) and HbA1c significantly influenced basal insulin secretion, particularly in donors with glucose intolerance and type 2 diabetes (T2D) (HbA1c ≥ 6.5%). Cluster analysis identified two distinct groups based on age, BMI/body surface area (BSA), and HbA1c, which strongly predicted insulin secretion patterns, whereas donor sex had no measurable impact. This large-scale study demonstrates the superiority of standardized perifusion over static incubation for resolving islet glucose responses. By capturing dynamic secretion profiles, perifusion reveals substantial donor heterogeneity, primarily driven by BMI and HbA1c through their effects on basal insulin secretion.

Keywords

islet transplantation, insulin secretion, GSIS, perifusion

[1]Inserm U1190, CHU Lille, European Genomic Institute for Diabetes (EGID), Institut Pasteur de Lille, Univ. Lille, Lille, France

*These authors contributed equally to the work.

Received: 26 March 2025; revised: 6 May 2025; accepted: 27 May 2025

Corresponding Author:
Valery Gmyr, Inserm U1190, CHU Lille, European Genomic Institute for Diabetes (EGID), Institut Pasteur de Lille, Univ. Lille, 59000 Lille, France.
Email: valery.gmyr@univ-lille.fr; vgmyr@univ-lille.fr

Graphical Abstract

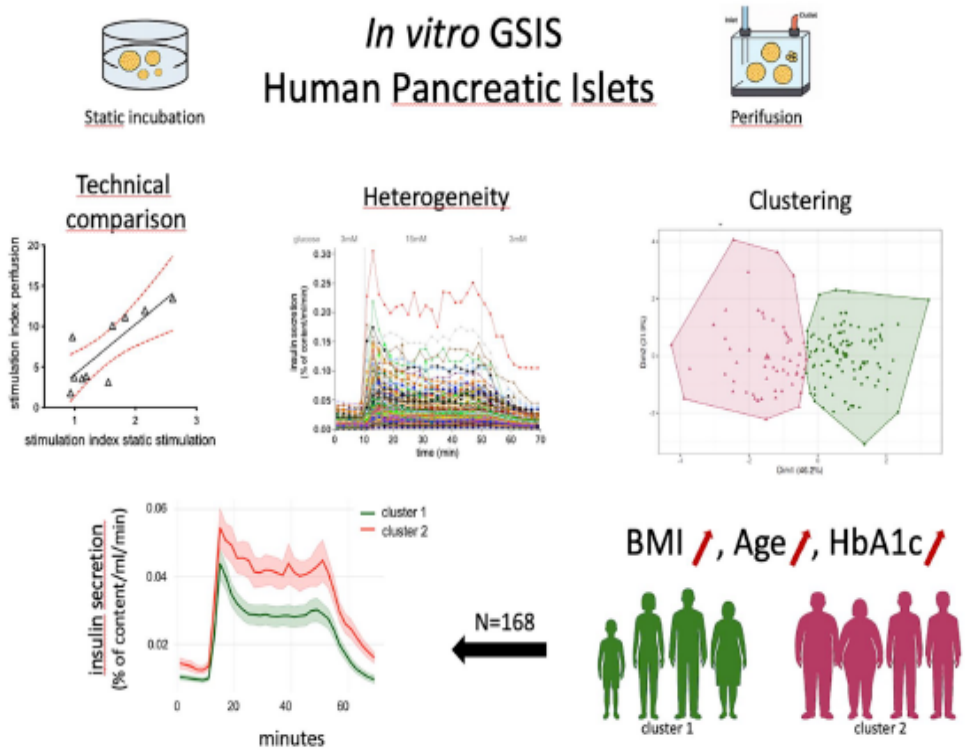

Introduction

Islet allotransplantation has emerged as an effective treatment for type 1 diabetes (T1D) patients with severe glycemic instability[1–3]. This cellular therapy has gained widespread recognition and reimbursement status across numerous countries, reflecting its integration as a standard therapeutic option[4,5]. Clinical outcomes demonstrate sustained benefits, with 28% of recipients maintaining insulin independence a decade posttransplantation in our cohort[6]. Despite significant advances in transplantation procedures, immunosuppression protocols, and overall safety profiles, the challenge of reliably assessing islet function before transplantation remains a critical barrier to optimizing clinical outcomes.

The complexity of islet biology necessitates comprehensive evaluation through multiple *in vitro* assays, including glucose-stimulated insulin secretion (GSIS), oxidative stress measurements, ATP/ADP ratios, oxygen consumption, mitochondrial integrity assessments, and cellular composition analysis[7–9]. However, the field lacks a standardized protocol or reliable predictive test that can definitively determine islet quality. Glucose-stimulated insulin secretion evaluation, the most widely adopted approach, employs either static incubation[9,10] or dynamic perifusion techniques[10–12]. The latter method offers distinct advantages by capturing biphasic insulin release kinetics in real-time, revealing both first- and second-phase secretions from various islet preparations[10,11,13–15]. This temporal resolution provides crucial insights into β-cell function that static methods cannot capture.

The interpretation of insulin secretion data is complex and influenced by various factors, including donor characteristics, such as sex, age, body mass index (BMI), body surface area (BSA), and islet preparation variables like size, purity, and cold ischemia[16]. While perifusion techniques have become widely adopted for islet characterization, the variability in protocols across different centers poses significant challenges for data comparison and standardization[17]. The implementation of standardized or centralized perifusion testing across islet production centers could improve quality assurance and enhance the predictability of outcomes[12,18]. Currently, the limited number of *in vitro* experiments conducted at each center, coupled with protocol heterogeneity, makes it difficult to establish reliable reference standards for human islet insulin secretion. Recommendation by Henquin[19] for greater consistency and rigor in reporting human islet *in vitro* studies highlights the critical need for standardization in therapeutic evaluation.

Table 1. Demographic and clinical characteristics of islet donors in static and dynamic perifusion studies.

	Static incubation	Perifusion	Range (static + perif)	*P* value
N	408	168		
Sexe (M/F) (n)	216/192	103/65		
Age (years)	48.9 ± 13.2	50.8 ± 13.0	13–86	0.111
Weight (kg)	78.2 ± 16.8	84.3 ± 19.9	42–150	*0.0002*
Height (cm)	170 ± 10	173 ± 10	140–203	*0.007*
BMI (kg/m^2)	26.8 ± 5.4	27.9 ± 5.6	16.6–46.9	*0.023*
BSA (m^2)	1.92 ± 0.23	2.03 ± 0.28	1.35–2.82	*<0.0001*
HbA1c (%)	5.7 ± 0.5	5.6 ± 0.6	4.2–9.3	0.175
ICU (days)	3.0 ± 2.7	2.9 ± 2.5	0.5–13	0.541

Comparison of donor characteristics between static incubation (n = 408) and perifusion (n = 168) groups. Data are presented as mean ± standard deviation or counts for categorical variables (sex). Range values represent the combined data from both groups. Statistical comparisons between groups were performed using unpaired nonparametric t tests, with significant differences ($P < 0.05$) indicated in italics. BMI: body mass index; BSA: body surface area; HbA1c: glycated hemoglobin; ICU: intensive care unit length of stay.

This study addresses these challenges by examining insulin secretion variability across a large cohort of human islets using both static and dynamic GSIS testing techniques. Furthermore, we investigated the impact of donor physiological variables on insulin secretion phases during glucose stimulation via perifusion, aiming to establish more reliable predictive markers for islet function assessment.

Materials and methods

Human islet donor information

Pancreata were procured from adult, brain-deceased donors through our clinical islet transplantation program (French "Agence de la BioMedecine": PFS16-008). The study was conducted in accordance with French Regulations and approved by the Institutional Ethical Committee of the University of Lille and the Centre Hospitalier Universitaire (CHU) in Lille, France. Next of kin provided informed consent for scientific research following consultation with the French National Registry of Organ Refusal. The study encompassed 576 human islet donors, with 408 donors allocated to static glucose-stimulated insulin secretion (GSIS) assessment and 168 to dynamic perifusion studies, and 10 donors included in both methods for direct comparison. The clinical characteristics of each donor are summarized in Table 1.

Pancreatic islets isolation, culture, and counting

Islet isolation followed the automated method of Ricordi et al.[20] with modifications[21]. Isolated human islets were maintained in custom CMRL 1066 medium (Thermo Scientific, Illkirch, France, containing 5 mM sodium pyruvate, 10 mM nicotinamide, 25 mM HEPES) supplemented with 0.625% human serum albumin, penicillin, streptomycin, and 0.18 mg/l insulin[21]. Prior to each experimentation, islets were systematically recounted to determine the number of islet equivalents (IEQ) required for static glucose stimulation or perifusion experiments[22].

Static incubation technique

For static GSIS assessment, 40 IEQs were placed on cell culture inserts (3 µm pore size, PITP01250, Merck Millipore, Cork, Ireland). Each donor sample (n = 408) underwent sextuplicate testing, utilizing 240 IEQ in parallel, islets were equilibrated for 50 minutes in KREBS buffer (124 mM NaCl, 4.8 mM KCl, 2.5 mM $CaCl_2$-H_2O, 1.2 mM $MgCl_2$-$6H_2O$, 25 mM $NaHCO_3$, pH 7.3) containing 3 mM glucose and 0.1% bovine serum albumin at 37°C. Glucose stimulation was performed by transferring inserts to KREBS buffer containing 15 mM glucose for 30 minutes. Following collection of supernatants, islets were resuspended in acid-ethanol solution (1.5% HCl, 70% EtOH, 28.5% ddH_20), sonicated, diluted 1/400, and stored with supernatants at -20°C pending insulin measurement as described[21,23].

Dynamic perifusion technique

Dynamic perifusion studies (n = 168) utilized 300 IEQ per reaction chamber, with continuous flow maintained at 1 ml/min and fractions collected every 2 minutes, as described[24]. The protocol employed KREBS buffer supplemented with 1 mg/ml Bovine Serum Albumin and consisted of three phases: 50-minute equilibration in 3 mM glucose without sampling, followed by sequential collection at 3 mM glucose (10 minutes, 0.54 g/l), 15 mM glucose (40 minutes, 2.72 g/l), and return to 3 mM glucose (20 minutes). Perifusion parameters, including flow rate (1 ml/min), temperature (37°C), and oxygenation (95% O_2/5% CO_2), were rigorously standardized across all experiments using automated, calibrated perifusion systems. Throughout the procedure, flow rate, pressure, temperature, and oxygen concentration remained constant. Each run included internal controls, and islet batches were randomly assigned across experimental days to minimize batch

effects. Additionally, all experiments were conducted using identical buffer compositions and glucose ramping protocols, ensuring consistency in stimulus delivery and measurement conditions. Postexperiment, islets were processed in acid-ethanol, sonicated, serially diluted (1/2114, 1/3844, and 1/5761), and stored with outflow fractions at −20°C.

Insulin measurement and determination of insulin secretion

Insulin quantification was performed using the automatic ACCESS II Access Immunoassay System (Beckman Coulter France, Villepinte, France). Intracellular insulin was extracted via ultra-sonication of acid-ethanol resuspended islets. Results were expressed as absolute values (IU/ml/min) or as percentage of secretion normalized to intracellular insulin content. For perifusion experiments, the stimulation index (SI) was calculated from the mean of first-phase peak (S1) with or without second-phase plateau (S2) at 15 mM glucose, relative to baseline (B) secretion at 3 mM glucose. Static incubation SI was determined as the ratio of combined first and second phase secretion (S1 + S2) at 15 mM glucose to baseline (B) secretion at 3 mM glucose.

Statistical analysis

Data analysis was performed using Prism 10.4.1 (GraphPad Software, La Jolla, USA), with results expressed as means ± SD or SEM. Statistical evaluation included Pearson correlation coefficients and linear regression analysis (beta coefficients and regression equations). Group comparisons were conducted using Kruskal–Wallis tests, with significance set at $P < 0.05$. Body surface area calculations employed Mosteller's[25] formula, incorporating height (cm) and weight (kg)

$$BSA(m^2) = \sqrt{Ht(cm) \times Wt(kg) / 3600}$$

Results

Dynamic characterization of insulin secretion

The perifusion system enabled real-time observation of insulin secretion kinetics from isolated human islets. When stimulated with glucose, islets (300 IEQ) demonstrated a characteristic biphasic response (Fig. 1a). At baseline (3 mM glucose), islets maintained stable basal secretion (B phase). Upon exposure to 15 mM glucose, insulin secretion exhibited two distinct phases: an initial rapid and intense peak (S1), followed by a sustained but lower plateau (S2). Return to 3 mM glucose resulted in gradual descent to baseline levels over 20 minutes. This secretion pattern remained consistent whether expressed in absolute terms (μIU/ml/min, Fig. 1a) or as a percentage of total insulin content (Fig. 1b).

System reproducibility and method comparison

To validate system reliability, parallel perifusion chambers were tested using the same islet preparations and conditions. While absolute insulin measurements (mIU/ml/min) showed approximately 1.6-fold variation between chambers (Fig. 1c), normalization to intracellular insulin content eliminated this sampling variation, yielding superimposable secretion profiles (Fig. 1d). Comparative analysis of static versus dynamic glucose stimulation was performed using matched islet preparations from 10 donors. Perifusion demonstrated greater dynamic range in Stimulation Indices (SI) (SI: 1.8–13.4) compared to static incubation (SI: 0.9–2.6) while maintaining a significant positive correlation ($r^2 = 0.652$, $P = 0.005$) between methods (Fig. 1e). This enhanced sensitivity of perifusion was further confirmed across the full dataset, with significantly higher SI in the perifusion group (4.28 ± 3.25, $n = 168$) compared to static incubation (1.88 ± 1.26, $n = 408$) ($P < 0.0001$, Fig. 1f).

Intracellular insulin content per IEQ showed comparable but statistically different values between static incubation (31.8 ± 21.9 ng) and perifusion (36.4 ± 22.8 ng) groups ($P = 0.024$, Fig. 1g), suggesting subtle variations in islet sampling or preparation methods between techniques.

Heterogeneity and impact of HbA1c and BMI on insulin secretion

Analysis of donor heterogeneity

Dynamic glucose stimulation of 168 islet preparations revealed substantial inter-individual variation in insulin secretion kinetics (Fig. 2a). Mean secretion rates were 0.011% ± 0.009 at low glucose (B phase) and 0.038% ± 0.034 at high glucose (S1 phase), yielding an average stimulation index of 4.25 ± 3.22. While all preparations demonstrated glucose responsiveness (SI > 1), the magnitude varied dramatically. The highest responding preparation showed a SI of 5.70 (B = 0.0412%, S1 = 0.2351%), while the lowest had a SI of 1.28 (B = 0.0021%, S1 = 0.0027%), representing remarkable inter-individual variations: 19.5-fold in basal secretion, 87-fold in stimulated secretion, and 22-fold in stimulation indices (Fig. 2b).

Correlation analysis of donor variables

Multiple donor characteristics were found to significantly influence islet function, as summarized in Table 2. Basal insulin secretion correlated significantly with BMI, HbA1c, and BSA, whereas insulin secretion under high-glucose conditions was primarily associated with BMI. In contrast, the SI correlated with a broader range of factors, including age, HbA1c, intensive care unit (ICU) duration, and cold ischemia time. Given the strong correlation between BSA and BMI ($r^2 = 0.62$, $P < 0.0001$), the specific effects of BSA are detailed separately in Supplementary Fig. 1.

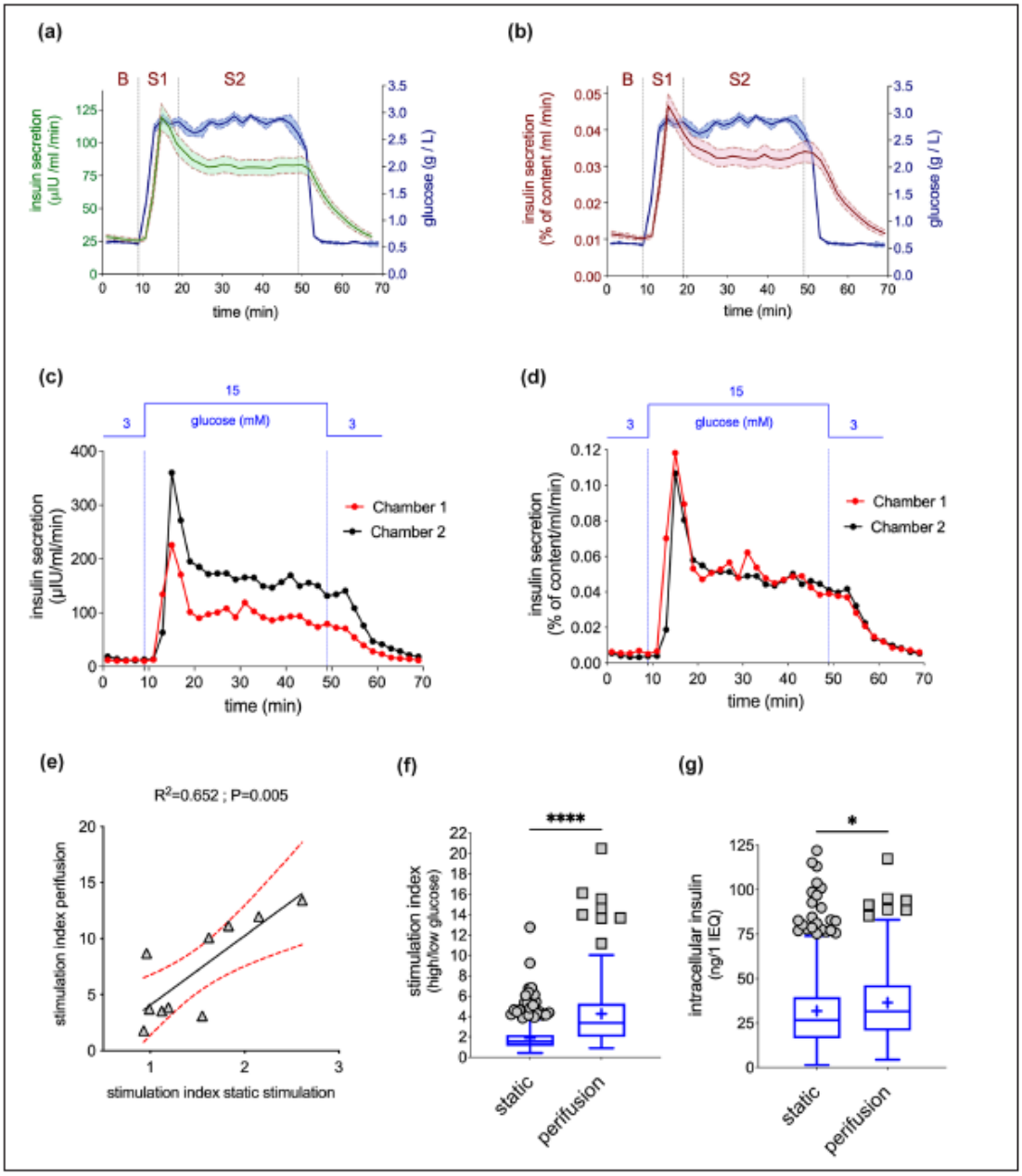

Figure 1. Dynamic glucose-stimulated insulin secretion profiles and method comparison. (a, b) Time-course analysis of insulin secretion from perifused islets (n = 168), expressed as (a) absolute values (mIU/ml/min) and (b) percentage of insulin content (%/ml/min). Phases of secretion are indicated: basal (B, 3 mM glucose), first-phase peak (S1), and second-phase plateau (S2) at 15 mM glucose. Blue line indicates glucose concentration. (c, d) Assessment of reproducibility using parallel perifusion chambers, showing insulin secretion expressed as (c) absolute values and (d) percentage of insulin content. (e) Correlation between static and dynamic stimulation indices (n = 10, r^2= 0.652, P = 0.005); red dotted lines indicate 95% confidence intervals. (f) Comparison of stimulation indices and (g) intracellular insulin content per islet equivalent (IEQ) between static incubation (n = 408) and perifusion (n = 168) techniques. Data in (a, b) are presented as mean ± SEM. Statistical significance was determined by unpaired nonparametric t test: *$P < 0.05$; ****$P < 0.0001$.

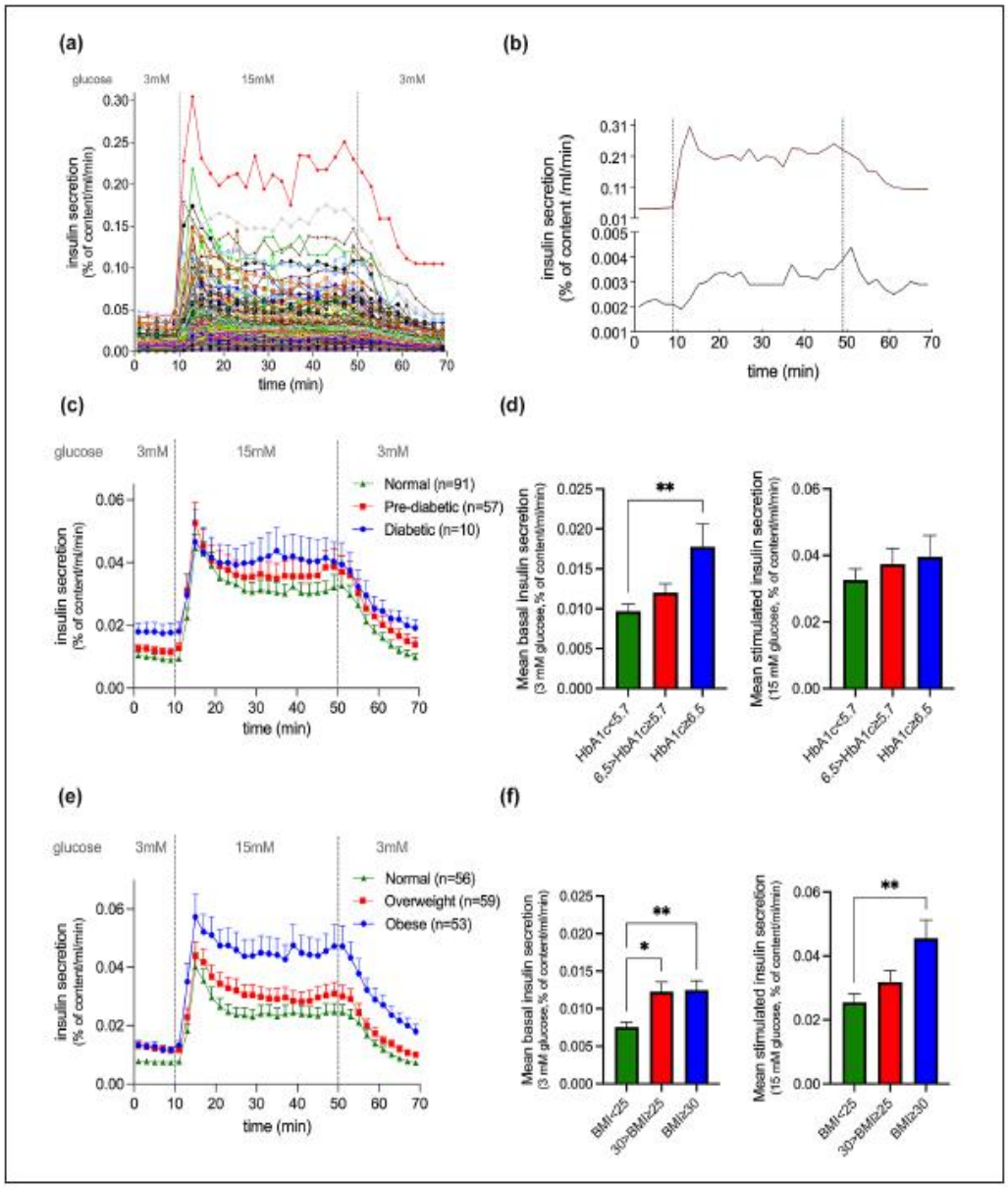

Figure 2. Analysis of insulin secretion heterogeneity and association with donor metabolic variables. (a) Individual insulin secretion profiles from $n = 168$ islet preparations during glucose stimulation (3 mM to 15 mM), expressed as percentage of insulin content. (b) Representative maximum (red) and minimum (black) secretion profiles illustrate the range of responses. (c) Insulin secretion kinetics stratified by donor HbA1c: normoglycemic (<5.7%, $n = 91$), prediabetic (5.7%–6.5%, $n = 57$), and diabetic (≥6.5%, $n = 10$). Data are presented as mean ± SEM. (d) Comparison of mean basal (3 mM glucose, left) and stimulated (15 mM glucose, right) insulin secretion across HbA1c groups. (e) Insulin secretion kinetics stratified by donor BMI: normal (<25 kg/m², $n = 56$), overweight (25–30 kg/m², $n = 59$), and obese (>30 kg/m², $n = 53$). Data are presented as mean ± SEM. (f) Comparison of mean basal and stimulated insulin secretion across BMI groups. Statistical significance was determined by unpaired nonparametric t test: $^*P < 0.05$; $^{**}P < 0.01$.

Table 2. Correlation analysis of donor characteristics with insulin secretion variables in dynamic perifusion studies.

N = 168	R^2	*P* value	Significant
Age vs B	0.005	0.359	NS
vs SI	0.003	0.473	NS
vs SI/B	0.023	*0.047*	*
BMI vs B	0.034	*0.015*	*
vs SI	0.029	*0.026*	*
vs SI/B	0.001	0.628	NS
HbA1c vs B	0.042	*0.009*	**
vs SI	<0.001	0.827	NS
vs SI/B	0.040	*0.011*	*
BSA vs B	0.047	*0.005*	**
vs SI	0.018	0.079	NS
vs SI/B	0.002	0.526	NS
UCI vs B	0.001	0.640	NS
vs SI	0.001	0.200	NS
vs SI/B	0.035	*0.015*	*
Cold ischemia vs B	<0.001	0.866	NS
vs SI	0.011	0.179	NS
vs SI/B	0.034	*0.017*	*

Linear regression analysis between donor physiological variables and insulin secretion kinetics (n = 168). Secretion variables were measured during basal stimulation (B, 3mM glucose), first-phase secretion peak (SI, 15mM glucose), and calculated as stimulation index (SI/B). R^2 represents coefficient of determination; *P*-values were determined using Kruskal–Wallis multiple comparisons test. Statistical significance is indicated as: NS: not significant. BMI: body mass index; BSA: body surface area; HbA1c: glycated hemoglobin; ICU: intensive care unit length of stay.
*$P < 0.05$; **$P < 0.01$.

Impact of glycemic status

Donors were stratified based on HbA1c levels following WHO criteria: normoglycemic (< 5.7%), prediabetic (5.7-6.5%), and diabetic (≥ 6.5%). Diabetic donors showed significantly elevated basal insulin secretion compared to normoglycemic donors (1.8-fold increase, $P < 0.01$), while prediabetic donors displayed intermediate levels (Fig. 2c, d). Despite these differences in basal secretion, all groups retained robust glucose responsiveness, showing comparable secretion kinetics during both stimulation and return to baseline phases.

Effect of BMI on insulin secretion

Donors were grouped by BMI into normal weight (<25 kg/m²), overweight (25–30 kg/m²), and obese (≥30 kg/m²). Clear differences in insulin secretion patterns emerged across groups (Fig. 2e, f). Both basal and glucose-stimulated insulin secretion increased progressively with BMI. Normal-weight donors showed significantly lower basal secretion compared to overweight ($P < 0.05$) and obese donors ($P < 0.01$). Under high-glucose conditions, obese donors demonstrated significantly higher insulin secretion compared to normal-weight donors ($P < 0.01$). Gender analysis revealed minimal overall impact; however, in the normal BMI group, females exhibited slightly higher glucose-stimulated secretion than males (1.3-fold, $P = 0.023$) (Supplementary Fig. 2).

Impact of donor physiological variables on insulin responses: clustering analysis

Identification of distinct donor clusters

A multivariate factorial mapping was conducted, incorporating key physiological variables, including age, BMI, HbA1c, and BSA, to explore underlying donor phenotypes. Despite strong correlations between some variables, such as BMI and BSA, all variables were retained to maximize analytical depth. Data were standardized through centering and reduction to ensure comparability. Clustering via the silhouette method identified two optimal donor groups (Fig. 3a), with no individuals excluded to ensure representation of clinically relevant extremes such as severe obesity and diabetes.

Cluster characterization

Distinct metabolic profiles emerged between the two clusters (Fig. 3b). Cluster 1 ($n = 102$) comprised donors with normal metabolic variables: mean BMI of 25.1 kg/m², normal HbA1c (5.5%), and BSA of 1.9 m². In contrast, Cluster 2 ($n = 56$) reflected a metabolically impaired cohort characterized by obesity (mean BMI: 33.6 kg/m²), elevated HbA1c (5.8%, prediabetic range), and higher BSA (2.3 m²). Age distribution was comparable between clusters (52.7 vs 48.3 years). Cluster robustness was confirmed through bootstrap techniques, with high Jaccard indices for both Cluster 1 (0.98) and Cluster 2 (0.99), exceeding the accepted stability threshold of 0.75.

Impact on insulin secretion dynamics

Comparison of insulin secretion profiles revealed significant functional differences between clusters. Both basal (3 mM glucose) and glucose-stimulated (15 mM glucose) insulin secretion were significantly higher in Cluster 2 (Fig. 3c; Wilcoxon test, $P = 0.012$ and $P = 0.014$, respectively). These differences were further illustrated in the full dynamic secretion curves (Fig. 3d), highlighting altered insulin kinetics in donors with metabolic dysfunction.

Gender analysis

Gender distribution analysis across clusters showed no significant impact on insulin secretion variables during perifusion (low glucose: $P = 0.13$; high glucose: $P = 0.18$). This was further confirmed by Pearson's chi-squared analysis ($P = 0.08$), indicating that metabolic variables, rather than gender, were the primary drivers of clustering.

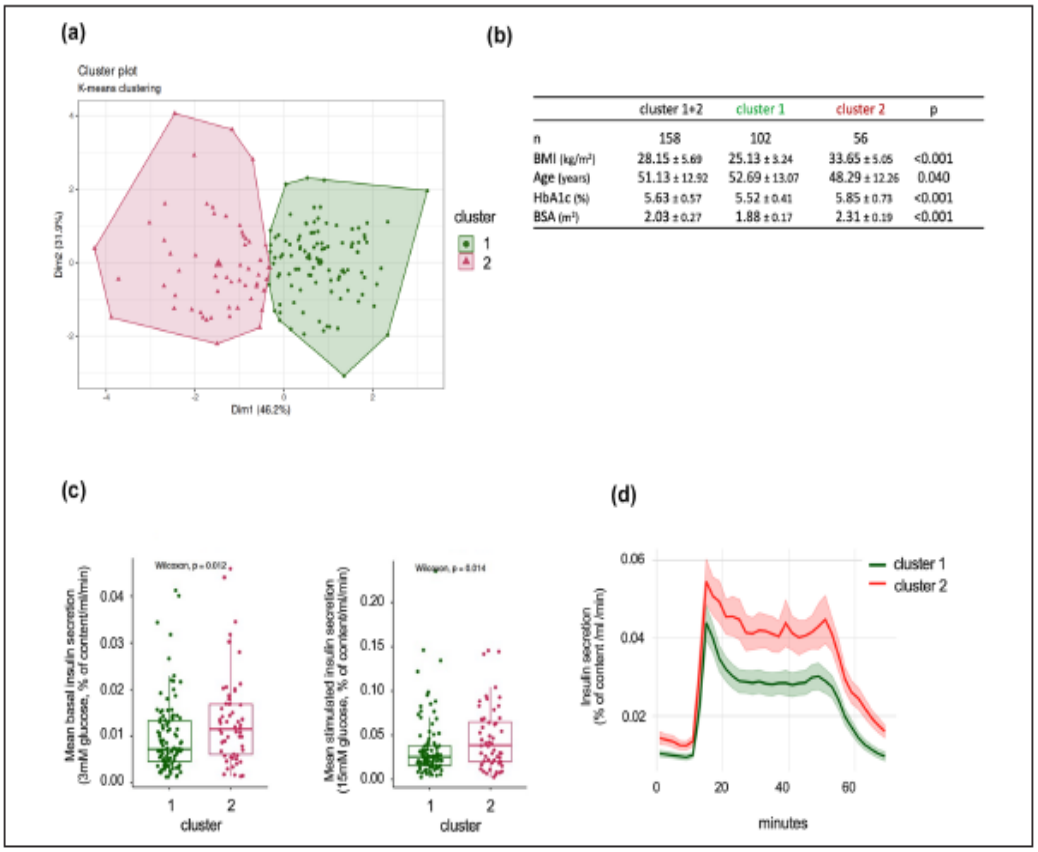

	cluster 1+2	cluster 1	cluster 2	p
n	158	102	56	
BMI (kg/m²)	28.15 ± 5.69	25.13 ± 3.24	33.65 ± 5.05	<0.001
Age (years)	51.13 ± 12.92	52.69 ± 13.07	48.29 ± 12.26	0.040
HbA1c (%)	5.63 ± 0.57	5.52 ± 0.41	5.85 ± 0.73	<0.001
BSA (m²)	2.03 ± 0.27	1.88 ± 0.17	2.31 ± 0.19	<0.001

Figure 3. K-means clustering of donor characteristics in relation to insulin secretion. K-means clustering was performed using donor age, BMI, HbA1c, and BSA in relation to insulin secretion at low (3 mM) and high (15 mM) glucose. (a) Two distinct clusters emerged from the analysis. (b) Cluster-specific data with statistical comparisons of individual variables using unpaired nonparametric *t* tests. (c) Wilcoxon test comparing insulin secretion medians between clusters at low and high glucose levels. (d) Time-course profiles of insulin secretion (mean ± SEM) for the two clusters.

Discussion

This large-scale, single-center study provides the first comprehensive comparison of insulin secretion between static (n − 408) and dynamic perifusion (n − 168) techniques using standardized experimental variables. While both methods showed comparable stimulation index measurements (r^2– 0.652), dynamic perifusion offered superior resolution in assessing secretion kinetics relative to donor physiological variables. Standardization was crucial given the intrinsic heterogeneity of pancreatic islets in size, endocrine cell distribution, and molecular expression patterns[26,27]. The observed variability in insulin secretion capacity, influenced by donor characteristics[28] and isolation center protocols[16,17,29], highlights the necessity for consistent assessment methods. Our approach of normalizing secretion to total islet insulin content effectively mitigated islet-specific heterogeneity[16,24]. Notably, we observed higher intracellular insulin content (~34 ng/IEQ) compared to previous multi-center studies (13.3 ng/IEQ)[19], emphasizing the impact of standardized protocols on measurement outcomes. The discrepancy likely reflects differences in islet isolation protocols, donor demographics (age, BMI, metabolic status), and measurement methodologies, including insulin quantification techniques and culture conditions. Variations in assay sensitivity and data normalization may further contribute to inter-study variability.

Our perifusion studies revealed substantial heterogeneity in stimulation indices (ranging from 1 to 20), consistent with previous findings[13,30]. The selected glucose concentrations (3 and 15 mM), while differing from other studies using 4–16 mM[13] or 5.6–16.7 mM[30], were intentionally chosen. The use of 3 mM glucose, below physiological fasting levels, provided valuable insights into hypoglycemic responses, which may be predictive of islet graft function in T1D patients. Furthermore, we chose 15 mM glucose as it

reliably elicits robust, physiologically relevant insulin responses, enabling clear resolution of secretion kinetics without inducing non-specific stress.

Analysis of donor variables traditionally associated with islet isolation yields[31] revealed novel insights into their influence on secretion kinetics. Our findings demonstrate that obesity and diabetes significantly affect both basal and stimulated insulin secretion, particularly under low glucose conditions. The enhanced insulin secretion observed under low glucose conditions in donors with obesity and prediabetes may reflect β-cell compensatory mechanisms in response to systemic insulin resistance. In these individuals, peripheral tissues exhibit reduced insulin sensitivity, prompting β-cells to increase basal insulin output to maintain euglycemia. This chronic compensatory demand may lead to an upregulation of glucose-independent insulin secretion pathways, including enhanced basal exocytosis and altered ATP-sensitive potassium channel activity. Additionally, low-grade inflammation and lipotoxicity associated with obesity may modulate islet function by sensitizing β-cells to non-glucose stimuli, such as free fatty acids, further contributing to elevated basal secretion. These adaptations, while initially protective, may precede β-cell dysfunction and are consistent with early-stage hyperinsulinemia seen in prediabetic individuals.

The combination of advanced age (>48 years), obesity (BMI > 33kg/m^2), and prediabetes (HbA1c > 5.8%) was associated with higher insulin secretion kinetics. These results extend previous observations about BMI's importance[16] and challenge earlier conclusions regarding age effects. Our *in vitro* findings align with clinical observations of primary insulin hypersecretion[32] and underscore the role of basal insulin secretion in glycemic regulation[33]. The absence of gender-based differences in our study aligns with existing literature[33], suggesting that while subtle hormone-mediated differences may exist, gender does not significantly impact insulin secretion capacity.

Regarding islet quality assessment, it's important to contextualize our findings alongside established donor scoring systems such as the North American Islet Donor Score (NAIDS)[35,36] and the Kansas City Islet Score[37]. These tools, developed to predict islet isolation outcomes based on donor characteristics like age, BMI, cold ischemia time, and HbA1c, have demonstrated utility in estimating islet yield and viability[2]. However, they do not directly assess functional potency. Our work aims to complement these predictive scoring systems by offering a high-resolution functional evaluation of islet insulin secretion via dynamic perifusion. By doing so, we provide additional insight into islet quality that may further inform graft selection and improve transplantation outcomes.

In conclusion, dynamic perifusion reveals that inter-individual heterogeneity in isolated islet insulin secretion is primarily driven by donor BMI and HbA1c, especially under hypoglycemic conditions. These findings have important implications for donor selection and the optimization of islet transplantation protocols, reinforcing the value of standardized quality criteria in advancing cell therapy outcomes.

Acknowledgments

We gratefully acknowledge the Biotherapy department at the Centre Hospitalier Universitaire (CHU) of Lille for providing access to their islet isolation facility. We extend our thanks to Sandrine Belaich and Bruno Lukowiak for their technical expertise and invaluable assistance during the islet isolation procedures. This work greatly benefited from the collaborative environment and research infrastructure provided by the Direction de la Recherche et de l'Innovation (DRI) at CHU Lille. We also thank the FRENCH organ procurement organizations Agence de la Biomédecine and the surgical teams involved in pancreas recovery, as well as the donor families whose generosity made this research possible.

ORCID iDs

Priyadarshini Gnanasekar https://orcid.org/0009-0001-7094-3093

Chiara Saponaro https://orcid.org/0000-0001-7336-7362

Markus Mühlemann https://orcid.org/0000-0002-8323-7331

Julien Thevenet https://orcid.org/0000-0001-6873-8640

Marie-Christine Vantyghem https://orcid.org/0000-0002-9369-0463

Caroline Bonner https://orcid.org/0000-0002-4430-8280

Valery Gmyr https://orcid.org/0000-0003-1236-359X

Ethical Considerations

This study is part of a research protocol approved by the French regulations on the Lille University Hospital site on the subject of "Design, development and optimization of production and evaluation tools to improve islet transplantation and evaluation of islet-parathyroid co-transplantation" # PFS16-008.

Author Contributions

P.Pa., V.G., C.S., M.M., C.B., F.P., and J.K.C. were involved in data acquisition, conceptualization, data analysis and visualization. A.C., P.Pe., J.T, N.D, A.H, V.G., M.C. and J.K.C. are involved in the pancreas procurement and islets isolation. G.P, V.L., A.C. and V.G. performed GSIS for the islet evaluation. I.G.M., M.C.V., V.G., F.P., C.B., and J.K.C. conducted data curation and formal analysis. C.A.A and V.R. participated in statistical studies (R software). V.G, P.Pa., C.S, M.M, F.P, C.B, and J.K.C. wrote the original draft and performed subsequent revisions.

All authors have read and approved the final manuscript.

Funding

The author(s) disclosed receipt of the following financial support for the research, authorship, and/or publication of this article: This research was supported by grants from the Agence de la BioMédecine (AOR "*Recherche et Greffe 2023*"), the Conseil Régional Hauts-de-France (CPER Tech Sante AAP2022), Fondation de la Recherche Médicale (EQU202303016330, Prix

Line-Renaud et Loulou-Gasté), Association pour la Recherche sur le Diabète, and the European Genomic Institute for Diabetes (ANR-10-LABX-46). Priyadarshini Gnanasekar-Panchatcharam was supported by a doctoral fellowship from the CPER Tech Sante program.

Declaration of Conflicting Interests

The author(s) declared no potential conflicts of interest with respect to the research, authorship, and/or publication of this article.

Statement of Human and Animal Rights

This article does not contain any studies with human or animal subjects.

Statement of Informed Consent

There are no human subjects in this article and informed consent is not applicable.

Data Availability Statement

Anonymized datasets generated and analyzed during the current study are available from the corresponding author upon reasonable request, subject to institutional data sharing policies and ethical considerations. Access to raw clinical data is restricted to protect donor privacy in accordance with French regulations and institutional guidelines.

Supplemental Material

Supplemental material for this article is available online.

References

1. Shapiro AM, Lakey JR, Ryan EA, Korbutt GS, Toth E, Warnock GL, Kneteman NM, Rajotte RV. Islet transplantation in seven patients with type 1 diabetes mellitus using a glucocorticoid-free immunosuppressive regimen. N Engl J Med. 2000;343(4):230–38.
2. Hering BJ, Clarke WR, Bridges ND, Eggerman TL, Alejandro R, Bellin MD, Chaloner K, Czarniecki CW, Goldstein JS, Hunsicker LG, Kaufman DB, et al. Phase 3 trial of transplantation of human islets in type 1 diabetes complicated by severe hypoglycemia. Diabetes Care. 2016;39(7):1230–40.
3. Vantyghem MC, de Koning EJP, Pattou F, Rickels MR. Advances in beta-cell replacement therapy for the treatment of type 1 diabetes. Lancet. 2019;394(10205):1274–85.
4. Berney T, Andres A, Bellin MD, de Koning EJP, Johnson PRV, Kay TWH, Lundgren T, Rickels MR, Scholz H, Stock PG, White S, et al. A worldwide survey of activities and practices in clinical islet of Langerhans transplantation. Transpl Int. 2022;35:10507.
5. Witkowski P, Philipson LH, Buse JB, Robertson RP, Alejandro R, Bellin MD, Kandeel F, Baidal D, Gaglia JL, Posselt AM, Anteby R, et al. Islets transplantation at a crossroads—need for urgent regulatory update in the United States: perspective presented during the scientific sessions 2021 at the American diabetes association congress. Front Endocrinol (Lausanne). 2021;12:789526.
6. Vantyghem MC, Chetboun M, Gmyr V, Jannin A, Espiard S, Le Mapihan K, Raverdy V, Delalleau N, Machuron F, Hubert T, Frimat M, et al. Ten-year outcome of islet alone or islet after kidney transplantation in type 1 diabetes: a prospective parallel-arm cohort study. Diabetes Care. 2019;42(11):2042–49.
7. Ichii H, Inverardi L, Pileggi A, Molano RD, Cabrera O, Caicedo A, Messinger S, Kuroda Y, Berggren PO, Ricordi C. A novel method for the assessment of cellular composition and beta-cell viability in human islet preparations. Am J Transplant. 2005;5(7):1635–45.
8. Papas KK, Colton CK, Nelson RA, Rozak PR, Avgoustiniatos ES, Scott WE 3rd, Wildey GM, Pisania A, Weir GC, Hering BJ. Human islet oxygen consumption rate and DNA measurements predict diabetes reversal in nude mice. Am J Transplant. 2007;7(3):707–13.
9. Street CN, Lakey JR, Shapiro AM, Imes S, Rajotte RV, Ryan EA, Lyon JG, Kin T, Avila J, Tsujimura T, Korbutt GS. Islet graft assessment in the Edmonton Protocol: implications for predicting long-term clinical outcome. Diabetes. 2004;53(12):3107–14.
10. Misun PM, Yesildag B, Forschler F, Neelakandhan A, Rousset N, Biernath A, Hierlemann A, Frey O. In vitro platform for studying human insulin release dynamics of single pancreatic islet microtissues at high resolution. Adv Biosyst. 2020;4(3):e1900291.
11. Henquin JC, Dufrane D, Kerr-Conte J, Nenquin M. Dynamics of glucose-induced insulin secretion in normal human islets. Am J Physiol Endocrinol Metab. 2015;309(7):E640–50.
12. Hart NJ, Powers AC. Use of human islets to understand islet biology and diabetes: progress, challenges and suggestions. Diabetologia. 2019;62(2):212–22.
13. Alcazar O, Buchwald P. Concentration-dependency and time profile of insulin secretion: dynamic perifusion studies with human and murine islets. Front Endocrinol (Lausanne). 2019;10:680.
14. Cabrera O, Jacques-Silva MC, Berman DM, Fachado A, Echeverri F, Poo R, Khan A, Kenyon NS, Ricordi C, Berggren PO, Caicedo A. Automated, high-throughput assays for evaluation of human pancreatic islet function. Cell Transplant. 2007;16(10):1039–48.
15. Henquin JC, Dufrane D, Gmyr V, Kerr-Conte J, Nenquin M. Pharmacological approach to understanding the control of insulin secretion in human islets. Diabetes Obes Metab. 2017;19(8):1061–70.
16. Henquin JC. Influence of organ donor attributes and preparation characteristics on the dynamics of insulin secretion in isolated human islets. Physiol Rep. 2018;6(5):e13646.
17. Nano R, Kerr-Conte JA, Scholz H, Engelse M, Karlsson M, Saudek F, Bosco D, Antonioli B, Bertuzzi F, Johnson PRV, Ludwing B, et al. Heterogeneity of human pancreatic islet isolation around Europe: results of a survey study. Transplantation. 2020;104(1):190–96.
18. Ewald JD, Lu Y, Ellis CE, Worton J, Kolic J, Sasaki S, Zhang D, Dos Santos T, Spigelman AF, Bautista A, Dai XQ, et al. Humanislets.com: improving accessibility, integration, and usability of human research islet data. Cell Metab. 2025;37(1):7–11.
19. Henquin JC. The challenge of correctly reporting hormones content and secretion in isolated human islets. Mol Metab. 2019;30:230–39.
20. Ricordi C, Gray DW, Hering BJ, Kaufman DB, Warnock GL, Kneteman NM, Lake SP, London NJ, Socci C, Alejandro R. Islet isolation assessment in man and large animals. Acta Diabetol Lat. 1990;27(3):185–95.
21. Kerr-Conte J, Vandewalle B, Moerman E, Lukowiak B, Gmyr V, Arnalsteen L, Caiazzo R, Sterkers A, Hubert T, Vantyghem MC, Pattou F. Upgrading pretransplant human islet culture tech-

nology requires human serum combined with media renewal. Transplantation. 2010;89(9):1154–60.
22. Gmyr V, Bonner C, Lukowiak B, Pawlowski V, Dellaleau N, Belaich S, Aluka I, Moermann E, Thevenet J, Ezzouaoui R, Queniat G, et al. Automated digital image analysis of islet cell mass using Nikon's inverted Eclipse Ti microscope and software to improve engraftment may help to advance the therapeutic efficacy and accessibility of islet transplantation across centers. Cell Transplant. 2013;24:1–9.
23. Vandewalle B, Douillard C, Kerr Conte J, Gmyr V, Riachi R, D'herbomez M, Pattou F, Lefebvre J. Human pancreatic islet quality control: easy assessment of metabolic functions. Exp Clin Endocrinol Diabetes. 1999;107(3):214–19.
24. Henquin JC, Dufrane D, Nenquin M. Nutrient control of insulin secretion in isolated normal human islets. Diabetes. 2006;55(12):3470–77.
25. Mosteller RD. Simplified calculation of body-surface area. N Engl J Med. 1987;317(17):1098.
26. Dybala MP, Hara M. Heterogeneity of the Human Pancreatic Islet. Diabetes. 2019;68(6):1230–39.
27. Saponaro C, Mühlemann M, Acosta-Montalvo A, Piron A, Gmyr V, Delalleau N, Moerman E, Thévenet J, Pasquetti G, Coddeville A, Cnop M, et al. Interindividual heterogeneity of SGLT2 expression and function in human pancreatic islets. Diabetes. 2020;69(5):902–14.
28. Buemi A, Mourad NI, Ambroise J, Hoton D, Devresse A, Darius T, Kanaan N, Gianello P, Mourad M. Donor- and isolation-related predictive factors of in vitro secretory function of cultured human islets. Front Endocrinol (Lausanne). 2024;15:1345351.
29. Nano R, Kerr-Conte JA, Scholz H, Engelse M, Karlsson M, Saudek F, Bosco D, Antonioli B, Bertuzzi F, Johnson PRV, Ludwing B, et al. Heterogeneity of human pancreatic islet isolation around Europe: results of a survey study. Transplant. 2020;104(1):190–196.
30. Kayton NS, Poffenberger G, Henske J, Dai C, Thompson C, Aramandla R, Shostak A, Nicholson W, Brissova M, Bush WS, Powers AC. Human islet preparations distributed for research exhibit a variety of insulin-secretory profiles. Am J Physiol Endocrinol Metab. 2015;308(7):E592–602.
31. O'Gorman D, Kin T, McGhee-Wilson D, Shapiro AM, Lakey JR. Multi-lot analysis of custom collagenase enzyme blend in human islet isolations. Transplant Proc. 2005;37(8):3417–19.
32. Trico D, Natali A, Arslanian S, Mari A, Ferrannini E. Identification, pathophysiology, and clinical implications of primary insulin hypersecretion in nondiabetic adults and adolescents. JCI Insight. 2018;3(24):e124912.
33. Investigators OT, Gerstein HC, Bosch J, Dagenais GR, Diaz R, Jung H, Maggioni AP, Pogue J, Probstfield J, Ramachandran A, Riddle MC, et al. Basal insulin and cardiovascular and other outcomes in dysglycemia. N Engl J Med. 2012;367(4):319–28.
34. Henquin JC. Glucose-induced insulin secretion in isolated human islets: does it truly reflect beta-cell function in vivo? Mol Metab. 2021;48:101212.
35. Wang LJ, Kin T, O'Gorman D, Shapiro AMJ, Naziruddin B, Takita M, Levy MF, Posselt AM, Szot GL, Savari O, Barbaro B, et al. A multicenter study: north American islet donor score in donor pancreas selection for human islet isolation for transplantation. Cell Transplant. 2016;25(8):1515–23.
36. Gołębiewska JE, Bachul PJ, Wang LJ, Matosz S, Basto L, Kijek MR, Fillman N, Gołąb K, Tibudan M, Dębska-Ślizień A, Millis JM, et al. Validation of a new North American islet donor score for donor pancreas selection and successful islet isolation in a medium-volume islet transplant center. Cell Transplant. 2019;28(2):185–94.
37. Ramachandran K, Huang HH, Stehno-Bittel L. A simple method to replace islet equivalents for volume quantification of human islets. Cell Transplant. 2015;24(7):1183–94.